The control of the surface topography of neutrophils

By

Maha Awadh Aljumaa

Neutrophil Signalling Group,

Institute of Infection and Immunity,

Cardiff University, School of Medicine,

Cardiff.

January 2018

Thesis submitted to Cardiff University for the degree of Doctor of Philosophy

ACKNOWLEDGEMENTS

In the name of Allah, the Most Gracious and the Most Merciful

First and above all I would like to thank ALLAH Almighty who gave me the courage, health and energy to complete my thesis in due time.

It is my great pleasure to express sincere gratitude to my country, Saudi Arabia for providing the sponsorship which allowed me to undertake this research.

I would like to extend thanks to several people who have been central in the achievement during my study, both academically and personally. This work and the time that I have spent engaged in research and writing, would have been much poorer.

Special mention goes to my supervisor Professor Maurice Hallett, for his supervision, support, patient guidance, encouragement and advice he has provided throughout my time as his PhD student. At many stages in the course of this research project I benefited from his comments and suggestions throughout the experimental and thesis work have contributed to the success of this research. Also he has given me the opportunity to attend conferences and meet so many interesting people. This made me confident through all my study and improved myself to be a better scientist. Maurice I am very lucky to have been under your supervision with your cared so much about my work, great scientific discussion, guidance and for everything you taught me and answered to my questions and queries so quickly.

I must express my gratitude to my parents Mrs Awadh Aljumaa and Ms Nada Alneweshi for their almost unbelievable support and encouragement during the hard times. They are the most important people in my world and I dedicate this thesis to them.

I also would like to thank the staff of the School of Medicine and in particular I would like to thank all volunteers who so generously donated blood for my project. Last but not the least; a deep thanks to my friends in the UK for their help and collaboration and special thanks go to my brother Mohmmad Aljumah for the fun times we have shared throughout the years in UK.

Finally, may Allah always bless us all.

SUMMARY

Neutrophils are characterised by undergoing rapid cell shape change, especially during cell spreading and phagocytosis. In both situations, the cell changes from a spherical to a non-spherical configuration. This must necessarily require additional cell surface membrane as a sphere is the minimum surface area to enclose a given volume. Although it has been proposed that this additional membrane may come from cell surface structures called wrinkles or micro-ridges, it has not been possible to directly test this hypothesis. In this thesis, a methodology was established that would permit such a test. By incorporating freely diffusible fluorescent molecules into the plasma membrane of neutrophils, a methodology was devised that allows the diffusion time into a subdomain within a photobleached area to be monitored. As the diffusion time depended on the diffusion pathlength, this gave a measure of the surface topography. In osmotically swollen cells, in the neutrophil tail and the phagocytic cup, it was found that the membrane was smooth. However, in the cell body, there was a significant delay in diffusion, consistent with the presence of surface wrinkles. These wrinkles were reduced by osmotic swelling, and as cells spread onto a substrate. The wrinkledness could be increased by osmotic shrinking. This was the first time that changes in cell surface topography could be monitored. In order to establish whether changes in cell surface topography were important for rapid cell shape change, cells were suddenly hyper-wrinkled (osmotically) during phagocytosis or chemotaxis. In both cases this procedure immediately arrested the cell behaviour. On restoration of normal surface topography (by return osmolality to normal), cells then continued to undergo shape change. In the hyper-wrinkled state an abnormal shape change could be induced by uncaging cytosolic IP_3 and so force a Ca^{2+} signal. The data presented in this thesis therefore confirms that surface wrinkling changes during neutrophil shape change, and that this was a key factor in neutrophil shape change.

PAPERS, ABSTRACTS AND CONFERENCE PRESENTATIONS

1. Maha Aljumaa and Maurice Hallett (2014) Sub-domain FRAP of cell surface molecules to monitor cell surface topography in living cells ***American Society for Cell Biology*** (ASCB)/International Federation for Cell Biology (IFCB) Meeting in Philadelphia, PA, 2014 December 6-10.

2. Maurice B. Hallett, Maha Al-Jumaa and Sharon Dewitt (2014) Optical Methods for the Measurement and Manipulation of Cytosolic Calcium Signals in Neutrophils. ***Methods in Molecular Biology***, 1124, 107-120

3. Maha Aljumaa and Maurice Hallett (2016) Sub-domain FRAP of cell surface molecules to monitor cell surface topography in living cells, The ***Scientific Society for Saudi Students*** in the United Kingdom

4. Maha Aljumaa, Sharon Dewitt and Maurice Hallett (2017) Topographical interrogation of the living cell surface reveals its role in rapid cell shape changes during phagocytosis and spreading. ***Science Reports*** 7, 9790. (Published online doi: 10.1038/s41598-017-09761-6)

CONTENTS

ABBREVIATIONS LIST

AM	**Acetotoxymethyl ester**
BSA	**Bovine serum albumin**
BSS	**Balanced Salt Solution**
$[Ca^{2+}]$	**Cytosolic free calcium ion concentration**
C3b	**Complement fragment 3b**
C3bi	**Complement fragment C3b (inactive)**
c IP_3	**Caged Inositol 1,4,5 trisphosphate**
CR1	**Complement receptor 1 (CD11a/CD18, LFA-1, $\alpha_L\beta_2$)**
CR3	**Complement receptor 3 (CD11b/CD18, Mac-1, $\alpha_M\beta_2$, Mo-1)**
D	**Diffusion constant**
Doc	**Deoxycholate**
DiI iodide	**1,1' - Dioctadecyl - 3, 3,3',3' – Tetramethylindocarbocyanine**
DMSO	**Dimethylsulfoxide**
EGTA	**Ethylene glycol aminoethyl ether tetraacetic acid**
FM 1-43	**N-(3-Triethylammoniumpropyl)-4- (4-(Dibutylamino)Styryl) Pyridinium Dibromide)**
Fc	**Conserved fragment of antibody**
FcR	**Fc receptor (immunoglobulin receptor)**
Fmlp	**Formylmethionylleucylphenylalanine (formylated peptide)**
FPR	**Formylated peptide receptor**
FRAP	**Fluorescence recovery after laser photo-bleaching**
GPX	**Glutathione peroxidase**
HBK	**Hepes Buffered Krebs medium**

Hepes	**Hydroxyethylpiprazine ethanesulphonic acid**
HOCl	**Hypochlorous acid**
ICAM-1	**Intercellular adhesion molecule-1**
IP_3	**Inositol 1,4,5 trisphosphate**
Kd	**Dissociation constant**
MPO	**Myeloperoxidase**
NADPH	**Nicotinamide adenine dinucleotide phosphate**
NK	**Natural killer cells**
NO	**Nitric oxide**
Oct	**Octanol**
$ONOO^-$	**Peroxynitrite**
PI-3-kinase	**Phosphatidylinositide 3-kinase**
PIP_2	**Phosphatidylinositol 4,5-bisphosphate**
PKC	**Protein Kinase C**
PLC	**Phospholipase C**
PMN	**Polymorphonuclear neutrophilic leukocytes (neutrophils)**
Prx	**Peroxiredoxins**
ROS	**Reactive oxygen species**
RNS	**Reactive nitrogen species**
sdFRAP	**Subdomain Fluorescence recovery after laser photo-bleaching**
SOD	**Superoxide dismutase**
Trx	**Thioredoxin**
TNF–α	**Tumour necrosis factor-α**
VDAC	**Voltage-dependent anion channels**

LIST OF FIGURES

Chapter 1

Introduction

1. The Immune system

1.1 Understanding the immune system

The immune system is a complex structure that defends the body against diseases. It is a collection of cells, tissues and molecules which have evolved to prevent infection and to eradicate established infections. The reaction of these cells and molecules are mediated by recognizing and detecting a wide variety of pathogenic infectious agents which stimulates an immune response. Pathogens such as viruses, fungi, or bacteria are usually recognised by proteins on their surfaces. The immune system distinguishes them from proteins on the cells of the body and reacts against them. This influences both health and diseases; the beneficial roles in health include preventing the growth of some tumours, the clearance of dead cells and repairing damaged tissues. However, abnormal immune responses can cause severe diseases known as inflammatory diseases (Abul *et al*., 2014).

The organs of the immune system include the lymphatic system which is responsible for the growth, development and distribution of lymphocytes. The lymphoid organs are classified as primary or secondary. The primary lymphoid organs, also called central lymphoid organs, include the bone marrow and the thymus. Immune cells develop in these sites in the absence of antigen. The secondary lymphoid organs, also known as peripheral lymphoid organs, include spleen, lymph vessels, lymph nodes, skin and liver in which the maturation of immune cells occurs which is driven by antigen. The cells of the immune system (Table 1.1) protect the body from infection via the immune response, or by the innate immune system (Klaus, 2009). Neutrophils form a key component of innate immunity.

1.2 Innate immune system

Innate immunity provides the primary protection against infection as it is able to respond quickly to limit or eliminate infection within a short period of time. The innate immune system is also called natural immunity or native immunity as it does not require prior exposure to the infecting agent and is the immunity with which the body is born. It is characterised by physical, biological and chemical barriers in addition to the specific immune cells and soluble molecules (Klaus, 2009). It is thus considered to be the first line of defence against infection (Abul *et al*., 2014). The main mechanisms for innate immunity are passive barrier defences and nonspecific reactive cellular responses.

The passive barriers defences are able to restrict unwanted materials from entering and damaging the tissues in our bodies. In fact, they are identified as layers that are found in the external surfaces that protect the deeper tissues of the body. However, once the pathogens have passed the layers, phagocytes are responsible for killing the invading microbes. The innate immune cellular response is mounted against infections by bacteria or fungi, although not against any particular strains. Innate immunity is mediated mainly by phagocytic cells that are ready to recognize these pathogens at the site of infection and become quickly stimulated to destroy them (Gregory, 2009).

Table 1.1 The mechanisms of the different cells of the immune system.

Cell type	Primary Role
Leukocytes	
-Neutrophils	**Phagocytosis and microbial killing**
-Basophils	**Release histamine and other chemicals involved in inflammation**
-Eosinophils	**Destroy multicellular parasites**
-Monocytes	**Move to sight of infection and differentiate into macrophages:**
-*Macrophages*	**Phagocytosis and antigen presentation**
Lymphocytes	
-B cells	**Make antibodies against antigens and develop into memory cells**
-T cells	
-Cytotoxic T cells	**Bind antigens on target cells/pathogens and destroy them**
-Helper T cells	**Release cytokines (to attract macrophages)**
-Supressor T cells	**Suppress immune responses**
-NK cells	**Kill virus infected and tumour cells**
-*Plasma cells*	**Produce large quantities of antibodies**
-*Mast cells*	**Degranulate upon activation and release inflammatory mediators**

1.3 Neutrophils

Neutrophils were discovered in 1908 by Elie Metchnikoff (Metchnikoff, 1905) and are small leucocytes (fig 1.1), having an average diameter of around 10μm (micrometres) (Segal, 1996). They can be simply isolated from other white blood cells due to their high density of 1.08-1.09g/ml. The main distinguishing feature of neutrophils is their distinctive morphology: the cytosol of the cell has a large multilobed nucleus, with 3 to 5 lobes (Schmid-Schonbein *et al*., 1980) which occupies more than 20% of the cell size and the rest of the cytosol contains granules. There are three major types of neutrophil granule; primary granules which are also called azurophilic granules; specific or small storage granules; and gelatinase-containing granules. Each population of granules differ in their contents and size. These granules store enzymes, receptors, pre-synthesised inflammatory mediators and other proteins. Neutrophils are not very metabolically active cells and contain only a limited number of mitochondria that account for only 0.2% of the total amount of the cell volume. Additionally, neutrophils have few organelles such as endoplasmic reticulum (ER) or Golgi, which accounts for less than 1% of the cell volume.

Neutrophils are a subtype of leukocytes (Borregaard and Cowland, 1997) which represents the most numerous white blood cells (Ellett *et al*., 2011), which constitute approximately 40–80% of the white blood cell population (Schmid-Schonbein *et al*., 1980), approximately $7x10^9$ neutrophils per litre of blood (Lewis *et al*., 2006). Homeostasis of this cell number is maintained through the continuous release of large numbers of the cells from the bone marrow and extravasation from the blood. The non-activated human neutrophils in

the circulation have a short lifespan of 3-5 days (Roth, 1993). After migration into the tissue, the activated neutrophils survive for only 1-2 days (Schmid-Schonbein *et al*., 1980).

At sites of infection, neutrophils are the first leukocytes to enter an area of inflammation. This is the result of signalling by microbes that have accessed the tissues and also from resident macrophages that activate local endothelial cells lining blood vessels and signal circulating neutrophils to extravasate at that location. Neutrophils are attracted to sites of infection by chemoattractants, such as IL-8, C3a, C5a and leukotriene B4, for which neutrophils have receptors, which both activate chemokinesis and guides the cells by chemotaxis (Schmid-Schonbein *et al*., 1980). Once neutrophils have migrated through the extravascular space to the site of inflammation or infection, neutrophils engage microbes or cell debris and internalise them by phagocytosis (Kobayashi *et al*., 2005). Within the formed phagosome, lytic enzymes are released from their granules and a membrane bound oxidase activated to produce reactive oxygen species (ROS), (Segal and Jones, 1979; Kaplan, 2013), both of which cause killing of the internalised material.

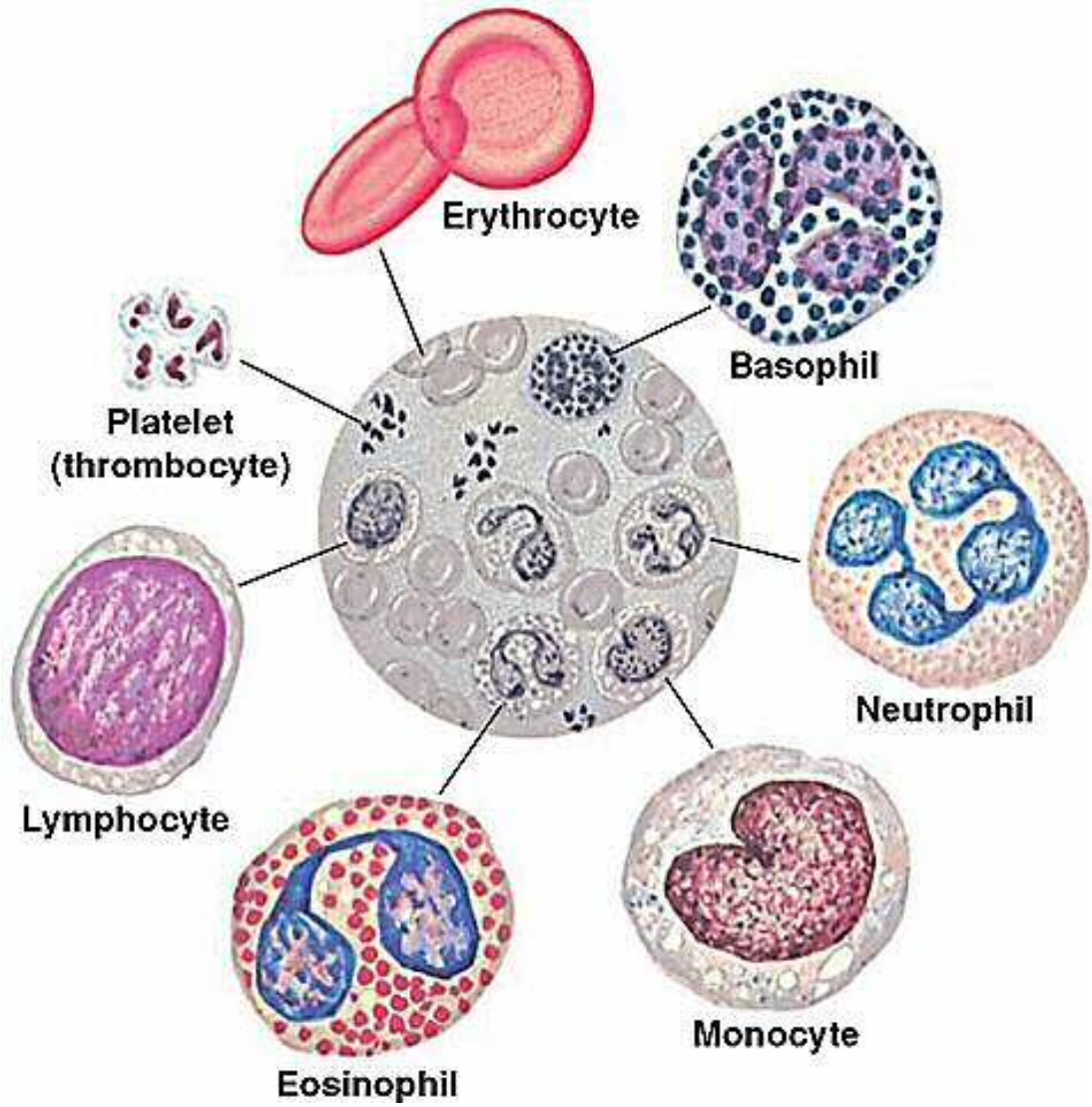

Figure 1.1 Blood cells. Blood cells are divided into three groups; red blood cells (erythrocytes); platelets (thrombocytes) and white blood cells (leukocytes). Leukocytes (neutrophils, eosinophils and basophils) with many nuclear lobes are called polymorphonuclear leukocytes or granulocytes. This figure was adapted from The Hematologic and Lymphatic Systems (http://what-when-how.com/nursing/the-hematologic-and-lymphatic-systems-structure-and-function-nursing-part-1/.)

1.3.1 Production of neutrophils

Neutrophils are produced by the haematopoietic system which is responsible for both neutrophil proliferation and differentiation. Production begins in the early embryo to form blood that comprised of various cell types with 175 billion red cells, 70 billion granulocytes (neutrophils, eosinophils, basophils), macrophages and other white blood cells and 175 billion platelets, that each have specialised functions (fig 1.1). The hematopoietic stem cells (HSCs) are capable of self-renewal and reside in the bone marrow (fig 1.2). However, they can also be isolated from the blood and but may not be active outside the bone marrow, except in umbilical cord vasculature where circulating HSCs spread from the venous system to the bone marrow (Spangrude, 1994). HSCs differentiate to a range of cell types. Many of the blood cells have a brief life and so must be continually produced each day; in humans it is estimated that at least one hundred billion new hematopoietic cells are produced daily. Thus, HSCs in the bone marrow are the only source for the production of all blood cell types, which then become committed to the central marrow cell lines of either erythroid, megakaryocytic, granulocytic, monocytic and lymphocytic lineages (Okuda *et al*., 1992).

Neutrophils derived from HSC in the bone marrow then undergo five stages of differentiation. It is crucial for life that the production of neutrophils is maintained, as they are in the circulation for between 4 and 10 hours only. The stages and differentiation processes which produce neutrophils is known as granulopoiesis. Studies by Chilvers *et al* in (1990) have shown that an adequate balance between granulopoiesis, bone marrow storage and release, intravascular margination, clearance and release is essential for the

maintenance of neutrophil homeostasis. In a normal adult human, $10^{11} – 10^{12}$ new cells are created per day in order to maintain steady state levels in the peripheral circulation. However during infections, this increases to compensate for an increased extravasation of cells. The release of neutrophils from the bone marrow is regulated by granulocyte colony stimulating factor (G-CSF), which is essential for turning on neutrophil production. The large amount of neutrophils in the bone marrow can be separated to three pools. The stem cell pool which contains undifferentiated haematopoietic stem cells (HSCs); the mitotic pool which includes committed granulocytic progenitor cells; and the post-mitotic pool that are maturing neutrophils yet to be released and thus form a bone marrow reserve (Chilvers *et al*., 1990).

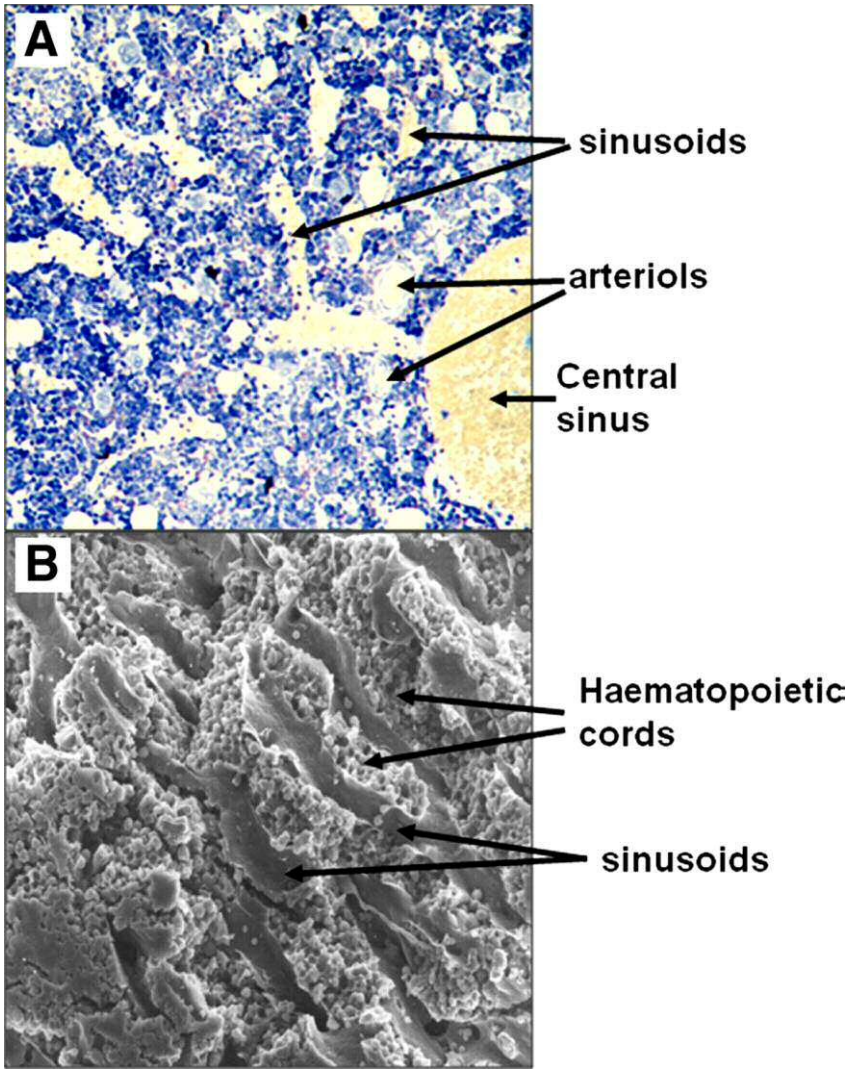

Figure 1.2 Light microscopy and scanning electron microscopy of guinea pig bone marrow. (A) Light microscopy of guinea pig bone marrow. (B) Scanning electron microscopy of guinea pig bone marrow [Taken from (Sara, 2010)].

1.3.2 Myelopoiesis

The combined production of monocytes and granulocytes is referred to as myelopoiesis. This is a regulated process in the bone marrow which begins with pluripotent stem cells which undergo mitotic division to generate two types of stem cells, myeloid or lymphoid stem cells (fig 1.3). The myeloid stem cell lineage is the source of neutrophil production as well as all other granulocytes, monocytes, platelets and erythrocytes. Neutrophils production begins with differentiation of myeloid stem cells, which form the neutrophil progenitor pool (NPP) (fig 1.4). Essentially, the cells form a CFU-GEMM (colony forming unit – granulocyte, erythroid, monocyte and megakaryocyte) which differentiates into the CFU-GM (colony forming unit– granulocyte, macrophage) and into the CFU-G (colony forming unit– granulocyte) (Okuda *et al.*, 1992).

The differentiation of CFU-G cells results in the granulocyte cell type, but individual cells at this stage are not completely committed to a particular granulocyte cell type. Consequently, the mitotic divisions in this step form myeloblastic promyelocytes that are able to divide once or twice to form the neutrophilic myelocytes that, in contrast to the other cells, are capable of up to four further divisions. The formation of these cells is the first step in the commitment to neutrophil differentiation. Within a period of one week, these cells add to the proliferative pool (NPP) and finally lead to mature neutrophils within the neutrophil storage pool (NSP). Mature neutrophils can be distinguished from other granular cells by their three or more segmented nucleus. After neutrophil production, they are no longer capable of cell division and their synthetic machinery becomes practically inactivated

(Okuda *et al.*, 1992). Lastly, mature neutrophils in the bone marrow are more deformable and migrate through the endothelial holes in the bone marrow and into the blood stream.

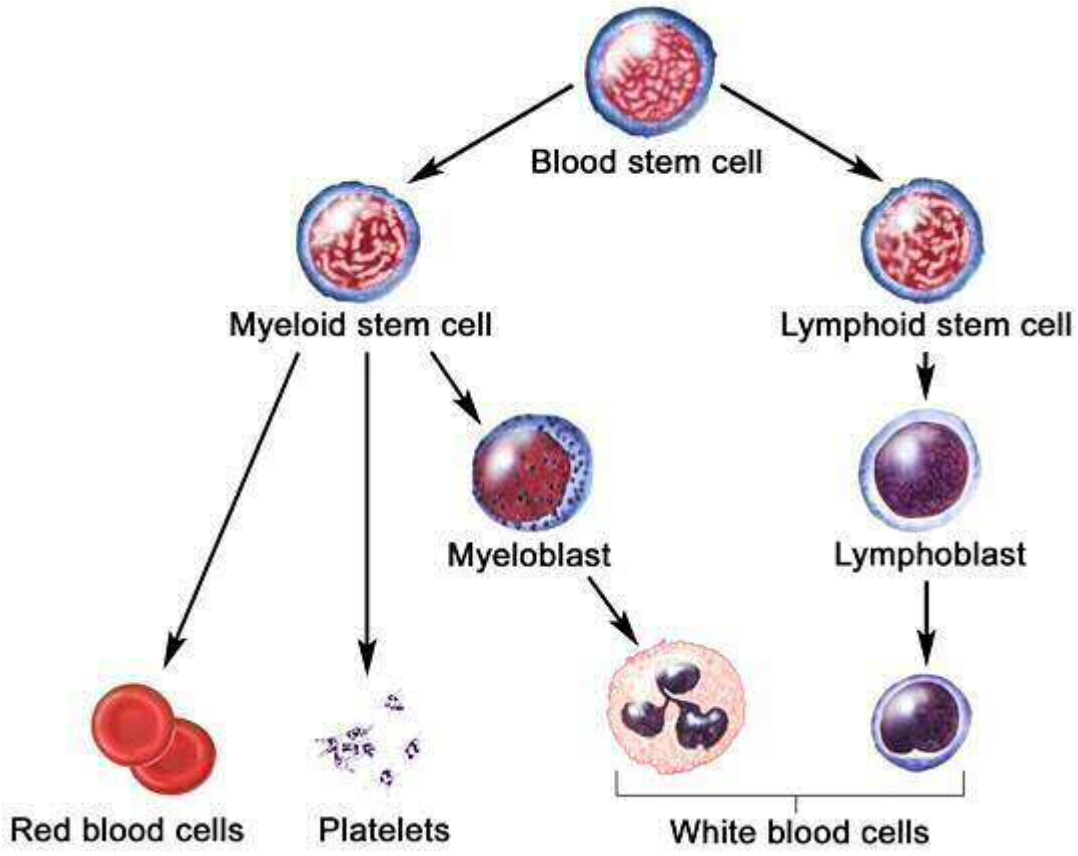

Figure 1.3 Production of blood cells from the pluripotent stem cell. This figure was adapted from National Cancer Institute (www.cancer.gov/about-cancer).

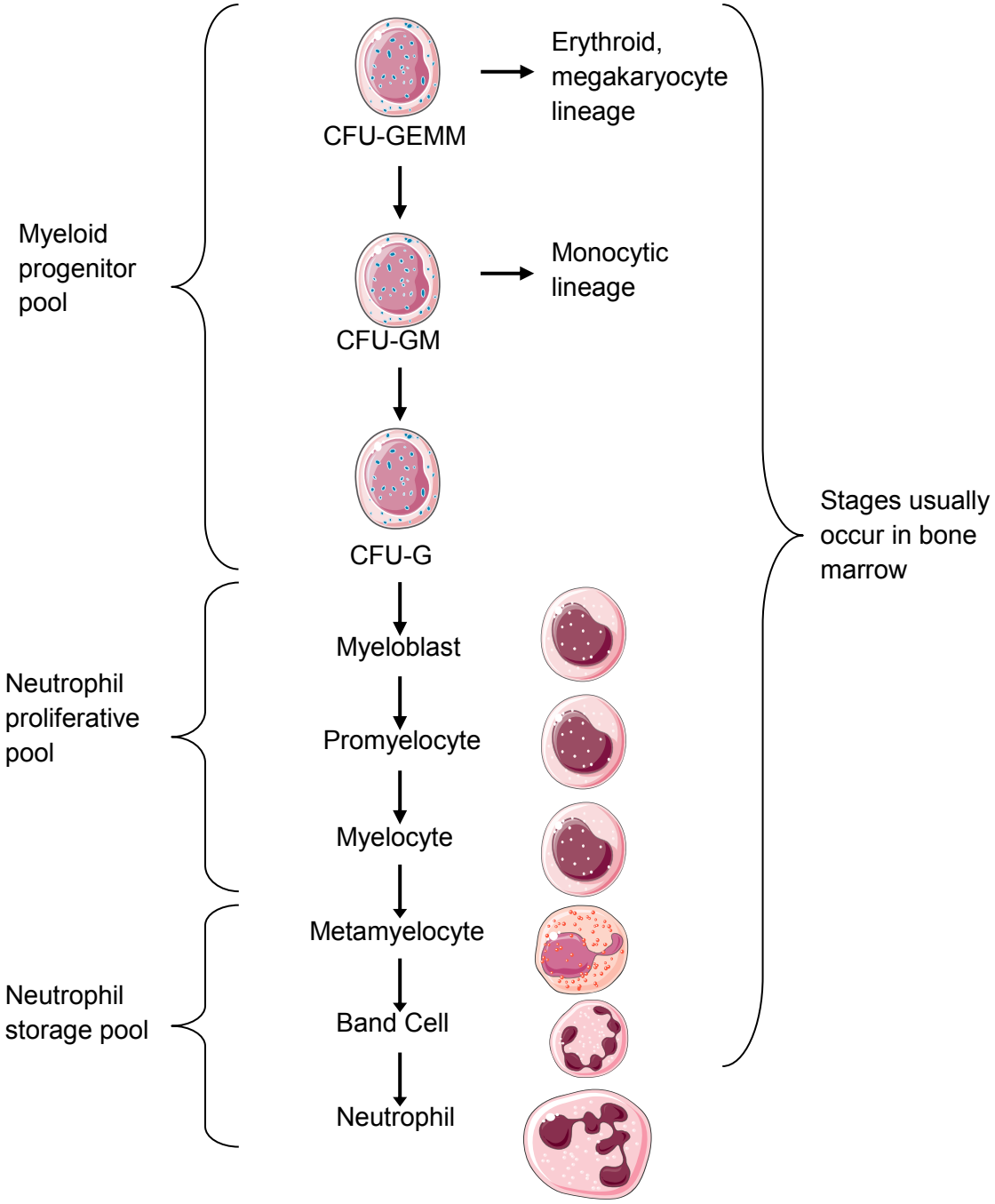

Figure 1.4 Neutrophil production. Figure produced using Servier Medical Art.

1.3.3 Granule formation during cell differentiation

During myeloid cell differentiation, neutrophil granules are developed and formed (selected granule content shown in Table 1.5). Primary granule maturation begins with the division of the promyelocyte. These granules, also known as azurophilic granules due to their staining by azure A, have a large size and have functions similar to the lysosomes of other cells. They fuse with phagocytic vacuoles to form phago-lysosmes. Primary granules are loaded with a wide range of anti-microbial defensins and contain myeloperoxidase, an enzyme that catalyses the formation of hypochlorous acid within the phagosome. Their maturation is fully completed at the myelocyte stage. Additionally, peroxidase negative granules develop which are separated into secondary and tertiary granules. Specific secondary granules are formed in the myelocytes and metamyelocytes steps. These are secretory vesicles that are rich in lactoferrin. However, during the band stage, non-lactoferrin granules are also formed and identified as gelatinase granules. They use the degranulation process to release several enzymes and antimicrobial peptides. Later, another population of secretory vesicles appear, consisting of a fourth category of granules in the last stage of neutrophil development at the band nuclear neutrophil segmentation (Borregaard *et al.,* 1995; Borregaard and Cowland, 1997).

Table 1.5 Content of neutrophils granules (adapted from Borregaard et al., 1996).

Granules	Membrane content	Matrix content
Azurophil(primary) granules	CD63, CD68	Acid β glycerophosphatase, acid mucopolysaccharide, α1-antitrypsin, αmannosidase, azurocidin/ CAP37, heparin binding protein, bactericidal permeability, increasing protein, βglycerophos-phatase,β-glucuronidase, cathepsins, defensins, elastase, lysozyme, myeloperoxidase, N-Acetly- β- glucosaminidase, proteinase-3, sialidase.
Specific(secondary) granules	CD15 antigens, CD66, CD67, cytochrome-b558, FMLP-R, fibronectin-R, G-protein α -subunit, Laminin-R, Mac-1 (CD11b/CD18), NB1 antigen, 19kD-protein, 155kD-protein, Rap1, Rap2, thrombospondin-R, TNF-Receptor, Vitronectin-R	β2-microglobulin, collagenase, gelatinase,histaminases, heparanase, lactoferrin, lysozyme, NGAL, plasminogen activator, sialidase, vitamin B12-binding protein.
Gelatinase (tertiary) granules	Cytochrome b558, Diacylglyverol, deacylating enzyme, fMLP-R, Mac-1(CD11b/CD18	Actytranferase, β2-microglobulin, gelatinase, lysozyme
Secretory vesicles	Alkaline phosphatase, CR1 (CD£%), cytochrome b 558, FMLP-R, MAC1 (CD11b/CD18), uroplasmingoen activator-R, CD10, CD13, CC45, Fcγ RIII(CD16), C1q-receptor, DAF	Plasma proteins including tetranectin

1.3.4 Neutrophil receptors

During differentiation, neutrophils acquire a number of receptors on their surface. These include G coupled receptors (Table 1.6 part 1), cytokine receptors (Table 1.6 part 2), “opsonin” receptors (Table 1.6 part 3), “adhesion” receptors ((Table 1.6 part 4) and pattern recognition/innate immunity receptors (Table 1.6 part 5). The following table (Table 1.6) lists these receptors and their agonists.

Table 1.6 (part1). G-coupled receptors on neutrophils and their agonists

RECEPTOR	AGONISTS	AGONISTS
Formyl-peptide receptors 1. FPR1 (FPR) 2. FPR2 (FPRL1) (lipoxin A_4 receptor) 3. FPR3 (FPRL2)	**Physiological** Bacterial Formyl-peptides	**Experimental** 1. f-met-leu-phe etc : N-terminal peptide Annexin I (Ac 9-25) 2. Peptides WKYMVM; MMK1 3. Peptide WKYMVM
Classical chemoattractant receptors 1. BLT1 (LTB4-receptor) 2. BLT2 (LTB4-receptor) 3. PAFR 4. C5aR	LTB4 LTB4 PAF C5a	2. U75302 (partial agonist) 3. PAF(C-16): Edelfosine
Chemokine receptors • CXCR1 (human) • CXCR2 • CCR1 • CCR2	Interleukin 8 $IL8R_A$ (alpha) $IL8R_B$ (beta) CCL 3; 4 ; 5 ;7 ;8 ;13 ;14 ;15 ;16 ;23 CCL 2	

Table 1.6 (part 2) Cytokine receptors and their agonists

RECEPTOR	AGONIST
Type I cytokine receptors	
• IL-4R	• IL-4
• IL-6R	• IL-6
• IL-12R	• IL-12
• IL-15R	• IL-15
• G-CSFR	• G-CSF
• GM-CSFR	• GM-CSF
Type II cytokine receptors	
• IFNAR (IFNα/β-receptor)	• IFNA (IFNα/β)
• IFNGR	• IFNG
• IL-10R IL-1R family	• IL-10 : IL-1
• IL-1RI	• IL-1
• IL1RII (decoy)	• IL1
• IL-18R TNFR family	• IL-18 : TNF
• TNFR1 (p55)	• TNF
• TNFR2 (p75)	• TNF)
• Fas	• CD95L (Fas ligand)
• LTβR	• LTβ
• TRAIL-R2	• TRAIL
• TRAIL-R3	• TRAIL

Table 1.6 (part 3) "Opsonin" Receptors on Neutrophils and their binding partners or agonists

RECEPTOR	AGONIST/BINDING PARTNER
Complement Receptors CR3 (CD18/CD11b: beta2 integrin; LFA1 etc)	C3bi (iC3b)
Fcγ-receptors • FcγRI • FcγRIIA (human) • FcγRIIIB (human) • FcαRI (human) Fcε-receptors • FcεRI • FcεRII	Antibody (Fc)

Table 1.6 (part 4) "Adhesion" receptors and their binding partners or agonists

RECEPTOR	AGONIST/BINDING PARTNER
Selectins • L-selectin • P-selectin glycoprotein ligand-1 (PSGL-1)	 • On endothelial cells: CD34 GlyCAM-1, MadCAM-1, (PSGL-1, low affinity). • P-selectin
Integrins • Mac-1 (αMβ2; CR3; CD18/CD11b: beta2 integrin etc) • LFA-1 (αLβ2)	•ICAM-1 (on endothelial cells): (C3bi (iC3b) opsonised microbes) •ICAM-1 (on endothelial cells):

Table 1.6 (part 5) Pattern Recognition/Innate Immunity Receptors

RECEPTOR	AGONIST/BINDING PARTNER
Toll-like receptors 1• TLR1 2• TLR2 3• TLR4 4• TLR5 5• TLR6 6• TLR8 7• TLR9	 1• Bacterial lipoprotein 2• zymosan (Beta-glucan): Bacterial peptidoglycans: Others 3• lipopolysaccharide (Gram-negative bacteria): fibrinogen: heparan sulfate: hyaluronic acid: others 4• Bacterial flagellin 5• Mycoplasma lipopeptides 6• Viral RNA (?) 7• Viral DNA (?)
C-type lectins • Dectin-1 • Mincle	β-1,3-linked and β-1,6-linked glucans from fungi glycolipids
Others • NOD2	Bacterial peptidoglycans

1.4 The neutrophil programme

The most important function of neutrophils is the effective killing of infecting microbes. In order to achieve this, neutrophils must first adhere to the endothelium of blood vessels and then leave the blood vessels and migrate to the site of invading microbes. Once the neutrophils have achieved all of these steps, they must recognise, phagocytose and kill the microbes. This can be thought of as “the neutrophil programme” which each individual cell must undertake successfully to provide an effective anti-microbial defence (fig 1.5).

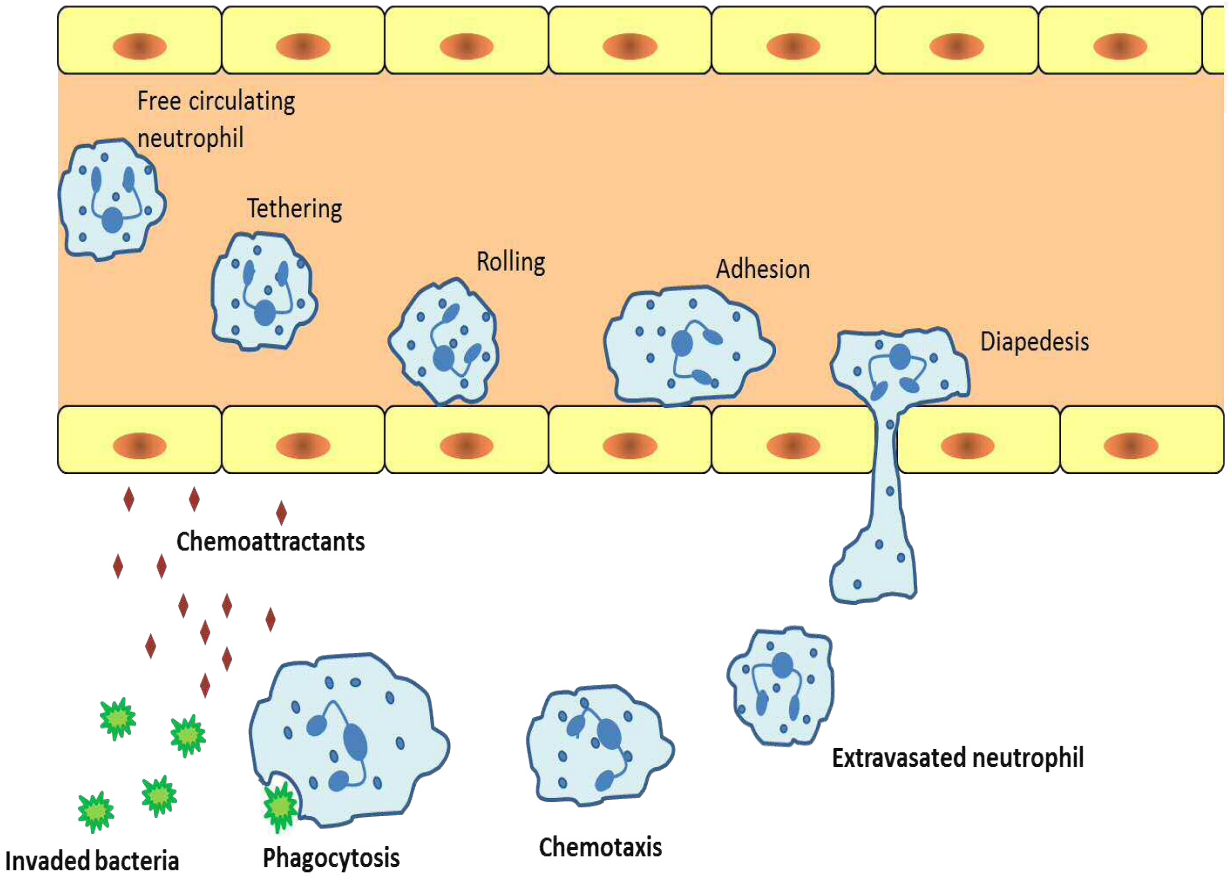

Figure 1.5 The neutrophil programme. Activation of endothelial cells by inflammatory mediators induces the expression of cell surface ICAM1, which binds to integrins on the surface of neutrophils leading to neutrophil extravasation, chemotaxis and then phagocytosis and killing of the microbes (Zarbock and Ley, 2008).

1.4.1 Neutrophil extravasation (diapedesis)

Extravasation means leaving the bloodstream ("vascular" referring to cells in the blood and "extra" meaning outside the vascular system). Neutrophil extravasation includes the following steps: (i) tethering of neutrophils to endothelial cells lining the blood vessels, (ii) rolling of the tethered cells along the endothelial layer, (iii) firm adhesion of neutrophils to the endothelium; flattening of neutrophils and reorganisation of the cell morphology and finally (iv) transmigration across the endothelial layer (fig 1.6). These steps are triggered by specific molecular signals, chemoattractants and other inflammatory mediators released from invading microbes, damaged cells and the cells surrounding them which act to direct the cells to contact the pathogens.

1.4.2 Neutrophil rolling (selectins)

A free circulating neutrophil is captured to the surface of the blood vessel endothelium via selectins which contain lectin domains that bind to carbohydrates. The binding between neutrophils and endothelial cells is mediated by the expression of P-selectin adhesion molecules on the surface of endothelial cells, within minutes of their stimulation by the cytokine TNFα. After 90 minutes, E-selectin which is a second surface adhesion molecule, is also produced. These two selectins are important in directing neutrophils to the site of infections. Other molecules such as IL-1 and LPS component also stimulate E and P-selectin expression (Kolaczkowska and Kubes, 2013). A 1997 study by McEver has showed that the microvilli of neutrophils and other leukocytes is the major site for expression of P selectin glycoprotein ligand 1 (PSGL1), which is a strong binding partner to the P-selectin molecule on

the endothelial cells. Interaction leads to slowing of neutrophils and initiates their rolling along the surface vessel wall in the direction of blood flow. This binding permits the slowed neutrophils to interrogate molecules on the endothelium that leads to them stopping and ultimately moving into the tissues (Kolaczkowska and Kubes, 2013).

Circulating neutrophils express L-selectin, which either tethers an already rolling neutrophil or produces a signalling event which directs neutrophils to adhere to the endothelial cells. L-Selectin is a type 1 transmembrane glycoprotein which mediates the rolling and activation of neutrophils by its binding to sialylated ligands that are expressed on the surface of the endothelial cells (Zarbock and Ley, 2008). Cytoskeletal interactions with L-selectin are essential for the formation of the tether and involve vinculin (Pavalko *et al*., 1995) and the ERM proteins such as ezrin and moesin by binding of its cytoplasmic domain to α-actinin (Ivetic *et al*., 2002). Rolling in such conditions requires the formation of a weak adhesion that permits a rolling motion; brief bonds are formed and broken between selectins and their ligands and results in the activation of β2 integrin (Simon *et al*., 1995).

1.4.3 Adhesion (integrins)

Integrins are heterodimers which represent the key metazoan receptors for cell adhesion that are also essential for the cell-cell contact and for the connections of cell-extracellular matrix (ECM). Integrin receptors are heterodimers which consist of two different chains, α (alpha) and β (beta) subunit. β2 integrins are expressed only on immune cells such as neutrophils and monocytes. Contact between neutrophils and the endothelium

via selectins allows them to roll slowly along the endothelium, sensing signals on the endothelium which enhance the expression of integrins on neutrophils and activate them into a higher affinity state. High levels of integrins are expressed on neutrophils, including LFA1 (αLβ2; β2 integrin, CD11a complexed with CD18) and MAC1 (αMβ2; CD11b/CD18) which both bind the ICAM1 and ICAM2 molecules that are expressed on the surface of the endothelial cells (Zarbock and Ley, 2008). Adhesion of the cells is mediated through the binding of these β2 integrins to the ICAM1 (Lawrence and Springer, 1991). In addition, high affinity binding of LFA1 promotes neutrophil arrest on the endothelium (Ding *et al.,* 1999). Resting neutrophils express Mac1 which are stored in their granules. Upon neutrophil activation, Mac1 is fused into the plasma membrane (Borregaard *et al.,* 1994). After neutrophils adhere to the endothelium as a result of integrin activation, they spread and then extravasate into the nearby tissues (Dunne *et al*., 2002).

1.4.4 Transmigration

Neutrophils have to seek the right place to leave the vasculature by transmigration through the endothelial cells into the surrounding tissue. They migrate through the endothelium which takes around 5 minutes and later penetrate the bottom of the membrane that may take up to 15 minutes (Kolaczkowska and Kubes, 2013). The penetration across the endothelial cell layer may occur by one of two different mechanisms; either between the endothelial cells (paracellular route) or through an endothelial cell itself (transcellular route) (fig 1.6).

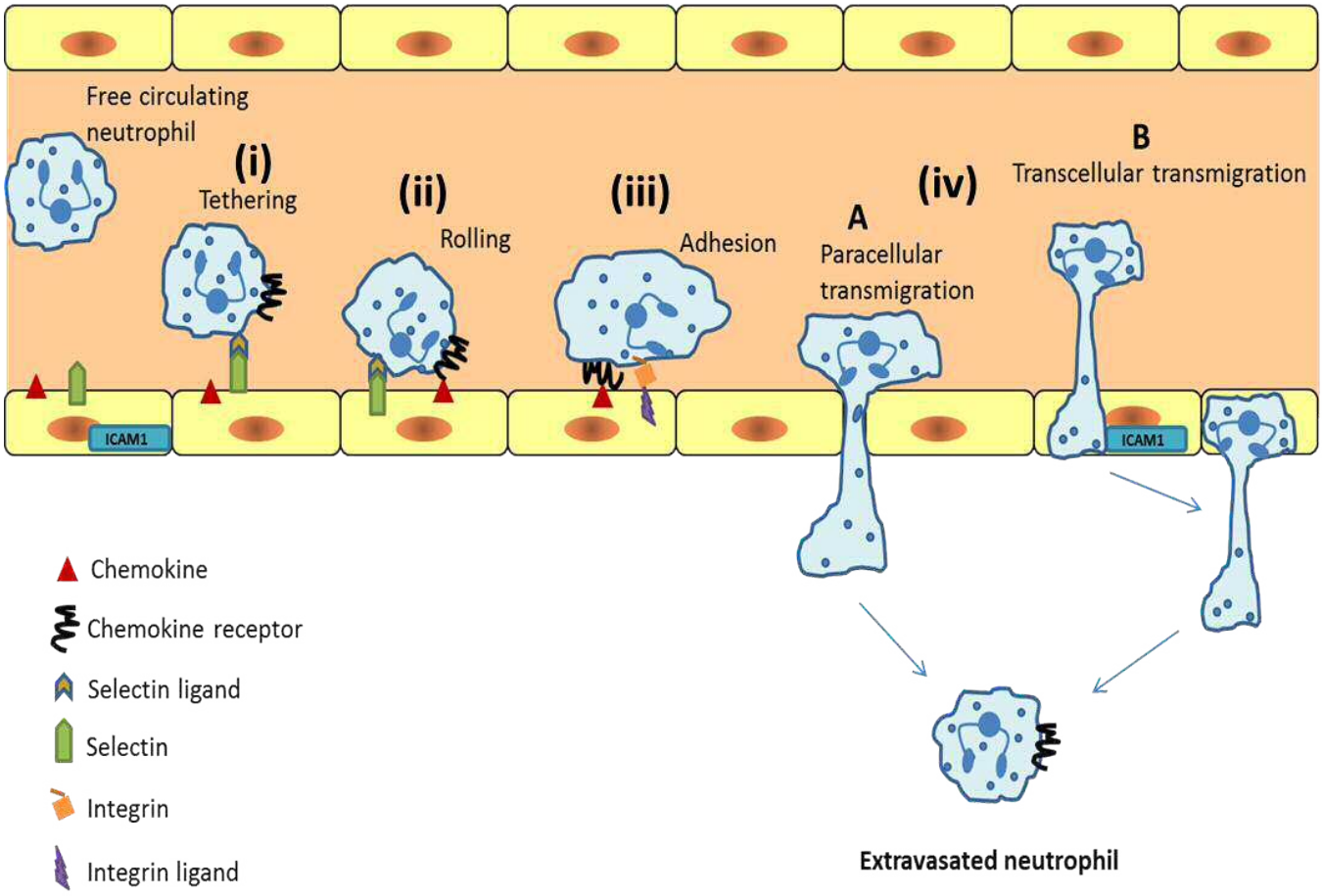

Figure 1.6 Neutrophil extravasation. Neutrophil recruitment to the site of infection follows four steps: tethering, rolling (which is dependent on selectins), adhesion (with integrin interactions) and transmigration. There are two routs of transmigration, ***A****) Paracellular transmigration between the endothelial cells or* ***B****) Transcellular transmigration, passing through an endothelial cell itself.*

1.4.5 Paracellular transmigration

Paracellular transmigration is probably the most common way for neutrophils to travel through the endothelium (fig 1.6 A). This mechanism is used when neutrophils migrate though the junction between the endothelial cells of the blood vessel wall in order to not cause any disturbance to their integrity. This process is controlled by molecules which are expressed on the endothelial cells, such as platelet-endothelial cell adhesion molecule 1 (PECAM1), also known as CD31 (Kolaczkowska and Kubes, 2013). It is a member of the immunoglobulin that is also expressed on leukocytes and platelets (Garrido-Urbani *et al*., 2008). In vivo, this molecule has a role in the extravasation of neutrophils which can be demonstrated by blocking with PECAM1 antibody in the inflamed peritoneal cavity of mice (Bogen *et al*., 1994). Although, PECAM1 is not completely necessary for the neutrophil transmigration, it might be involved by playing two different roles which help to arrest neutrophils before the cells pass through the basement membrane and also after passing through the cell junctions (Nakada *et al*., 2000, Wakelin *et al*., 1996).

Paracellular transmigration demands the release of junction intercellular proteins such as vascular endothelial cadherin (VE-cadherin) from the plasma membrane of endothelial cells within the adherent junction (Garrido-Urbani *et al.*, 2008). Although lost during neutrophil transmigration, cadherin is replaced once the neutrophil has migrated through the endothelial cell layer (Shaw *et al*., 2001). A 1997 study by Gotsch *et al* has shown that in vivo, the entry of neutrophils into inflamed peritoneum in mice is caused by antibody mediated inhibition of VE- cadherin. This suggests that there is a significant effect of VE-cadherin during neutrophil extravasation by its ability to control the opening of the

endothelial barrier that is necessary for the cells transmigration (Gotsch *et al*., 1997). Also, it has suggested that neutrophil transmigration can be decreased by the inhibition of VE-cadherin that has been phosphorylated through the engagement of ICAM1 (Allingham *et al*., 2007).

Other molecules required during cell transmigration are known as junctional adhesion molecules (JAMs). JAMs comprise three classical members JAM A, JAM B and JAM C. JAM A and JAM B are both expressed on the endothelial cells whereas JAM C is expressed at the intercellular junctions of high endothelial venules (Aurrand-Lions *et al*., 2005).

1.4.6 Transcellular transmigration

Transcellular transmigration is when the neutrophil passes through the endothelial cell itself. A possible explanation of the way transcellular transmigration may occur is shown in the diagram (fig 1.6 (B)). A study by Feng *et al* in (1998) provided evidence for transcellular transmigration using electron microscopy studies, which showed that the stimulation of neutrophils with fMLP component led to the transmigration of the neutrophil through endothelial cell itself (Feng *et al*., 1998) and this involved ICAM1 clustering on the endothelial cell. This is an important step by which the ICAM1 is translocated to caveolin rich domains in the plasma membrane. Neutrophil migration depends on the availability of a route that the cells can follow. The generation of the route can be seen through the internalisation of the ICAM1 that can then be trancytosed to the basal plasma membrane of the endothelial cells over the caveolae (Millan *et al*., 2006). Although there is some

experimental evidence for neutrophil transmigration by either ways, the mechanisms by which these occur are still not completely understood.

1.4.7 Neutrophil apoptosis

Neutrophils are short-lived cells which leave the blood stream to enter the tissues and sites of potential infection; in humans mainly to the lungs and the gut. They leave the body by these routes to be replaced by new circulating neutrophils from the bone marrow (see section 1.3.1). However, neutrophils also leave the blood stream to sites of localised infection, or inflammation, such as cysts or, in inflammatory joint disease, to the joint fluid. Under these conditions, neutrophils cannot exit the body directly and will die at these localised sites. In order to prevent the release of proteolytic enzymes from necrotic cells which lyse, neutrophils undergo spontaneous apoptosis (Haslett, 1997). The process of apoptosis, also known as a programmed form of cell death, maintains the integrity of the plasma membrane during cell death. Thus, apoptosis of neutrophils prevents the uncontrolled release of potentially tissue-damaging enzymes which would exacerbate the inflammation and cause accumulating damage to the extracellular matrix at the site of localised infection. It has been reported that the prevention of neutrophil apoptosis will lead to necrosis of the cells, with the release of their cellular contents resulting in tissue damage and autoimmune diseases (Cheah *et al.,* 2005). Apoptotic neutrophils are no longer capable of chemotaxis, phagocytosis, respiratory burst and degranulation (Whyte *et al.,* 1993). This is important, as the apoptotic cells are removed, along with anything they have previously phagocytosed, by phagocytosis into macrophages. It is also important in the production of anti-inflammatory mediators that prevent the inflammation continuing (Erwig *et al.,* 2007). Neutrophil apoptosis involves characteristic changes involving internucleosomal DNA

fragmentation and shut down of cellular processes which results in a decrease in cell volume, mitochondrial depolarization, nuclear condensation, cellular crenation and vacuolated cytoplasm (Savill *et al*., 1989; Kamada *et al*., 2005).

Neutrophils undergo constitutive apoptosis via two classical cellular apoptotic pathways. The extrinsic pathway, which requires an extracellular signal that activates the tumour necrosis factor-alpha (TNF-α) receptors or Fas on the plasma membrane, will lead to activation of a cascade of enzymatic activity, which includes proteases such as initiator caspases (caspase-8). A second route is the intrinsic pathway which may also be triggered by an intracellular signal such as irreparable damage to DNA or severe metabolic cell stress. Due to damage, the balance of the B cell lymphoma (Bcl)-2 family of proteins is altered which causes mitochondrial permeabilization. This leads to the release of cytochrome *c* into the cytosol and also stimulation of the apoptosome and initiator caspase-9. Caspase-8 is also important by activating the pro-apoptotic Bcl-2 homology-3-interacting domain death agonist protein (Bid). DNA fragmentation is caused by endonucleases and the entry of caspase-3, -6 and -7, into the nucleus. There is a common last step to both pathways. There are characteristic changes in nuclear morphology which involve karyorrhexis and pyknosis (Savill *et al*., 1989; Kamada *et al*., 2005).

Clearance of the apoptotic inflammatory neutrophils from sites of inflammation or infection is determined by changes to the cell surface such as externalization of phosphatidylserine (PS) that allow phagocytes, such as resident macrophages in the spleen,

liver and bone marrow, to recognise the apoptotic cells and remove them from the circulation or tissue via phagocytosis. Apoptotic neutrophils are then identified and phagocytosed by macrophages through release of their histotoxic components (Savill *et al.*, 1989). During the course of phagocytosis, the tethering of non-inflamed apoptotic cells to macrophages is essential via a surface molecule CD14, usually including bacterial lipopolysaccharide (LPS), that has an effect on neutrophil survival in addition to the activation of TLR4 (Devitt and Marshall 2011). However the apoptotic neutrophil has excellent LPS-binding capacity, thereby decreasing the LPS stimulation of viable, responding cells (Sarah *et al.,* 2010). Stimulation of macrophages by exposure to externalised PS does not only trigger phagocytosis via their receptors but also stimulates the production of some cytokines such as IL-10 and TGF-β in high amounts, which contribute to the resolution of the inflammatory response and also supports the healing tissue (Miller *et al.,* 2006; Scannell *et al.,* 2007). It is thought that neutrophil apoptosis is also influenced by the production of ROS, which can delay apoptosis via interference with the actions of caspases or else cause necrosis of the neutrophil by direct toxicity before they can undergo apoptotisis (Fadeel *et al*., 1998, Geering and Simon, 2011; Scheel-Toellner *et al*., 2004). Apoptosis can also be delayed by microbial components and by pro-inflammatory stimuli in damaging tissues.

Briefly, neutrophil apoptosis probably involves different pathways to the classically defined pathways of apoptosis in other cell types and is not yet completely understood (Tak *et al.,* 2013).

1.4.8 The oxidative killing mechanism in neutrophils.

The generation of reactive oxygen species (ROS) by neutrophils is a non-mitochondrial process, often referred to as the respiratory burst. It is crucial for the destruction of particles and microorganisms within the neutrophil phagosome. It may also be important as a signalling molecule or a mediator of inflammation, for example by causing endothelial dysfunction by oxidation of essential cellular signalling proteins such as tyrosine phosphatases (Manish *et al.,* 2014). ROS are produced when the nicotinamide adenine dinucleotide phosphate (NADPH) oxidase is activated to generate superoxide by one electron reduction of oxygen (fig 1.7). The NADPH oxidase is found in a range of cells such as the professional phagocytes and endothelial cells. In resting neutrophils, there are four cytosolic subunits of the oxidase; p47-^{phox}, p40-^{phox}, p67-^{phox} and Rac. When p47-^{phox} is phosphorylated by activated protein kinase C (PKC), a complex forms which combines with cytochrome b_{558} (comprised of gp91^{phox} and p22^{phox}) in the phagosomal membrane (Manish *et al.,* 2014). The vectorial arrangement across the phagosomal membrane of the assembled and active oxidase results in the release of superoxide into the phagosome, where it dismutates to form peroxide (H_2O_2), the substrate for the major intraphagosomal enzyme myeloperoxidase (MPO). MPO is abundantly expressed in neutrophils and catalyses the conversion of H_2O_2 to highly reactive hypochlorous acid (HOCl). HOCl chlorinate numerous bacterial proteins to bring about bacterial death (Manish *et al.,* 2014).

Also, in the presence of Fe^{2+}, the Fenton's reaction generates the highly toxic hydroxyl radical ($OH^{\bullet}$) which rapidly destroys the 3D structures of biological molecules, especially proteins within the phagosome. The lifetimes of superoxide and especially hydroxyl radicals

are extremely short so that diffusion from the source of generation cannot be more than a fraction of a micron. H_2O_2 is longer lived (semi-stable) and may leak from the phagosome. However, antioxidant enzymes in the cytosol, such as catalase, glutathione peroxidase (GPX), or peroxiredoxins (Prx) e.g. thioredoxin (Trx), "scavenge" H_2O_2 by its conversion to O_2 (fig 1.7) (Manish *et al.,* 2014). The NADPH oxidase in the phagosome membrane also provides superoxide for a reaction with nitric oxide (NO) at a diffusion limited rate ($k=5\text{-}10x10^9 M^{-1}s^{-1}$), following the formation of highly reactive nitrogen species (RNS), such as peroxynitrite ($ONOO^-$). It is three to four times faster than the dismutation of superoxide anion (O_2^-) which has been suggested to show an important effect in antimicrobial defence. The RNS, in turn, induces nitrosative stress, which adds to the proinflammatory burden of ROS. Likewise, because of the negative charge on superoxide O_2^-, its passage through biological membranes is regulated by voltage-dependent anion channels (VDAC) (Manish *et al.,* 2014).

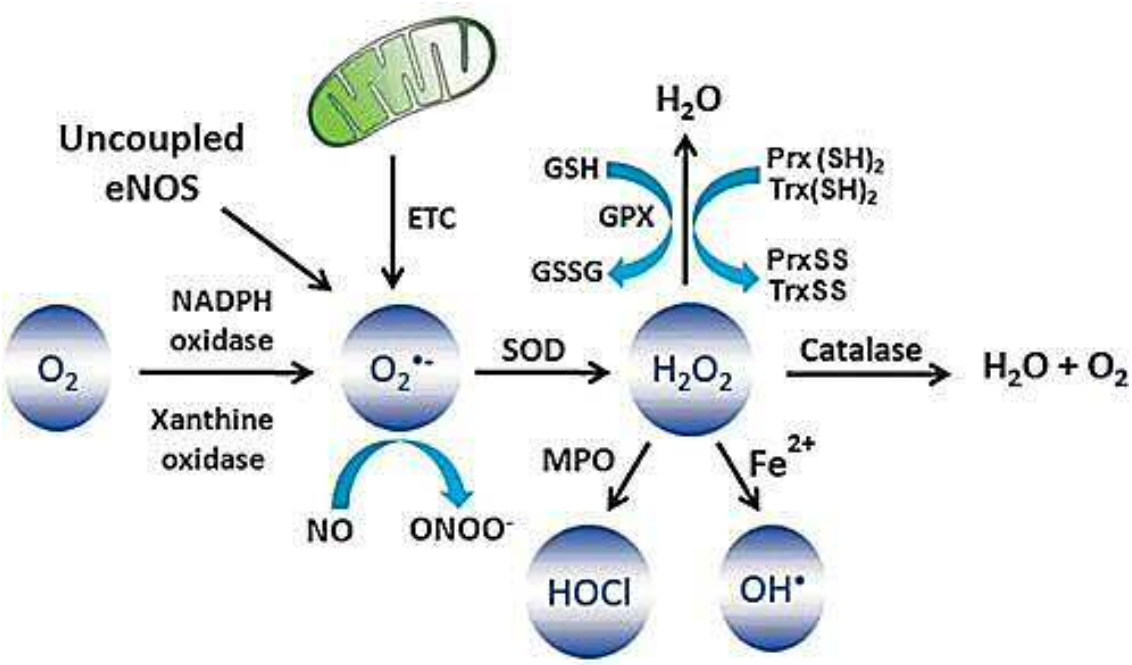

Figure 1.7 Routes to the generation of reactive oxygen species. The diagram shows the conversion of molecular oxygen (O_2) to superoxide ($O_2^{\cdot-}$); its conversion to hydrogen peroxide (H_2O_2) by superoxide dismutase (SOD); conversion to hypochlorite (OCl^- /HOCl) by myeloperoxidase (MPO). The Haber-Weiss reaction is shown below the main diagram together with antioxidants steps. (Taken from Manish et al., 2014).

1.5 Calcium signalling in neutrophils

1.5.1 Ca^{2+} Signalling

Cytosolic free Ca^{2+} ions control a number of different cellular processes in a wide variety of cell types, including exocytosis, muscle contraction, gene transcription, proliferation and cell death. Although in biological systems, the concentrations of many ions are controlled, the Ca^{2+} ion is probably the most tightly regulated. It is important for life to keep the cytosolic Ca^{2+} ion concentration low in order to prevent precipitation by forming insoluble calcium salts with phosphates, sulphate and carbonate. Of course, the major insoluble extracellular component of bone, calcium phosphate, is produced as a result of the higher extracellular concentrations of Ca^{2+}. As the extracellular Ca^{2+} concentration is normally high (around 1 - 5mM), eukaryotic cells require an energy-depended mechanism to achieve low concentration of free Ca^{2+} inside the cell. The cytosolic level of Ca^{2+} is maintained at around 100nM, by homeostatic systems which pump Ca^{2+} out of the cell to balance the inward leak of Ca^{2+}. This makes a considerable concentration gradient across the plasma membrane. Once significant additional amounts of Ca^{2+} enter the cytosol, the free Ca^{2+} concentration would considerably change, especially close to the channel gate that facilitated the entry. The generation of calcium signals inside a cell occurs as a result of two interdependent mechanisms; (i) by releasing Ca^{2+} from intracellular Ca^{2+} stores and (ii) by Ca^{2+} influx from the extracellular medium. There are three types of intracellular Ca^{2+} stores with inward facing Ca^{2+} pumps, sarco/endoplasmic reticulum (S/ER), membrane bound vesicles and possibly mitochondria. The SERCa pumps pass Ca^{2+} from the cytosol into the luminal space of the S/ER and also control channels which facilitate the release of Ca^{2+} once stimulation has occurred.

1.5.2 General Signalling System

Although individual cell types utilise Ca^{2+} signalling for different outcomes, they all use the same "toolkit" of mechanisms. Thus the general structure of any Ca^{2+} signalling pathway follows the same method. It begins when a receptor is occupied by its agonist and signals a pathway which usually includes a cascade leading to activation of enzymes (fig 1.8). Depending on which proteins are expressed in the particular cell type, the Ca^{2+} signal can thus generate outcomes that differ widely from cell-type to cell-type.

As with a number of cell types, the "Ca^{2+} cascade" begins with activation of phospholipase C (either β or γ) which cleaves phosphatidylinositol 4,5-bisphosphate (PtdIns(4,5)P_2, PI(4,5)P_2, or PIP_2) in the inner leaflet of the plasma membrane to liberate the head group as inositol 1,4,5-trisphosphate *($InsP_3$;* IP_3) to diffuse into the cytosol and leave diacylglyercol (DAG) in the plasma membrane (fig 1.8). Both products act together to activate DAG /Ca^{2+} dependent isoforms of protein kinase C (PKC). DAG acts directly by binding to PKC, whereas IP_3 acts indirectly by triggering the Ca^{2+} response (see section 1.5.3 and fig 1.9). In neutrophils, one of the important functions of PKC is the phosphorylation of $p47^{phox}$ to form an activate NADPH oxidase in the phagosomal membrane. Since the phagocytic stimulus is localised to the contact site between the particle and the neutrophil surface, DAG generated locally would be diluted by diffusion in the membrane. However, once a phagosome had closed, no such dilution would be possible and DAG concentration in the phagosomal membrane may rise to activate PKC locally and so activate the NADPH oxidase locally. Since it has been postulated that locally high Ca^{2+} driven by Ca^{2+} influx activates calpain to allow pseudopodia formation (see section 1.6), the outcome of PLC

activation would provide both localised psuedopodia formation and following this localised oxidase activation.

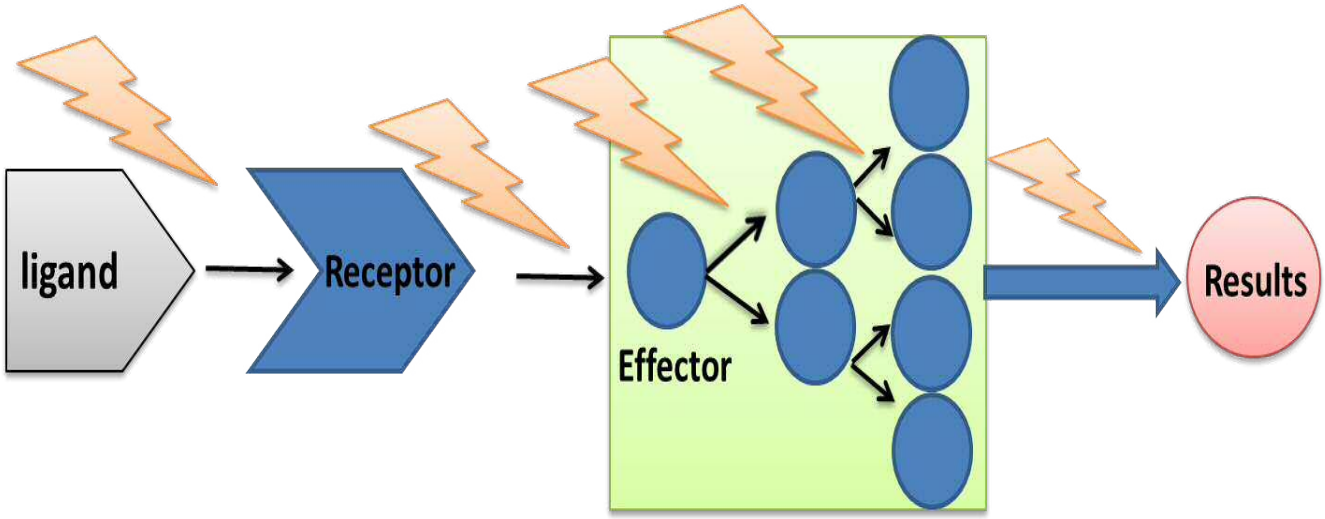

Figure 1.8 General signalling systems. From occupation of the receptor to the cell response (indicated as results) as series of step, including amplication cascades occur. The lightning bolts at each step of the pathway are control points at which cross-talk can occur with other pathways.

1.5.3 Calcium signalling in neutrophils

1.5.3.1 Cytosolic free calcium homeostasis

The level of cytosolic free Ca^{2+} is essential for the regulation of most neutrophil functions including phagocytosis, cell spreading and possibly chemotaxis. In neutrophils, similarly to all mammalian cells, the concentration of cytosolic free Ca^{2+} is regulated at different states of the neutrophil, i.e. resting and activated. In the resting neutrophil, the cytosolic free Ca^{2+} concentration is kept at approximately 100nM. However, with an extracellular calcium concentration of 1mM, the Ca^{2+} concentration across the neutrophil plasma membrane is 10,000:1. The maintenance of this gradient arising from the low permeability to Ca^{2+} of the plasma membrane of resting neutrophils and the pumping out of Ca^{2+} ions back across the plasma membrane. Fluctuations of concentration in cytosolic free Ca^{2+} are also reduced due to the high Ca^{2+} buffering capacity of the proteins within the neutrophil cytosol. The Ca^{2+} storage organelles in neutrophils also contribute to Ca^{2+} buffering at locations where the intracellular Ca^{2+} is actively sequestered. The effect of Ca^{2+} releasing from stores, as well as from channel opening at the plasma membrane, causes the global intracellular Ca^{2+} concentration to rise to about 1μM (Demaurex *et al*., 1992). However more recently, it has been shown that in microdomains such as the cytosol within membrane wrinkles of activated neutrophil, the Ca^{2+} concentrations may reach in excess of 30μM (Brasen *et al*., 2010).

1.5.3.2 The storage of calcium in neutrophil

Neutrophils are able to buffer Ca^{2+} via their various intracellular Ca^{2+} stores. Thus, in the cytoplasm, the concentration of Ca^{2+} sequestered within intracellular Ca^{2+} stores is high in resting cells. However, the store Ca^{2+} concentration is lowered significantly when it is released into the cytosol. There are intracellular Ca^{2+} stores near the plasma membrane sites that can produce Ca^{2+} during CD11b/CD18 crosslinking and also at a juxta nuclear site, possible vestigial ER or golgi (Davies *et al*., 1991), which can release Ca^{2+} in response to fMLP stimulation (Pettit and Hallett, 1998b). It has been reported that 'calciosomes' are an additional IP_3 sensitive calcium storage site in neutrophils. When the neutrophil undergoes phagocytosis, it has been shown that these intracellular calcium stores redistribute around the phagosome (Favre *et al*., 1996; Stendahl *et al*., 1994). Ca^{2+} can be pumped into these IP_3 sensitive calcium storage sites via SERCA2b calcium ATPase pumps, which have been identified within all of these stores. Pumping of Ca^{2+} into the stores can be prevented by various inhibitors, such as thapsigargin and cyclopiazonic acid (Favre *et al.,* 1996).

1.5.3.3 Cytosolic free Ca^{2+} signalling in neutrophils

In neutrophils, there are a vast number of receptors (see Table 1.6). Ca^{2+} signals are caused by the seven transmembrane spanning domain receptors (7TM) and by "cross-linking" stimuli such the opsonic receptors. Both are able to trigger the release of Ca^{2+} from intracellular calcium stores and open plasma membrane channels which permit Ca^{2+} influx. IP_3 is generated by the action of phospholipase C on PIP_2 and diffuses through the cytosol to trigger the release of Ca^{2+} from Ca^{2+} stores, which in turn prompts Ca^{2+} influx. Most of the

neutrophil effector functions rely on Ca^{2+} influx. It is essential for activation of all their responses, because the simple removal of extracellular Ca^{2+} is able to inhibit the neutrophil response. The intracellular Ca^{2+} stores which release calcium are also able to produce Ca^{2+}, which may play an important role for local activation. This liberating of Ca^{2+} from stores is thus crucial for the Ca^{2+} signalling (Hallett & Campbell, 1984).

When stimulated, the cytosolic Ca^{2+} concentration rises rapidly in the neutrophil. In the absence of extracellular Ca^{2+}, the Ca^{2+} signal is severely attenuated, showing that Ca^{2+} influx phase is the dominant phase. However, activation of neutrophils by both receptor classes gives different relative contributions of Ca^{2+} influx and Ca^{2+} store release. Although they are strongly coupled in the case of the (7TM) receptors, they are not so with the cross-linking stimuli. However, neutrophil responses rely mainly on the Ca^{2+} influx phase.

1.5.3.4 Cytosolic free Ca^{2+} signalling by seven transmembrane receptors (G protein coupled receptors)

Activation of 7TM receptors on neutrophils causes Ca^{2+} signalling that includes the release of calcium from intracellular Ca^{2+} stores at a juxta nuclear location (Davies *et al.*, 1991) and this triggers the opening of channels at the plasma membrane which allow an influx of calcium across the plasma membrane (Pettit and Hallett, 1995). Upon the activation of the 7TM receptors, a G protein is activated at the inner surface of the plasma membrane which activates phospholipase C-β(PLCβ) (Cockcroft and Gomperts, 1985). Activation of PLCβ causes PIP_2 in the membrane to be cleaved to generate IP_3, which releases calcium from IP_3

sensitive calcium stores. This may stimulate the opening of TRPM2 channels in the plasma membrane (Du *et al*., 2009) and so cause Ca^{2+} influx stage (fig 1.9). Diffusion of signalling molecules from the plasma membrane to intracellular calcium stores requires a measureable period of time (Hallett and Lloyds, 1995), which can cause a short but measureable delay between 7TM receptor activation and the global rise in cytosolic calcium (Hallett *et al*., 1990).

1.5.3.5 Cytosolic free Ca^{2+} signalling by cross-linking of stimuli (Integrin engagement)

Another way to generate the signalling of cytosolic free Ca^{2+} in neutrophil is by cross-linking of IgG receptors such as Fc (CD16/CD32) receptors (Roberts *et al*., 1997) or else by integrin such as CD11b/CD18 receptors. The mechanism for the generation of this cytosolic free Ca^{2+} signalling by cross-linking of stimuli is yet to be fully determined (Morgan *et al*., 1993). However, it shares features with the mechanism involved with 7TM receptors activation (Hellberg *et al*., 1996). The Ca^{2+} signal that is caused by the cross-linking stimuli originates from intracellular Ca^{2+} stores (Davies and Hallett, 1995). This release of Ca^{2+} from stores may not be enough to cause Ca^{2+} influx activation (Pettit and Hallett, 1997). There may also be a difference between the site of the Ca^{2+} store release between the cross linking and the 7TM receptors; the stores being peripheral with cross linking receptor (Pettit and Hallett, 1996) rather than central with 7TM (Davies and Hallett, 1995). There is evidence from electron microscope studies which supports the presence of motile Ca^{2+} storage sites close to the plasma membrane. It has been shown that Ca^{2+} storage sites are located near the plasma membrane (Hoffstein, 1979). It has been suggested that the delay which occurs between receptor ligation and the calcium signal is connected to the period of time that is

required by the receptors to diffuse in the plasma membrane to form sufficiently large cross-linked aggregates to generate the Ca^{2+} signal (Roberts *et al*., 1997).

Some inhibitors of tyrosine kinases (Morgan *et al*., 1993) and the actin bundling protein, L-plastin (Rosales *et al*., 1994) are able to stop this Ca^{2+} signal suggesting that the signal from the plasma membrane is transduced by the tyrosine phosphorylation and the actin cytoskeleton. It has been proposed that Ca^{2+} signalling by cross linking of stimuli and 7TM receptors have similarities and that integrin engagement activates tyrosine kinase dependent Ca^{2+} mobilisation, via PLCγ2 phosphorylation and a rise in IP3 (Hellberg *et al*., 1996). A potential mechanism is shown in (fig 1.9).

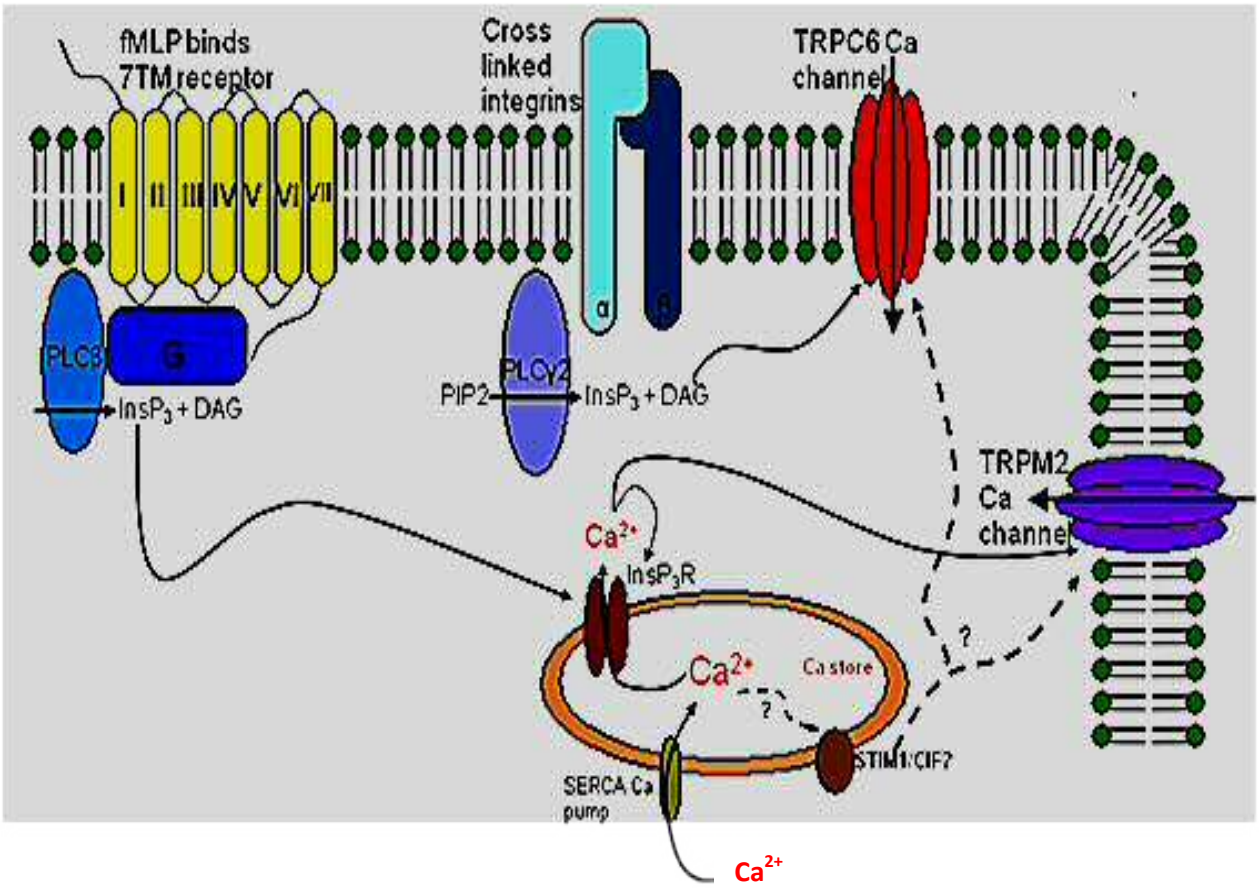

Figure 1.9 Schematic graphic for Ca^{2+} signalling in the neutrophil. The release of calcium into the cytosol is followed by the activation of a 7TM receptor by a chemoattractant such as fMLP. The ligated receptor activates a G protein that is able to stimulate PLCβ which converts PIP_2 into IP_3 and DAG. IP_3 is capable of activating IP_3 receptors on the Ca^{2+} stores and so release Ca^{2+}into the cytosol. The calcium released from Ca^{2+} stores could also be stimulated by cross linking of integrins through phosphorylation and activation of PLCγ2 in the neutrophil plasma membrane which causes the release of IP_3 and DAG which triggers the release of calcium from Ca^{2+} stores. Channels in the plasma membrane prompt calcium influx into the cytosol. This figure shows a possible mechanism that might occur, but the real mechanism of calcium influx from channels in the plasma membrane of neutrophil is still not identified. DAG actives calcium channels, calcium influx factor (CIF) is the calcium channels activation through liberating of calcium from stores or a diffusible second messenger.

1.5.3.6 Calcium influx in neutrophils

Upon the liberation of Ca^{2+} from intracellular stores in neutrophils, as a result of either 7TM receptors or cross-linking of stimuli, there will be Ca^{2+} influx through channels in the plasma membrane. However, the mechanism for Ca^{2+} influx is still not completely understood. Inhibition of many neutrophil responses can be realised by discontinuing Ca^{2+} influx (Hallett and Campbell, 1984, Marks and Maxfield, 1990). It is clear that when the Ca^{2+} stores are no longer able to release Ca^{2+}, Ca^{2+} influx occurs in order to refill the Ca^{2+} stores (Smyth *et al*., 2006). For example, inhibition of the SERCA pumps using thapsigargin or cyclopiazonic acid, empties the Ca^{2+} stores and results in the opening of Ca^{2+} channels in plasma membrane. Ca^{2+} influx is triggered by diffusion of small molecules and results in a delay of tens of milliseconds between the addition of the stimulus to neutrophil and the global Ca^{2+} influx. Micro-injection of the IP_3-receptor blocker heparin has the ability to block Ca^{2+} influx from channels in plasma membrane when triggered by the 7TM receptor agonist fMLP (Davies-Cox *et al*., 2001). However, Ca^{2+} influx cannot be prevented when triggered by IgG immune complexes, suggesting an IP_3-independent mechanism may also occur in neutrophils (Davies and Hallett, 1995). In addition, C5a stimulation of anucleated neutrophil cytoplasts fails to trigger calcium signal generation pointing to the importance of the juxtanuclear calcium store (Gennaro *et al*., 1984).

There is also a difference in the time delay of the Ca^{2+} signal triggered by the two distinct mechanisms. Stimulation of neutrophils with fMLP releasing Ca^{2+} from intracellular stores results in a total delay of around 500ms before Ca^{2+} influx (Pettit and Hallett, 1995). In contrast, cross-linking of integrin on the plasma membrane requires between 10s and

100s before opening of Ca^{2+} channels occurs (Pettit and Hallett, 1996). The delay difference cannot be explained by the two different intracellular Ca^{2+} stores, each coupled to the two distinct receptor types and is more likely to result from the time required to form receptors clusters. It has recently been shown that within the plasma membrane, TRPM2 channels are opened directly as a result of a rise in cytosolic calcium, leading to Ca^{2+} influx following their activation by IP_3 receptors. This gives an indication that Ca^{2+} signalling in neutrophils that occurs via 7TM receptors leads to the release of calcium from IP_3 sensitive juxtanuclear calcium store that is necessary following the generation of the calcium influx (Du *et al*., 2009).

1.6 Neutrophils and cell surface topography

Phagocytosis is a complex event and changes in both the biochemistry and structure of neutrophils occur to facilitate the process. This may include dynamic changes at the level of the cell surface membrane, which apparently expands significantly by extension of pseudopods leading to engulfment of the foreign body. These changes may also be seen during the process of extravasation when the cells undergo chemotaxis and spreading, stages which represent movement of the neutrophil following activation on the endothelium, when an apparent increase in the cell membrane surface area of neutrophils has been attributed to 'flattening' of wrinkles (Dewitt & Hallett, 2007). There are a few other theories which have been proposed to explain the phenomenon of the membrane expansion in neutrophils (fig 1.10).

It has been shown that during the formation of phagosomes in macrophages, the membrane of endoplasmic reticulum (ER) fuses with the cell surface membrane (Gagnon *et al*., 2002). This may provide the additional membrane for phagocytosis in these cells. It has been found that there was only a residual amount of the ER in neutrophils and that is deeply embedded within the cell. It is thus unlikely that this mechanism for providing additional membrane during phagocytosis could occur in neutrophils (Bessis, 1973). In fact, the authors of this original paper showed that ER was not involved in phagocytosis by neutrophil. It should be noted that the ER theory even in macrophages remains controversial (Gagnon *et al.*, 2002).

It has been suggested that fusion of intracellular vesicles to the membrane might be another source of the extra membrane. However, the amount of 2500 vesicles would be necessary to provide sufficient additional membrane. This would amount to the total vesicle compliment of the neutrophil. Exocytosis of vesicle contents would also occur with an accumulation of extracellular degradative enzymes and hydrolases (Hallett & Dewitt 2007). This would be harmful for the surrounding healthy tissue and is unlikely to occur during normal phagocytosis. Also exocytosis only results from the fusion of vesicles that are close to the membrane and limits the possible maximum to about third of the total vesicle content. It has been discussed the last point against this theory. The authors of this original paper studied that membrane expansion by applying suction through a micropipette held at the neutrophil surface and measuring the force required to deform the membrane. It was found that a significant expansion could be achieved by simply a physical effect, which was

independent of exocytosis. Furthermore from calculation of the force required, it was found to be consistent with localised “unwrinkling” of the membrane (Herant *et al*., 2006).

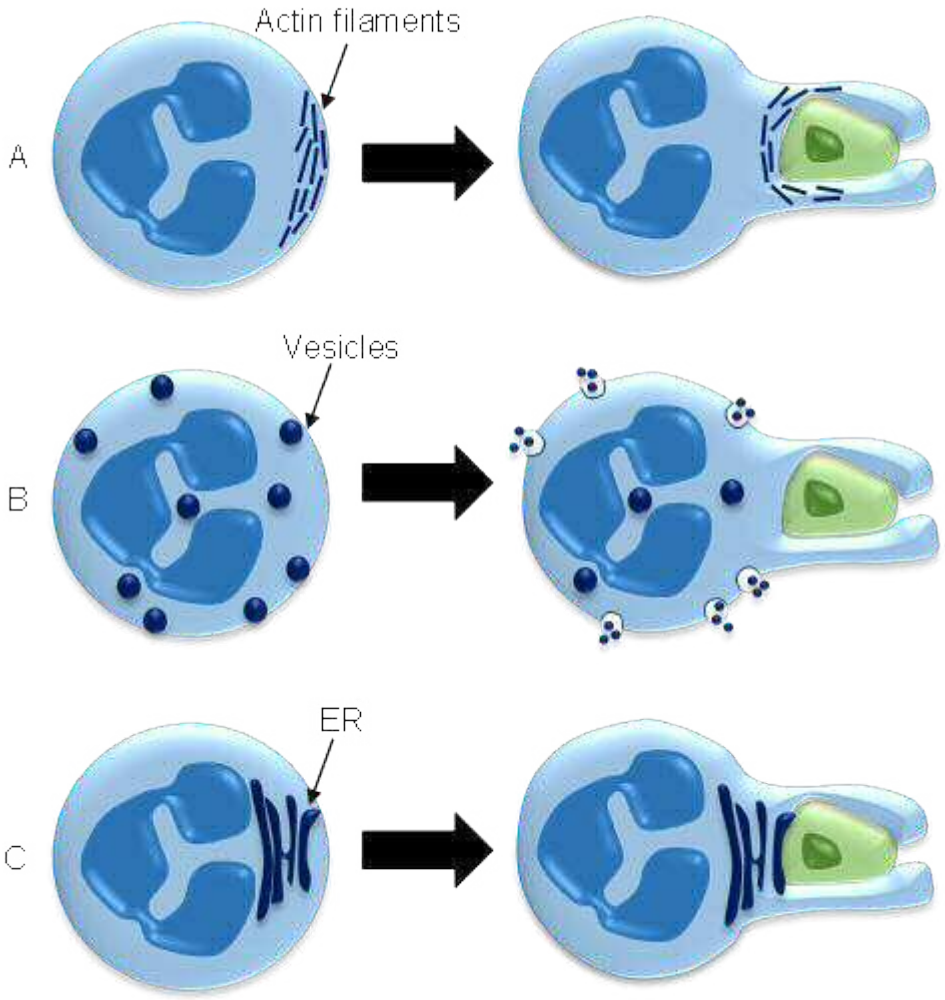

Figure 1.10 Diagram presenting several theories of membrane expansion during phagocytosis by neutrophils. (A) The stretching model: formation of pseudopodia by actin filaments pushing and stretching the plasma membrane. (B) The vesicle model: fusing of intracellular vesicles to the plasma membrane adding membrane. (C) The endoplasmic reticulum (ER) model: fusion of ER to the cellular membrane to afford additional membrane.

1.6.1 Possible methods of membrane expansion

The importance of cell surface area regulation in neutrophil activity has been an area of intense research and speculation. Imaging these changes in neutrophils is complex and although atomic force microscopy has not been successfully used in these experiments, there is the potential for scanning electron micrography (SEM) to identify morphological changes on a sub-micron level. However, this has not been completely studied and therefore more work is needed to verify this approach. Experiments with SEM demonstrate that the cell surface of neutrophils is irregular (fig 1.11) and characterized by numerous surface wrinkles, folds or ruffles and projections such as filopodia and microvillus extensions (Hallett *et al*., 2007).

Wrinkles are believed to play an important role in determining cell surface binding and morphological change in response to elevated levels of cytosolic Ca^{2+}. However, how the apparent extra membrane is achieved has not yet been resolved. It is thought that these wrinkles might be a membrane reservoir which can be utilised when necessary. For example, SEM images show that when the neutrophil undergoes phagocytosis, membrane wrinkles are lost locally. This provides the possibility that when neutrophils undergo shape changes, unfolding of the wrinkled plasma membrane provides the extra membrane (Hallett *et al*., 2007). It is thus necessary to determine the nature of the surface wrinkles in neutrophils and the mechanisms that maintain or regulate these wrinkles (fig 1.11).

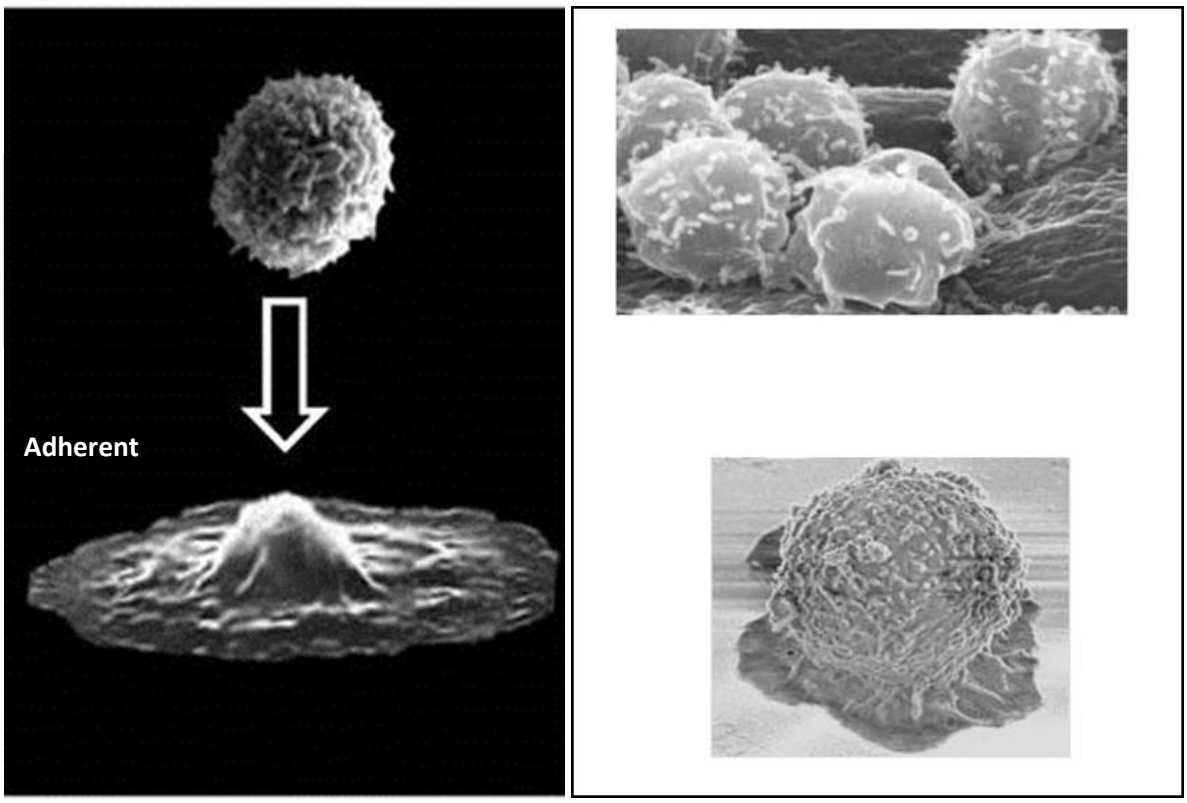

Figure 1.11 Scanning electron micrographs of multiple wrinkles on the neutrophil surface membrane which are lost in regions where the neutrophil spreads (images from Dewitt and Hallett, 2007).

Applying suction to the plasma membrane of neutrophils through micropipettes is useful for measuring the “tightness” of surface membrane wrinkles in neutrophils. The results of these studies identified that a limited amount of suction could expand the membrane into the mouth of the micropipette and accounted for around 5% of the total surface area. However, a greater force could produce an additional expansion of the cell plasma membrane (Herant *et al*., 2003; Dewitt and Hallett 2007; Hallett and Dewitt 2007). These data were interpreted as reflecting a limited amount of slack within the wrinkles, but that extra force could "unwrinkle" the remainder of the membrane, as if the wrinkles were held in place by a molecular "velcro" (Herant *et al*., 2003).

The "velcro-like" molecular structures which hold the wrinkle together, includes two main binding molecules. The first molecule is the membrane linker protein ezrin, which may also hold L-selectin in place on the wrinkled membrane. The second molecule is the membrane linker protein talin, which may also hold β2-integrin in place in the wrinkle valleys. Within the wrinkled region, the different locations for these molecules can be observed at the SEM level where L-selectin is only placed in peaks and β2-integrin is only placed in valleys (Herant *et al*., 2003). These locations are probably important in explaining their roles in neutrophil capture by the endothelium and subsequent cell spreading (see section 1.4).

1.6.2 Neutrophils under tension

Polarization and migration of neutrophils in response to chemoattractants results from the formation of protrusions at the leading edge of the cell, which are balanced by shrinkage at the back of the cell. The maintenance of cell polarization is essential for effective and constant migration. This maintenance is a continuous response to an anisotropic environment that results in the migration of the neutrophil up a chemoattractant gradient. It has been proposed that there is a semi-autonomous excitable network that maintains polarization of the cell (Afonso and Parent, 2012), which involves both positive and negative feedback loops. It has been suggested that actin, PI3K and small GTP binding Rac and Ras proteins are positive feedback loops which are useful in controlling protrusions at the leading edge of the neutrophil (Brandman and Meyer, 2008; King and Insall, 2009).

A study by Chen *et al* (2006) has shown that positive feedback loops include the action of extracellular signals. For example, the stabilisation of neutrophil polarization and migration occurs after the secretion of ATP at the leading edge of the cell (Chen *et al*., 2006). Such positive feedback loops need a balancing inhibitory factor so that neutrophils spread protrusions throughout their leading edge. In addition to this, whole cell spreading occurs when pseudopodia are formed uniformly over the whole cell-substrate contact surface. It has been identified that a mechanism for avoiding inappropriate protrusions formation that is linked to membrane tension, acts as an inhibitory factor in neutrophils (Houk *et al*., 2012) (fig 1.12).

Devreotes and Janetopoulos (2003) have shown that the main inhibitory signals behind membrane tension might be characterised as a “sink” for limiting factors. For example, key proteins for establishing protrusion have to be isolated to the front of the cell and eliminated from the back. Also, within the leading edge of the cells, there may be the generation of a fast-diffusing soluble molecule that acts as the inhibitory signal. The formation of this molecule establishes a uniform inhibitory signal that is essential to restrict the positive signal to the leading edge of the cells. However, the dominant effect within pseudopodia is the mechanical force which is the inhibitory signal. Hence, the front pseudopodium has a mechanical force which also exerts its effect at the back of the cell (Devreotes and Janetopoulos, 2003).

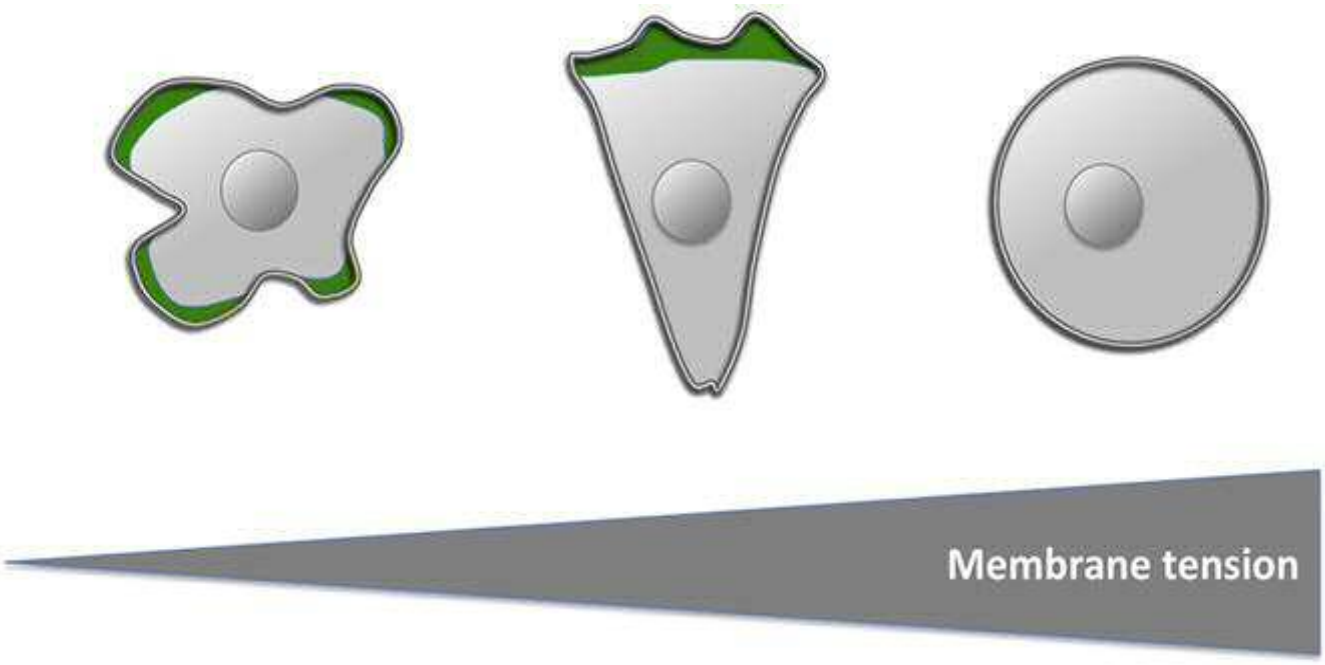

Figure 1.12 Membrane tension within polarised neutrophils. Neutrophils freely polarise and are able to localise activating signals at leading edges (green colour) in response to chemoattractants. Cell membrane tension acts to prevent the signals at the leading edge, so the polarisation becomes stable. The cell behaviour depends of the action of the membrane tension. (Left of the diagram) shows effects of reduction in membrane tension which results in the spread of protrusions at the leading edge and pseudopods reach the whole cell. (Right of the diagram) shows opposite effects throughout the inhibition of protrusions as a result of rise in membrane tension (Figure adapted from Alfonso & Parent (2012)).

1.6.3 The mechanism of mechanical tension

The study by Houk *et al* (2012) has shown that mechanical tension is a long range inhibitory mechanism which controls the cell body behaviour. This hypothesis was tested by the demonstration of some enhanced effects by increasing the surface area, doubling the membrane tension for long range inhibition of Rac activation and inhibition effects through reducing activity of membrane tension. It has been widely assumed that the mechanism of the long range inhibition usually involves the generation of diffusible molecules or requires sequestration at the leading edge. However, from this finding, the most important aspect of the long range inhibition is the constraint in increasing at membrane plasma area during leading edge protrusion. This effect prevents secondary fronts from generating, away from the cell front (Houk *et al*., 2012).

Although it has long been speculated that a diffusion based inhibition is one of the important hypothetical inhibition mechanisms for maintaining cell polarisation (Jilkine and Edelstein-Keshet, 2011; Houk *et al.*, 2012), provided an elegant demonstration that cell membrane tension was the key in neutrophils for controlling pseudopod formation. Neutrophils were exposed to a brief heat shock to generate elongated cells, the front of which actively formed pseudopodia while the cell body was inactive. A thin tether connecting the front and the body would restrict diffusion of any factor from front to back. This thin tether could be severed spontaneously or by a focused laser beam without causing any damage to the cell body or the pseudopod (fig 1.13 A). Within 70s of cutting the link, psuedopdia formed on the previously inert cell body of about 47% cells. The reanimated cell body became extremely protrusive and able to generate a new pseudopod (fig 1.13 B). The

authors showed that without laser cutting, the tethers also cleaved spontaneously at a low frequency. Again, within 1 min of severing, reanimation of 26% of the cell bodies occurred and new pseudopodia formed (fig 1.13 C). After severing the tether, the fast reanimation of the cell body could not be explained by a slow resynthesis of an inhibitory factor and instead demonstrates that inhibition of the cell body was the result of a reduction in the mechanical tension. This conclusion verified that membrane tension is essential and enough for preventing the spreading of membrane protrusions after neutrophils are exposed to uniform chemoattractant stimulation (Houk *et al*., 2012).

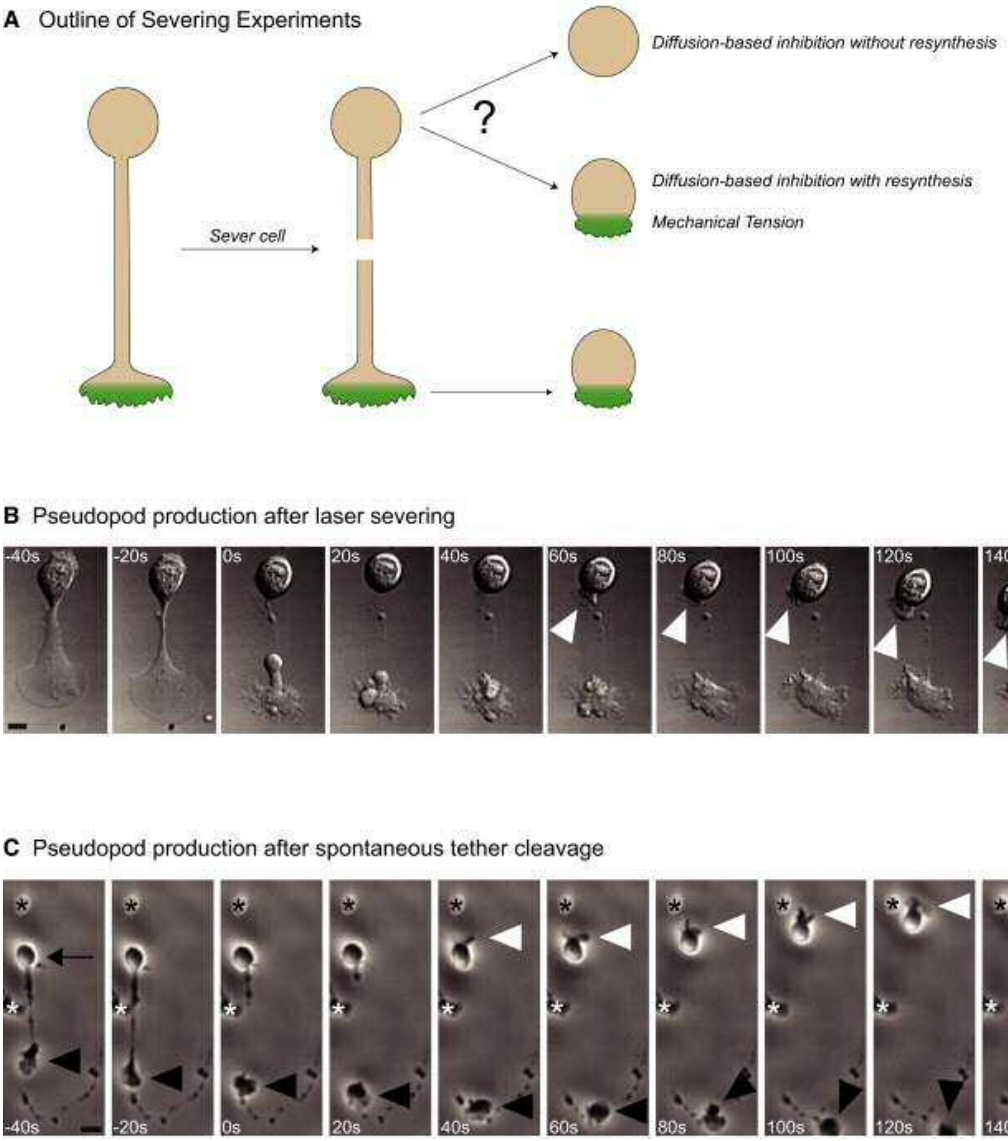

Figure 1.13 The formation of a new pseudopod in neutrophils after severing. (A) A summary of laser-based severing experiments. The results present information of the cell body behaviour upon the polarisation and then removal of the pseudopod. Mechanical tension could generate a brief inhibitor at the leading edge, which would be consistent with the reanimation upon pseudopodia after severing. This inhibitor might be either a rapidly synthesised limiting component or a diffusible inhibitor with a short half-life. (B) A summary of formation of new pseudopod after laser-based serving experiments. At zero seconds, a laser beam severs a tethered HL-60 cells. After the cell is severed in about 47%, a new pseudopod is made (white arrow) by the previously inactive cell body. (C) A summary of formation of new pseudopod after spontaneous tether cleavage. At zero seconds, the pseudopod is spontaneously cleaved from the cell body (black arrow). Within 50s of severing (white arrow) a new pseudopod is generated from the cell body, initiating migration. The cell body is able to reanimate after spontaneous tether cleavage in 26% of cells (This figure is from Houk et al., 2012).

1.6.4 Unwrinkling theory and the role of calcium

The basic idea behind the cell surface wrinkle theory is that the cell surface wrinkles maintain tension in the membrane, which prevents pseudopodia formation until required. When the membrane unwrinkles, tension is released and additional membrane is provided for an increase in cell surface area. It has been proposed that wrinkles are released to provide the extra membrane required for phagocytosis (Hallett and Dewitt, 2007) and cell spreading (Dewitt and Hallett, 2007). For 20 years it has been recognised that during spreading by neutrophil and macrophages, there is a huge increase in the level of cytosolic free Ca^{2+}. Furthermore, Ca^{2+} elevation induced by uncaging cytosolic Ca^{2+} or inositol 1,4,5-trisphosphate (IP_3) (Pettit and Hallett, 1998) triggers cell spreading. It has been shown that there is also a need for a rise in cytosolic free Ca^{2+} during phagocytosis (Dewitt and Hallett, 2002) which accelerates the rate of the pseudopod extension around the particle, an effect linked to μ-calpain activity, a protease activated by Ca^{2+}. Within the cell, active calpain can cleave substrates important for maintaining the wrinkled surface (Molinari and Carafoli, 1997; Dewitt and Hallett, 2002) (fig 1.14).

During lymphocytes adhesion via ß2-integrin, cell flattening also occurs as results of the calpain activation (Stewart *et al*., 1998; Leitinger *et al*., 2000). It has shown that μ-calpain has two separate binding sites; the ezrin, radixin and moesin homology (FERM) domain, that binds to membrane-associated proteins and an actin-binding domain, linking to the actin cytoskeleton (Dewitt and Hallett, 2007; Hallett and Dewitt, 2007). Activation of μ-calpain via Ca^{2+} influx would thus provide a mechanism for liberating the molecular “velcro”,

through proteolytic cleavage of the calpain-sensitive cytoskeletal elements, leading to the extra membrane required to realise pseudopod formation.

As a result of calpain activation via elevated Ca^{2+}, the link between the cell surface membrane and the underlying actin cytoskeleton is disconnected. Pharmacological inhibition of calpain activation reduces the process of phagocytosis, cell spreading and extravasation. It is therefore possible that μ-calpain may be a therapeutic target for the treatment of autoimmune conditions (Michetti *et al*., 1997). There is abundant evidence in the literature to support this proposal, both in vitro and in animals. For example, the onset of experimentally induced RA and inflammation in rats is significantly decreased by inhibition of μ-calpain (Shahi *et al*., 2011). However, more work is needed in order to prove the role of μ-calpain in the unwrinkling theory.

Calpastatin is an endogenous binding partner of activated μ-calpain, via A, B and C domains (Wendt *et al*., 2004). From this binding it is possible to indicate the location of the activated calpain in the cell. Thus, domain IV of μ-calpain binds to domain A and domain VI of μ-calpain binds domain C. However, domain B requires binding between A and C domains in order to permit the binding to the activated μ-calpain (Bokor *et al*., 2005). Thus, domains A and C increase calpain activation, whereas domain B inhibits calpain activation (Yang *et al*., 1994; Takano *et al*., 1995).

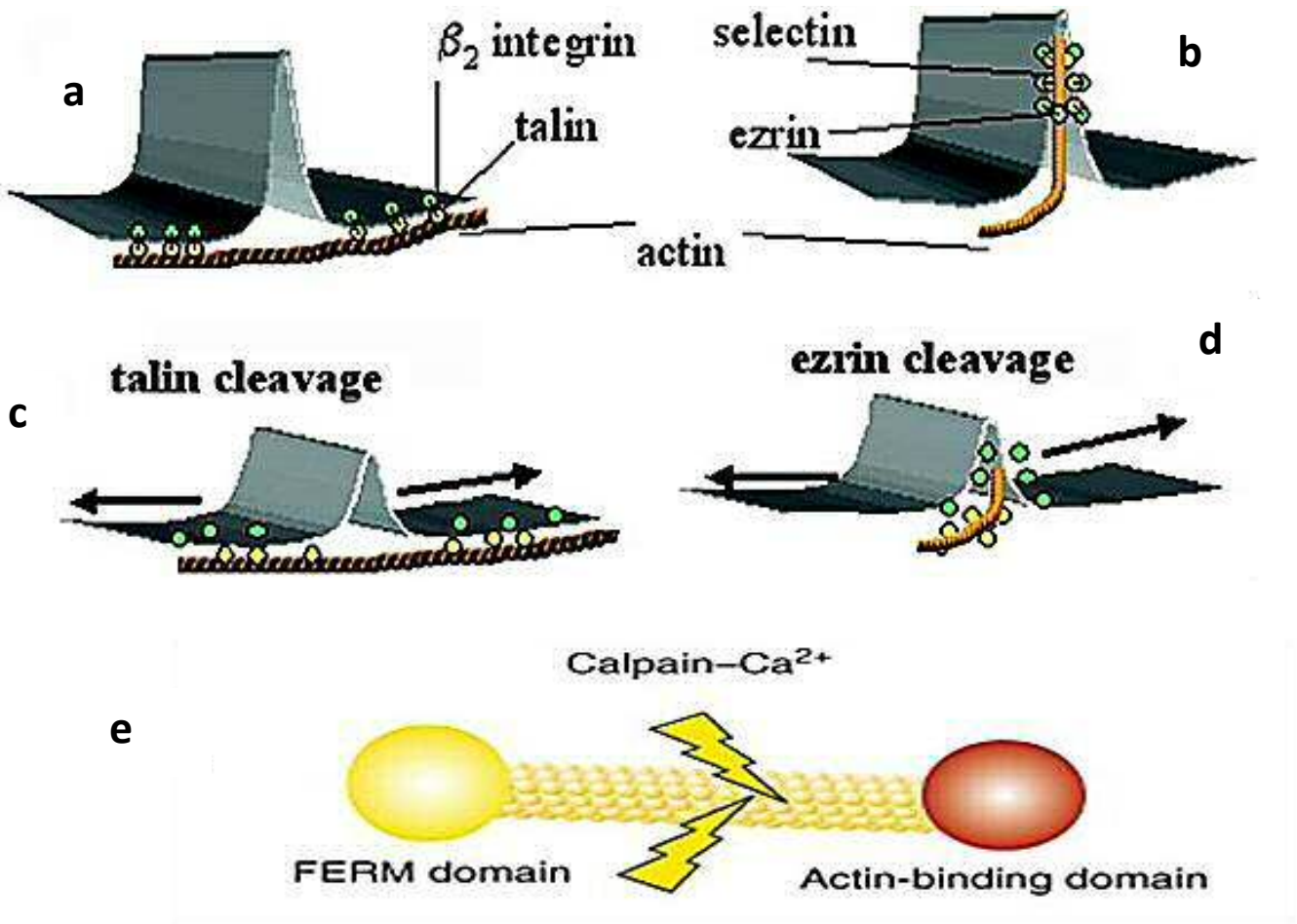

Figure 1.14 Mechanism for wrinkle release to provide the extra membrane needed for cell morphology changes. Holding wrinkles in two structure, (a) actin across the wrinkles by talin and (b) actin within the wrinkles by ezrin. Release of the additional membrane is proposed through the cleavage of both (c) talin and (d) ezrin, as a result of Ca^{2+} influx, allowing pseudopodia to be formed. (e) The possible connection between talin and ezrin is shown, whereby the FERM and actin-binding domains link to the calpain cleavage site. This figure is adapted from Hallet and Dewitt (2007).

1.7 Aims of the work in this thesis

As discussed in the above overview of neutrophil function and cell surface topography, neutrophils are characterised by undergoing rapid cell shape change, especially during cell spreading and phagocytosis. In both situations, the cell changes from a spherical to a non-spherical configuration. This must necessarily require additional cell surface membrane as a sphere is the minimum surface area to enclose a given volume. Although it has been proposed that this additional membrane may come from cell surface structures called wrinkles or microridges, it has not been possible to directly test this hypothesis.

The work in this thesis therefore aims to test these proposals.

The aims can be put under three headings.

1. Developing and establishing the validity of a novel methodology that can be used to monitor the cell surface topography (wrinkledness) of living neutrophils.

2. Use this novel methodology to investigate whether changes in the surface topography that occur during neutrophil shape change in a manner consistent with the hypothesis that wrinkles provide the additional membrane for the shape change.

3. To establish whether changes in cell surface topography were required for rapid neutrophil cell shape change.

Chapter 2

Materials and Methods

2.1 Materials

Product	Product source	volume	Chapter Used in
Heparin	CP Pharmaceuticals Ltd, U.K.	100µl	Chapter (3 ,4 & 5)
Dextran	Sigma-Aldrich Ltd, Dorset, U.K.	2.5ml	Chapter (3 , 4 & 5)
Fluo-4 AM	Invitrogen Ltd, Paisley, U.K.	1µl	Chapter (4 & 5)
Zymosan A	Sigma-Aldrich Ltd, Dorset, U.K.	10mg/ml	Chapter (4 & 5)
IP_3 (Caged)	Enzo Life Sciences, Exeter, U.K.	1.5µl	Chapter (5)
fMLP (N-Formyl-Met-LeuPhe)	Sigma-Aldrich Ltd, Dorset, U.K.	2µl/ml	Chapter (5)
Bovine Serum Albumin (BSA)	Sigma-Aldrich Ltd, Dorset, U.K.	100µl	Chapter (3, 4 & 5)
HEPES	Fisher Scientific, Leicester, U.K.	1ml	Chapter (3, 4 & 5)
KCl	Sigma-Aldrich Ltd, Dorset, U.K.	1ml	Chapter (3, 4 & 5)
NaCl	Sigma-Aldrich Ltd, Dorset, U.K.	50µl (1.2M)	Chapter (3 & 5)
KH_2PO_4	Sigma-Aldrich Ltd, Dorset, U.K.	1ml	Chapter (3, 4 & 5)
$MgSO_4$	Sigma-Aldrich Ltd, Dorset, U.K.	1ml	Chapter (3, 4 & 5)

$CaCl_2$	Sigma-Aldrich Ltd, Dorset, U.K.	1ml	Chapter (3, 4 & 5)
Octanol	Sigma-Aldrich Ltd, Dorset, U.K.	10µl / 1ml	Chapter (5)
Sucrose	Sigma-Aldrich Ltd, Dorset, U.K.	50µl / 1.2M	Chapter (5)
DiI	Sigma-Aldrich Ltd, Dorset, U.K.	1.1mM	Chapter (3, 4 & 5)
Deoxycholate	Sigma-Aldrich Ltd, Dorset, U.K.	100µl	Chapter (3 & 5)

Table 2.1 Laboratory Reagents & Chemicals

2.1 Laboratory Equipment

2.1.1 Microscopy

CLSM Confocal Microscope (Leica, Milton Keynes, U.K).

Leica SP5 resonant laser scanning microscope equipped with a UV diode laser (405nm) suitable for uncaging.

Scanning Electron Microscope (SEM).

2.1.2 Cell Counting equipment

Cellometer® Automated Cell Count (Peqab Ltd., Fareham, U.K).

2.2 Software

Software	Source
Microsoft Excel 2010	Microsoft, Redmond, Washington,U.S.A.
Microsoft PhotoEditor 3.0	Microsoft, Redmond, Washington,U.S.A.
Microsoft Word 2010	Microsoft, Redmond, Washington,U.S.A.
Leica Application Suite Advanced Fluorescence	Leica Microsystems
Microsoft Paint Version 5.1	Microsoft, Redmond, Washington,U.S.A.

Table 2.2 Computer software

2.3 Buffers

Human neutrophils were suspended in Hepes Buffered Krebs (HBK) medium which had the following constituents.

Substance	Concentration
NaCl	120mM
HEPES	25mM
KCl	4.8mM
KH_2PO_4	1.2mM
$MgSO_4.7H20$	1.2mM
$CaCl_2.2H_20$	1.3mM
Bovine Serum Albumin (BSA)	0.1% (v/v)

Table 2.3 Constituents of Hepes Buffered Krebs

2.3.1 HBK preparation:

- The HBK was prepared in double distilled water.
- The NaCl and HEPES stock solutions were kept at 4°C.
- The chemicals KCl, KH_2PO_4, $MgSO_4.7H_20$ and $CaCl_2.2H_20$ were dispensed into aliquots (20ml) which were kept at 4°C until required for use.
- In order to generate fresh HBK medium, the BSA was prepared by diluting 10% (w/v) in ddH_2O and frozen in aliquots of 1ml. For a concentration of 0.1% (w/v), the BSA was added to all the stock solutions in order to make a fresh HBK medium for every experiment and adjusted to pH7.4 using NaOH.

2.3.2 Balanced Salt Solution (BSS)

BSS (0.13M-Nacl, 2.6mM-KCL, 8.0mM- Na_2HPO_4 and 1.83mM-KH_2PO_4, pH 7.4), was made in 5 litre batches with double distilled water using the following quantities:

40g-NaCl,

1g-KCl,

5.75g-Na_2HPO_4

1.0g –KH_2PO_4.

This was then adjusted to pH7.4 using NaOH, aliquoted and heat autoclaved 20Psi for 30mins.

2.4 Labelling & Detection Products

2.4.1 Membrane probes

The following fluorescent membrane markers were used.

Product Name	Chemical Structures	Manufacturing
DiI	1,1' - Dioctadecyl - 3,3,3',3' - tetramethylindocarbocyanine iodide	Sigma-Aldrich Ltd, Dorset, U.K.
FM 1-43	(N-(3-Triethylammoniumpropyl)-4-(4-(Dibutylamino)Styryl) Pyridinium Dibromide)	Sigma-Aldrich Ltd, Dorset, U.K.
PHK26	-	Sigma-Aldrich Ltd, Dorset, U.K.

Table 2.4: Fluorescent probes tested for suitability for membrane labelling.

2.4.2 Deoxycholate

Deoxycholate (Doc) is a water-soluble ionic detergent. It was stored at 4°C. In order to avoid a formation of MW ~2000 micelles, it is necessary ensure the concentration does exceed 2mM in solution. Also failure to control the concentration can lead to a toxic cellular effect. In the studies reported here, Doc was used as an artificial plasma membrane expander (Rohm and Haas, 2006) (See Chapter 3 and 6 for details).

2.4.3 Properties of deoxycholate

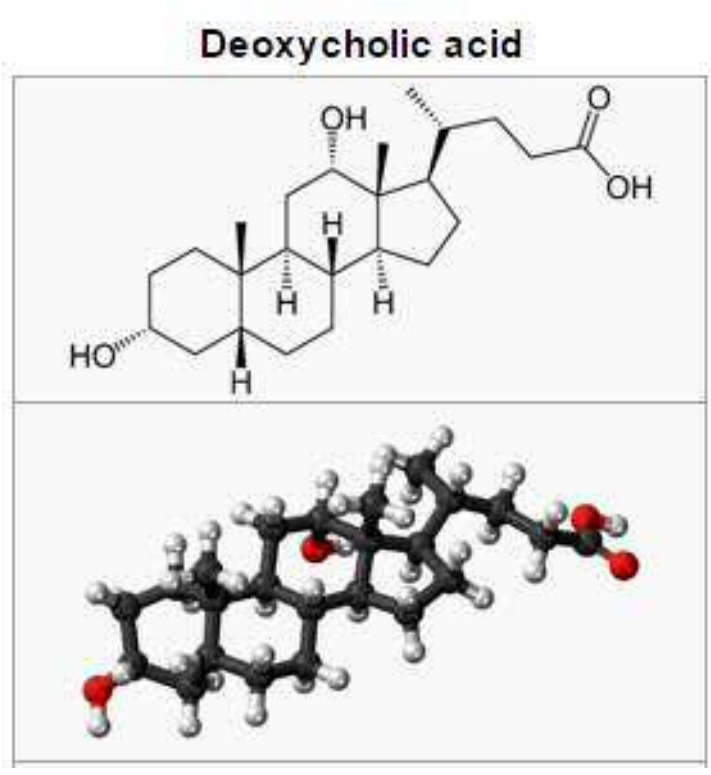

***Figure 2.1 The chemical structure of deoxycholate*.**

The following lists the properties of Deoxycholate

Alternative Names	**Sodium deoxycholic acid; deoxycholate, sodium salt**
Chemical Name	3, 12-α-Dihydroxy-5β-cholan-24-oic acid, monosodium salt
Molecular Formula	$C_{24}H_{39}O_4Na$
Molecular Weight	414.6g
Detergent Class	Ionic (anionic)
Solubility (in water at 20°C)	≥5%
Absorbance (1% Detergent Solution)	340nm <0.02; 280nm <0.04; 260nm <0.06
pH (1% Solution)	5 to 9
Purity (by HPLC)	≥98%
Aggregation Number	5 (average)
Micelle Molecular Weight	2000g (average)
Critical Micelle Concentration (CMC)	2 to 6 mM (0.083 to 0.249%, w/v)
Cloud Point	Unknown
Dialyzable	Yes
Form	Powder
Product Size	5g
Regent Type	Detergent (Pure)

Table 2.5 The chemical structure and Properties of Deoxycholate, *taken from website: www.thermofisher.com.*

2.5 Methods

The following are methods that were used in the results chapters.

2.5.1 Blood collection and neutrophil isolation protocol

Neutrophils were isolated from the blood of healthy human donors ranging from 20-60 years old in all experiments as follows below:

Stage 1: Blood collection

A volume of blood (10ml) was drawn and transferred in a tube containing of 100µl heparin (WOCKHARDT) as anti-coagulant (100µl/10ml blood; final concentration of 50IU per ml of blood). Blood samples were mixed gently after collection.

Stage 2: Dextran sedimentation

A volume of (2.5ml) of 6% dextran solution which was dissolved in BSS (6g dextran dissolved in 100 ml BSS, stored at 4°C) was added to the sample. This was determined to be the optimal dextran concentration to isolate the leukocytes. Sedimentation was allowed to proceed by leaving the cells for 30 mins at room temperature until three layers appeared: (from bottom to top) erythrocytes (red blood cells), leucocytes (buffy coat) and platelet-rich plasma. The buffy coat layer, consisting of white blood cells and plasma, was carefully aspirated and placed into clean tubes. This sample was centrifuged at 500g (RCF) for 1 min (break speed 3). Distilled water (1ml) was added to the cell pellet (re-suspended gently for 10s) before osmolarity was restored by the addition of BSS (20ml). The sample was spun at 500g for 1 min (break speed 3) and the cell pellet resuspended in Krebs buffer (1ml) and cooled in an ice bath until required (fig 2.1).

Stage 3: Ficoll

As experiments were to be performed on single cells, further purification was rarely necessary (living neutrophils were easily identified under phase contrast microscopy by virtue of their physical/morphological characteristics). Also centrifugation through Ficoll-paque can have adverse effects on neutrophil subsequent behaviour. If it was required, however, the ficoll paque was layered under the white cell/granulocyte suspension produced in step 2 to form a physical gap between the ficoll: cell interface and the base of centrifuge tubes. Centrifugation at 350g (RCF) for 30 mins was undertaken and the interface cells discarded. The pelleted cells were carefully resuspended (to avoid mechanical activation) and washed 3 times to remove the ficoll.

Stage 4: Cell viability

The morphological observation demonstrated that neutrophils had an intact plasma membrane (trypan blue exclusion) and 2-5 lobed nuclei (acridine orange staining). Freshly isolated human neutrophils were stained with DiI and studied for their morphology. All stained cells were viewed and imaged under the confocal microscope.

2.5.2 Serum preparation

Human blood was taken without anticoagulant and left in glass universal vial to clot overnight at 4^{o}C. Human serum was separated from clotted blood by centrifugation (10 mins at 1300g) to force fluid from the clot. This fluid was collected and centrifuged for a further (20,000g; 5 mins) in order to clear the fluid of red blood cells. The supernatant serum was stored at -20^{o}C until required.

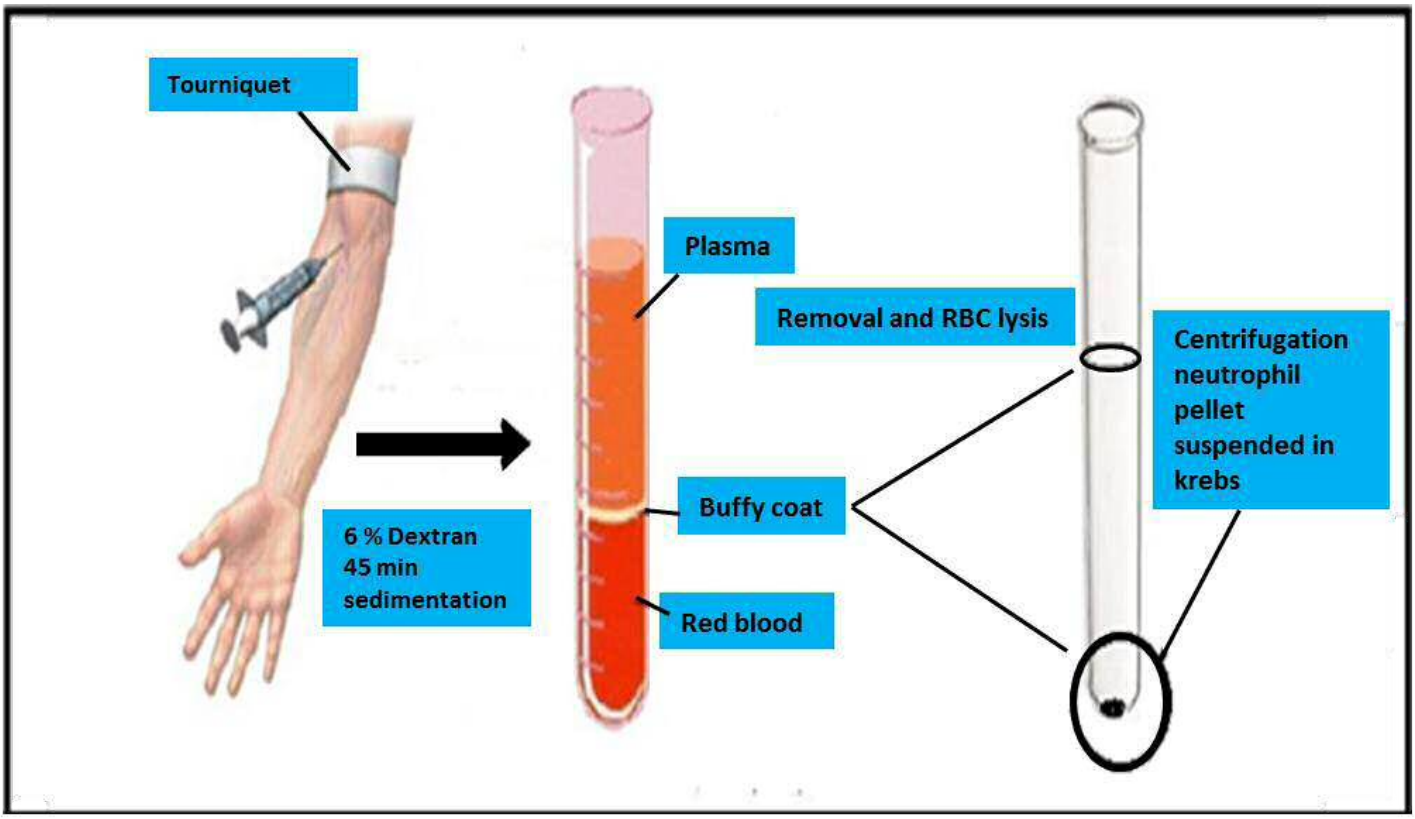

Figure 2.2 Blood neutrophil isolation.

2.5.3 Fluorescent labelling and detection (cell membrane labelling)

The fluorescent marker to be used in this project must have a good uptake into the plasma membrane and be reasonably photostable but also readily photo-bleachable when exposed to high laser intensity. Ideally, the marker should remain in the cell membrane without significant redistribution into other organelles, giving images with a bright thin layer around the cell. The markers listed in Table 2.4 were tested and DiI was identified as the most suitable marker. Membrane labelling was thus carried out using DiI in all experiments. DiI is a lipophilic carbocyanide (fig 2.3) which is weakly fluorescent in water, but highly fluorescent and moderately photostable when incorporated into cell membranes (Kobbert *et al.,* 2000). Upon application of DiI, lateral diffusion occurs and staining of the entire cell membrane was observed, with minimal or no cellular toxicity. Therefore, DiI was utilised as an effective means of establishing fluorescence in neutrophil cell membranes.

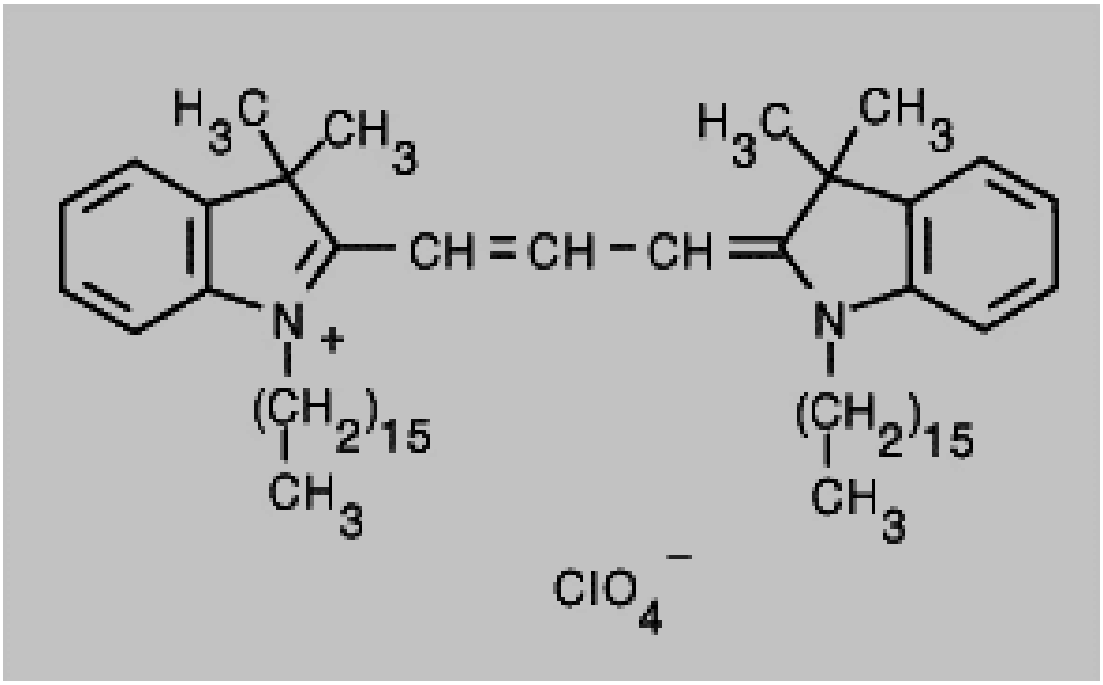

Figure 2.3 The structure of DiI.

The properties of DiI are listed below.

Alternative name	**DiI, D282 and $DiIC_{18}$**
Chemical name	1,1'-dioctadecyl-3,3,3'3'- tetramethylindocarbocyanine perchlorate
Molecular formula	$C_{59}H_{97}ClN_2O_4$
Molecular weight	933.87g/mol
CAS number	41085-99-8
Storage	Store liquid/solid at room temperature (RT)
Solubility	Soluble in ethanol, methanol, DMF, DMSO
Platform	Fluorescence Microscopy
Detection Method	Fluorescent
Sub-Cellular Localization	Cell Membranes & Lipids

Table 2.6 Properties of DiI, *taken from website: www.thermofisher.com****.***

2.5.4 Fluorescence spectra

The fluorescent properties of DiI (fig 2.4) give the possibility of imaging without bleaching, yet also allowing bleaching when required. The DiI-labeled plasma membrane of neutrophils was imaged using a Leica SP5 resonant laser scanning microscope and SP5 Leica software. Excitation at 543nm gave good fluorescence imaging with the emission collectors set to 600–750nm, but with little or no bleaching. When exciting at 488nm, photobleaching was achievable by increasing the laser power of the argon laser. This step was used to give good bleaching when required (see section 2.5.6). Imaging was therefore routinely achieved at 543nm excitation and photobleaching at 488nm (high power).

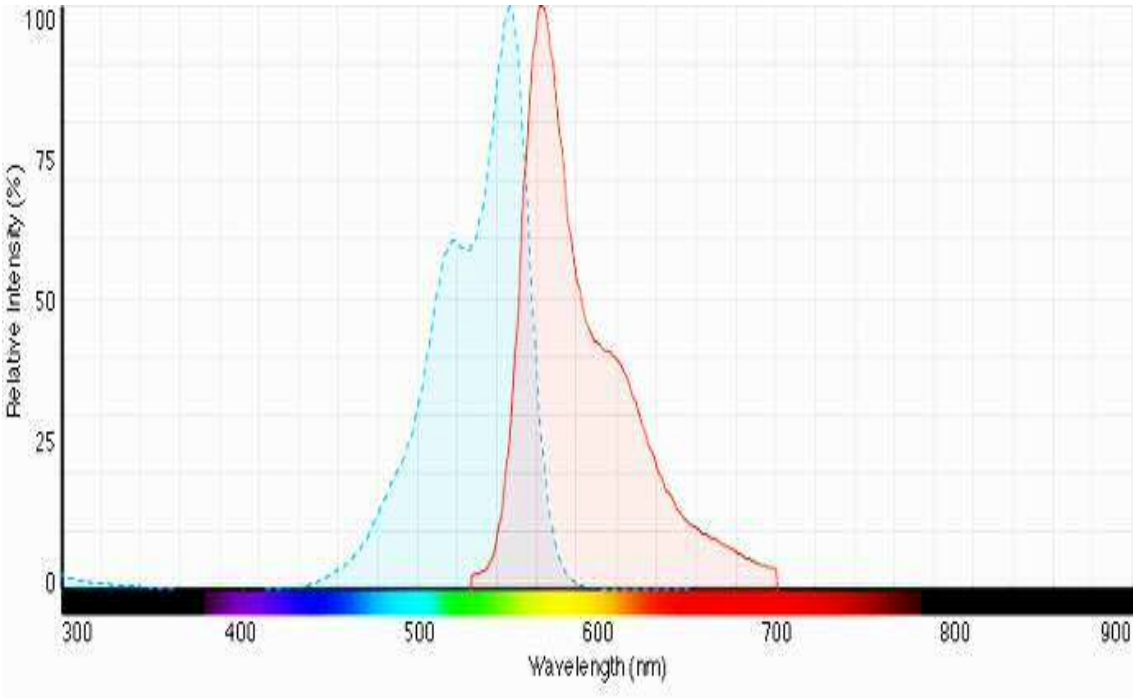

Figure 2.4 Fluorescence Spectra.

This image is taken from Dil Stain (https://www.thermofisher.com/order/catalog/product/D282).

2.5.5 The mechanism of labelling the cell membrane

DiI is a red-orange fluorescent, lipophilic carbocyanine marker which is able to insert the two long (C18 carbon) hydrocarbon chains into the plasma membrane and diffuses rapidly around the phospholipid bilayer of the membrane in order to stain the whole cell surface (Shiraishi *et al.,* 1992). It was usually applied to cells in a DMSO solvent but generated DiI crystals when added to the cell suspension. The contacting between a crystal and a cell gave a rapid staining of the cell membrane.

2.5.5.1 DiI staining method

Stock 1 solution: 10mg/ml in DMSO to give 1.1mM

Stock 2 solution: Stock 1 diluted in DMSO 1:11 (to give 1mM)

The Stock 1 and Stock 2 solutions were stored at room temperature

On day of experiment:

1- Stock 2 was diluted in Krebs (4µl in 1000µl) to provide 4µM.

2- This was added 1:1 to neutrophils on the cover slip (usually 100µl added to 100µl) to provide final concentration of 2µM.

3- After 2 minutes, non-cell associated extracellular DiI was removed by washing.

4. A well stained cell was selected on which to undertake experiment.

2.5.6 Confocal imaging

Confocal microscopy of neutrophils was performed using an oil immersion lens at 63×/1.2 NA. The microscope was equipped with an argon ion laser (for 488nm), a helium neon laser (for 543nm) and a helium-neon laser for (633nm). In order to avoid detection of autofluorescence background signals in images, laser intensities never exceeded 4% for the argon ion and 10% for the helium-neon laser, individually. The microscope was also equipped with an oil immersion objective ECPlan-Neofluor 40×/1.30 NA. During the experimental procedures, the neutrophils were kept active by maintaining the stage incubator temperature at 37°C. The images were analysed with the Leica Advanced Fluorescence software.

2.5.7 Leica Microsystems

Leica Microsystems provides an advance fluorescence imaging software which was used for imaging. Image J (NIH) and purpose written software plugins were used for cell counting and other analysis of the data in this thesis.

The following simple steps for data analysis were:

• Leica microsystems image analysis software and Image J are available online from a number of free sources was installed on the analysis computer.

• Using the Leica software, Open the chosen experimental data file from the saved experiment file. Choose “quantify”.

• If the image sequence is an AVI.file, or a TIF series it is necessary to “import” the data.

• The images can then be quantified from within regions of interest (ROIs) selected in the field to produce date streams for numerical analysis within Excel. Scale bar and time stamps are automatically provided with the Leica software which is recalculated as the image size is adjusted (an example of screenshots is shown below).

Screenshots from the Leica Analysis software showing analysis of raw data

2.5.8 Sub-domain FRAP procedure

FRAP experiments were performed on a Leica SP5 resonant scanner confocal microscope using a 63x objective. A region of the cell to be photobleached was identified by prior inspection. The zoom, rotation controls and image format (e.g. 512 x 512 pixels = full frame, 32 x 512 pixels = a "letter box" shape) was used to limit the scan area to the desired region of the cell. Data were acquired from this restricted zone of the cell and photobleaching achieved when required by transiently stepping up the power of the argon laser. This resulted in a pulse of photobleaching restricted to that part of the cell. Data acquisition was continuous throughout the bleach pulse and the subsequent recovery cycle. This cycle could be repeated several times to give reproducible results or "before and after" treatment comparisons.

Neutrophils were maintained at 37^{o}C using an air-stream incubator and photobleaching was facilitated through a 40mW argon laser at 30% power; rectangular slices of 488nm and 543nm lines were utilized. For each bleach pulse, a single iteration was performed lasting between 1-10s. For examination of recovery of fluorescence, the intensity of the 488nm laser was reduced to zero and imaging continued at the lower laser intensity 543nm line. The fluorescence recovery at subdomains within the bleached area was recorded.

2.5.9 DiI as a membrane label

Honig and Hume have used DiI for studying anterograde and retrograde neuronal tracing (Honig and Hume, 1986). Hence, DiI is fluorescent lipophilic membrane stain that has a hydrophilic head and hydrophobic tail which embeds in the plasma membrane of the cell. Within the hydrophobic plasma membrane, its two lipophilic hydrocarbon side chains are

restrained and the quantum yield of the fluor increases (see the structure of DiI in fig 2.3). Before DiI is combined into the plasma membrane, it is therefore weakly fluorescent (Hofmann and Bleckmann, 1999; Honig and Hume, 1986). However, within the plasma membrane bilayer, it is extremely fluorescent and quite photostable (Michelle and Fox, 2007). Sherazee and Alvarez have shown that over the cell membrane, DiI is able to diffuse along the lipid bilayer of membranes. DiI diffusion laterally (Hofmann and Bleckmann, 1999; Honig and Hume, 1986) is sufficient to highlight dendrites and outline their spinous protrusions (Sherazee and Alvarez, 2013). Because of its hydrophobicity, movement of DiI between membranes is typically insignificant (Hofmann and Bleckmann, 1999; Honig and Hume, 1986).

DiI is ideal for confocal laser scanning microscope and gives an extremely strong and robust fluorescence (Gan *et al*., 1999; Lanciego and Wouterlood, 2011). A study by Terasaki *et al* in (1994) has discovered that DiI stains many different live cell types and also can be used with fixed tissue (Terasaki *et al.,* 1994). In addition, it is significant in labelling various species for example rodents, primates and zebrafish (Gan *et al*., 2000; O'Brien and Lummis, 2006; Seabold et al., 2010; Arsenault and O'Brien, 2013). Within brain tissue, a "gene gun" for gene injection has been used with "DiO listic labelling," i.e. drops of DiI that are coated with the lipophilic dye (Lo *et al*., 1994).

5.10 DiI Labelling procedure (staining of neutrophil plasma membrane)

In 2011, a study by Westmark *et al* established protocols for DiI application (Westmark *et al*., 2011). Labelling with DiI was achieved by direct application of the dye crystal to the neutrophil plasma membrane. The preparation of DiI membrane staining solutions is shown in

section 2.5.5. Briefly, staining was achieved by applying dye working solution to 100µl of neutrophil on a coverslip. DiI solution and any crystals were washed by using 100µl of Krebs. Stained cells were identified by confocal microscopy and kept at 37°C. All images and movies of the cells were taken as soon as possible after the labelling, in order to reduce intracellular membrane staining.

2.5.11 Subdomain FRAP Theory

The theory behind the proposed methodology is that knowledge of the distance of diffusion of DiI in the membrane can be acquired from the rate of recovery after photobleaching. This can be seen by simulating the effect using Fick's law of diffusion.

2.5.11.1 Fick's Law simulation

Fick's Law was used to simulate diffusion in the plane of the membrane. The effect of distance from the bleach front was thus theoretically observed. Essentially a section of membrane is considered to be divided into equal compartments, with the same area of contact to the next such that the flux in unit time (J) from each compartment to the next is driven to the concentration difference across the boundary between compartments. Fick's Law is that J (C2-C1) where J is the flux from one compartment to the next and C1 and C2 are the concentrations in each compartment. The concentrations at each unit step in time can thus be calculated in each membrane compartment (distant from the diffusion front) and be followed over time.

At the start, all compartments within the bleached zone are empty; and the concentration at the bleach boundary is 1000 molecules. If a constant of proportionality is taken to be 0.1, at the next time step, there will be 100 molecules in the first compartment

within the bleach zone. At the second time step, there will be 10 molecules in second bleach compartment (a tenth of the molecules previously in compartment 1), but 180 molecules in the first compartment as 10 molecules which are lost to compartment 2 but 90 molecules enter from the boundary (i.e. 0.1x(C2-C1)). At the third time step, there will be 1 molecule in the third compartment (a tenth of the molecules previously in compartment 2), 27 molecules in compartment 2 (1 molecule lost to compartment 3 but 18 molecules arrive from compartment 1 i.e. a tenth of the molecules previously in compartment 1) and 271 molecules in compartment 1 (18 lost to compartment 2 but 82 arrive from outside the bleach zone (i.e. 0.1 x (C2-C1) and so on. It can be seen that the number of molecules increases in each compartment over time, but that the relationship between distance from the bleach zone and time is not obvious. For this reason the number of molecules in each compartment was calculated time step by using an algorithm in Excel.

Using standard Excel calculation (shown in fig 2.5) the concentration in "cell D13", for example is calculated as D13=D12+(C2*C12)-(C2*D12) where Xn is the fraction of molecules in compartment X at time step n and C2 is the fraction of molecules moving in each time step. By plotting the increase in concentration in each compartment over time the effect of distance from bleach front was observed (fig 2.5). Validation of the principle of sdFRAP, namely that the increase in fluorescence at various distances would depend on the distance therefore required an experimental demonstration that the way in which the fluorescence increased would be similar to that predicted by Fick's Law. For this reason, smooth (non-wrinkled) cell membrane was required, so that the linear distance could be measured. In both the smooth membrane of the fully stretched neutrophil tail and in the osmotically swollen cells where the membrane was fully stretched (prior to osmotic lysis), it was found that the

kinetics of the increase in intensity was similar to that predicted by Fick's Law. Fick's Law simulation was used here only to illustrate the expected relationships if the membrane was smooth (as in the tail and swollen cell membranes) and so provide validation of the theory underlying the sdFRAP methodology. Fick's Law was not used to estimate diffusion distances in wrinkled membranes, as the difference in distances between smooth and wrinkled membranes were small. Instead, advantage was taken of the relationship between time and diffusion given by Einstein's diffusion relationship: $D \quad x^2/\tau$ where the diffusion coefficient, D, is proportional to the square of the distance travelled (x^2) divided by the characteristic time taken (τ). In the stretched membrane situation this relationship was shown to hold, as the diffusion coefficient, D, was similar when calculated at various distances. The timing on the arrival of molecules at a defined distance from the bleach front simply followed Einstein's equation.

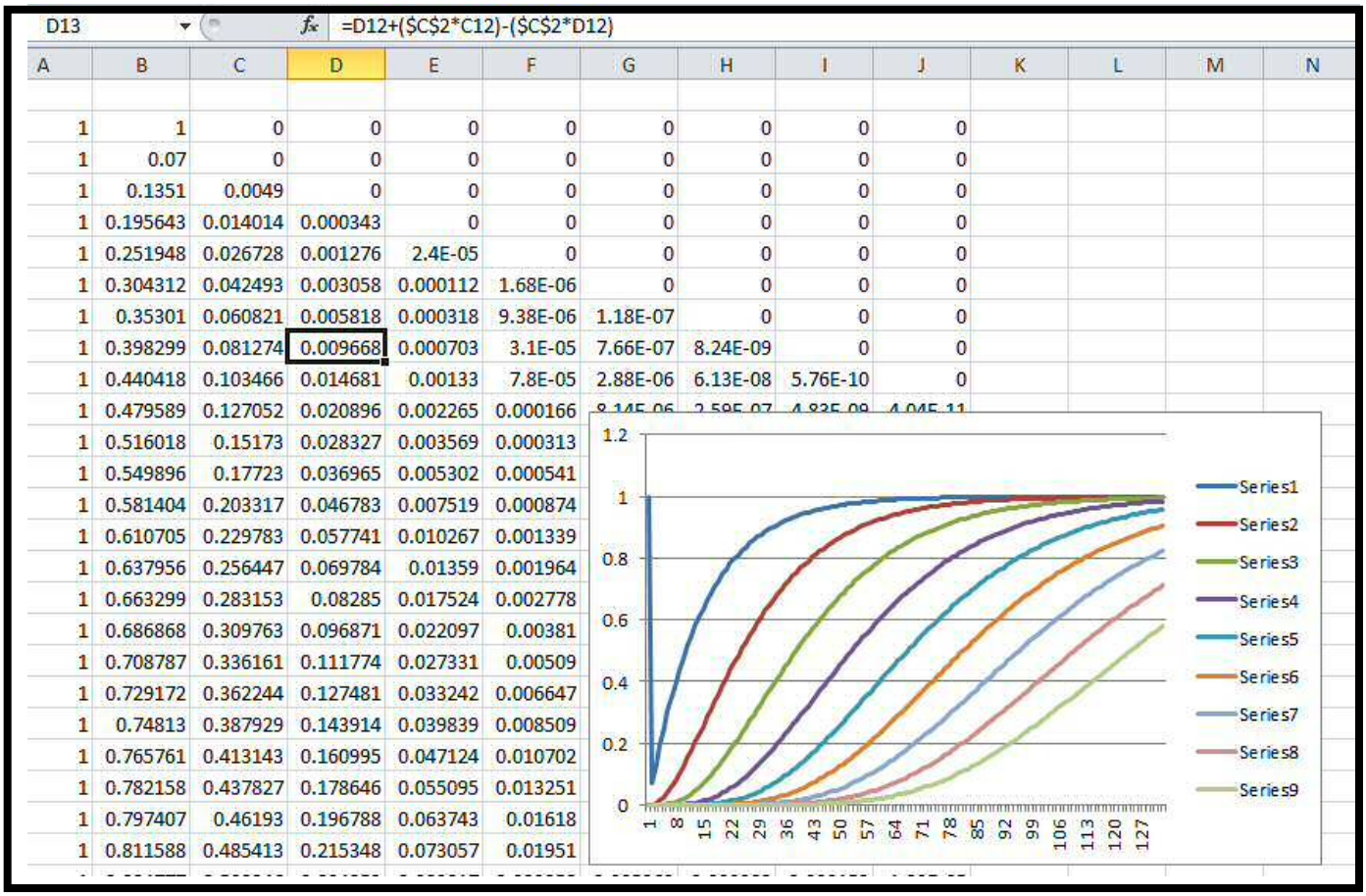

A	B	C	D	E	F	G	H	I	J
1	1	0	0	0	0	0	0	0	0
1	0.07	0	0	0	0	0	0	0	0
1	0.1351	0.0049	0	0	0	0	0	0	0
1	0.195643	0.014014	0.000343	0	0	0	0	0	0
1	0.251948	0.026728	0.001276	2.4E-05	0	0	0	0	0
1	0.304312	0.042493	0.003058	0.000112	1.68E-06	0	0	0	0
1	0.35301	0.060821	0.005818	0.000318	9.38E-06	1.18E-07	0	0	0
1	0.398299	0.081274	0.009668	0.000703	3.1E-05	7.66E-07	8.24E-09	0	0
1	0.440418	0.103466	0.014681	0.00133	7.8E-05	2.88E-06	6.13E-08	5.76E-10	0
1	0.479589	0.127052	0.020896	0.002265	0.000166	8.14E-06	2.58E-07	4.83E-09	4.04E-11
1	0.516018	0.15173	0.028327	0.003569	0.000313				
1	0.549896	0.17723	0.036965	0.005302	0.000541				
1	0.581404	0.203317	0.046783	0.007519	0.000874				
1	0.610705	0.229783	0.057741	0.010267	0.001339				
1	0.637956	0.256447	0.069784	0.01359	0.001964				
1	0.663299	0.283153	0.08285	0.017524	0.002778				
1	0.686868	0.309763	0.096871	0.022097	0.00381				
1	0.708787	0.336161	0.111774	0.027331	0.00509				
1	0.729172	0.362244	0.127481	0.033242	0.006647				
1	0.74813	0.387929	0.143914	0.039839	0.008509				
1	0.765761	0.413143	0.160995	0.047124	0.010702				
1	0.782158	0.437827	0.178646	0.055095	0.013251				
1	0.797407	0.46193	0.196788	0.063743	0.01618				
1	0.811588	0.485413	0.215348	0.073057	0.01951				

*Figure 2.5 Fick's Simulator. The figure shows a screen-shot of the Excel calculation used to predict diffusion using Fick's Law Fluxα (C1-C2), where the flux in unit time is proportional to the concentration difference between compartments C1 and C2. In the Excel sheet, column A is the unit-less time step (here simply a constant 1), the rows show the calculation for each subsequent time step, columns B - J are calculations for the signal increase at 9 adjacent "compartments" in the bleach zone and the insert shows the increase in fluorescence taken from the simulation by plotting the signal in 9 compartments against time. In this example, the concentration outside the bleach zone was unity (see cell B2), so that the recovery of fluorescence can be seen as a return to the starting value i.e. F/F_0. The highlighted cell (D13) shows the algorithm in the upper function box (fx= D12 + (C2*C12)-(C2*D12)) which was used in all cells.*

2.5.11.2 Relationship between diffusion rate to subdomain and cell surface topography

The diffusion coefficient, D (for DiI is a purely physical parameter), the time to arrive at a subdomain, depends on the actual diffusion distance. In the equation D x^2/τ, x^2 is the actual mean square displacement in time τ, which could be measured independently on smooth membranes. In membranes of unknown topography, y^2 is the apparent mean square displacement on a wrinkled surface in time τw. Given that the diffusion constant D for the molecule is unchanged $y^2/ x^2=\tau w/\tau$. Y/x is thus a ratio of the diffusion path lengths on the smooth and wrinkled surfaces and is calculated from the measured parameters √ ($\tau w/\tau$). Since the area of a smooth and wrinkled surface is proportional to the pathlength squared, ($\tau w/\tau$) gives a measure of the wrinkledness of the surface between the photobleach front and the subdomain; and is used in this thesis as the topographical index (Ti).

Thus Ti= $\tau w/\tau s$, where τw is the characteristic times for diffusion to the subdomain on the wrinkled cell surface and τ is the characteristic time for diffusion to the subdomain on a smooth surface.

2.5.11.3 Measurement of sdFRAP recovery rate constant

The recovery of fluorescence intensity in the subdomain will follow the exponential recovery curve,

$$\textit{Intensity} = 1 - e^{-kt,}$$

k is the recovery rate constant (s^{-1}) and t is the time after bleaching. The value of k was measured by curve fitting the recovery curve to this theoretical curve. This was done by

subtracting the background fluorescence after bleaching and dividing by the maximum fluorescence that was reached i.e. the normalised data was calculated as (I_t-I_0)/(I_{max}-I_0), where I_t is the intensity at any time after bleaching, I_0 is the intensity after bleaching (time zero) and I_{max} is the intensity after full recovery (at infinite time). The recovery curve therefore moves from zero (after bleaching) to unity (after full recovery). The exponential rise in fluorescence is defined by the exponential rate constant k (fig 2.6). By varying the value of k, the best fit of the data to the curve was obtained (fig 2.7). It is seen that a small change in estimated k value causes a large mismatch to the actual data (fig 2.7). The "best fit" had the minimum residual error. The value of k was easily estimated from the data, as when k = t the theoretical curve would give a value of $1\text{-}e^{-1}$ (0.63). The time at which this value is achieved would be 1/k seconds. In the example shown, the k value was found to be $0.17s^{-1}$ by curve fitting; and the reciprocal value (the characteristic time of the curve) of 5.8 seconds is shown on the curve. Knowledge of the characteristic time (or the k value) describes the entire recovery curve.

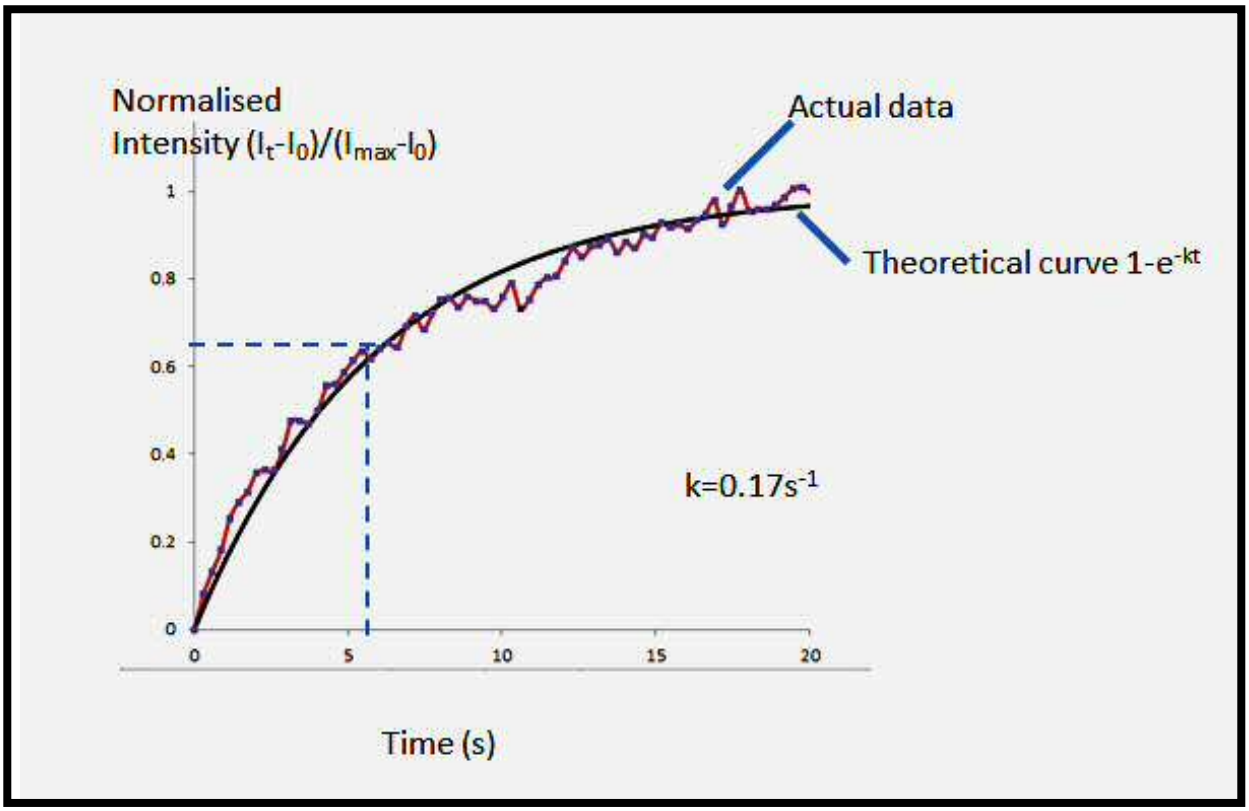

Figure 2.6 A typical recovery curve with the theoretical curve superimposed. The Curve was calculated for a k value of 0.17s^{-1} and was the best fit. The dotted lines show the position of the curve at 1-(1/e) which is 0.63. This gives a characteristic time of 5.8s (or 1/0.17s^{-1}).

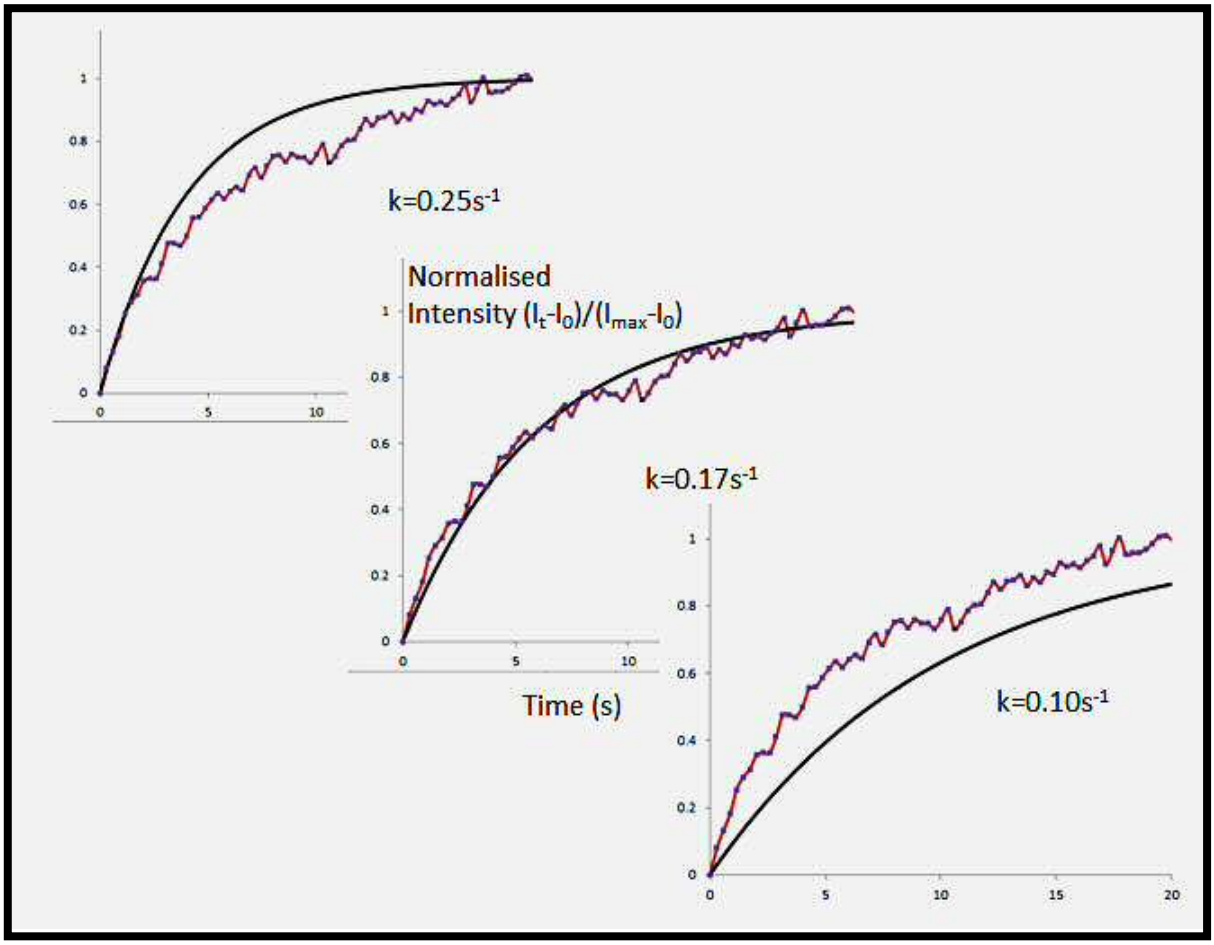

Figure 2.7 The effect of varying the value of k over a narrow range (0.1-0.25s^{-1}) in fitting the theoretical curve (smooth line) to the same experimental data. With a k value of 0.25s^{-1}, the predicted line reaches the maximum too soon. With a k value of 0.10s^{-1}, the predicted line reaches the maximum too slowly. However, with the "best fit" k value of 0.17s^{-1}, the predicted line follows the actual data over the recovery period from zero to unity.

2.5.11.4 Comparison of sdFRAP recovery curves.

In order to compare fluorescent recovery curves, it was first necessary to normalise the data by calculating the "normalised intensity" i.e. $(I_t-I_0)/(I_{max}-I_0)$, where I_t is the intensity at any time after bleaching, I_0 is the intensity after bleaching (time zero) and I_{max} is the intensity after full recovery (at infinite time). As the zero and maximum values are set, it allows the time of recovery (and the rate constant) to be compared directly. The reproducibility of the system was shown by the effects of two photo-bleaches performed under control conditions, (i.e. without any experimental manipulation between successive photo-bleaches). When undertaking this, it was found that the rate constants for each recovery were virtually identical. In many experiments, the same zone was bleached twice to test an experimental intervention between the first and second photo-bleach. Experimental manipulations were repeated on different cells and the resultant rate constants (K values) were compared experimentally using paired t-test (before and after treatment).

In the example shown in fig 2.8, successive bleaches have been compared. The raw data, the normalised intensity curves with fitted theoretical curves; and the two successive photo-bleaches can be superimposed. The curves were also compared on a point by point basis (rather than as a single rate constant). The residual difference between the curves or residual "error" being the value at time t from curve 1 minus the value at the same time for curve 2, divided by the value in curve 1 i.e. residual = (Ix1-Ix2/Ix12). If the curves are the same and difference are simply due to random noise, the sum of residuals would be zero (Σ (res) = 0), as result of the equal likelihood of positive and negative deviations. The mean of the residuals and the standard deviation of the data points was therefore used to perform a one sample t-test that the null hypothesis that the residual were not significantly different from zero. In the example shown in

fig 2.7, the mean residual was 0.00475 ± 0.037 (SD); n = 77. This was not significantly different from zero (p = 0.27) and showed that the curves were not significantly different. If this test failed, it would show that there was a different recovery rate (and hence diffusion path) after the two photobleaches. In all experiments shown, in which double bleaching was performed, the reproducibility was adequate to allow detection of differences in the rate constant if they occurred after experimental manipulation.

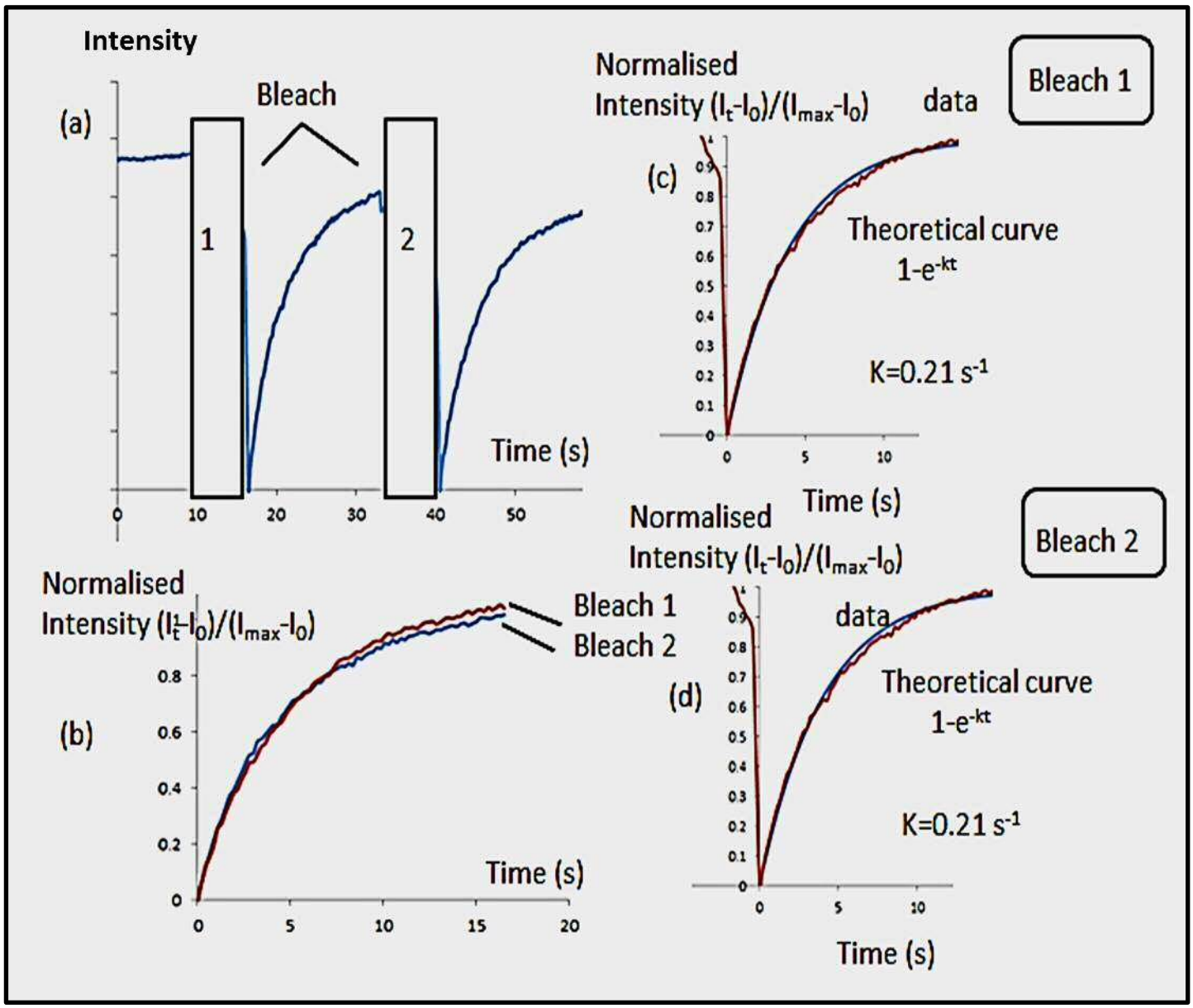

Figure 2.8 Reproducibility of sdFRAP recovery. (a) Shows a typical experiment in which double photobleaching of DiI on a labelled neutrophil is shown. The fluorescence intensity is shown as it changed with time. At zones 1 and 2 photobleaching was performed. (b) Displays the same data that have been compared for each recovery after normalisation. (c & d) Indicate the rate constant, k was estimated from the first and second bleaches. In both cases it was 0.21s^{-1}.

2.5.11.5 Necessity of fluorescent signal normalisation (F/F_0)

It was necessary to normalise the fluorescence intensity between different experiments because there were differences in the amount of DiI loaded into each cell and the detection sensitivity (laser strength and the PMT voltage) would be set to different parameters on different days. The standard method for normalising in this situation is to calculate the unit-less parameter F/F_0, which will be a value of between zero (total bleaching) and 1 (total recovery). The fluorescence intensity in the zone on the cell which was bleached was measured after full recovery and taken F_0 (i.e. the theoretical fluorescence at time zero being the recoverable fraction at photobleaching). The fluorescence intensity at every subsequent time point after bleaching (F) was divided by F_0. This ensured that for every cell the theoretical initial fluorescence was unity (i.e. F_0/F_0) and was a minimum of zero (e.g. when bleaching reduced the intensity to zero). The recovery after bleaching was always between zero and 1 and the timing of recovery could easily be compared. For example, when the fluorescence had recovered to 50% of the initial value, F/F_0 would always be 0.5 regardless of the starting intensity of the cell. As each bleach step on the same cell was a separate determination of recovery before and after a treatment, there would be two F_0 values, one for each pre-photobleach step. F/F_0 values were then calculated after the first photobleach, taking F_0 as the theoretical pre-photobleach intensity and F/F_0 values were calculated for the second bleach using the intensity before the second bleach as the F_0 value. In this way, recovery of F/F_0 values in the same cell could be compared.

2.5.11.6 Change in membrane wrinkle coverage after osmotic treatment

Before osmotic shrinking or swelling, the actual surface area (SA) of the cell is $W.4\pi R^2$, where R is apparent radius of the cell and w is the factor by which wrinkled membrane increases that area. After osmotic shrinking or swelling, the surface area (SA) = $w.4\pi r^2$ where r is the apparent new radius and W is the new factor by which wrinkled membrane increases that area.

Since the actual SA does not change during osmotic shrinking or swelling:

$$W.4\pi R^2 = w.4\pi r^2 \qquad \text{or} \qquad \mathbf{W/w = (r/R)^2}$$

Thus, if osmotic swelling causes the cell diameter to increase from 10μm to 11μm, the ratio W/w is $\sqrt{}$ (5/5.5) = approx. 0.95, i.e. the swollen cell has 5% less wrinkle coverage. If osmotic shrinking reduces the cell diameter from 10μm to 8μm, the W/w is $\sqrt{}$ (5/4) = 1.12, i.e. the shrunk cell has 12% more wrinkle coverage.

2.5.11.7 Relationship between fluorescence recovery rate constant at the subdomain and diffusion distance

The relationship x^2 t for sdFRAP recovery at subdomains at defined distances times can be shown experimentally. The plasma membrane of the tail region of a spread neutrophil, labelled with DiI, was photobleached and fluorescence recovery recorded in 100nm square subdomains, 500nm apart as shown in the example in Chapter 3 (fig 3.9). Recovery from the entire region (FRAP) and from the subdomains (sdFRAP) within the bleached area are shown, together with half times of recovery from the equally spaced subdomains estimated from the raw data. The graphs show the relationship for all subdomains taken from 2 successive photobleaches. The insert shows the untreated data and the main graph the relationship between time and the square of the distance with the fitted linear regression (R^2 = 0.97). However, estimating the $t_{1/2}$ value is prone to error as it is taken from a single time point. In contrast, the characteristic time τ can be estimated using all the data in the recovery curve.

Since the rise in fluorescence follows a simple exponential recovery $I_t = 1\text{-}e^{-kt}$ (where I_t is the intensity (as F/Fo) and time t and k is the rate constant (s^{-1}), the reciprocal of the rate constant, k, the characteristic time, **τ,** also describes the whole curve. Thus, fitting the recovery curve to the exponential equation to give the characteristic time is a robust descriptor of the sdFRAP recovery curves. It can simply be shown that the characteristic time, **τ,** is the sdFRAP diffusion distance in the same way as the half-time, as follows.

The diffusion of molecules from a constant source (of n_0 molecules) into the bleached zone follows the following relationship:

$$n(x,t) = n_0 \operatorname{erfc}\left(\frac{x}{2\sqrt{Dt}}\right).$$

n(x,t) is the concentration of molecules (n/n_o) at point x from the source at time t from onset of the concentration boundary (Berg, 1977; Bokshtein *et al.*, 2005; Crank, 1980).

Using the first 2 terms of the Taylor series to approximate the error function (erfc) gives the following simple expression.

$$n(x,t) = n_0\left[1 - 2\left(\frac{x}{2\sqrt{Dt\pi}}\right)\right]$$

The concentration of fluor (or intensity as F/F0) after photobleaching within the subdomain at a distance x from the bleach front is thus given by

$$F/F_0(x,t) = 1 - \left(\frac{x}{\sqrt{Dt\pi}}\right)$$

Thus, an intensity (conc. of fluor molecules) reaches a fraction of F_0 (i.e. when $F/F_0 = f$) within a subdomain at distance x when time is t:

$$\mathbf{x^2 = (1\text{-}f)^2 . \pi . Dt}$$

The time for the intensity to rise to a defined fraction of the final concentration is in proportion to the square of its distance from the source. This is a fundamental property of diffusion. The time to reach ½ the equilibrium concentration (half time, $t_{1/2}$) is thus given by $x^2 = (\pi/4)\, Dt_{1/2}$. The time to reach $(1/e)^{th}$ (characteristic time τ) of the equilibrium concentration is given by $x^2 = (0.4)\, \pi\, .\, D\tau$. Both half time ($t_{1/2}$) and characteristic time (τ) thus obey the relationship x^2 t and so give information of the diffusion distance.

2.6 Phagocytosis

2.6.1 Induction of Phagocytosis

Phagocytosis was induced using zymosan particles (10mg/ml) which were allowed to adhere to the glass coverslip. Free zymosan particles were washed away before allowing neutrophils to also adhere to the glass. On addition of normal human serum (1/10 dilution), complement was activated at the zymosan surface resulting in opsonisation of the particles (iC3b) and generation the chemoattractant C5a. Neutrophils near zymosan particles were thus induced to move towards the particles and undergo phagocytosis. The neutrophils were labelled by adding the DiI and then washed by adding Krebs medium. The images were taken during phagocytosis and FRAP experiments performed on chosen neutrophils at various stages of phagocytosis, including within phagosomes which were closed and those which were yet to close (i.e. open phagosomes).

FITC–conjugated zymosan particles were sometimes used, especially during the experimental manipulation of the surface topography by osmotic change. This enabled easier

analysis of the extent and rate of phagocytosis. Confocal images (or images sequences) were obtained during the process of phagocytosis.

2.6.2 Preparation of adherent zymosan

Zymosan particles, the cell wall of yeast saccharomyces cerevisiae comprising protein-carbohydrate complexes, were used as the phagocytic stimulus in these experiments. Zymosan was stored as a powder and suspended for use in physiological Krebs medium by vortex mixing to give 1mg/ml zymosan suspension. Microscopic inspection of the zymosan suspension was made to check that there were few large aggregates and further vortex mixing undertaken if necessary to produce single zymosan particles, ellipsoid in shape having a larger diameter of about 2-3μm (Pillemer and Ecker, 1941). Zymosan particles were allowed to adhere to glass coverslips by placing a droplet of zymosan suspension on a clean coverslip and left at room temperature for at least 15 mins. Adherence of zymosan particles was monitored microscopically and incubation extended if necessary. Adherent zymosan particles were easily identified as their Brownian motion ceases when firm adherence is made. Non-adherent zymosan particles were washed away by the addition of excess medium with the aim of producing a sparse coverage of adherent zymosan particles with sufficient space between particles and neutrophils, so that they occupy the cover glass without touching. An ideal coverage was about 1-2 zymosan particle/ 400μm^2. These zymosan-coated coverslip could be prepared in advance of the experiment.

2.6.3 Induction of phagocytosis of adherent zymosan by neutrophils

While observing microscopically, human neutrophils were added to the coverslip coated with adherent zymosan particles. A field was selected in which a neutrophil and a particle were within the same field of view. The zoom facility was used to provide good imaging conditions. Normal human serum (prepared as previously described, section 2.7) was added to give a 1/10 dilution. The reaction between complement within the serum and the zymosan cell wall generates C3bi, which opsonises the particle and at the same time C5a, a chemo-attractant, is produced. Within a short time (0-30s) neutrophils start to move towards the particle. Imaging sequences were often acquired at this time in order to capture the phagocytic event, which occurs when the front of the neutrophil is in contact with the zymosan particles.

2.6.4 Preparation of C3bi- opsonised zymosan particles

In some experiments, zymosan particles were opsonised with C3bi in vitro, so that the neutrophils were not exposed to C5a. Zymosan particles were opsonised by addition to the freshly prepared serum and incubated at 37^{o}C for 30 mins. The zymosan was then centrifuged and washed repeatedly to remove the activated serum (containing C5a). These particles were treated as outlined in section 2.6.2. Under these conditions, contact between the neutrophils and the particles were allowed to occur by random chance.

2.7 Fluorescent methods for measuring cytosolic Free Ca^{2+} concentration in neutrophils

2.7.1 Fluorescent Ca^{2+} indicators

Fluorescent probes for monitoring cytosolic free Ca^{2+} signalling using the confocal techniques have been assessed in neutrophils. The fluorescent probe Fluo-4 AM was normally

used to detect and measure Ca^{2+} changes in cells. It is a green fluorescent calcium indicator that can be loaded quickly into neutrophils. Fluo-4 AM stock solutions, prepared by diluting 50µg of it into 10µl of a dry anhydrous DMSO, were kept at 20^{o}C until required. 1µl of the prepared stock was loaded in a 1ml suspension of the cells. In order to let the cells take up the dye and convert the acetoxymethyl ester to the free acid (i.e. Fluo-4 AM to Fluo-4), they were left at the room temperature for 30 mins before starting the experiment.

2.7.2 Monitoring Ca^{2+} changes during FRAP experiments

After loading the cells with the Fluo-4 indicator, cells were left on the cover slip for about 5-8 mins at 37°C using an air-stream incubator. The cells were stained with DiI using the same methods described in (section 2.5.5). The changes of the Ca^{2+} were obtained throughout the bleaching of the tagged molecules in the neutrophil membrane using the sub-domain FRAP procedure described in section 2.5.8 and Chapter 3. Photobleaching was undertaken in two steps, one photobleach before stimulating of an elevating cytosolic Ca^{2+} and the other photobleach after stimulating an of elevating cytosolic Ca^{2+}. The stimulation was achieved either by adding FMLP to the cells (1µM) or by uncaged cytosolic IP_3 using brief UV exposure. The fluorescence Ca^{2+} indicator was excited by 488nm light and emitted light collected at 510 - 550nm. DiI was excited using the laser line at 543nm and bleaching performed as previously described (section 2.5.8) with maximum output of the 488nm laser line. There was no cross-talk between the signals.

2.8 Measurement of cell spreading

2.8.1 Measurement of spreading neutrophil diameters in cell populations

The Cellometer automated cell counter machine was used as an automatic method for counting cells of defined diameter. Although this device is conventionally used for cell counting, the software uses a size threshold algorithm to distinguish "cells" from noise or debris. However, by setting size thresholds at different levels, a cell size distribution was generated so that a change in cell diameters within a population of cells was obtained in real time as they spread onto a surface. Thus, the spreading competencies of the whole neutrophil populations were achieved to determine the measurements for an individual cell. To measure and calculate the cell populations diameters in this experiment, the cell sizes were set from 7 to 20µm. In order to determine neutrophils spreading on a glass surface, it was necessary to modify the counting chamber by setting glass coverslips between the top and the bottom half of the chamber (fig 2.9). Neutrophils (10µl suspended in 500µl HBK medium) were added onto the adjusted Cellometer slides, using Pipette 20µl and left for two minutes to settle on the glass and spread spontaneously. The measuring time to the spreading diameters of neutrophils in the populations was within 15 mins. Data and images of the neutrophils spreading were recorded at defined intervals.

The data are described as mean +/- S.E.M. The means from different experiments were compared by one-way analysis of variance. The comparisons were made using Student's *t*-test for unpaired values and the statistical significance set at $p<0.05$. Each of these experiments was repeated at least 5 times on different cell populations and at least 500 cell diameters recorded.

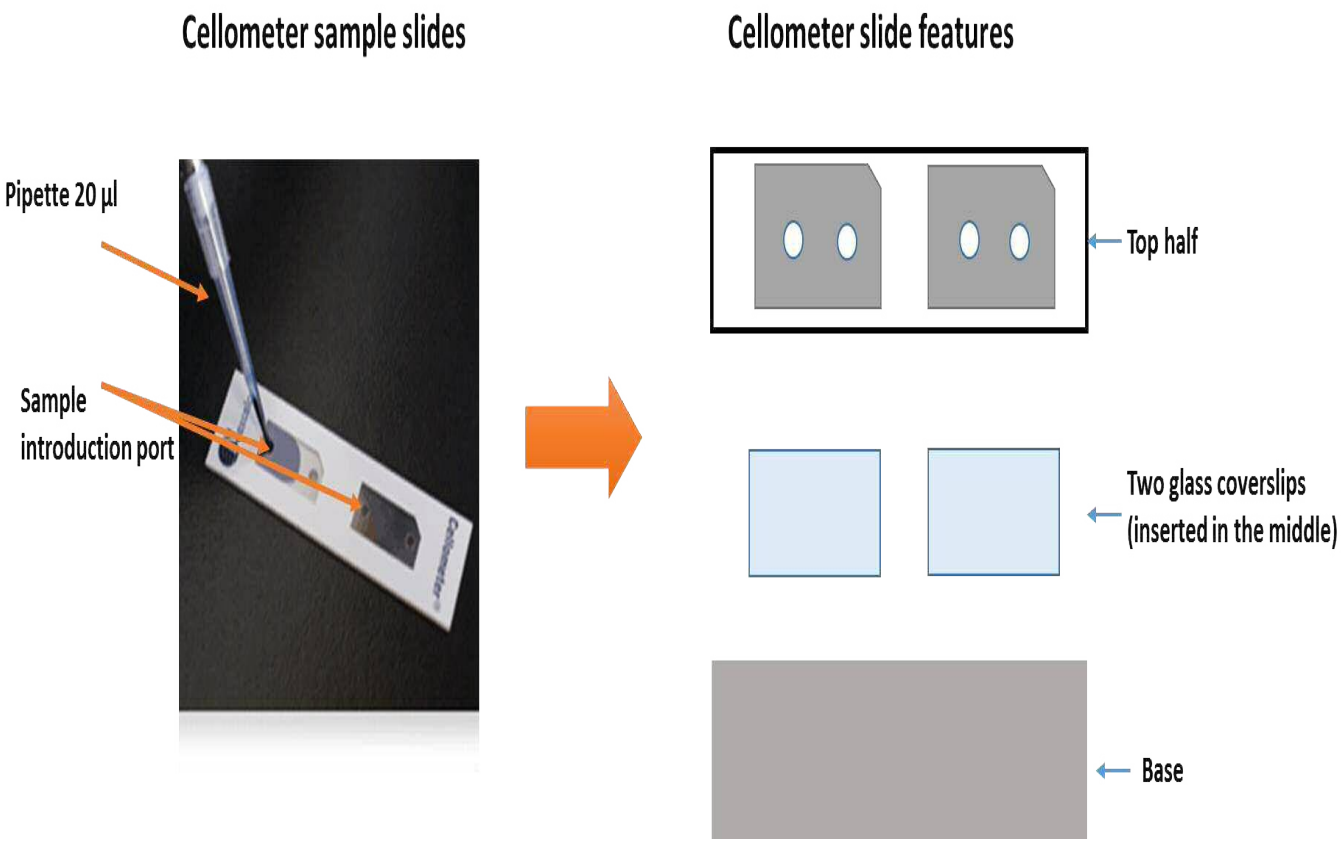

Figure 2.9 The Cellometer slides and glass coverslips for measuring the change in neutrophils diameters within a population. Inserting the glass coverslips allows spreading of the cells onto the surface and the slides were then attached back together.

2.8.2 Single neutrophil spreading measurements

In order to establish the time course of spreading of individual cells, rather than a shift in population distribution of sizes, individual neutrophils were allowed to sediment onto glass coverslips at 37^{O}C whilst acquiring confocal images and the complete spreading event recorded. The diameter of the cell on each image of the recorded sequence was measured and the time of onset of spreading and maximum spread size determined.

2.9 Scanning Electron Microscopy

Neutrophils were fixed in suspension with glutaraldehyde (4%) overnight. The fixed cell suspension was filtered on to porous membranes to produce a stable population of fixed cells for dehydration and sputter coating with gold. Sputter coating is an ultra-thin coating of electrically-conducting material, deposited by low vacuum coating of the sample. This is done to produce a faithful reflection of the surface contours of the cells and to increase the amount of secondary electrons that can be detected from the surface of the sample, thereby increasing the signal-to-noise ratio. It also prevents charging of the specimen which would occur during imaging by the accumulation of static electric fields as a result of electron irradiation. The gold-coated sedimented neutrophils were imaged using a JEOL 840A scanning electron microscope (Joel UK, Hertfordshire, UK) within the Electronic Microscopy Unit of Cardiff University Medical School, operated by Dr Chris von Ruhland. Images were acquired using analySIS (Munster, Germany) and quantified using ImageJ.

2.10 Statistical analysis

Data in this thesis were analysed using Excel or GraphPad Prism 5.01 software (GraphPad software Inc). Where possible, one-way ANOVA of variance with Bonferroni post-hoc testing (with correction for multiple tests) or t-test was performed for normally distributed data. For non-parametric data the comparisons were made using Kruskal-Wallis test/ Dunn's Multiple Comparison post-tests or Mann Whitney U tests especially when the sample size was small. Results were viewed as statistically significant when the *p* value <0.05.

Chapter 3

Developing a new method for monitoring cell surface topography in live cells

3.1 Introduction

At present, there are no methods for investigating surface topography in living cells. A new method is therefore needed. In this chapter, I will describe how subdomain FRAP (fluorescence recovery after photo-bleaching) may be used to provide information of the cell surface topography. It is well known that fluorescence tagged molecules within living cells are useful for examining and measuring dynamic cellular events. FRAP has been employed to study the movement of molecules within living cells. As the method depends on monitoring the recovery of fluorescence following photobleaching of tagged molecules, it may also be useful for monitoring cell surface topography (Reits and Neefjes, 2001). In this chapter, data will be presented to show that the movement of cell surface fluorescent molecules can reveal the distance that diffusion has occurred, this can be used to examine the cell surface topography.

3.1.1 Fluorescence and photobleaching

Within cold bodies, fluorescence is an optical phenomenon that results from absorbance of light of a specific wavelength by certain molecules. After a short delay, the same molecule emits a lower energy photon and hence light of a longer wavelength. The delay is known as the fluorescence lifetime. The change in energy between the absorbed and produced photons is the result of molecular vibrations during absorbance (excitation). As a result of the absorbance of energy by the molecule, bonds can be broken and covalent modification occurs such that the fluorophore is no longer fluorescent. This photon-induced chemical damage is irreversible and is called photobleaching and the features of photobleaching differ in each fluorophore. Before the molecules of the fluorophore are irreversibly photobleached, they experience a number of

absorption-emission cycles. The average number of excitation and emission cycles is determined by the local environment and by the molecular structure and fluorophore-specific property (Dittrich and Schwille, 2001).

Photobleaching is linked to the process of transition from an excited singlet state to the excited triplet state, a method termed intersystem crossing. However, the particular photobleaching mechanism is not yet identified. When the excited molecules withdraw from the absorption-emission cycle, they have a much longer timeframe and are able to undergo chemical reactions with components in the environment, which may form the basis for bleaching reactions. This is because the triplet state is relatively long-lived with respect to the singlet state. Emitting a few photons will cause rapid bleaching to some fluorophores. However, more robust fluorophores may possibly go through thousands or millions of cycles before bleaching (Dittrich and Schwille, 2001).

3.1.2 Principle of confocal laser scanning microscopy

In the mid-1950s, the basic concept of confocal microscopy was first established by Marvin Minsky (Minsky, 1988). This microscopy is known to be an important tool for a wide collection of studies in the biological and medical sciences. Thus, it has the ability to image thin optical sections in living and fixed samples reaching around 100µm in thickness. Also, it is considered to be a great standard tool for achieving FRAP experiments. The modern tools have been equipped with 3 to 5 laser systems that are regulated via high-speed acousto-optic tunable filters (AOTFs). Photomultiplier tubes, connected to the confocal microscope, have the

ability to measure the emission of fluorescence between 400 and 750nm. Through this connection, it shows high quantum efficiency in the near-ultraviolet, visible and near-infrared spectral regions. The laser systems are useful for very specific control of wavelength and excitation intensity. Also, this microscopy has spectral imaging detection systems that enable advanced refinement of the technique. This includes fluorophore resolution with overlapping spectra and also provides the ability to compensate for autofluorescence (Minsky, 1988).

Synthetic and naturally occurring molecular probes such as fluorescent proteins and quantum dots have been improved due to the recent advances in fluorophore design. Therefore, these molecular probes may display a great level of photo stability and target specificity (Pawley, 1995). The light source of a laser scanning microscope is one or more laser(s). The use of a laser as illumination source has two major consequences. The excitation light bandwidth is determined by the source and not by an excitation filter and thus is much narrower than in fluorescence microscopy (2 - 3nm rather than 20 - 30nm).

Illumination of the total visual field is achieved by scanning the sample with the laser beam sequentially point by point and line by line. The photomultiplier tube (PMT) is used to measure the fluorescence emitted at each point and the image construction is achieved through collecting all the pixel data into single image (fig 3.1). There is a huge benefit of this technique of illumination through the possibility of selecting regions of the visual field to illuminate. The fundamentally significant point to the confocal method is realised by eliminating the out-of-focus light in specimens. This can be seen using a spatial filtering technique with thickness, which is able to go above the immediate plane of focus. PMT can record only light

from the focal plane due to its location behind the pinhole. Thus, confocal microscopy is able to image optical slices of the specimen, that can be done either by high contrast or through high resolution in x, y and z. From the focal plane, it is possible to record (optical slices) single images once the focus plane is moved in z-direction and then processing the slides together will provide a reconstructed image of the 3-dimensional object (Michael, 2015).

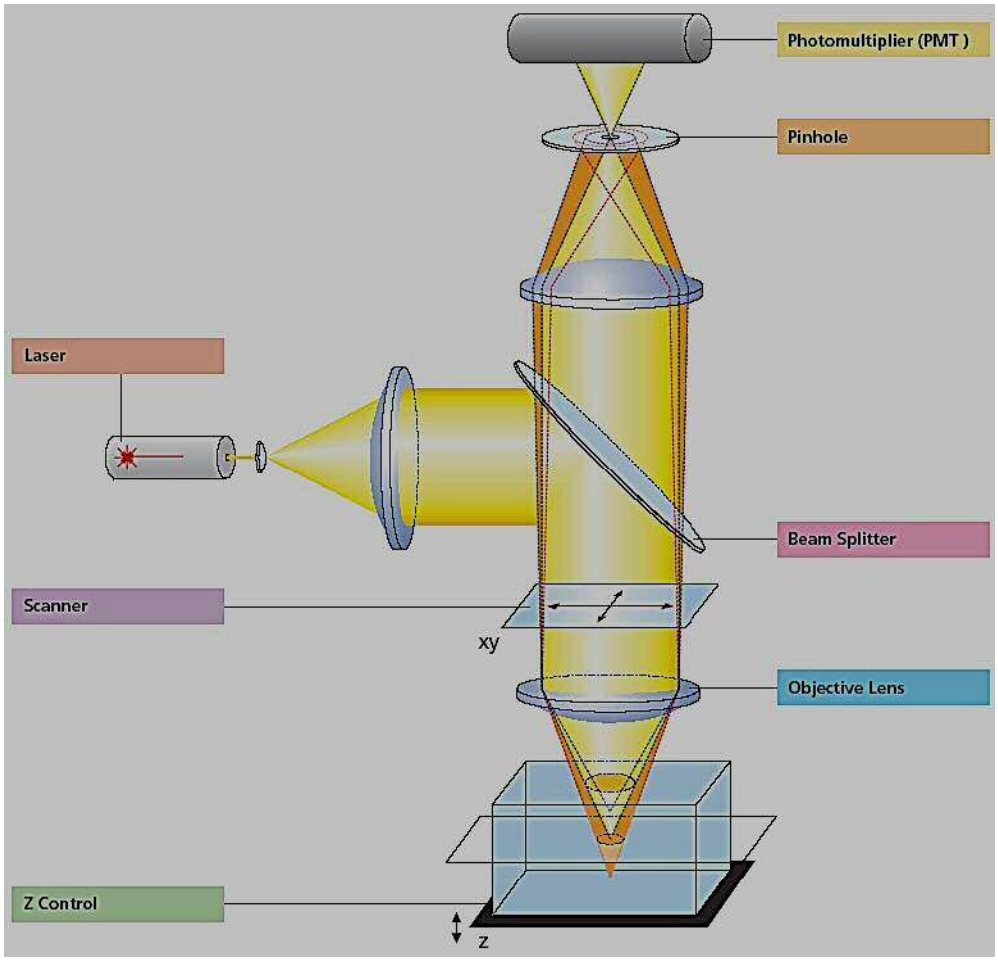

Figure 3.1 Confocal laser scanning microscope. The whole visual field is achieved and scanned due to the laser beam that causes the illumination. The out of focus light is decreased by a pinhole [Taken from (Michael, 2015)].

3.1.3 Theory of FRAP experiments

FRAP is achieved by introducing a rapid shift away from the steady-state distribution of fluorescent molecules without disrupting the actual concentration of the molecule under study (Robert and Misteli, 2001). FRAP experiment is realised when irreversible photobleaching of fluorescent molecules in the cell membrane are bleached by an increased localised focus argon laser beam (Reits and Neefjes, 2001) (fig 3.2). This generates conditions where the probe molecules in the illuminated region are bleached and recovery occurs when they are replaced by fluorescent molecules in the surrounding unilluminated region. This leads to a mixture of fluorescent and non-fluorescent molecules over time until a steady-state distribution is reached (Robert and Misteli, 2001). The movement of the non-bleached fluorescent molecules into the bleached area leads to a recovery of fluorescence, which is recorded at low laser power (Robert and Misteli, 2001). The rate of recovery of fluorescence is limited by diffusion and the distance molecules must travel. If a subdomain within the bleached area is monitored, the distance of the subdomain to the bleach front is known in 1 dimension (D) and thus the time taken for molecules to arrive is limited by its 2D travel distance (fig 3.3). Since the diffusion constant of a particular probe is fixed, changes in the recovery rate will reflect changes in the distance travelled by the molecule (Reits and Neefjes, 2001) in 2D but also as a result of the 'non-flat' topography (fig 3.3). This will therefore give an indication of the cell surface topography in the bleached region of the cells.

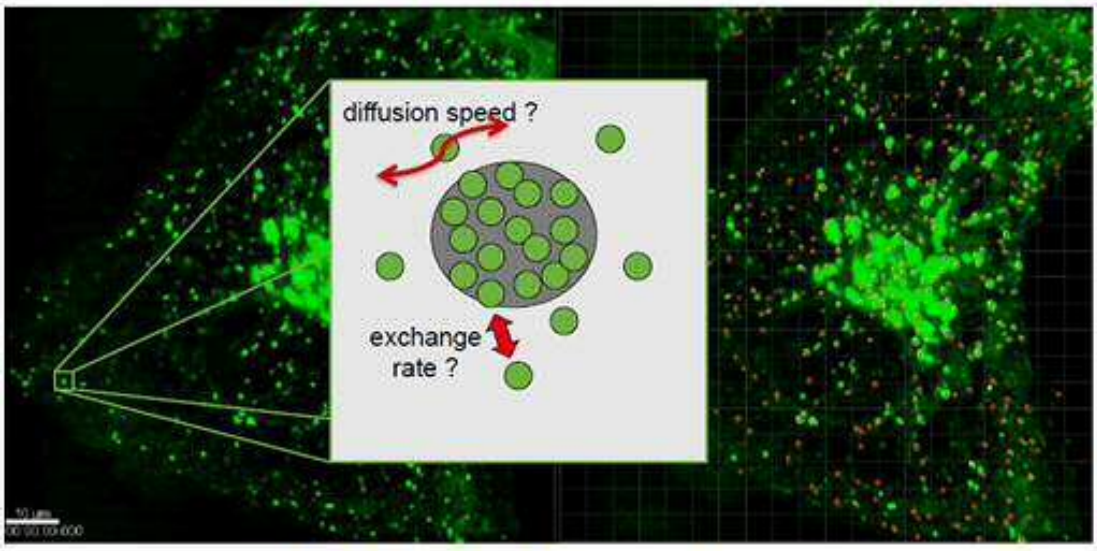

Molecular Dynamics

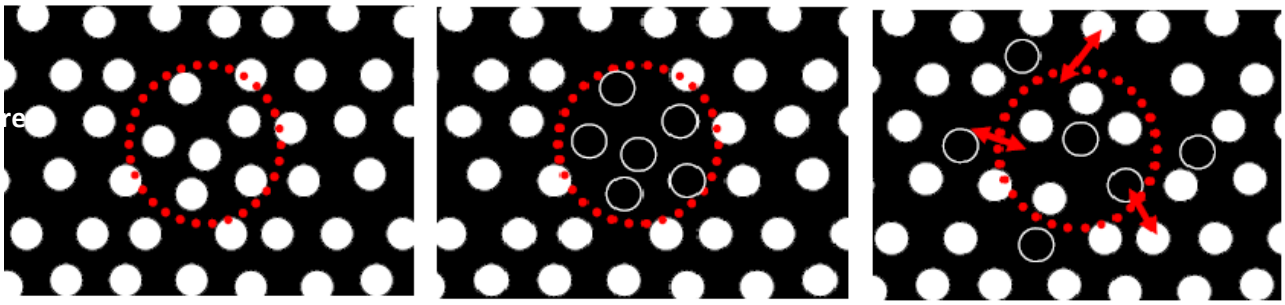

Fluorescence recovery after photobleaching

Figure 3.2 Representation of the FRAP process. These diagrams illustrate the process of photobleaching of fluorescent-labeled cell molecules. The images [taken from (Terjung, 2011)], illustrate the need to consider the diffusion speed and exchange rate between the bleached and non-bleached regions. The lower time series (pre-bleach, bleach within red zone and post-bleach recovery of fluorescence) demonstrates that fluorescently labelled molecules can be specifically bleached and that diffusion follows this process, leading to delineation of the bleached area and a rise in relative fluorescence.

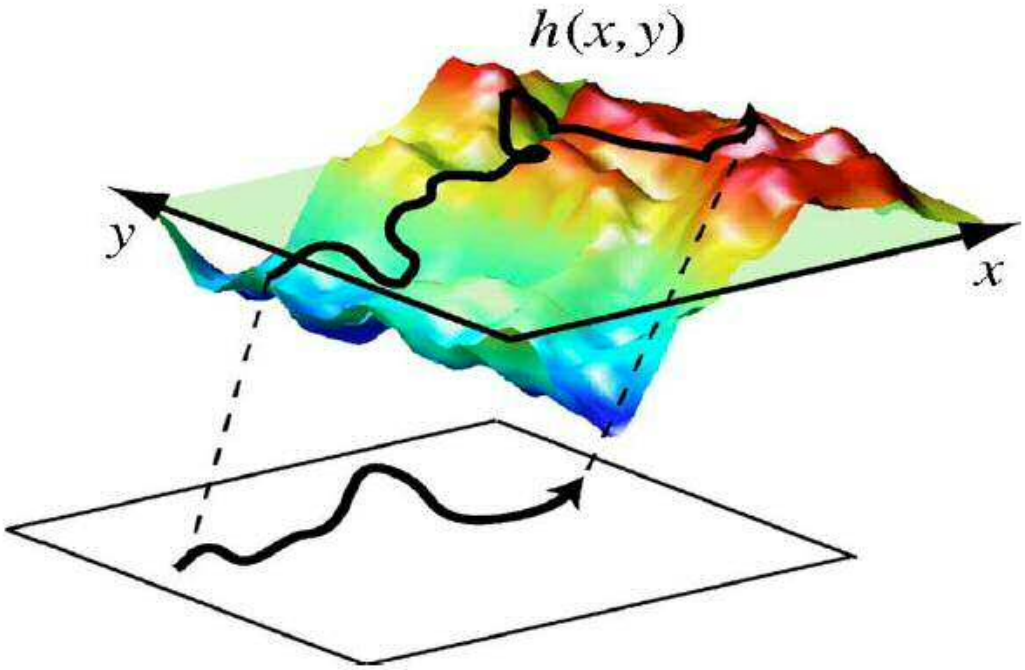

Figure 3.3 The diagram shows the apparent diffusion distance of a molecule in 2D and the actual 3D distance travelled as a result of a non-flat topography. [Taken from (Naji and Brown, 2007)]

3.2 Aim of this chapter

The aim of the work in this chapter is to develop a method for monitoring the cell surface topography. This will be achieved by using a novel variation on standard FRAP whereby the recovery of the fluorescent signal at a bleached region of membrane is recorded at a define distance from the bleach front. The time for molecules to arrive at this region (or sub-domain) will depend on the pathlength for diffusion. The methodology will be set up, optimised and the validity of these measurements established by experimental manipulation of the neutrophil plasma membrane. The new method is called subdomain FRAP (sdFRAP) to distinguish it from conventional FRAP.

3.3 Results

3.3.1 Fluorescent labelling the neutrophil plasma membrane

Initial experiments were conducted in order to determine the most suitable means of labelling neutrophil membranes for fluorescence detection. Several probes were investigated of which DiI, PHK26 and FM generated significant plasma membrane staining (fig 3.4 A). However, FM1-43 and PHK26 dyes were not suitable markers to label the plasma membrane of the cells, as they provided low quality images and resulted in a large number of crystals that might affect the experimental outcomes. In contrast, DiI was a more appropriate dye giving specific and clear membrane labelling. Therefore, cells labelled with DiI were investigated regarding their bleaching properties. Significant bleaching was achieved at 488nm illumination, 15s of bleaching reducing the signal from 200 to 60 arbitrary units. It was apparent that DiI labelling varied between different cells, with staining appearing 'thicker' in some cells than others. This was attributed to the ability of DiI to report on the extent of membrane wrinkledness (thicker staining), more wrinkled, (fig 3.4b). It was also seen that two different cells bleached at the same time, had different results, one cell bleaching very slowly and recovering very quickly; and the second bleaching very quickly and recovering very slowly.

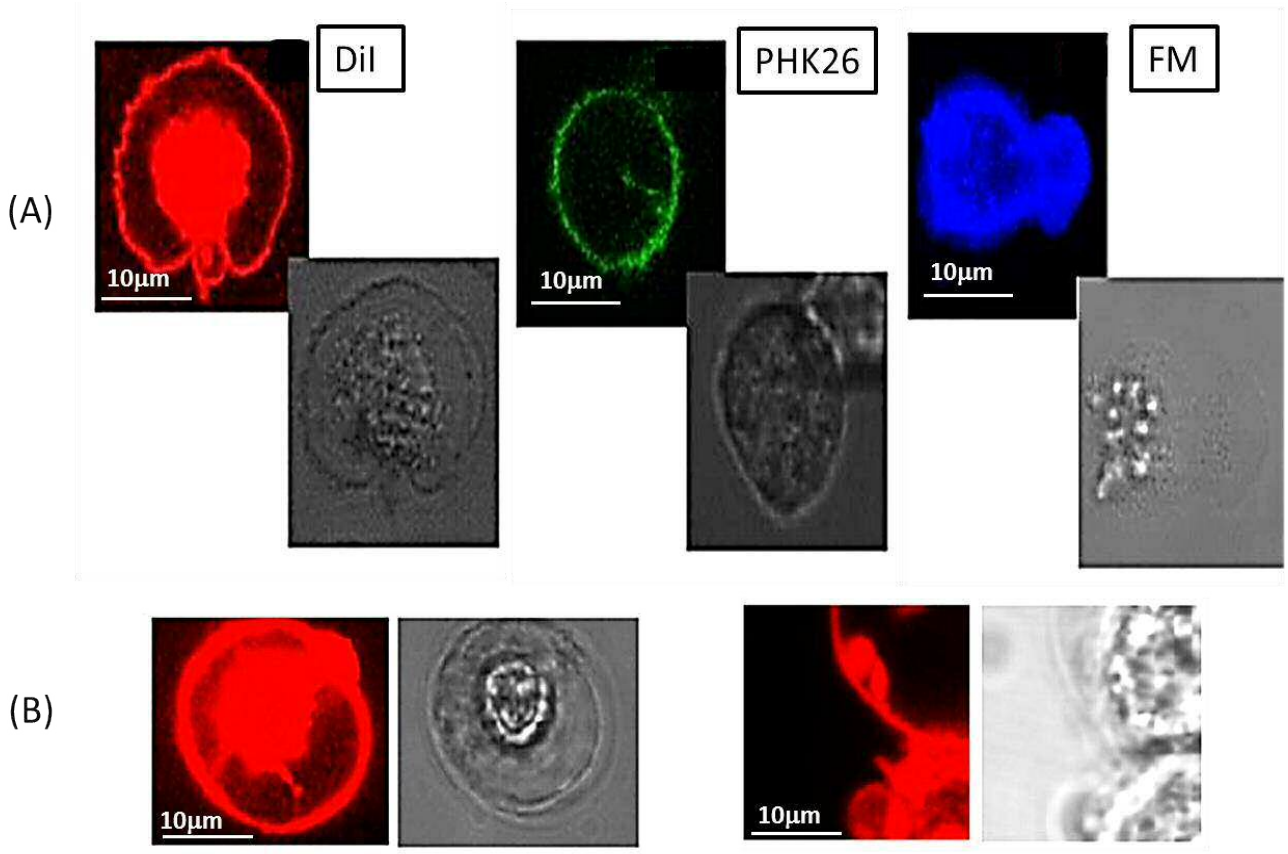

Figure 3.4 Efficiency of markers for cell surface topography measurements. (A) The fluorescent and phase contrast confocal images of living neutrophils stained with DiI, PHK26 or FM1-43 are shown. (B) Visual inspection of the apparent thickness of peripheral DiI staining in spread and "bloated" cells suggested that the DiI reported different states of membrane wrinkledness and thus these preliminary results suggested that the signal from DiI was sensitive to surface topography. Each image shown is typical of at least 10 other cells observed. This experiment was achieved four times on a single day and it was repeated six alternative days and neutrophils were sourced from four separate donors.

3.3.2 Photo-bleaching and recovery characteristics of DiI in the neutrophil membrane

Following identification of DiI as a suitable marker for cell surface topographic changes, it was necessary to characterize FRAP in order to understand these changes during further experimentation. The FRAP signal from normal neutrophils is shown in the explanatory diagram (fig 3.5), where (a) indicates the initial intensity at the membrane, (b) the fluorescence intensity decrease as a result of photo-bleaching, (c) a gradual recovery in intensity as diffusion occurs to the point of measurement and (d) the steady state level reached within 70s. The pre- and post-bleach levels indicated as x and y values were used to calculate the equilibrium recovery of fluorescence ((y/x) x 100 = % recovery).

In this example, the bleach zone was about 10% of the cell surface and thus 10% of the molecules were bleached. This means that at full recovery, the intensity cannot be 100% of the starting value; but instead it is (100-10)% i.e. 90%. When calculating recovery kinetics (or recovery time), it is obviously important that final equilibrium level is used (defined as F_0). The extent of the reduction in the equilibrium level after photobleaching is dependent on the area bleached and, importantly, the duration of the photobleaching. If photobleaching requires too long a duration, because it is inefficient (or the probe is resistant to bleaching), diffusion of fluorescent marker molecules into the slowly bleaching zone will occur and they will also become bleached. If bleaching is very slow, all the molecules in the cell will be bleached. Thus, it is important that DiI can be bleached efficiently so that sufficient fluorescent molecules remain for the recovery to be measured. The data shown in (fig 3.5), therefore show that DiI has acceptable “bleach-and-recovery” characteristics to be used in this study.

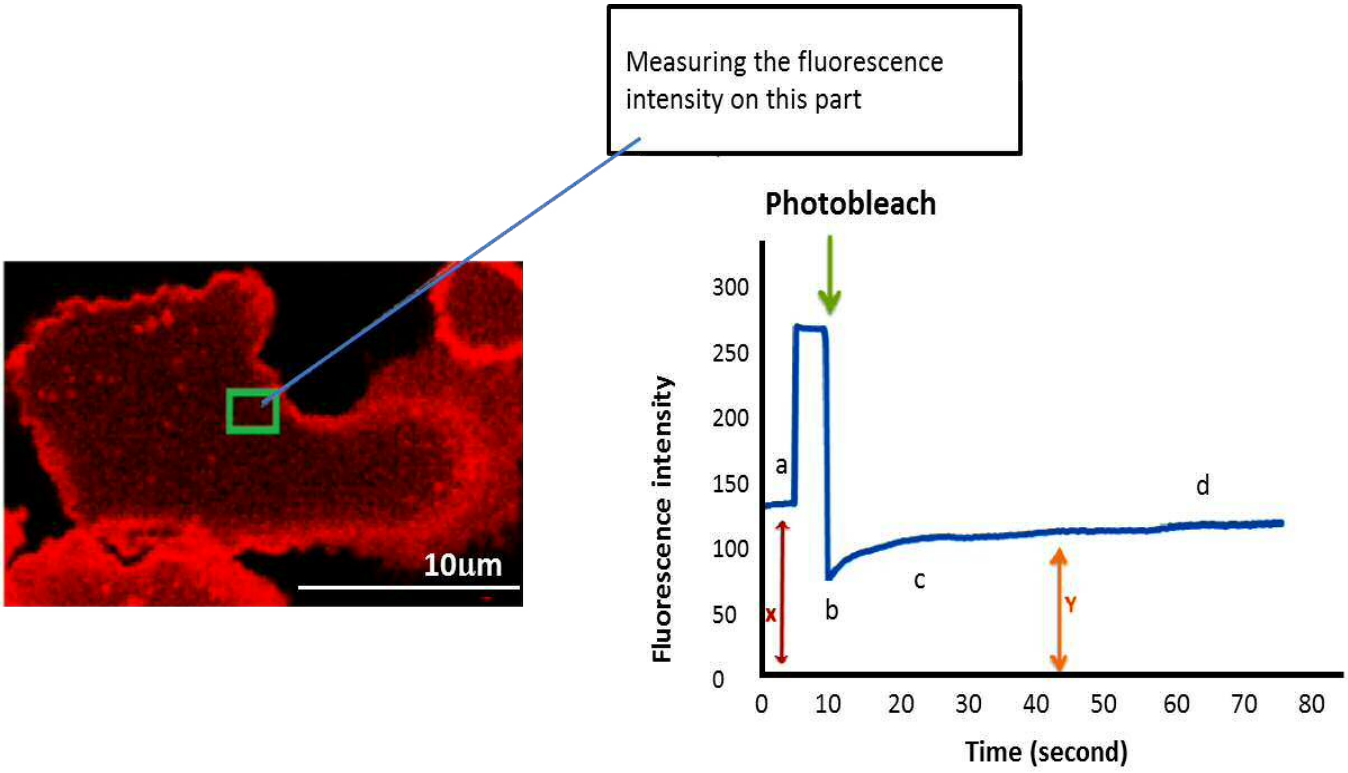

Figure 3.5 Bleach-and-Recovery of DiI in the neutrophil plasma membrane. The data are taken from a typical "bleach-and-recovery" experiment. (a) Is the initial intensity before the elevation of the signal at the point of photobleaching (resulting from the increased laser strength required for photobleaching, it peaks at 255 units, the maximum (8 - bit) signal of the detection system). As this is not relevant to the data, in most other examples given in this thesis it has been removed. However, for completeness, it is shown here together with (a) the initial intensity at the membrane, (b) the fluorescence intensity after photo-bleaching, (c) the recovery phase and (d) the steady state level. X and Y show the pre- and post photobleach fluorescence levels used to calculate the percentage recovery.

3.3.3 Validation of sdFRAP as a measure of distance

The aim of the sub-domain FRAP (sdFRAP) methodology is to measure the diffusion distance on the neutrophil surface. In this way, information will be gained about the cell surface topography. In order to assess the ability of sdFRAP to monitor diffusion distance, a flat membrane with no topographical features would be required. Once spread onto a glass surface, neutrophils polarise to form a leading edge and a uropod or "tail". The "tail" can spread to a surprising degree and will form a large flattened membrane. The 2D distance on this flat surface will be equivalent to the diffusion distance and so provided a test of the sdFRAP methodology. The diffusion of DiI into the tail region following photobleaching showed that diffusion was unimpeded and DiI diffused into the main part of the tail and along its smaller "branches" (fig 3.6). This experiment clearly showed that the recovery kinetics depend on the position of the measurement subdomain, the further from the bleach front, the slower the recovery of fluorescence (fig 3.7). The recovery after photobleaching was monitored by confocal laser scanning microscopy as a continuous time course (which can be viewed as a movie).

By recording the intensity of DiI in defined regions within the bleached tail (i.e. FRAP subdomains), there was a clear delay in achieving half maximum signal which was related to the distance from the bleach front. At 4μm and 8μm from the boundary the half times were 11s and 32s, respectively (fig 3.8). These times correspond to the same diffusion constant (of about 1.43μm^2/s) and are thus consistent with simple diffusion on a flat surface. The shape of the recovery curves was also dependent of the distance. A simulation of the kinetics of diffusion over a linear path can be generated using Fick's law of diffusion (fig 3.8).

Briefly, in this diffusion simulator (see Chapter 2.5.11.1: Fick's Law simulation), a section of membrane, divided into equal compartments, with the same area of contact to the next such that the flux in unit time (J) from each compartment to the next is driven by the concentration difference across the boundary between compartments. This follows Fick's Law: J (C2 - C1) where J is the flux from one compartment to the next and C1 and C2 are the concentrations in each compartment. The concentrations at each unit step in time in each membrane compartment (distant from the diffusion front) were thus calculated and the change in concentration over time plotted for different subdomains (fig 3.8). In this simple simulation, the effect of measuring the concentration at distances remote from the bleach front can be seen (fig 3.8), with delays in fluorescence recovery occurring at increasing distances, as well as differences in rates of recovery.

It can be seen that there is an agreement between the theoretical (fig 3.8) and observed (fig 3.7) shapes of the recovery curves. sdFRAP would therefore be potentially useful in interrogating the surface topography of neutrophils. A deviation from the "flat" diffusion kinetics which was seen in the flat tail, would indicate that the diffusion pathlength was longer and thus that the surface was not flat but had "hills and valleys". Furthermore, there is a relationship between the diffusion distance and the half time for fluorescence recovery at the subdomains is shown in figure 3.9. As before, the plasma membrane of the tail region of a spread neutrophil, labelled with DiI, was photobleached. The fluorescence recovery was recorded in 100nm square subdomains, each 500nm apart. The graphs show the relationship for all subdomains taken from 2 successive photobleaches and the method for determining the relationship between time and the square of the distance. As predicted, the diffusion constant

for DiI constant, D, $t_{(0.5)}$ was proportional to the diffusion distance, with a linear regression R^2 = 0.97. This relationship between either the half time or the characteristic time (see section 2.5.11.7) can be used to establish the diffusion distance (section 2.5.11.3). As the characteristic time is the inverse of the rate constant, it will be important to use the recovery data curve to find the rate constant.

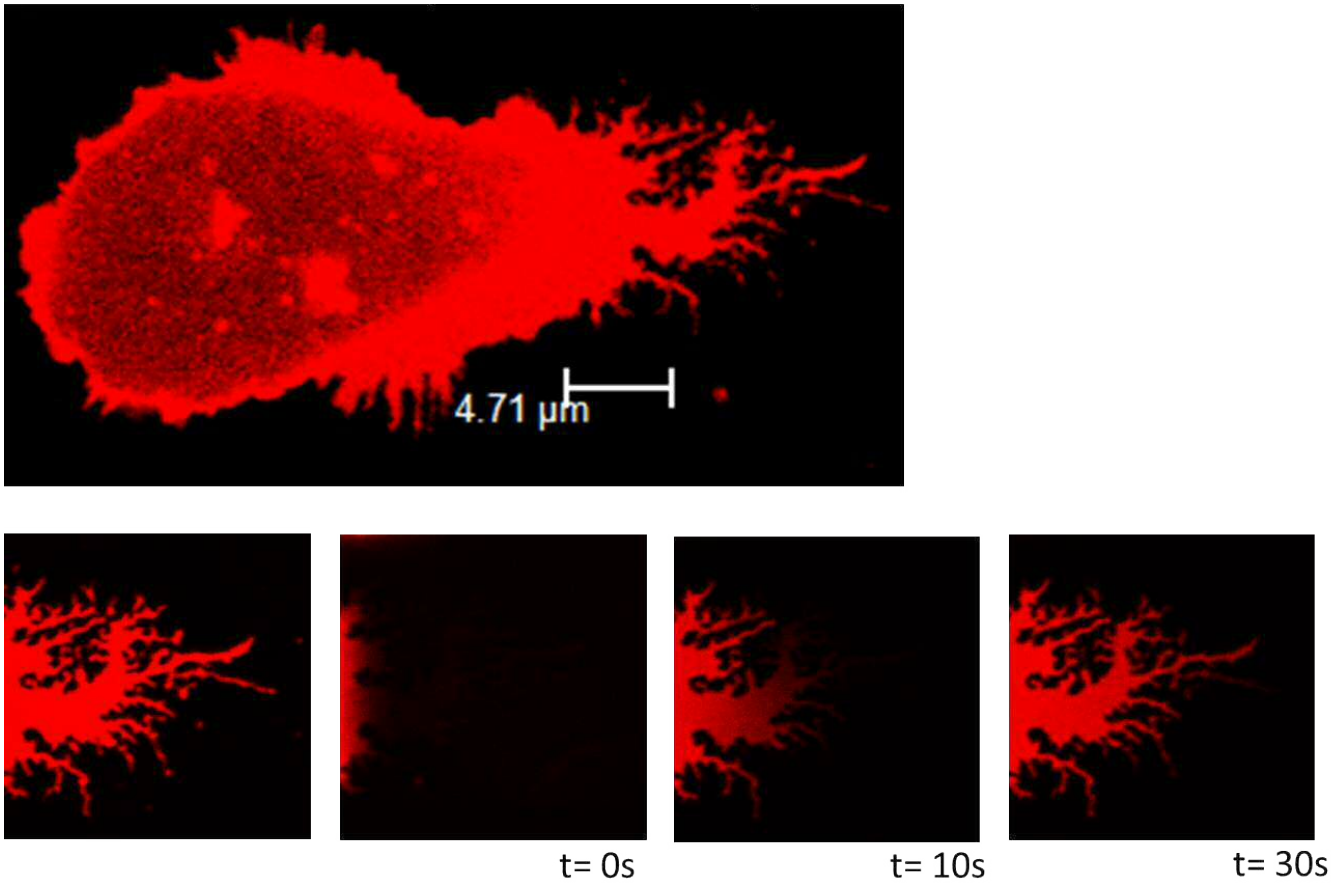

Figure 3.6 Diffusion of DiI into the flattened neutrophil tail. The upper image shows the distribution of DiI in the membrane of an entire spread and polarised neutrophil with the cell body and the flattened and branching tail (to the right). Photobleaching was achieved by zooming in to the required region of the cell as indicated in the lower panel. The 488nm laser intensity was then increased to maximum sufficient time to achieve significant photobleaching (1 - 15). Areas of the cell outside the bleach zone were not exposed to this high intensity laser excitation. The lower set of images show the tail region within the bleach zone before and at the time of photobleaching (time zero), followed by images at 10 and 30 seconds after bleaching. This experiment gave similar results when performed on at least five similar polarised cells from two different blood donors on two separate days and similar quantitative results were obtained from at least 20 subdomain locations.

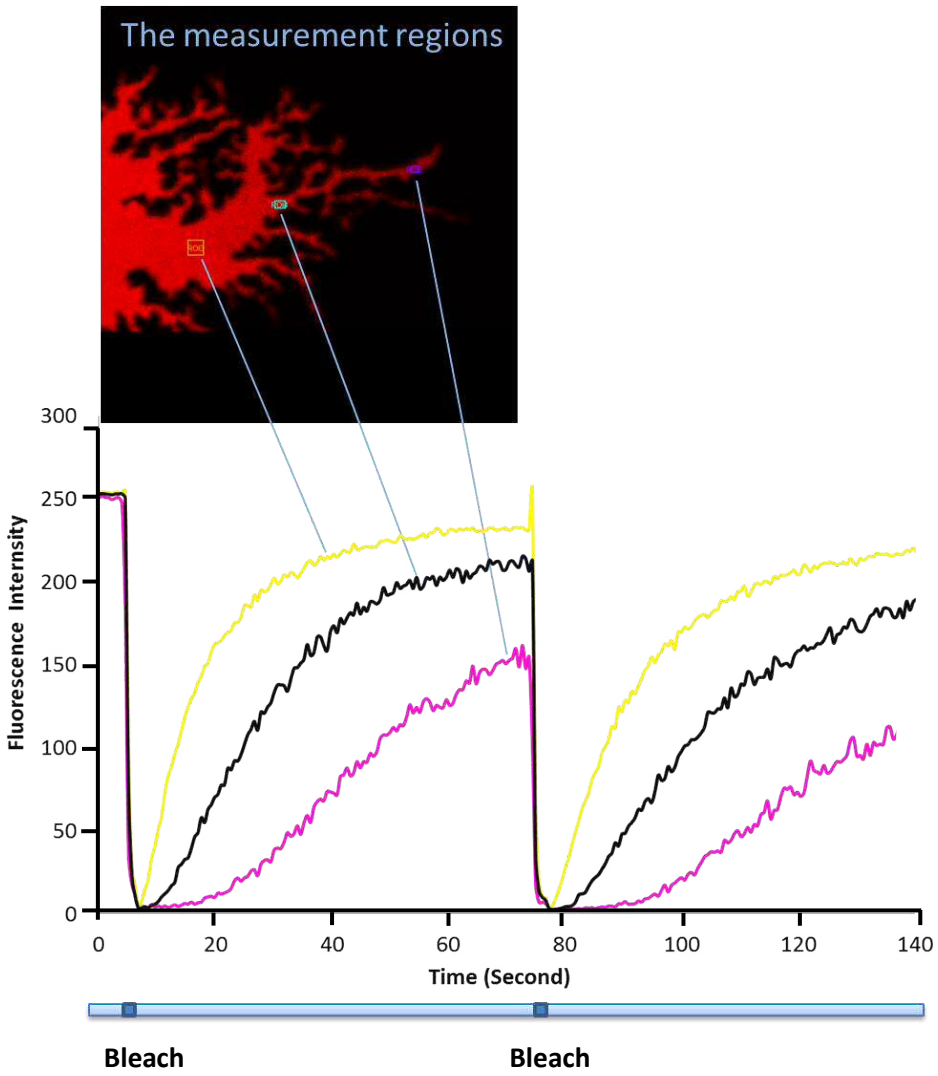

Figure 3.7 Kinetic sdFRAP measurement in the neutrophil tail. The image shows the position of three measurement subdomains within the bleach zone (see fig 3.6); each zone is 4μm apart i.e. 4, 8, 12μm from the photo-bleach front. The raw data from each subdomain is shown as indicated on the continuous recording below, with the yellow line being at 4μm from the bleach front and the black and pink lines being at 8μm and 12μm from the bleach front. In this experiment, two cycles of bleach and recovery were taken. Both cycles gave the same results and the estimated diffusion constant D (= dist^2/time) gave similar values from all the sites. Scale bar is 4.71μm. Similar quantitative results were obtained from at least 20 subdomain locations.

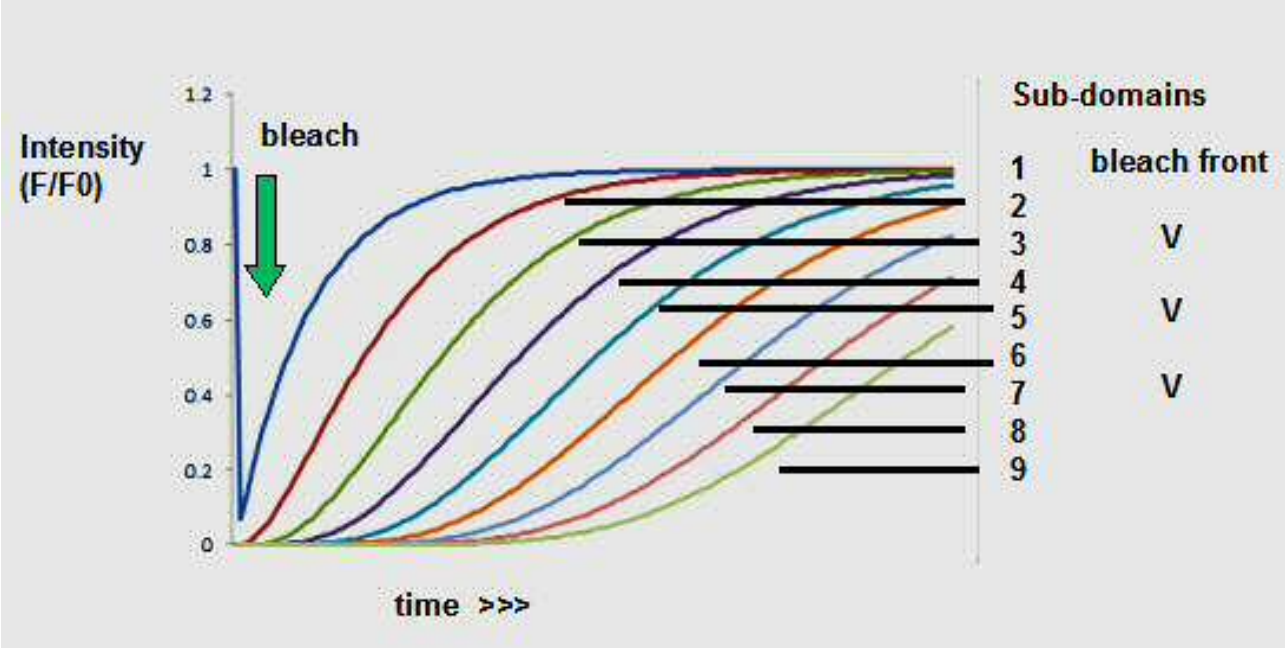

Figure 3.8 Fick's law simulation of sdFRAP. The graph shows the result of simulating Fick's Law of diffusion in silico. Each curve shows the recovery of fluorescence at a subdomain increasingly remotes from the photobleach front. The distance between subdomains (x = distance from subdomain) and the time (t) for recovery are in arbitrary units but are linked by the diffusion constant relationship D, $x^2 \alpha t$. The intensity is given as (F/F_0) on the y axis. (See section 2.5.11.5 for explanation of (F/F_0)).

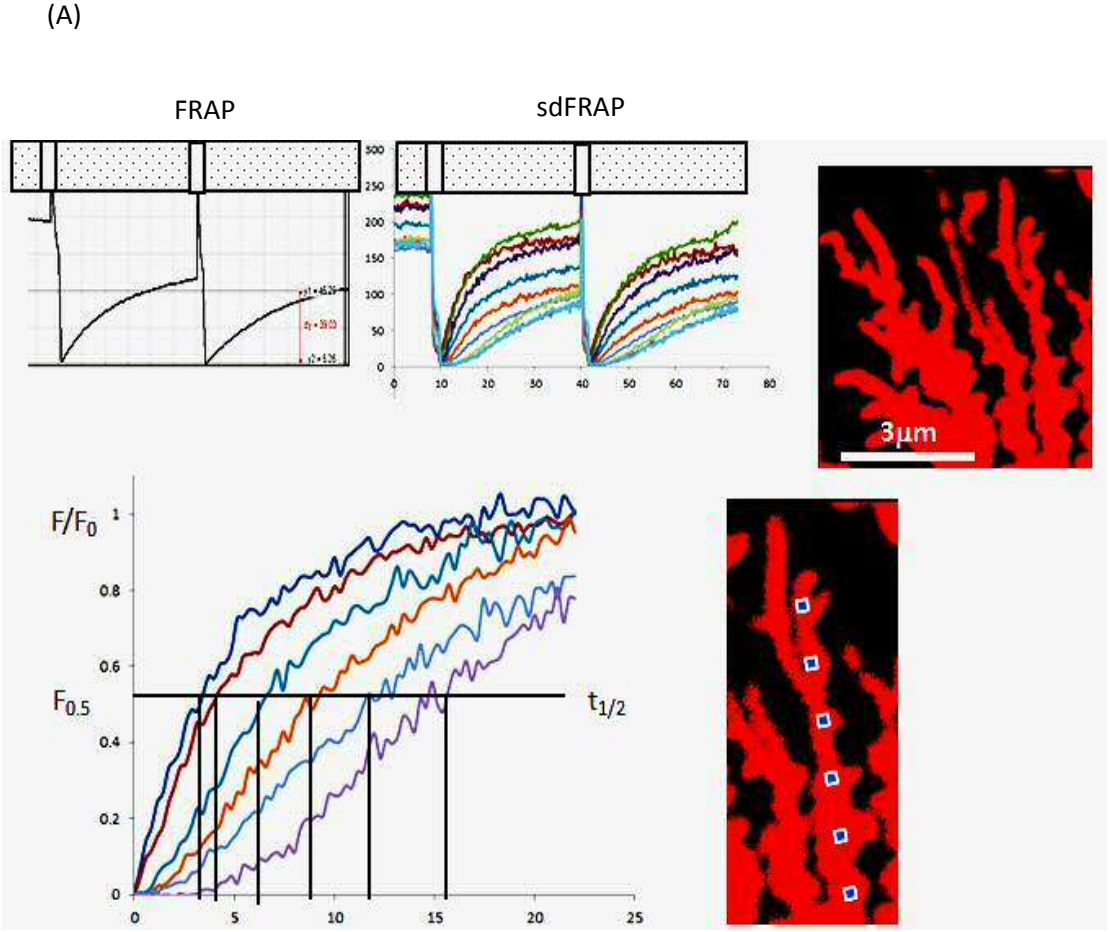

Figure 3.9 The relationship between diffusion distance and sdFRAP recovery. The DiI-labelled r fluorescence recovery recorded in 100nm square subdomains, 500nm apart as shown in the images. (A and from equally spaced subdomains (sdFRAP) are shown (top panel). Fluorescence recovery after two half times ($t_{1/2}$) of recovery for each subdomain is shown (lower panel). (B) The relationship between from bleach zone at all subdomains is shown. The raw $t_{1/2}$ data is in the insert, with the main graph sho the square of the distance with the fitted linear regression ($R^2 = 0.97$).

3.3.4 sdFRAP of DiI in the stretched neutrophil plasma membrane

In order to test whether sdFRAP would accurately measure diffusion distance in regions of smooth neutrophil plasma membrane other than the tail, it was necessary to generate smooth plasma membrane in regions of the plasma membrane that were not adhered to the underlying substrate. This was achieved by osmotically swelling the cells to near their lytic point, when any wrinkled membrane would be unfurled by lateral tension. Neutrophils were therefore subjected to extreme osmotic swelling to generate "bloated" spherical cells with a smooth (non-wrinkled) surface by dilution of the bathing physiological medium (fig 3.10).

The recovery of fluorescence in subdomains within the smoothed membrane (fig 3.11) also followed the prediction made from the Fick's Law simulation. Also, the recovery curves gave a similar estimate of the diffusion constant D as in the neutrophil tail, D = 1.2 ± 0.3 $\mu m^2/s$ (n = 3) but was slightly reduced from the value obtained in the flattened tail region of the cell. This may suggest that the swollen cell membrane was not as fully extended as the tail region. Testing the rates of recovery in subdomains on a smooth (non-wrinkled) surface (which was not adherent to the glass) was a further demonstration that our system monitors diffusion distances. From these studies, it was concluded that sdFRAP could monitor the diffusion distance when used in the lateral diffusion along the membrane.

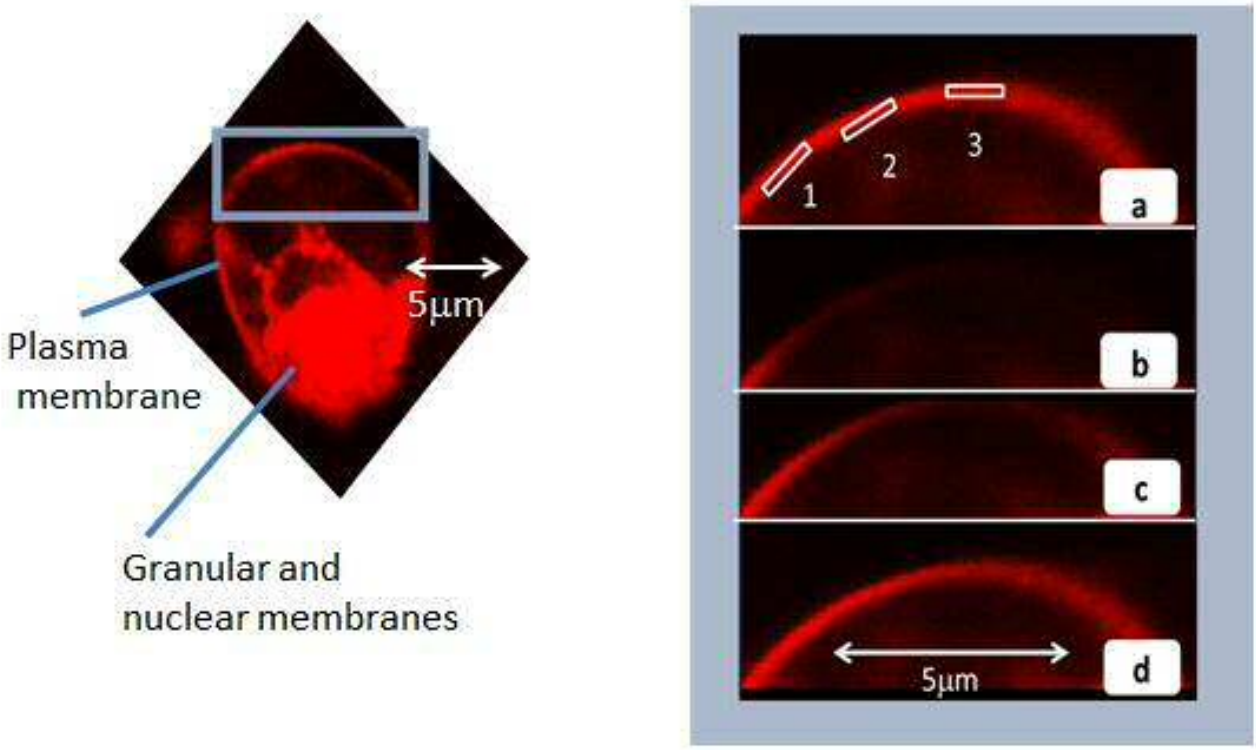

Figure 3.10 Lateral diffusion of DiI in the stretched neutrophil membrane. The confocal image on the left shows the DiI distribution in an osmotically swollen neutrophil. A region of plasma membrane remote from the nuclear and granular content (which also stains with DiI as indicated above) was chosen as indicated. This region was subjected to photobleaching and the recovery monitored in 3 sub-domains as shown in image (a) on the right. The sequence on the right shows (a) the region of stretched plasma membrane before photobleaching, (b) immediately after bleaching, (c) 10s, (c) 20s and (d) 30s after the bleaching.

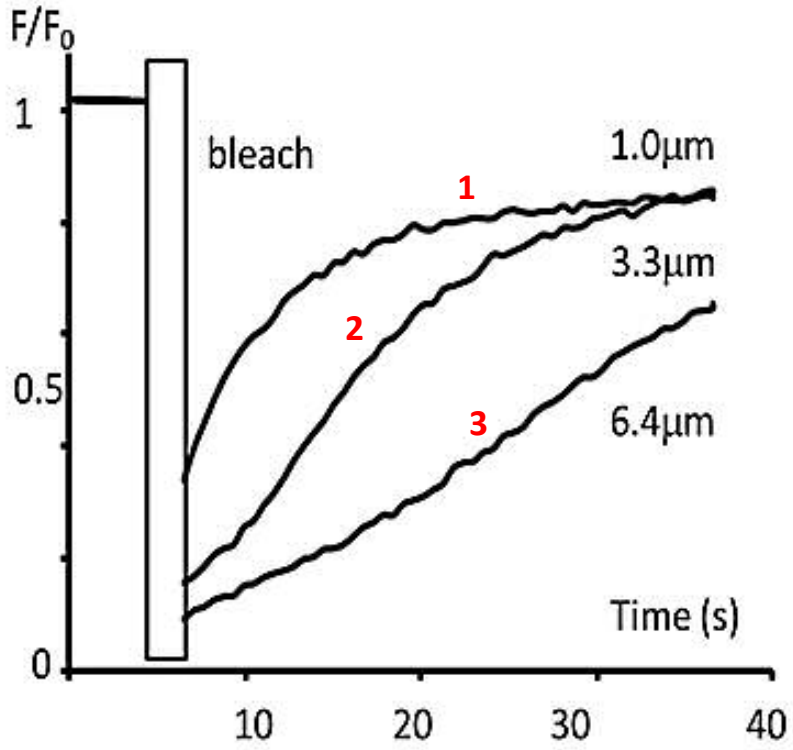

Figure 3.11 Kinetic sdFRAP measurement in the stretched neutrophil membrane. The measurement of the sdFRAP was taken in the three subdomains shown in fig 3.10 a. The diffusion distances from the bleach front are indicated alongside the three lines (1, 2 and 3). The sdFRAP on a swollen cell surface showed the same relationship between subdomain distance and recovery (i.e. time to recovery increases with increasing distance). It is interesting that this is not quite as quick as in the tail (figure 3.7) and therefore it is possible that there were still some wrinkled regions of membrane even under these conditions. This experiment was typical of five other experiments, which were repeated on different days with neutrophils from at least two blood donors.

3.3.5 Sub-domain FRAP characterisation of topography of non-spread neutrophils

In these previous experiments, the time delays before fluorescence appeared at a subdomain were evident. This was because the diffusion distances were large. For example, the tail length was over 10µm. It would not be possible to achieve such large diffusion distances in other regions of the neutrophil (e.g. the phagocytic cup is only 2-3µm diameter). Therefore, in the remainder of experiments reported here, simple time delays cannot be recorded and instead the rate of recovery was measured at a defined location within the bleach zone (i.e. a sub-domain) for comparisons between different neutrophil states. The recovery rate, k, (s^{-1}) is the inverse of the characteristic time(s) for recovery (see section 2.5.11.3 for the calculation of k value). After bleaching part of the non-stretched membrane of the neutrophil, the sdFRAP signal was similar to those observed previously (fig 3.12). The fluorescence recovery can be fitted to an exponential curve (fig 3.13).

$$F/F_0 = 1-e^{-kt} \qquad \textbf{equation 1}$$

F_0 is the equilibrium fluorescence; F is the fluorescence at time, t, after the photobleach and k is the exponential decay constant in units of s^{-1}.

The value of k was estimated using a log transformation of the recovery of fluorescence, which was linear with a slope equal to -k. In four normal cells (Table 3.1), at a 2µm subdomain, k was found to be 0.15 ± 0.02s^{-1} (mean ± sd). The rate constant is the

reciprocal of the "characteristic time" (τ) (see section 2.5.11.2 in for explanation) in the standard diffusion equation:

$$D \alpha x^2/\tau \qquad \textbf{equation 2}$$

D is the diffusion constant ($\mu m^2/s$), τ is the characteristic time in seconds and x is the distance in μm.

In the spread neutrophil tail (see section 3.4.3), the characteristic time at a 2µm subdomain was approx. 2.86s; giving a k value of $0.35s^{-1}$. The characteristic time in normal neutrophils was significantly longer than in stretched membrane ($p<0.05$). This analysis shows that in round (non-spread) neutrophils, the surface is significantly more wrinkled that in the tail of the spread neutrophil. The diffusion path length compared to the flat tail will be given by $\sqrt{}$ ($\tau w/\tau s$) and the wrinkled area is simply $\tau w/\tau s$ (where τw and τs are the characteristic recovery times for the wrinkled and smooth surfaces) (see section 2.5.11.2 for explanation).

The sdFRAP data therefore shows that the normal neutrophil has a wrinkled topography that increases the diffusion distance on the cell surface by 1.6 fold and also increases the surface area by 2.56 fold. Thus, the cell body has wrinkles that would provide approximately 150% additional membrane which would be sufficient to act as a reservoir for either cell spreading or phagocytosis. For simplicity, the term $\tau w/\tau s$ will be called the

topographical index (Ti), as this indicates the apparent fold increase in diffusion area in 2D as a result of surface topography in 3D. It has been difficult to quantify this parameter previously in either fixed cells using SEM or AFM, or in live cells using AFM. This quantitation may thus represent the first direct measurement of the extent of the membrane “reservoir” afforded by cell surface topography in a living cell.

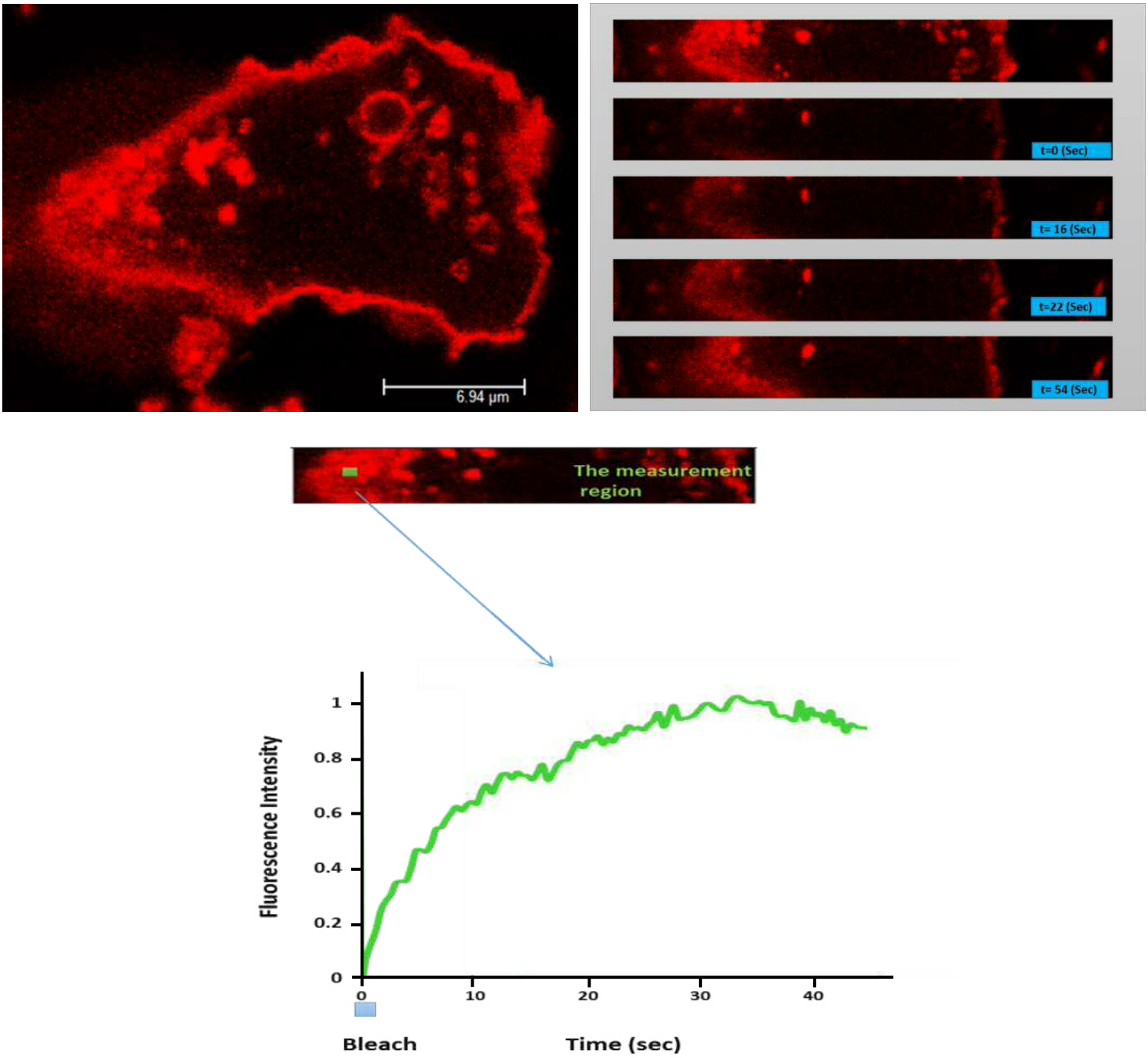

Figure 3.12 Recovery of DiI fluorescence in a subdomain after photobleaching in non-spread neutrophils. The data shown is from a typical experiment in which the plasma membrane of a non-fully spread neutrophil (top left) has been photo-bleached in the area shown on the top right sequence of bleach and recovery (pre-bleach and 0, 16, 22 and 54s post bleach). Recovery was measured in the sub-domain (indicated in lower panel) from the sequence of recovery images and the subdomain recovery time course is shown (graph). This experiment is typical of four other experiments which were studied on two different days. Two different donors provided the blood.

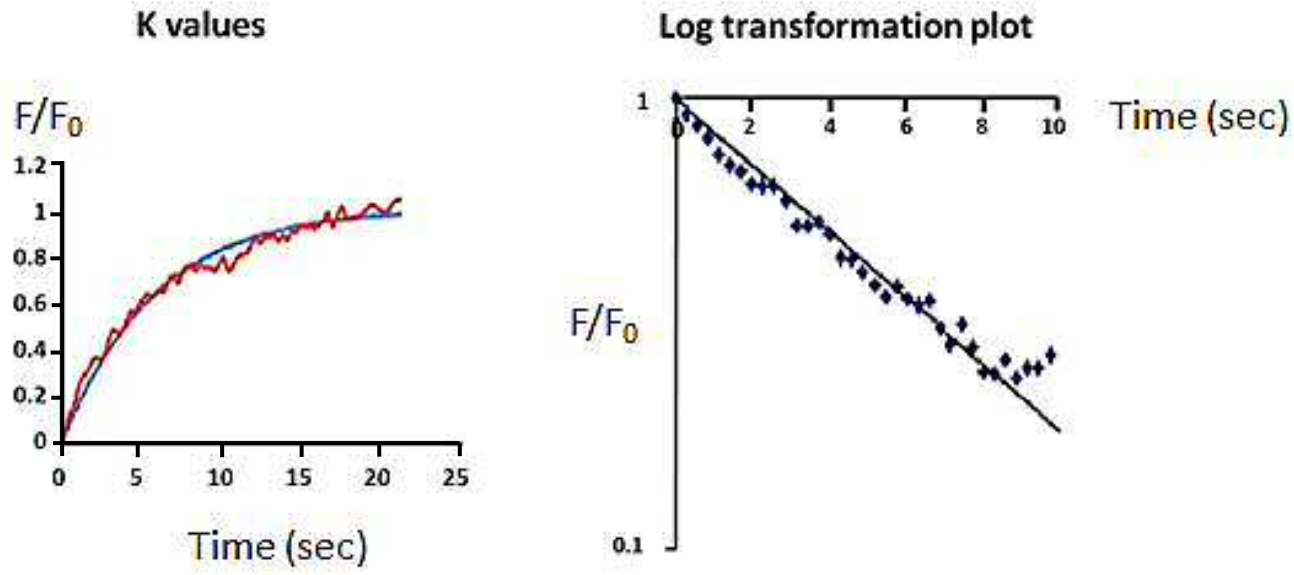

Figure 3.13 Analysis of kinetics of sdFRAP recovery. On the left is the recovery kinetics of the experiment shown in fig 3.12 with a superimposed smooth line for $F/F_0 = 1\text{-}e^{-kt}$. The value of k was adjusted to give the "best fit". In this case k was estimated to be $0.17s^{-1}$. On the right the log transformed data is shown. This confirms that when t = 0, $F/F_0 = 1$ and that the relationship is linear with a slope of – k.

Normal cell	K (s^{-1})
Cell 1	$0.17s^{-1}$
Cell 2	$0.15s^{-1}$
Cell 3	$0.15s^{-1}$
Cell 4	$0.13s^{-1}$
Mean	$0.15s^{-1}$
sd	0.01633
sem	0.008165

Table 3.1 K values estimated from 4 random cells using the analysis shown in fig 3.13. The mean, the standard deviation (sd) and the standard error of the mean (sem are also shown).

3.3.6 Sub-domain FRAP of DiI in the plasma membrane of artificially wrinkled neutrophils

In order to test whether a change in cell surface topography would impact on the measured sub-domain recovery rate constant, the effect of osmotically shrinking neutrophils was investigated. As the cell volume would be decreased as a result of osmotic shrinking, but the plasma membrane would not, the surface area of the cell would necessarily increase its wrinkledness at both microscopic and sub-microscopic levels. When sdFRAP analysis was performed on neutrophils shrunk by an increased extracellular NaCl concentration, there was a striking decrease in the measured k value from $0.14s^{-1}$ before shrinking to $0.03s^{-1}$ (fig 3.16 a). The characteristic recovery times increased from 7s before shrinking to 33s in the shrunk state (fig 3.15, fig 3.16). Cell shrinking caused a significant decrease in value K value from $0.12 \pm 0.2s^{-1}$ to $0.04 \pm 0.03s^{-1}$ (mean sd, n = 3) (fig 3.17, Table 3.2). Since these data were derived from before and after measurements on the same cell, a paired t-test was used and showed the difference to be highly significant (p<0.004).

These observations were consistent with the increased diffusion distance expected in the shrunk cell. It was concluded that the increase in cell surface wrinkledness induced by shrinking could be easily detected by this method.

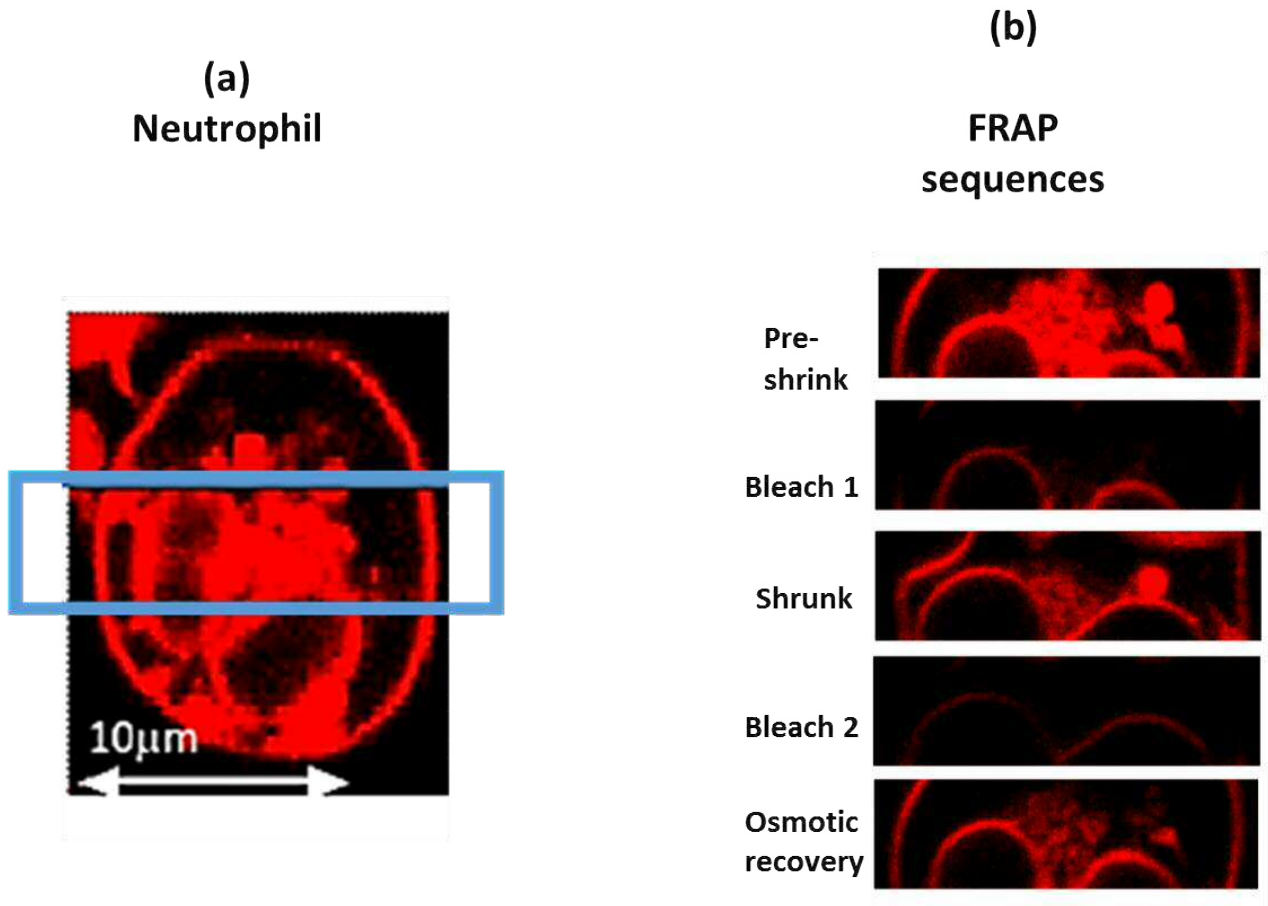

Figure 3.15 Osmotic shrinking of DiI labelled neutrophils. (a) A confocal image of a DiI loaded neutrophil prior to the experiment. The rectangle shows the region expanded on the right. (b) The expanded region at various stages of the experiment i.e. before osmotic shrinking and at the first bleach; then after osmotic shrinking (shrunk) with NaCl and then at the second bleach. The final image of the sequence shows the ability of the cell to recover its initial non-shrunk state. This experiment was repeated four times on neutrophils isolated from the blood of at least three different donors, on three separate days.

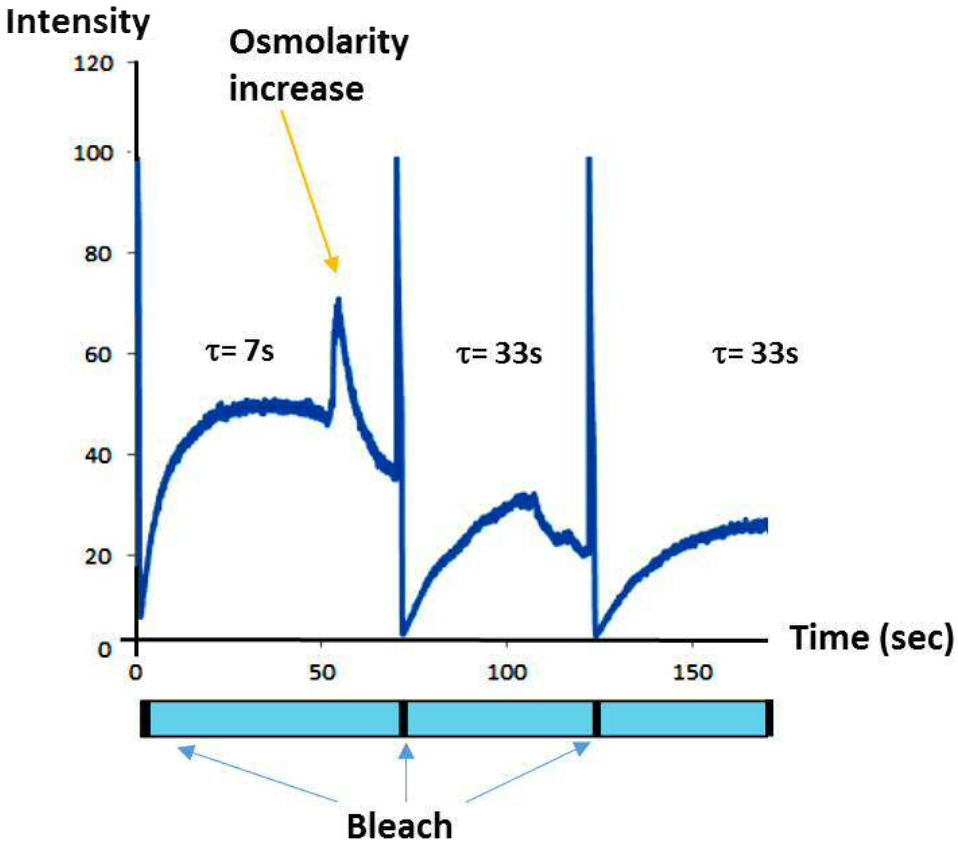

Figure 3.16 The effect of osmotically induced wrinkles on the kinetics of sdFRAP. The measurement of the sdFRAP was taken before and after osmotic shrinkage. The characteristic diffusion times are indicated after each bleach recovery cycle. At the arrow, the osmotic strength was increased by the addition of NaCl (300mM) generating an optical artefact as indicated.

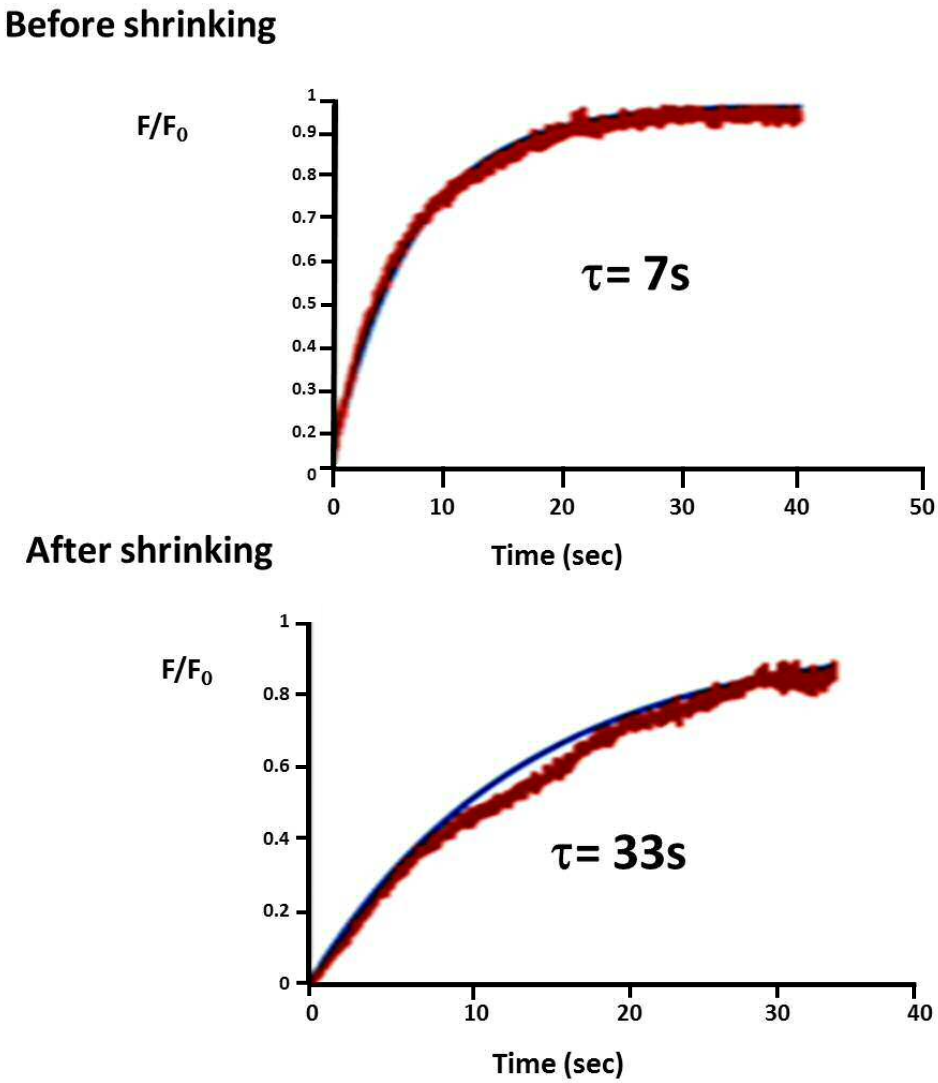

Figure 3.16a The effect of osmotically induced wrinkles on the kinetics of sdFRAP. The kinetics of fluorescence recovery at subdomains before and after osmotic shrinkage, which was induced by the addition of NaCl (300mM). The graphs show the acquired data with the theoretical curve $1-e^{-kt}$ fitted to estimate the k value (s^{-1}). The reciprocal of this gives the characteristic time in seconds (τ) as shown.

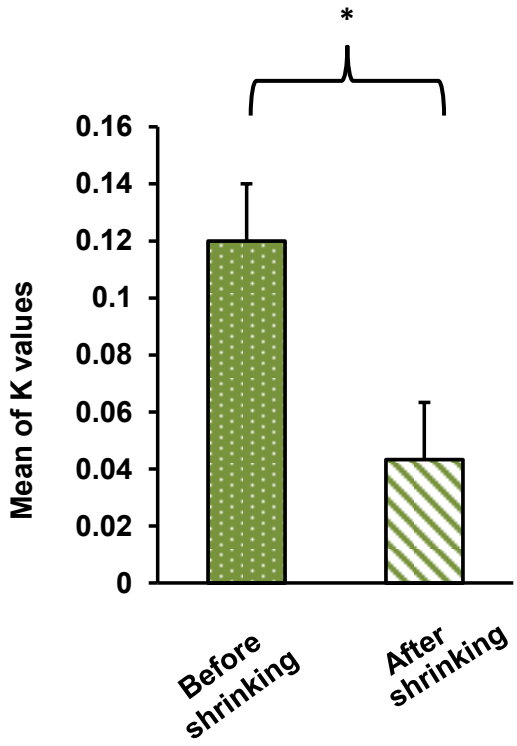

Figure 3.17 Effect of shrinking on neutrophils as measured by recovery rate constant (k values). Results show a marked significant reduction in recovery after shrinking, reflecting an increase in membrane topographical features. The raw data are shown in Table 3.2.

K (s^{-1})	Before shrinking	After shrinking
Cell 1	$0.12s^{-1}$	$0.05s^{-1}$
Cell 2	$0.14s^{-1}$	$0.07s^{-1}$
Cell 3	$0.1s^{-1}$	$0.01s^{-1}$
Mean	$0.12s^{-1}$	$0.043s^{-1}$
sd	0.016	0.025
sem	0.01	0.017
n	3	3

Table 3.2 Effect of shrinking on neutrophil as measured by recovery rate constant (k values). The raw data are presented as K values of three different cells from three healthy donors before and after the effect of shrinking with mean ± sem. The differences between the means of the population (unpaired) and from individual cells (paired data) were statistically significant and were shown in the fig 3.17: $p<0.05$ and $p<0.004$ respectively.

3.3.7 sdFRAP of DiI in the plasma membrane of artificially expanded neutrophils

To further test whether sdFRAP reflected cell surface topography, the cell surface membrane was expanded by addition of the hydrophobic lipid membrane expander, deoxycholate (Doc). Unlike osmotic shrinkage, where wrinkles form as a consequence of a cell volume change, Doc incorporates into the lipid bilayer and thus adds more "membrane" to the cell without a decrease in the cell volume. This procedure generated neutrophils which in SEM appeared "bloated" with inflated wrinkles of a "loose bag" rather than the "tight bag" of untreated cells (see data in Chapter 4).

Using confocal microscopy of living cells, the bloating resulted in a loss of fine detail (fig 3.18). The subdomain recovery rates of the DiI, measured in the same cells before and after the addition of Doc, showed that the diffusion path was extended by the addition of Doc (fig 3.19 a and b). In 4 cells, the population mean rate constant (k) before the addition of Doc was 0.65 ± 0.21s^{-1}, whereas after DOC incorporation, this was reduced to 0.47 ± 0.07s^{-1}. Although this difference was not statistically significant at $p<0.01$, a paired t-test of the data from individual cells (see Table 3.3) showed that the effect of Doc was highly significant ($p<0.01$). It was therefore concluded that sdFRAP was sensitive to a perturbation of the neutrophil surface topography in the absence of a change in cell volume.

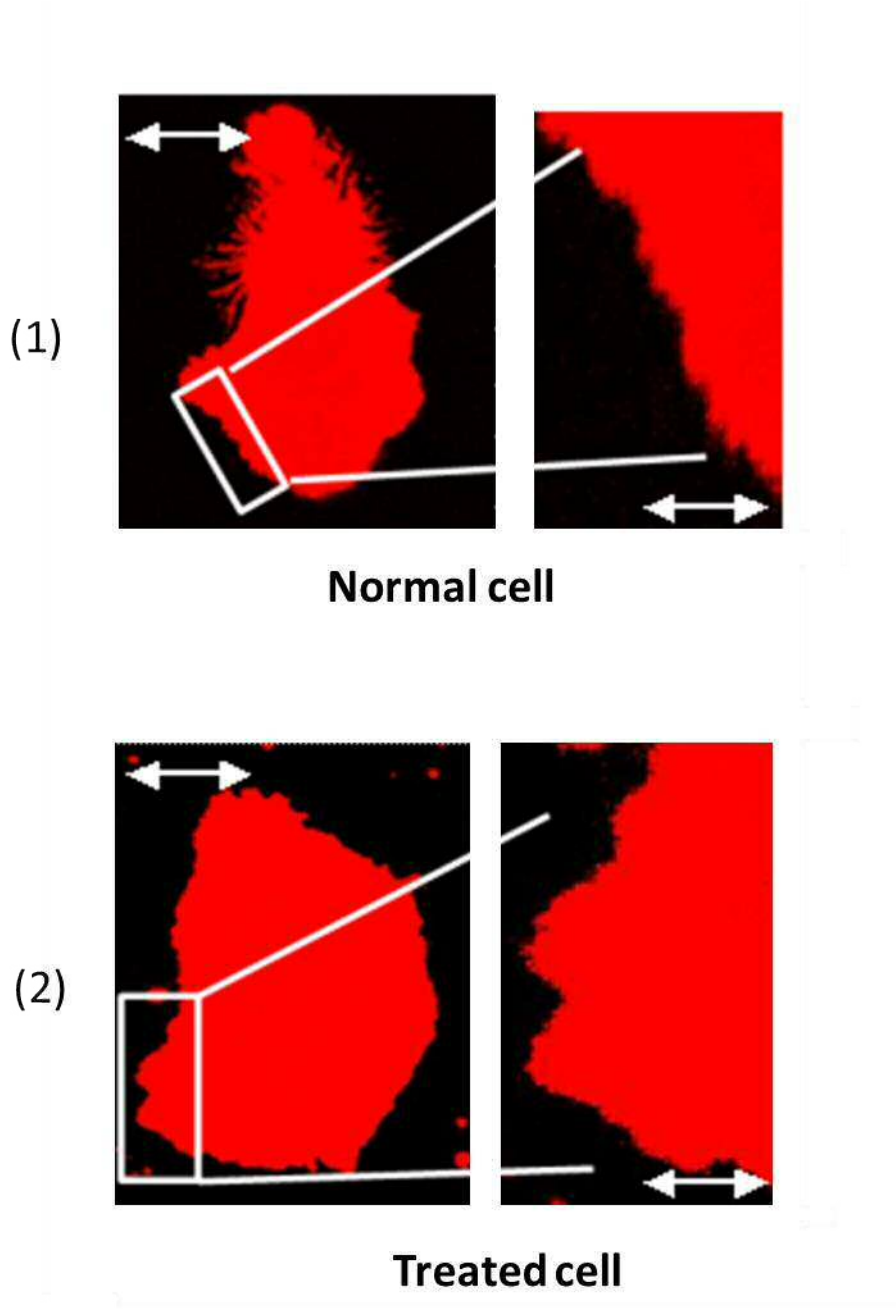

Figure 3.18 The effect of the membrane expander, deoxycholate, on neutrophil morphology. The image pairs show the same neutrophil (1) before and (2) after the addition of deoxycholate 400μM. In the right hand images, a magnified region of the cell (shown superimposed on the left hand image) is shown. The scale bars indicate 2μm in the right hand pair of images and 5μm in the right hand pair of images.

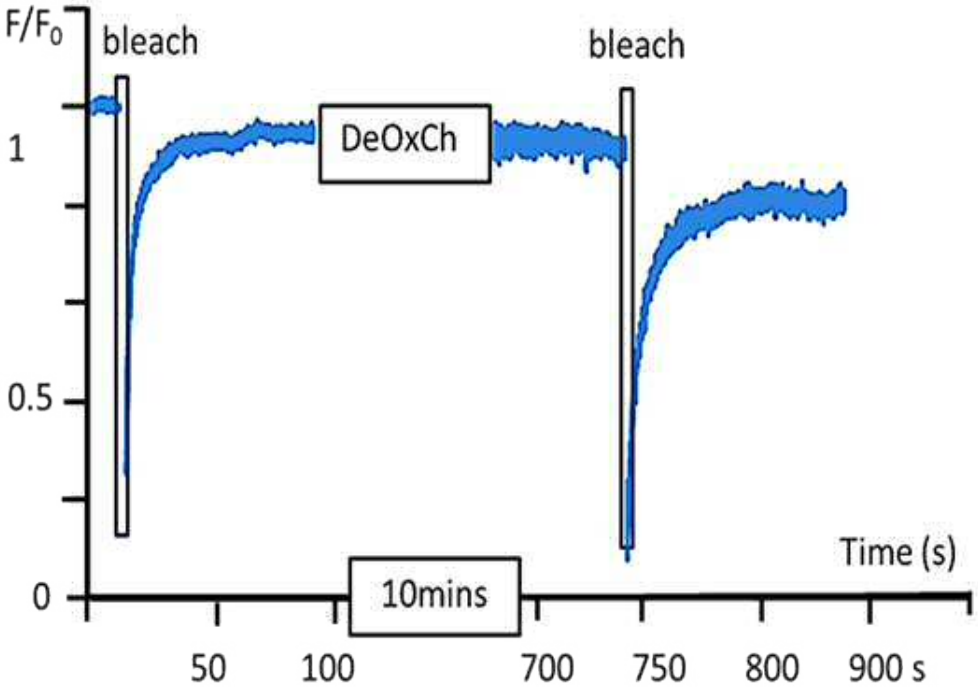

Figure 3.19a The effect of deoxycholate-induced bloating on the kinetics of sdFRAP. The data from a typical experiment are shown in which sdFRAP was measured both before and after deoxycholate (400μM) incorporation into the neutrophil membrane as indicated (DeOxCh). The 10 mins deoxycholate incubation on the time course on the left have been omitted from the record for clarity. This experiment was repeated four times on four different days from different donors for each day.

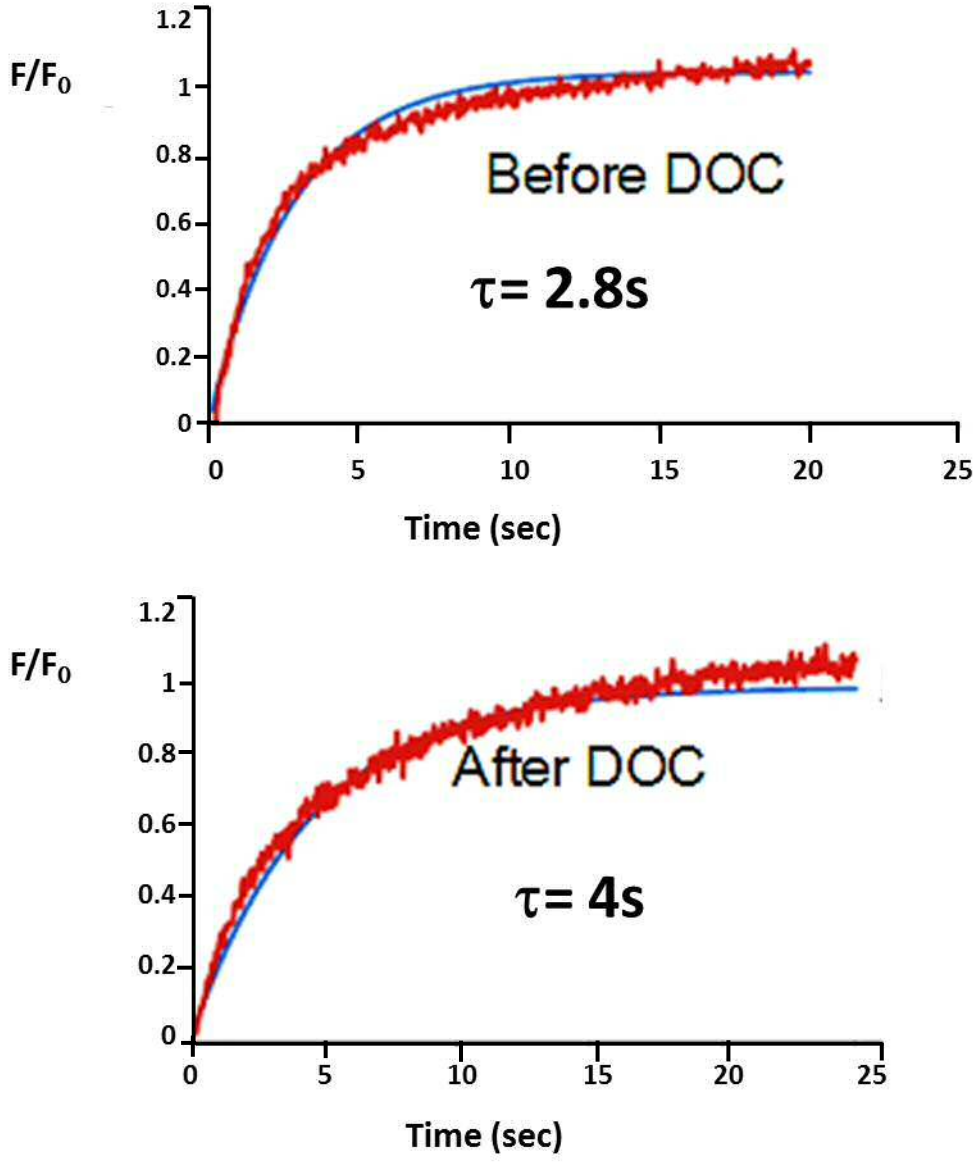

Figure 3.19b The effect of the membrane expander, deoxycholate, on neutrophil morphology. Curve fitting of the "before" and "after" DOC recovery kinetics applied to the data from fig 3.19a.

K (s^{-1})	Before Doc	After Doc	Diff	ratio	1/ratio
Cell 1	1	0.65	0.35	0.65	1.538462
Cell 2	0.65	0.45	0.2	0.692308	1.444444
Cell 3	0.6	0.35	0.25	0.583333	1.714286
Cell 4	0.35	0.25	0.1	0.714285714	1.4
Mean	0.65	0.43	0.23	0.66	1.52
sdev	0.23	0.15	0.09	0.05	0.12
sem	0.12	0.07	0.05	0.02	0.06

Table 3.3 The complete data for 4 cells treated with deoxycholate as shown in fig 3.19. The before and after deoxycholate values were estimated from curve fitting as shown in fig 3.19b and the means sd and sem for all data is given. In each cell, there was a decrease in k value (significantly different from zero) and the ratio or inverse ratio was again significantly different from unity (i.e. non change). The t-test p values for the before and after k values were p (paired) = 0.02 and p (unpaired) = 0.21; n = 4.

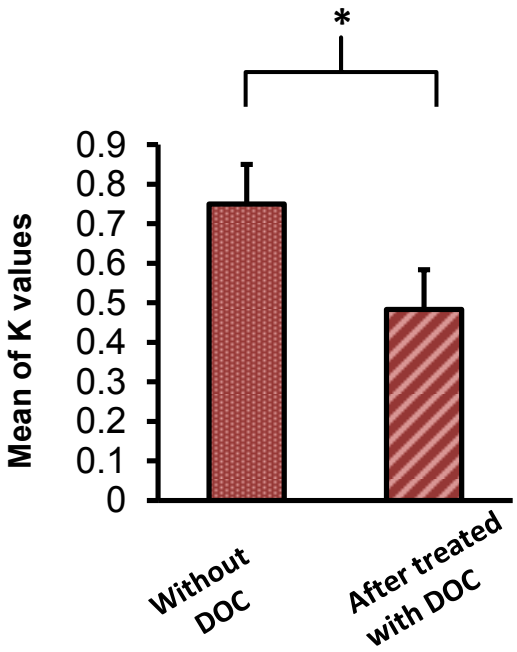

Figure 3.20 The effect of deoxycholate on sdFRAP recovery rate (k). The population data shown in Table 3.3 is shown graphically for ease of understanding. The values are the mean ± SEM. For the three cells studied.

3.4 Discussion

In this chapter I have shown that sdFRAP can report changes in cell surface topography of neutrophils. This was established under two conditions where the diffusion distance was measureable (i) the flattened tail of the neutrophil and (ii) in osmotically swollen cells where the membrane was "stretched" to nearly its maximum extent. The ability of sdFRAP to monitor changes in the cell surface topography was tested by two experimental procedures that increased the wrinkledness of the cell surface: (i) osmotically shrinking the cell volume to induce hyper-wrinkling at the cell surface; and (ii) adding a membrane expander, deoxycholate, to add extra surface features to the cell. In both cases sdFRAP was sufficiently sensitive to measure the change in cell surface topography within individual cells. Using sdFRAP it was shown for the first time that in the resting neutrophil, cell surface wrinkles were significant and could be the membrane reservoir required for phagocytosis and cell spreading.

Although there have been no previous attempts to monitor cell surface topographical changes in living cells, a non-imaging optical approach, based on right angle light scattering which has been reported to monitor neutrophil "shape change" (Wymann, *et al.,* 1987; 1989; Kernan *et al.,* 1991; Ehrengruber *et al.,* 1995, 1996). Essentially, the 90^{o} scattering of light by particles in suspension can be calculated from Mie scattering theory (Mie, 1908). This predicts that light scattering by particles of the same order of magnitude as the wavelength of the incident light will be profound in some granular cells (Meyer, 1979; Ruban

et al., 2007). In the granular cytoplasm of neutrophils (granule diameters 0.2 – 0.3μm), the attenuation coefficient could be as high as 700mm^{-1} (Prahl, 2007), depending on the number of granules/volume of cytoplasm (Dewitt *et al.,* 2009) Changes in the right angle scattering from suspension of neutrophils may thus result from changes in the "shape" of the neutrophil giving changes in the granular density. Remarkably, using flow cytometry to interrogate individual cells in the population, this approach shows that populations of suspended neutrophils change "shape" synchronously in a sinusoidal oscillation if pre-treated with the PI3-kinase inhibitor, wortmannin (Wymann *et al.,* 1987; 1989). However, the underlying principle of this measurement is unclear and the interpretation has been challenged (Keller *et al.,* 1996). These authors concluded that it is not possible to determine whether a particular "shape change" had occurred e.g. spherical to polarized or to nonpolar cells. Furthermore, they concluded that "forward or right angle scatter changes are not a reliable measure for changes in "cell volume" of human PMNs (Keller *et al.,* 1996). Without knowledge of whether light scattering measurements report cell volume or surface area changes, or whether it is related to surface "reflection properties" or, more likely, cytosolic granular density, these data obviously cannot be interpreted or used to make proposals of changes in the neutrophil cell surface topography.

Prior to the work reported in this chapter, the only methodologies for monitoring the cell surface topography were based on direct imaging. Electron microscopy has sufficient resolution to image the cell surface topography, but is only applicable to fixed cells. The cell surface topography can be observed directly using scanning electron microscopy (SEM) or in

2D in sections cut through the cell in transmitted electron microscopy (TEM). As both methodologies require the cell to be fixed and exposed to an electron beam in a vacuum, these methods cannot be used on living cells and hence no effects of experimental or physiological manipulation can be observed directly on the same cell. Atomic force microscopy (AFM) can achieve a similar resolution and in theory can be used with living cells. However, there are two problems. The first is that the time required for acquisition of the image (scanning with the atomic force probe can require several minutes) is slower than the time scale of neutrophil movement (e.g. neutrophils can spontaneously move at 0.1μm/s). This results in a severe "blurring" of the image such that quantitative measurement of the surface is impossible. Secondly, as the cell body of the neutrophil is pliant, the probe downward force is sufficient to "smooth" out surface features (see Al Jumaa *et al.,* 2017). AFM works well when the neutrophil is firmly adhered to a solid substrate (giving a non-yielding resistance to the probe) or on fixed cells. Thus, this method is also not suitable for studying living cells.

The sdFRAP approach in the flattened neutrophil membrane of the fully spread tail was used to estimate the diffusion constant, D in order to compare it with values obtained by other techniques. It was found that the entire tail region of these cells had a homogeneous flattened topography, with measurements of the diffusion constant being approx. 1.43μm^2/s at all locations. This is significantly less than the diffusion constant for DiI (C18 (3)) reported in pure lipid layers of 9.8μm^2/s measured (Gullapalli, Demirel and Butler, 2008). Presumably, membrane associated proteins which exclude DiI in the neutrophil membrane, by which are

absent in the pure lid bilayer, account for this difference. Interesting, the value obtained here in the flattened tail is higher than those reported in several cell types (Pucadyil and Chattopadhyay, 2006; Bag, Yap and Wohland 2014). As the reported values in other cell types did not take account of the possibility of cell surface topography, the diffusion constant was underestimated. In "spherical" erthrocyte ghosts which have an apparently simple and smooth topography with a reported D value for DiI (C18) of 0.2$\mu m^2/s$ (Thompson and Axelrod, 1980) was surprisingly low compared to other reports. This may be accounted for by the fragility of the red cell ghost membrane which once detached from underlying spectrin reforms in a variety of geometries including surface "spicules", which depends on the precise osmotic resealing conditions. The value found here, of 1.4$\mu m^2/s$ is, however close that previously reported in neutrophil membrane of 1.7$\mu m^2/s$ (Petty, Hafemann and McConnell, 1981). Since the D value estimated by sdFRAP in the neutrophil tail was constant regardless of the distant at which it was measured, it was concluded that there was no significant variation in wrinkledness in the tail region.

However, it was not the aim to achieve an accurate measurement of the diffusion constant of DiI but to provide a reporter system for changes in the surface topography. The sdFRAP methodology depends on the measurement of changes in sdFRAP rather than calculation of the absolute values of D, the diffusion constant (see section 3.4.5). These changes could be as a result of experimental manipulations (such as in this chapter) or as a consequence of cell behaviour (e.g. spreading, phagocytosis or elevated cytosolic Ca^{2+} in later chapters): or it may between different loci within an individual cell.

As the tail is a fully “stretched” region of the cell, it may be assumed that this was the maximum rate of DiI diffusion on a smooth surface in our system. Osmotic swelling of the cells was used to reduce the cell surface wrinkles in regions of the cell which were not adherent. This was difficult as once the cell volume is increased by osmotic pressure, lysis often results. Presumably the wrinkles were held in place securely until a critical point when expansion occurred which led swiftly to bursting point. However, if the cell was expanded in this way but remained intact, the diffusion length was reduced to almost the 2D measured length as was seen in the stretched neutrophil tail.

In order to validate the method, in this chapter I have shown data from experimentally altering the cell surface topography. By shrinking the cell osmotically, the cell surface must necessarily be altered. As the cell volume is decreased, the excess surface area is taken up by surface folding. It was expected that additional folds would be superimposed on the already wrinkled surface and that an increase in the path-length for diffusion would be evident. It was therefore very important that the effect of shrinkage was easily detectable (fig 3.15; 3.16). The change in sdFRAP recovery rate, or the characteristic recovery time were significantly different when either comparing population means or the responses within individual cells. This gave a validation of method.

The cell surface membrane was also expanded artificially by the inclusion of deoxycholate (DOC). This has been shown previously to expand the membrane and reduce

surface tension (Raucher and Sheetz, 2000). Again it was important to use Doc carefully with neutrophils, deoxycholate could also lyse cells. However, in the experiments reported here, it was possible to see effect on the surface topography. Blebs and abnormal topography were generated as a result of expansion of the membrane without physiological control or other signals to induce spreading. This was easily measurable by sdFRAP as an increase in pathlength. These approaches therefore demonstrated the validity and sensitivity of the sdFRAP approach to monitor cell surface topography in neutrophils.

Although it has not been possible before to measure the membrane reservoir in neutrophils or other cells, theoretical considerations of the additional membrane required for either phagocytosis or cell spreading suggest that the wrinkles must contain an excess of membrane more than 172% and 210% respectively (Dewitt & Hallett 2007; Hallett and Dewitt, 2007). Here the sdFRAP approach found that, compared to the flat tail of the neutrophil, the cell body was significantly wrinkled. It was estimated that the extra wrinkledness accounted for an additional area which increased the area of a flat surface by 256% (section 3.3.5). This is an interesting value which is in line with previous estimates.

3.5 Summary

In summary, the data presented in this chapter have established a methodology which can report changes in cell surface topography. The methodology was based and a novel technique called sdFRAP in which the recovery rate at subdomain at a defined distance from the photo-bleach front of a region of plasma membrane was used to estimate the diffusion pathlength. This approach has found that the tail region of the neutrophil is smooth and the cell body is wrinkled; and that the cell surface topography can be altered experimentally by osmotic changes or chemical membrane expanders.

Chapter 4

Topographical changes of the cell surface during neutrophil phagocytosis and spreading

4.1 Introduction

4.1.1 The pathway of phagocytosis

The major anti-bacterial role of neutrophils is the phagocytosis of infecting microbes. Phagocytosis can be defined as a receptor-mediated, clathrin-independent but actin-dependent, process whereby particulates (>200nm) are internalised by the cell (Mukherjee *et al*., 1997, Aderem and Underhill, 1999). There are four professional phagocytic cell-types in the mammalian immune system; neutrophils, monocytes, macrophages and dendritic cells (Rabinovitch, 1995). Phagocytosis is triggered in these cells by pathogen-specific receptors or by opsonin-mediated (C3bi or antibody) binding. "Recognition" of the invading microbe, by activation of these receptors by binding of the particle to the cell surface, starts the process of phagocytosis (fig 4.1). This results in a localised actin polymerisation which produces pseudopodia by "pushing out" against the plasma membrane to form a phagocytic cup, holding the particle firm before ultimately internalising the particle within a closed phagosome (Mukherjee *et al*., 1997; Rabinovitch, 1995). The phagosome fuses with granules containing hydrolytic and degradative enzymes to produce a phagolysosomes (Rabinovitch, 1995; Fratti *et al*., 2001) (fig 4.1).

Complement receptor C3bi and Fc-receptors (FcR), scavenger receptors and pathogen-specific receptors, like Toll-like receptors (TLRs), mannose receptors and lectins (Aderem and Underhill, 1999; Underhill and Ozinsky, 2002) may all be involved in the initial binding event. C3bi is formed by complement activation via one of the three pathways, (i) the alternative pathway, (ii) the classical pathway and (iii) the mannose binding lectin pathway (Aderem and

Underhill, 1999); and results in the cleavage of C3 into C3a and C3b. C3b undergoes a further chemical change to the opsonin, C3bi (or iC3b) and binds tightly to the surface of the bacterium in a process called opsonisation. When antibodies against the microbe are produced, they bind to and coat (opsonise) the microbe. Fc receptors on the surface of phagocytes bind to the Fc region of antibodies. Immobilisation of opsonin receptors on the phagocyte surface is produced through interaction with C3bi or Fc regions of antibodies, which result in tyrosine phosphorylation of immune receptor tyrosine activation motifs (ITAMs). This activation is essential to cause Syk kinases activation that have important roles in cytoskeleton changes, actin assembly and downstream transcriptional activation of inflammatory cytokines (Cox *et al*., 1996, Majeed *et al*., 2001). It is known that Scavenger receptor A (SR-A) binds to whole microbes, recognizing LPS and lipoteichoic acids (Pearson, 1996). Likewise, macrophage receptor with collagenous structure (MARCO) recognises a variety of Gram-positive and Gram-negative bacteria (Elomaa *et al*., 1995) as well as artificial latex and TiO2 (Palecanda *et al*., 1999), silica (Hamilton *et al.,* 2006) and polystyrene particles (Kanno *et al*., 2007). The both receptors are considered to be the major scavenger receptors for the process of phagocytosis. The binding between receptors such as TLRs on the surface of the phagocyte cells and the moiety on the surface of pathogens is sufficient to trigger intracellular signalling and the internalisation and the release of pro-inflammatory cytokines such as IL-6, TNF and IL-1β (see Table 1.6, Chapter 1).

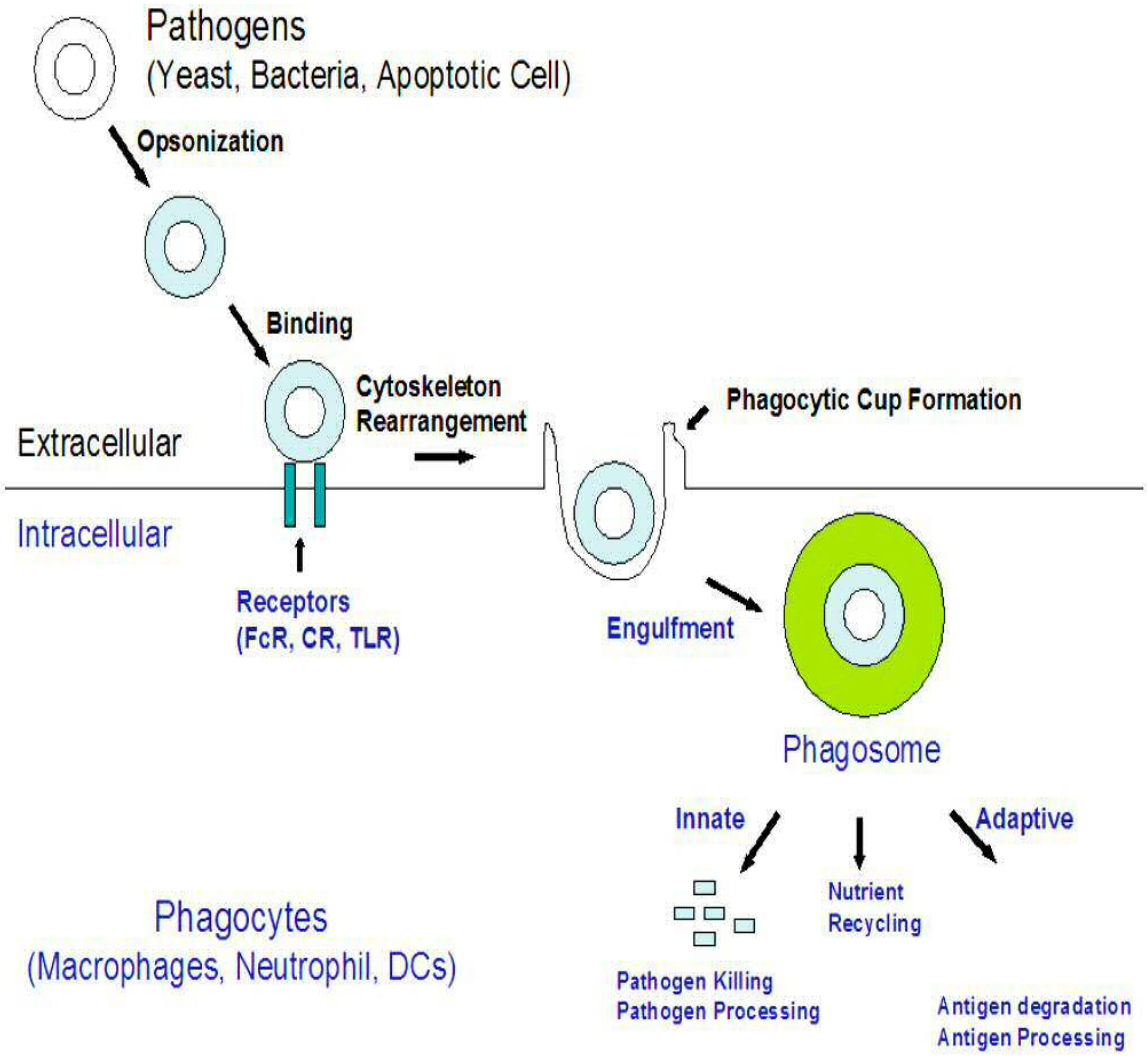

Figure 4.1 Phagocytosis pathways in immune cell. The diagram summarises some of the routes to phagocytosis in immune cells including neutrophils. The yeast or bacterial "pathogen" is recognised by opsonic receptors on the phagocyte surface such as FcR= Fc receptor, CR= complement receptor and TLR= toll-like receptor, which leads in phagocytic cup formation as a result of actin polymerisation and membrane expansion. Internalisation of the particle forms a phagosome which in neutrophils is the goal and results in killing of the pathogen by activation of the phagosome oxidase system and the action of non-specific proteolytic enzymes (labelled "innate"). Other fates are possible in other cell-types, including "nutrient recycling" and importantly in antigen presenting cells (labelled "adaptive").

4.1.2 Phagocytosis by neutrophils

Perhaps the major phagocyte for host protection is the neutrophil, being the initial cell to phagocytose and kill bacteria and fungi (Lee *et al.,* 2003, Segal, 2005). Some studies of neutrophil phagocytosis have been undertaken, using light and electron microscopy for capturing the progressive events in phagocytosis including recognition, attachment, engulfment and phagosome-lysome fusion. Phagocytosis of specific particles by neutrophils usually ends with lysis and degradation of the internalised particulate, as a result of the action of hydrolases and antibacterial proteins within the phagolysosome (Bainton, 1973). In neutrophils, the lysosomes are highly specialised and are called neutrophil granules. Primary azurophilic granules contain myeloperoxidase (MPO), proteases, lysozyme and acid hydrolases (Pryzwansky *et al*., 1979). Specific or secondary granules also have lysozyme and lactoferrin (LF). These granules are formed in early myelocytes stage.

It has been possible to study neutrophil degranulation and secretion through the use of immunocytochemistry with antisera against MPO and LF. During phagocytosis of E. coli by neutrophils, degranulation begins just 5s after the onset of phagocytosis which can result in MPO and LF markers on the neutrophil surface (Pryzwansky *et al*., 1978). Recognition of opsonised particles is essential for neutrophil phagocytosis and its failure results in lack of recognition and subsequent killing of the attacking microorganism (Roos *et al*., 1981). Experimentally, the binding of neutrophils to opsonised zymosan particles is useful, as these particles are sufficiently large to be distinguished within the cell and phagocytosis can be

controlled by micromanipulation or zymosan immobilisation techniques. This technique allows the contact between the particle and the cell to be timed and the subsequent pseudopodia formation, phagocytic cup and then internalisation to be followed in real-time microscopically. As the process is quick, it requires live real-time cell imaging for detailed observation. However, a SEM study of fixed cells by MacRae and Pryzwansky in (1984) was able to quantify some aspects of the process. They reported that after 30s incubation with opsonised zymosan, phagocytic cups, i.e. incomplete phagosomes having open cavities, had formed. The phagosome was complete within the next minute; and the bulging outline of the internalised zymosan could be detected within the cell in 3 mins (MacRae *et al*., 1980). During these events, there is an apparent increase in the surface area of the neutrophil plasma membrane to provide the pseudopodal membrane and the phagosomal membrane. As discussed in Chapter 1, it has been proposed that this is the result of localised unwrinkling of surface wrinkles to provide the additional membrane.

4.1.3 The process of cell shape change

Although in the circulation or in cell suspension, neutrophils appear “spherical”, once adherent, the shape of neutrophils changes and its shape change is highly dynamic. The phenomenon is primarily driven by actin polymerisation beneath the cell surface which pushes against the plasma membrane. It is an important property which underlies chemotaxis and movement of the cell to the site of infection. This was first observed by Van Leeuwenhoek in 1675. He described cell movement and the crawling of the cells on his

microscope slide. The cell movement is realised when some physical, chemical, diffusible or non-diffusible signals are sent from the surrounding environment of the cell. The cell membrane has receptors which are responsive to chemoattractant signals and trigger directed movement (Alberts *et al*., 2002). Cell movement includes the constant restructuring of the actin cytoskeleton and involves three different steps (fig 4.2). The first step is actin polymerization at the leading edge of the cell, locally forcing the membrane forward. The second step is adhesion to the underlying substrate at the leading edge and releasing at the cell body and tail. The last step is retraction of the cell rear and the translocation of the cell body when contractile forces, possibly generated by the action of the acto-myosin network, pull the cell forward. All these phases are determined by physical forces which are created by unique segments of the cytoskeleton (Abercrombie, 1980).

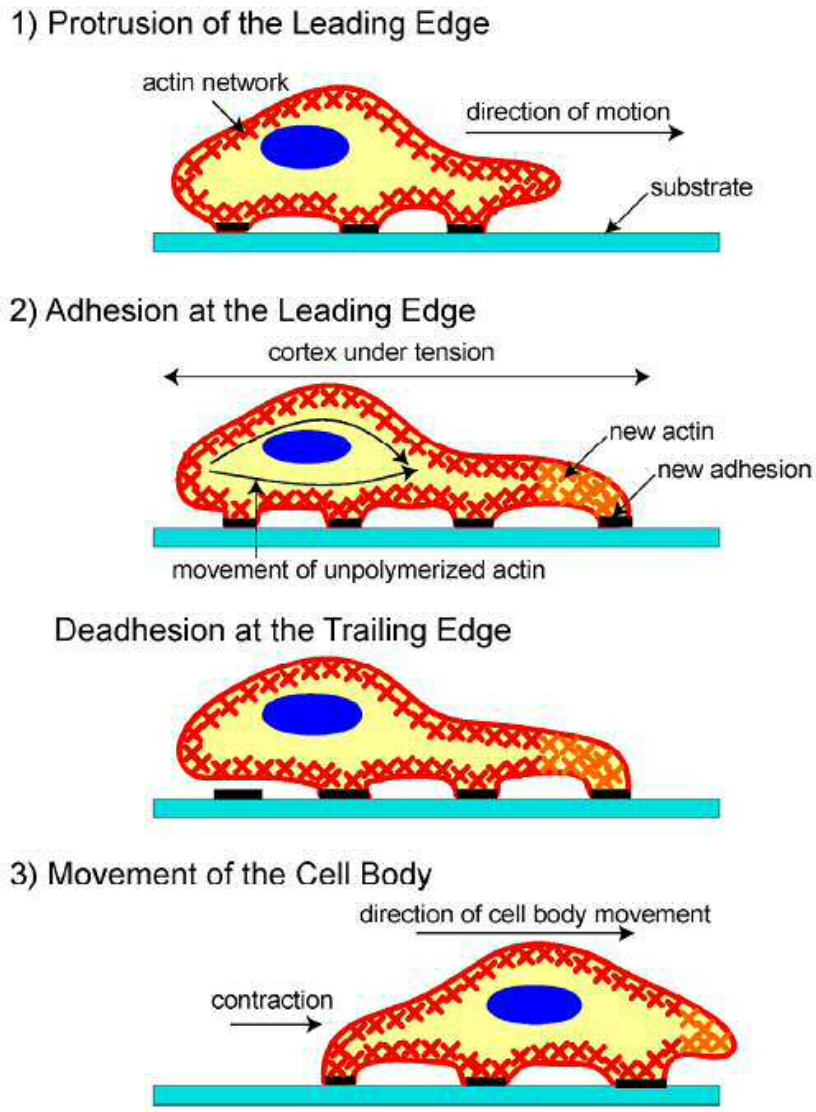

Figure 4.2 The three phases of cell movement. Cell migration starts with a leading edge protrusion, once the direction of motion has been determined. This can be seen through the process of actin polymerisation at the leading edge of the cell. In order to achieve movement, the leading edge adheres to the surface and then the rear detaches. Contractile forces made at the cell body and as well as at the rear result in the whole cell body being pulled forward. [Image is adapted from (Revathi and Allen, 2007)].

4.1.4 The Brownian Ratchet and the action of actin

A key step in this process and also in the formation of pseudopodia during phagocytosis is the “pushing” force of actin polymerisation. In contrast to muscle contraction, where actin reacts with myosin and consumes ATP, in non-muscle cells, the pushing force generated is not contractile but is outward. For example, the protrusion is the first phase of cell movement requires the force to be outward to produce a leading edge. Within the leading edge of the cell, the force is exerted by the mechanical connection between the actin cortical network and the plasma membrane; and the underlying mechanism is termed the Brownian ratchet (Grebecki, 1994). Essentially, actin monomers can be added to the leading monomer of polymerised actin, provided the concentration of free monomeric actin is above its critical concentration. In vitro, actin monomers will simply add to the polymer chain to generate ever lengthening chains of polymerised actin. However in the cell, this process will be impeded when the actin polymer is in contact with the plasma membrane. There will be no space for additional actin monomers to be added to the actin chain despite there being plenty of monomeric actin available. However, the actin polymer may flex a little or the position of the plasma membrane may fluctuate a little due to thermal agitation (Brownian movement). If sufficient space for an actin monomer to be added at the leading edge occurs, the membrane will be unable to relax back to its initial position which is now displaced by the length of 1 actin monomer. It will have been forced to a new position. This is the Brownian ratchet effect. Of course, the force of the Brownian ratchet can only push the plasma membrane if t the actin polymer is firmly tethered at the distal end. This is achieved by crosslinking and branching of actin polymers which involves

WASP proteins and other crosslinking proteins. The Brownian ratchet at the end of plasma membrane will continue until the growing actin filament is forced against the plasma membrane and Brownian movement of either the filament or the membrane is insufficient to permit the addition of any further actin monomers. Under these conditions, there is however, a potential pushing force, which would be evident if the thermal fluctuations increased or the resistance to thermal fluctuation at the plasma membrane is decreased. The latter would result from the unwrinkling of the plasma membrane. This underlies the protrusion of plasma membrane at the leading edge and at locations where pseudopodia actively form e.g. during phagocytic cup formation (Pollard and Borisy, 2003). It can be shown by computer simulations and mathematical calculations, that the Brownian ratchet provides a significant force and that there is no requirement for any additional "motors". The Elastic Brownian Ratchet Model (Mogilner and Oster, 1996) is a variation on the original proposal which suggests that as an actin monomer is 2.7nm long, it is able to add itself between the filament and membrane once bending of the filament away from the mebrane occurs is sufficiently large (i.e. when bending angle is > ~30°). This occurs when the filament length is > ~70nm. Each addition of a monomer "ratchets" the membrane, which implies that this process prohibits backward movement of the membrane and ensures that there is only a net forward motion of the cell edge.

The key event which would allow the Brownian ratchet to operate is the increase in spacing between the polymerizing actin and the plasma membrane. If this is provided by unwrinkling of the cell surface wrinkles, this proposal requires that the cell surface would be

altered from a wrinkled to a less wrinkled topography. The decrease in cell surface wrinkles has been observed in SEM studies of macrophages which had undergone phagocytosis (Petty *et al.,* 1981), but the dynamics of the process (which requires living cells) has not been observed. Also, since SEM can visualise only the cell surface, there can be no information on the wrinkledness of the formed phagosome which is within the cell. There are thus key questions as to whether the event precedes or follows phagocytosis; whether the unwrinkling is localised to the region of particle contact; and at what stage of phagocytosis unwrinkling is triggered. Clearly, the sdFRAP methodology for examining the cell surface topography in living cells (developed in Chapter 3), gives an opportunity to explore these questions.

4.2 Aims of this chapter

From the discussion above, it can be seen that the unwrinkling of the plasma membrane on the neutrophil would provide the additional membrane required for phagocytosis and to allow the Brownian ratchet to operate and so push out pseudopodia. The aim of the work in this chapter is therefore to investigate whether unwrinkling of the microridges occurs during phagocytosis and can be detected by a change in cell surface topography; and then to use this to discover whether the unwrinkling is localised to the region of the cell where phagocytosis is occurring.

Specifically the objectives are to:

1- Measure cell surface topography using the sdFRAP in living neutrophils having undertaken phagocytosis and spreading.
2- Compare plasma membrane topographical wrinkledness in the same individual living neutrophil before and after phagocytosis.
3- Compare the topography of membrane in the forming phagosome (phagocytic cup) and fully formed phagosomes with the topography of the rest of plasma membrane in the same cells.

4.3 Results

4.3.1 The topography of membrane of complete phagosomes

Having established that sdFRAP is a sensitive monitor of changes in cell surface topography, it was used initially to investigate whether there were regional differences in cell surface topography following phagocytosis. The confocal nature of the methodology allows examination of both the phagosomal membrane within the cell and the plasma membrane. This is impossible using SEM, as it can visualise only the cell surface, there can be no information on the wrinkledness of the membrane surrounding the intracellular closed phagosome. Initially, therefore, the topography of closed phagocytic cups was assessed using the sdFRAP technique. This was achieved by allowing DiI labelled neutrophils to internalise C3bi opsonised zymosan and performing sdFRAP in bleach zones which included the phagosomal membrane of closed phagosomes (fig 4.3 a). As the area of the phagosomal membrane is significantly smaller than the whole cell, it therefore had fewer DiI molecules. This means that it was important to establish a condition where it was possible to reproducibly measure the recovery rate within the phagosome without depleting its membrane of DiI. Fortunately, by simply reducing the bleach zone area, this was achieved using the standard methodology shown in Chapter 3. Although, this still reduced the fluorescence intensity to a level which was significantly lower than the pre-bleach level (fig 4.3 b), within the closed phagosome, recovery rates could be measured which were reproduced by a second sdFRAP (fig 4.3 c). Both the first and second recovery data, when normalised to (F/F_0) as described in section 2.5.11.5. This was fitted to the same recovery curve ($1-e^{-kt}$) over the entire recovery curve (Chi square (X2) “goodness of fit” test gave a

probability (p>0.89). The variation between the closed phagosomes was also acceptable, with the estimate of the recovery rate constants from independent cells having a relative standard error of 10.5% of DiI diffusion in the phagosomal membrane. This provided information on the apparent diffusion distance (Table 4.1).

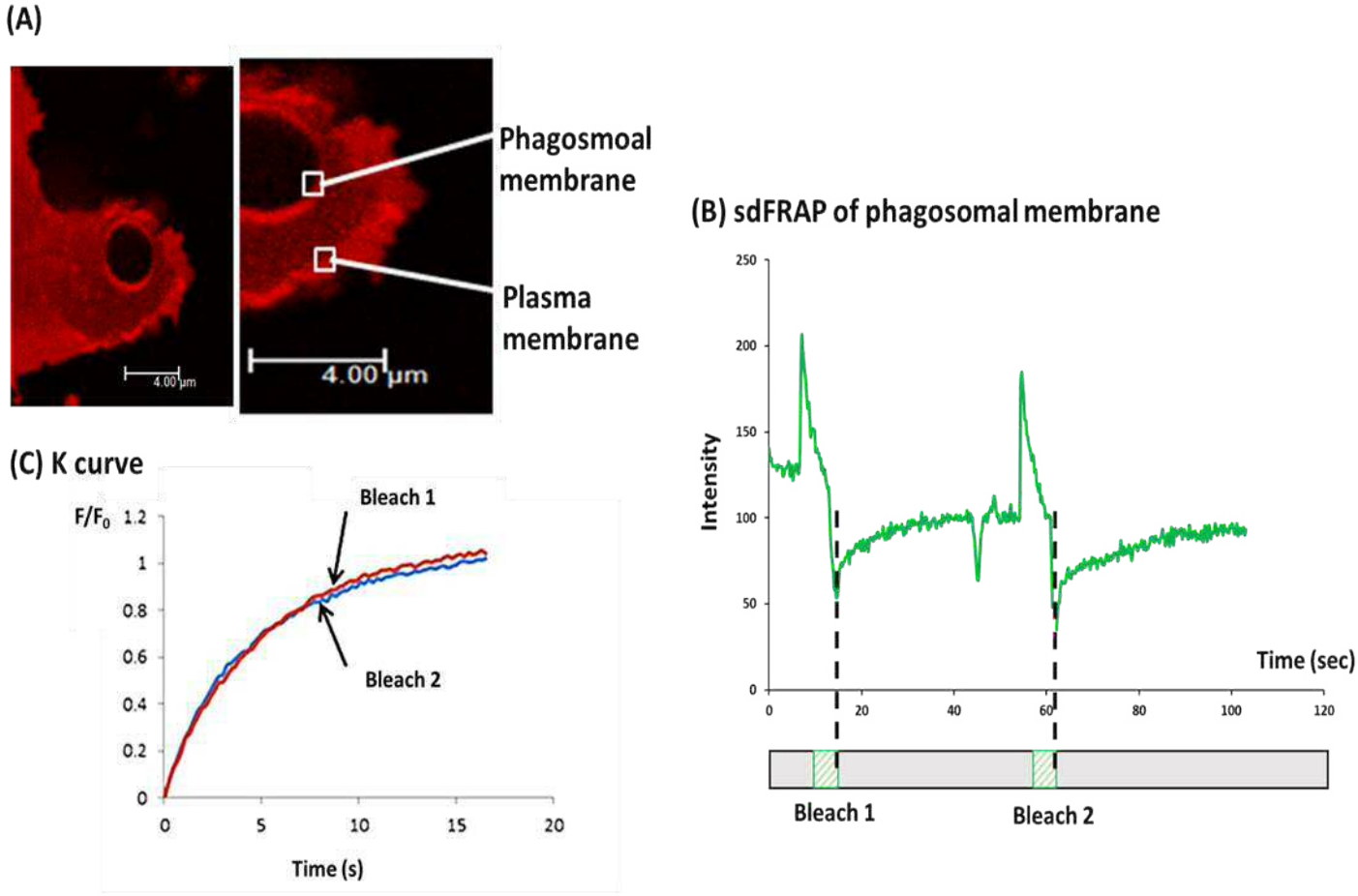

Figure 4.3 Demonstration of sdFRAP on phagosomal membrane. A confocal slice through a DiI-labelled neutrophil after internalisation of C3bi opsonised zymosan. The membrane around the closed phagosome can be distinguished from the plasma membrane, as shown in the enlarged image on the right. (b) The raw data from a typical experiment in which DiI in the phagosomal membrane were photo-bleached twice. On increasing the laser power, the signal increases and then reduces as bleaching takes place. After the photo-bleach step, the fluorescent signal recovers over the subsequent 20s. (c) The recovery curves after the two bleach steps were normalised as F/F_0 and superimposed to illustrate the reproducibility over the entre recovery curve.

	sdFRAP k value (s^{-1})
Cell 1	$0.23s^{-1}$
Cell 2	$0.24s^{-1}$
Cell 3	$0.15s^{-1}$
Cell 4	$0.30s^{-1}$
Cell 5	$0.25s^{-1}$
Mean	$0.23s^{-1}$
SD	0.048
SEM	0.022
RSE	10.5%
n	5

Table 4.1 Five independent measurements of the recovery constant, k, of phagosomal DiI. The recovery rate constant, k, was determined in the closed phagosomal membrane from five random cells, using the analysis shown in fig 4.3. The mean, the standard deviation (SD), the standard error of the mean (SEM) and the relative standard error (RSE) are shown. The source of neutrophils was from different blood donors for each cell measurement.

Using this approach, a comparison was made between the topography of the closed phagosomal membrane and the plasma membrane surrounding the body of the same cell. This was achieved by measuring sdFRAP within the phagosomal membrane and the plasma membrane within the same bleach slice through the same cell (fig 4.4). The conditions for recovery at both cellular loci were therefore identical and could be compared directly. A typical experiment is shown in fig 4.4 in detail, with the two loci, one at the phagosomal membrane and the other at the plasma membrane, shown. The sdFRAP recovery curves from these two loci, together with the fitted recovery curves are significantly different over the entire recovery curve (X^2 goodness of fit $p<0.001$). In all cells examined (4/4 cells), the characteristic time for recovery, **τ,** was calculated and it was found that the fluorescence recovery was significantly faster within the phagosomal membrane indicating the membrane was smoother i.e. the diffusion path was shorter than the plasma membrane in the same cell (Table 4.2). The mean sdFRAP diffusion rate of DiI (k) was $0.325 \pm 0.043 s^{-1}$ within the phagosomal membrane compared to $0.197 \pm 0.021 s^{-1}$ at the plasma membrane of 4 cells (fig 4.5). It is seen that the relative standard error of these two measurements was approximately 10% (as seen in Table 4.1). However, comparing these parameters within individual cells (where the measurement conditions were identical at the two loci) by taking a ratio has a relative standard error of only 3.4% (Table 4.2). This illustrates the value of experimentation on individual cells, when cell-to-cell variation is not relevant. The ratio of sdFRAP diffusion constants in the plasma membrane and phagocytic membrane of 1.65 ± 0.056 is significantly different from a value of 1, which would be true if the two membrane

had the same wrinkledness (p<0.01). It was thus concluded that the phagosomal membrane was significantly smoother than the plasma membrane.

The ratio is also useful for comparison with the diffusion path-length divided by the apparent diffusion distance, giving a topographical index (related to area). By definition, a completely smooth membrane has a Ti = 1 and the plasma membrane of adherent or spreading cells has a Ti between 1.6 and 2. Thus, the Ti of spreading cells is about 1.6 - 2 times that of the smoothest membrane (see sections 3.3.5 and 2.5.11.2). This is similar to the difference between the wrinkledness between the phagosomal membrane and the plasma membrane of the cell membrane, with a ratio of 1.65 ± 0.056 (Table 4.2) and suggests that the two membrane membranes are near the extremes of membrane wrinkledness, the phagosome being totally smooth and the plasma membrane being near its physiologically expected degree of wrinkledness.

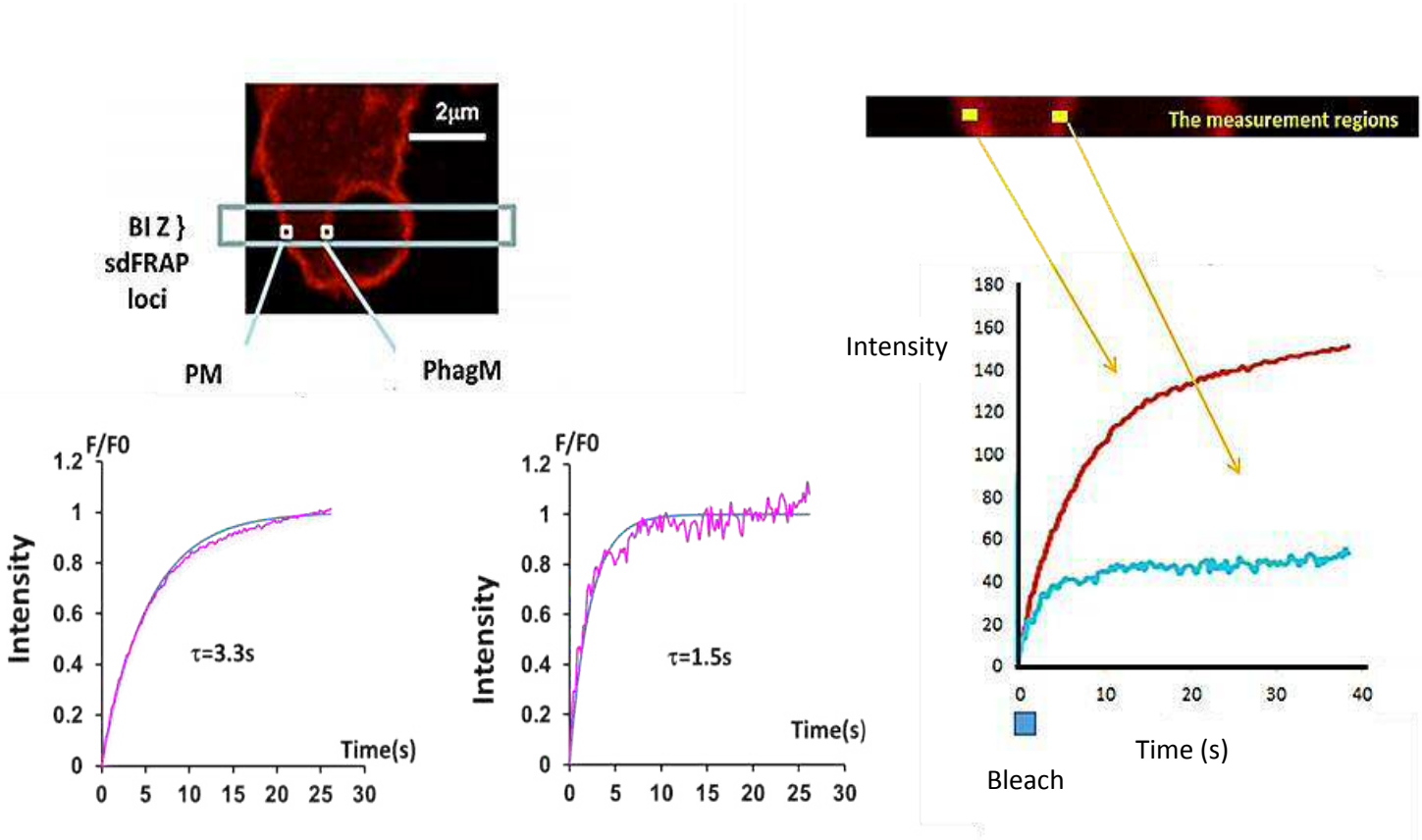

Figure 4.4 Comparison of membrane topography of the phagosomal membrane and the plasma membrane. The image (top left) shows the DiI staining of a portion of a neutrophil which has undergone phagocytosis of an opsonised zymosan particle, with the photo-bleached zone (Bl Z) and the loci of two measurement regions (sdFRAP loci) marked. The two graphs below (left) show the sdFRAP recovery of DiI fluorescence at the two regions indicated, i.e. the plasma membrane (PM) and the phagosomal membrane (PhagM) with the fitted curves ($1-e^{-kt}$), where k is the rate constant (see section 2.5.11.2) used to determine the characteristic times, τ, as shown in the figure. The graph on the right shows the raw data (without normalisation). The experiment shown was representative of at least 4 phagosomes measured.

K (s^{-1})	*Phagosomal* membrane	Plasma *membrane*	*PhagM/PM Ratio*
Cell 1	$0.45s^{-1}$	$0.25s^{-1}$	1.8
Cell 2	$0.3s^{-1}$	$0.19s^{-1}$	1.6
Cell 3	$0.25s^{-1}$	$0.15s^{-1}$	1.7
Cell 4	$0.3s^{-1}$	$0.2s^{-1}$	1.5
Mean	0.325	0.197	1.65
SD	0.087	0.041	0.11
SEM	0.043	0.021	0.056
RSE	13.2%	10.7%	3.4%
n	4	4	4

Table 4.2 Measurement of recovery rate constant, k values of plasma membrane and phagosomal membrane. The data show the sdFRAP recovery rate constants, k values of the plasma membrane and the closed phagosomal membrane in four cells. The population mean, standard deviation (SD), standard error of the mean (SEM) and relative standard error (RSE) are shown. Paired T-test of data was significantly different $p<0.05$, ($p = 0.0067$ unpaired t-test); and the ratio was significantly different from 1 ($p<0.05$).

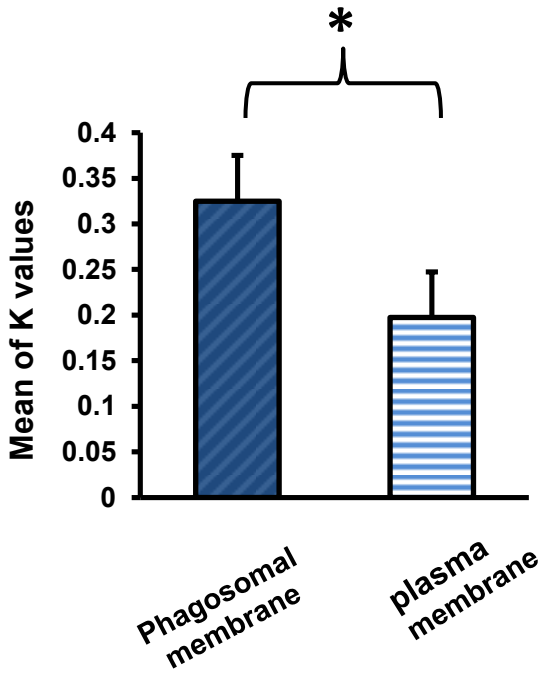

Figure 4.5 Graphical representation of the recovery rate constants for DiI diffusion in the closed phagosomal membrane and the plasma membrane. The histogram shows the mean and standard error of the mean of recovery rate constants (k, s^{-1}) for DiI diffusion in the closed phagosomal membrane and the plasma membrane. The data are also shown in Table 4.2.

4.3.2 Kinetics of phagocytosis of opsonised zymosan particles by human neutrophils

Two questions arise from the discovery that unwrinkling of the plasma membrane occurs locally at the site of phagocytosis. Firstly, at what stage in the process does plasma membrane unwrinkling occur (e.g. on particle contact, cup formation before phagosome closure or after closure) and secondly, if it occurred earlier, how restricted was the plasma membrane unwrinkling. This would obviously require performing sdFRAP on cells at an earlier stage of phagocytosis.

Since phagocytosis by neutrophils is a rapid and dynamic process, before attempting to monitor changes in the cell surface topography during phagocytosis, it was necessary to assess the kinetics of the process using zymosan attached to the glass coverslip (see section 2.6.2). When phagocytosis was induced between glass-adherent zymosan particles and the human neutrophils, there were two distinct stages. Following contact with the particle, a phagocytic cup formed within approximately 30s of contact (fig 4.6). The formed cup remained without any major change for up to 40-120s (fig 4.6), before the pseudopodia advanced rapidly to complete phagocytosis within the subsequent approximately 100s (fig 4.6). A similar time course of phagocytic cup formation has been previously observed when non-adherent zymosan is presented to neutrophils. The time at which the extension of pseudopodia accelerates correlates with the time Ca^{2+} signalling occurs (Dewitt and Hallett, 2002).

The initial phase of phagocytic cup formation and the final pseudopodial acceleration phases would present technical problems for using sdFRAP as the rapid movement of the cellular membranes distorted the recovery curves which could not be fitted simply to the expected kinetics. Also as the membranes of interest were moving, dual photo-bleaching of the same subdomain was not possible. However, the prolonged delay after phagocytic cup formation was ideal for surface topography monitoring as this delay gave sufficient time to undertake localised sdFRAP. In the demonstration experiment shown (fig 4.6), the membrane probe DiI was added at 76s to show that the delay was not the result of DiI labelling the neutrophil and further that DiI labelling did not arrest phagocytosis at this stage, but phagocytosis could continue to completion and formation of a fully internal phagosome (in this case within 120s of DiI addition). Thus, it was concluded that DiI did not interfere with the phagocytotic kinetics.

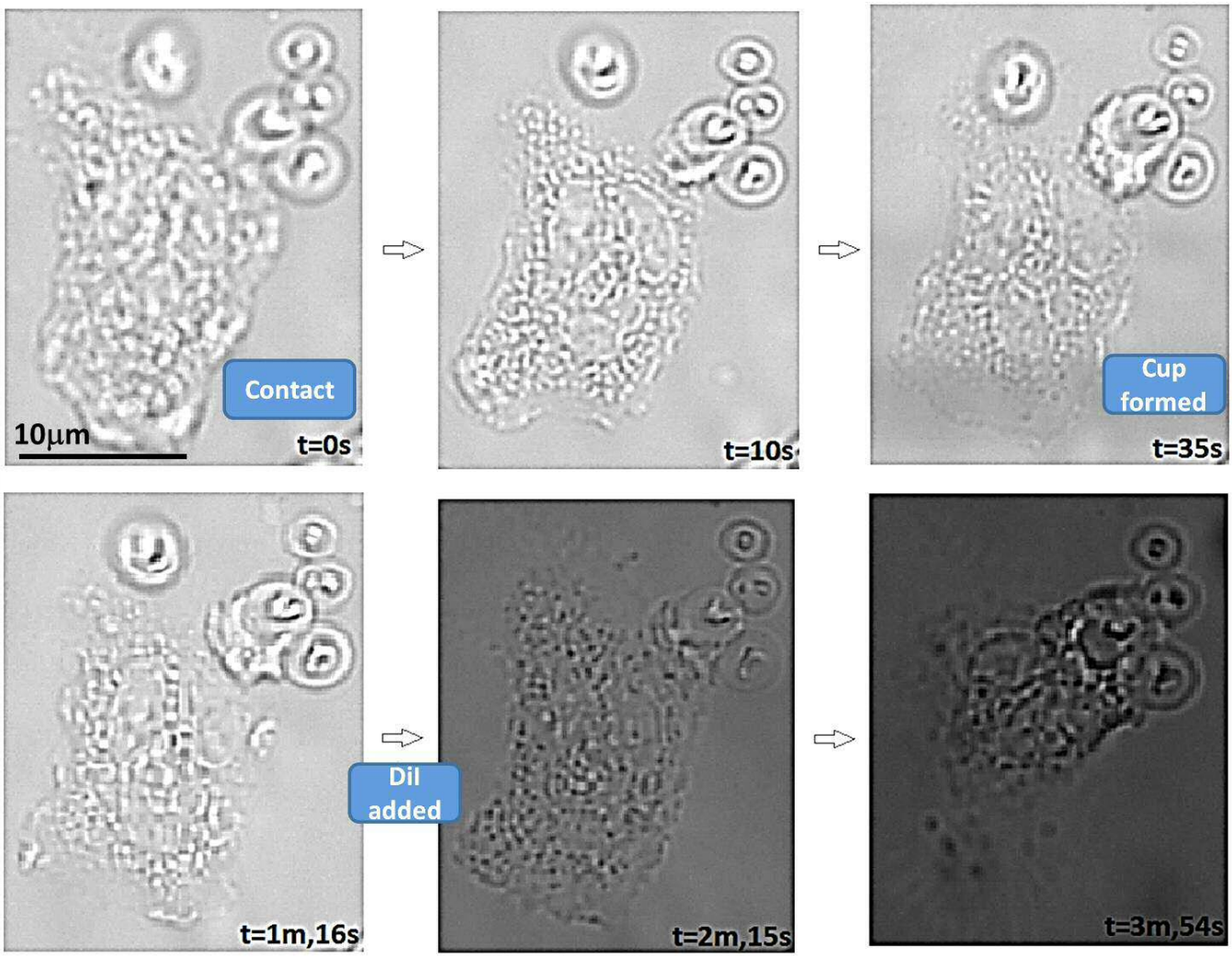

Figure 4.6 Kinetics of phagocytosis of opsonised zymosan by human neutrophils. Phase contrast images are shown which illustrate the process of phagocytosis under the experimental conditions adopted (see section 2.6.2). The time is shown at the bottom of each frame as t = xm, ys. The phagocytic cup which is formed around approximately 50% of the zymosan surface at 35s persisted until 76s (1 min and 16s). In this experiment, DiI was added to the cells at this point and in order to demonstrate that phagocytosis was able to continue to completion. This experiment was repeated on at least eight other cells from five different days and the sources of cells were from at least three blood donors, resulting in similar kinetics.

4.3.3 The topography of membrane comprising phagocytic cups

It was found from the sdFRAP kinetics of DiI in the forming phagocytic cup, that this membrane was significantly smoother than the adjacent plasma membrane. This suggested that the unwrinkling of the plasma membrane preceded complete closure and was probably the rate limiting step at this stage, as neutrophils often pause with an open cup before the Ca^{2+} signal is elicited and the process moves to completion (Dewitt and Hallett, 2002). In a series of experiments, this observation was very reproducible, but difficult to quantify accurately because during phagocytic cup formation, the speed of membrane movement relative to the time required for photobleaching and sdFRAP measurement was too great. However, as shown in section 4.3.2, there was a significant delay after phagocytic cup formation, before completion of phagosome formation. It was therefore possible to use sdFRAP to establish whether unwrinkling of membrane occurred earlier when the phagocytic cup was formed.

By changing the zymosan particle surface density, it was possible to induce multiple phagocytic events by a single neutrophil. In figure 4.7, a neutrophil is shown that had three phagocytic cups arrested at different stages. This gave an opportunity to perform sdFRAP simultaneously on the three cups and the adjacent plasma membrane within the same individual cell. There was a statistical difference in the rate of sub-domain fluorescence recovery in each of these loci compared to the plasma membrane (Table 4.3). The characteristic recovery time determined from k values found for curve fitting (fig 4.7) indicated that the plasma membrane around the forming phagocytic cup was significantly

less wrinkled that the non-phagocytic membrane, (as was shown in fig 4.4) even when the cell was forced to attempt phagocytosis of multiple targets (fig 4.7). This suggested that the membrane reservoir provided by the wrinkled surface of the neutrophil was significant and could account for a number of separate phagocytotic events without the need for a global Ca^{2+} signal and unwrinkling of the entire cell surface wrinkles.

Using the goodness of fit statistical method (Chi square as in section 4.31 and 4.3.2) to compare rate curves, the "normalised intensity" i.e. $(I_t-I_0)/(I_{max}-I_0)$, where I_t is the intensity at any time after bleaching; I_0 is the intensity after bleaching (time zero): and I_{max} is the intensity after full recovery (at infinite time) was calculated so that the zero and maximum values were fixed at zero and unity. This allowed the time of recovery (and the rate constant) to be compared directly and also for the curves to be compared for similarity or difference. The residual difference between the curves = $\Sigma\,((Ix1-Ix2)^2/Ix12)$, where I is the intensity at time x in curve 1 or curve 2 (see section 4.3.1). If the curves are the same and apparent difference are simply due to random noise, the sum of residuals would be zero; Σ (res) = 0, with an equal likelihood of positive and negative deviations. The 3 phagocytic cups represent the pre-stage before cup formation (cup1), cup formation at approx. 50% of the zymosan surface (cup2) and a further advanced cup (cup3) with approximately 80% of the zymoson surface covered. It was found that the rate of recovery in the pre-cup (cup1) was significantly different from either the later phagocytic cups (cups 2 and 3). These topography of the advanced phagocytic cups were not significantly different from each

other. Importantly, the rate of recovery of DiI within a single phagocytic cup was reproducible between the two bleaches and was not statistically different (Table 4.3). Using this determination, a map of the distribution of topographical indices was generated by sampling subdomains from multiple loci on the three phagocytic cups within the same photo-bleach slice (fig 4.8).

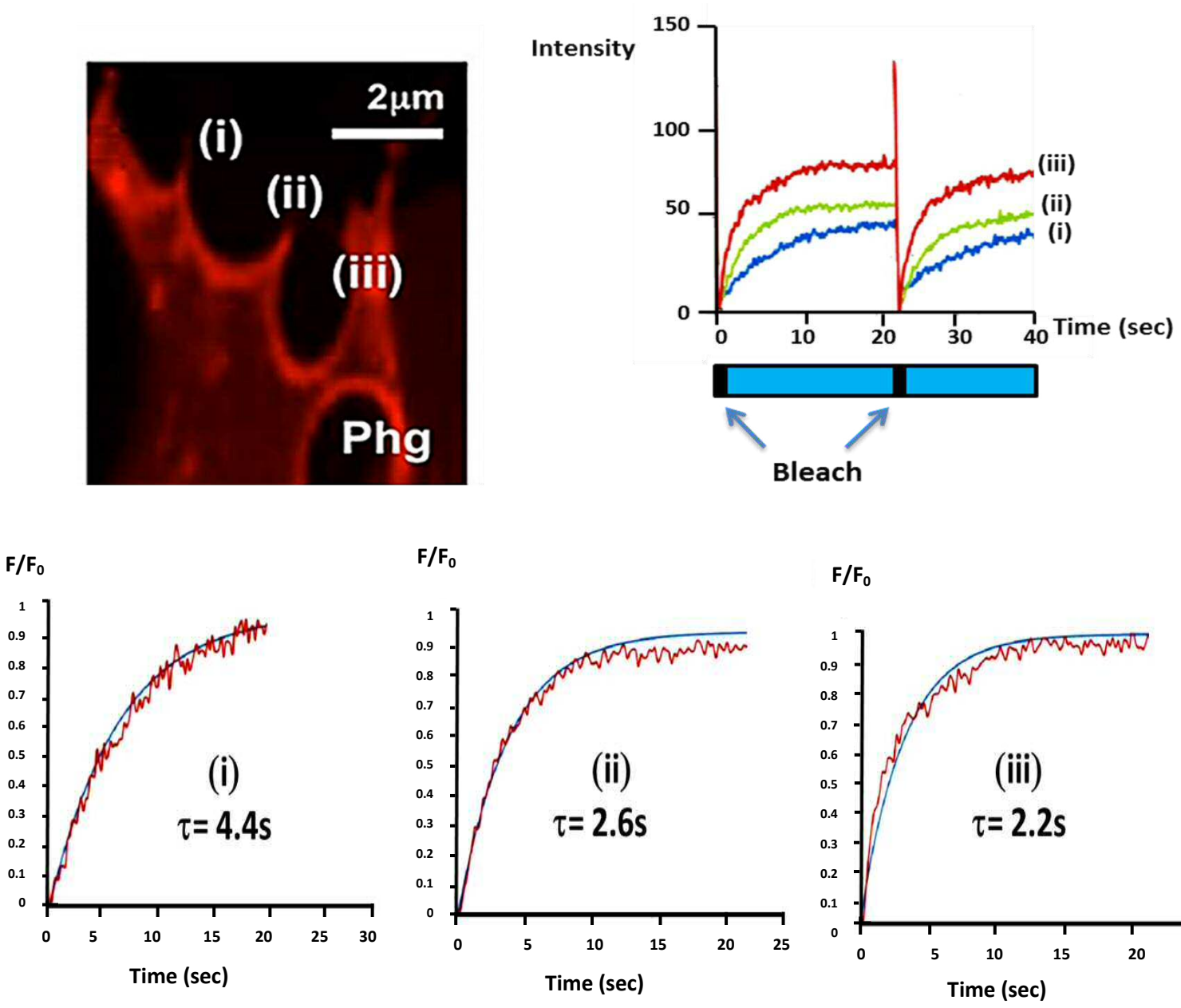

Figure 4.7 Neutrophil with multiple phagocytic cups. The image (top left) shows the DiI staining of a portion of a neutrophil which has completed phagocytosis of an opsonised zymosan particle (marked "Phg") and has three phagocytic cups marked i, ii and iii) en route to full phagocytosis. The graphs to the right shows the raw data from two photo-bleaches measured at three loci one each within the membrane of the three phagocytic cups. The graph below shows the sdFRAP recovery of fluorescence in the three phagocytic cups with the fitted curves from which the characteristic times, τ, were estimated.

P values (n = 77)	Bleach 1 v Bleach 2	Cup 1	Cup 2	Cup 3
Cup 1	0.27		<0.0001*	<0.0001*
Cup 2	0.28	<0.0001*		0.29
Cup 3	0.35	<0.0001*	0.29	

Table 4.3 The statistical significance of recovery rates from the 3 phagocytic cup within the same cell. For each sdFRAP recovery curve (normalised to F/F0), the 77 time paired points from bleach to recovery were compared between the first and second photobleaches (column 1) and between phagocytic cups 1, 2 and 3 as indicated in columns 2, 3 and 4 using the chi square (goodness of fit) parameter $\Sigma.(O-E)^2/E$*, where E is the expected value from the* $1-e^{-kt}$ *curve fit to the cup indicated on each row and O is the corresponding observed value from the cup shown in each row. The table shows that the replicate bleaches from each cup were not significantly different (column 1), nor were cups 2 and 3 significantly different from each other. In contrast, the recovery rate in cup 1 (the pre-cup (i) at an early stage of cup initiation/formation) is highly significantly different (*p =* $c.10^{-38}$-10^{-16}*) from either cup 2 or cup 3.*

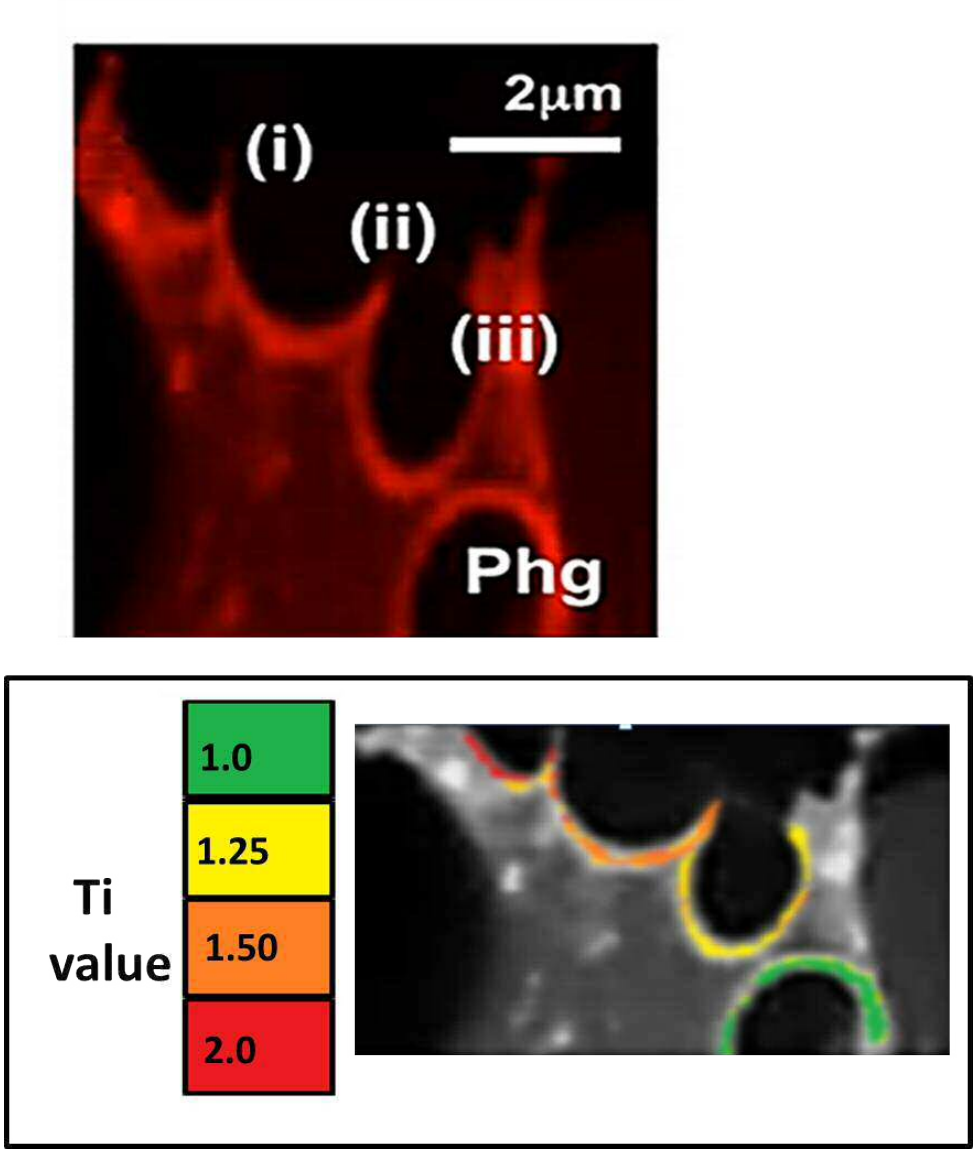

Figure 4.8 Topographical map of phagocytosis. The upper image shows the DiI loaded confocal image of the region of a neutrophil with the three phagocytic cups of interest labelled. The lower image shows the corresponding phase contrast image of the cell shown with a pseudo-colour overlay to illustrate the distribution of Ti values as a measure of the wrinkledness of the membrane, where a Ti value of 1 is smooth and higher values indicated increasing surface features. The colour bar shows the cut-offs used where green was used for Ti values of 1 - 1, 25; yellow 1, 25 - 1.5; orange 1.5 - 2.0 and red for greater than 2.0.

4.3.4 The topography of the plasma membrane after cell spreading

The second dramatic cell shape change which neutrophils undergo occurs when spreading on a surface. This has been likened to the localised "spreading" of the neutrophil membrane over a phagocytic particle, but on a larger scale so that the surface (having infinite curvature) cannot be internalised. Neutrophil spreading can occur on a glass surface (e.g. a glass coverslip) and is thought to involved immobilisation of neutrophil integrin receptors on the charged glass surface and so mimic physiological spreading. Like phagocytosis, it occurs quickly, complete within 100s and depends on a large Ca^{2+} signal which is triggered by contact with the glass (Kruskal *et al.,* 1986; Marks *et al.,* 1990; Dewitt *et al.,* 2013). It has been postulated that, as with phagocytosis, the additional membrane required for the transition from non-spread to spread is provided by the reservoir of membrane within the wrinkled surface (Raucher *et al.,* 2000; Dewitt & Hallett, 2007). sdFRAP was therefore applied to cells in the process of spreading. It was found that in every cell, sdFRAP of neutrophils membrane before and after spreading was significantly accelerated (fig. 4.9). The sdFRAP recovery rates (k) were 0.20 ±- $0.03s^{-1}$ before spreading and 0.11 ±- 0.022 (n = 3), giving a reduction in the topography index of the cell body from 2.6 ± 0.4 to 1.43 ± 0.29 (n = 3). These differences were statistically significantly different at the $p<0.1$ level ($p = 0.082$). The difference was greater in the tail region of spread neutrophils, where the Ti value was unity (as shown in Chapter 3; figure 3.3). This was consistent with the loss of surface wrinkles contributing to the additional membrane needed for spreading.

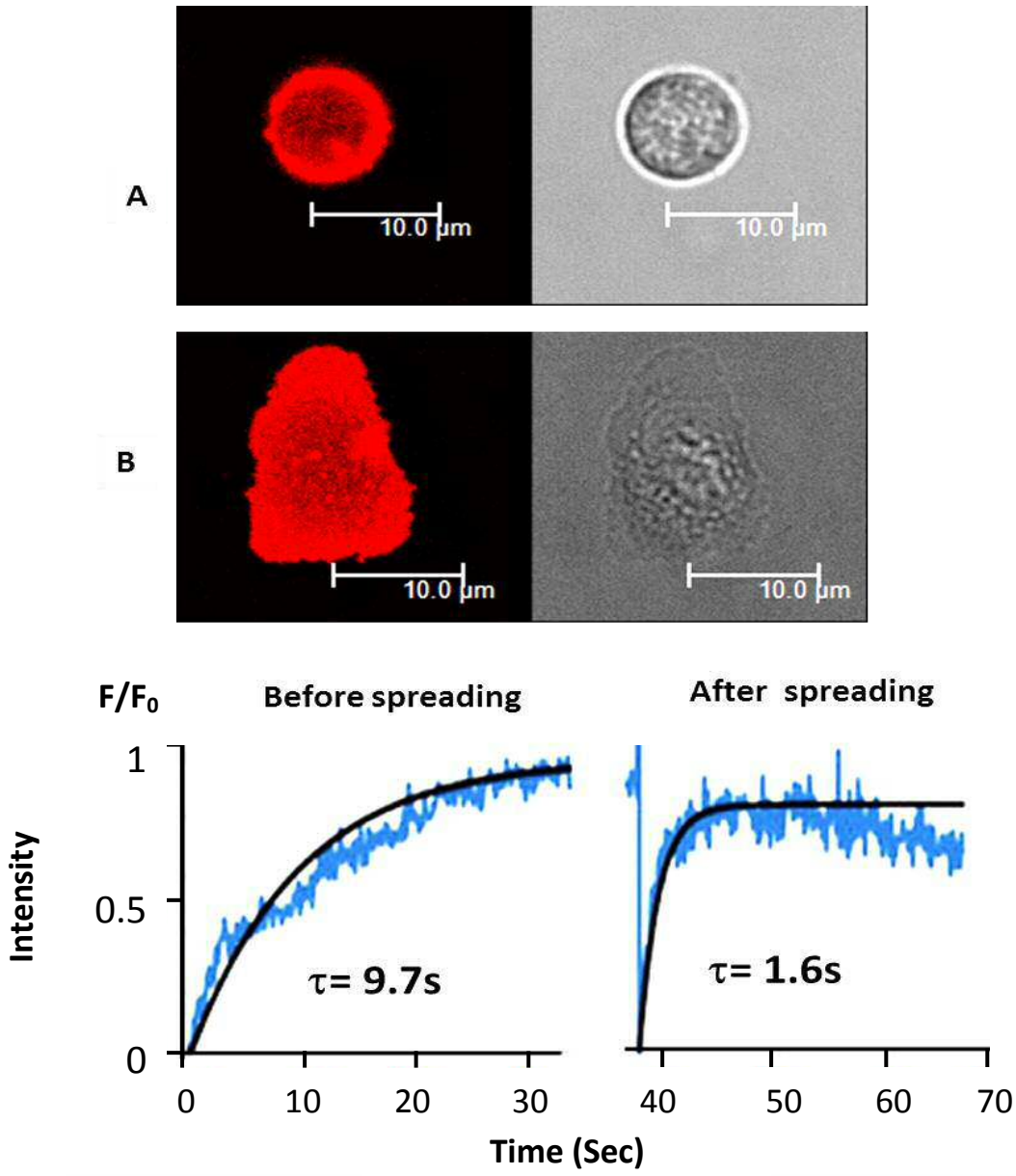

Figure 4.9 The effect of neutrophil spreading on cell surface topography. Cell surface topography during cell spreading was established by sdFRAP measurement before and after cell spreading of individual neutrophils. An example of the change in sdFRAP signal from an individual neutrophil is shown in (A) before and (B) after spreading onto a glass coverslip. The inset phase contrast images show the gross morphological difference in the cell before and after spreading. The fluorescence recovery curves before and after cell spreading are shown together with the fitted curve ($F/F_0 = 1-e^{-kt}$) and the characteristic time for recovery (τ). As both images were taken at the same magnification, the scale bar applies to both images. This experiment was typical of at least three other similar experiments on three different days from different donors for each day.

4.3.5 Cell surface topography changes induced by transient Ca^{2+}influx

It has been known for 30 years that an elevation of cytosolic Ca^{2+} precedes the neutrophil spreading response (Kruskal et al, 1986; Marks and Maxfield, 1990) and that inducing a Ca^{2+} signal, triggers neutrophil spreading (Pettit & Hallett, 1998; Dewitt *et al.,* 2013). Similarly, a Ca^{2+} signal is required for the localised cell shape change that is required for rapid phagocytosis (Lew *et al.,* 1985; Kruskal & Maxfield, 1987; Dewitt & Hallett, 2002). The evidence points to a permissive role for Ca^{2+} signalling for neutrophil shape change, by the localised activation of calpain, a cytosolic Ca^{2+} activated protease which cleaves the cortical actin-plasma membrane linker proteins, such as ezrin. While elevating cytosolic Ca^{2+} by photolytic uncaging of "caged Ca^{2+}" can induce spreading (Pettit & Hallett, 1998), this required a global cytosolic Ca^{2+} rising to a level which was not physiologically observed. In contrast, uncaging IP_3 induces neutrophil spreading in response to physiological Ca^{2+} levels (Dewitt *et al.,* 2013). This is attributed to the indirect effect of IP_3 by inducing Ca^{2+} influx, which mathematical modelling suggests can elevate cytosolic Ca^{2+} within the wrinkles to sufficiently high levels to activate calpain (Brasen *et al.,* 2010). As uncaging IP_3 triggered a Ca^{2+} influx, which induced cell spreading, it would not be able to distinguish between an effect on cell surface topography as the result of Ca^{2+} influx or to cell spreading. As cell spreading was shown to alter the cell surface topography, in order to test whether an elevation of Ca^{2+} influx alone was sufficient to alter the cell surface topography, a plastic film substrate to which neutrophils cannot adhere or spread was used. The effect of photo-lytically uncaging IP_3 in neutrophils under

these conditions was established. It was found that an IP_3-driven Ca^{2+} influx had a significant effect on sdFRAP in the absence of cell spreading (Ti = 4.0 ± 0.3 and 2.7 ± 0.4 before and after uncaging respectively, n = 4: sig diff $P<0.05$). After the Ca^{2+} signal, sdFRAP indicated a decreased diffusion path-length (fig. 4.10), which would result from flattening of the cell surface wrinkles even in the absence of cell spreading.

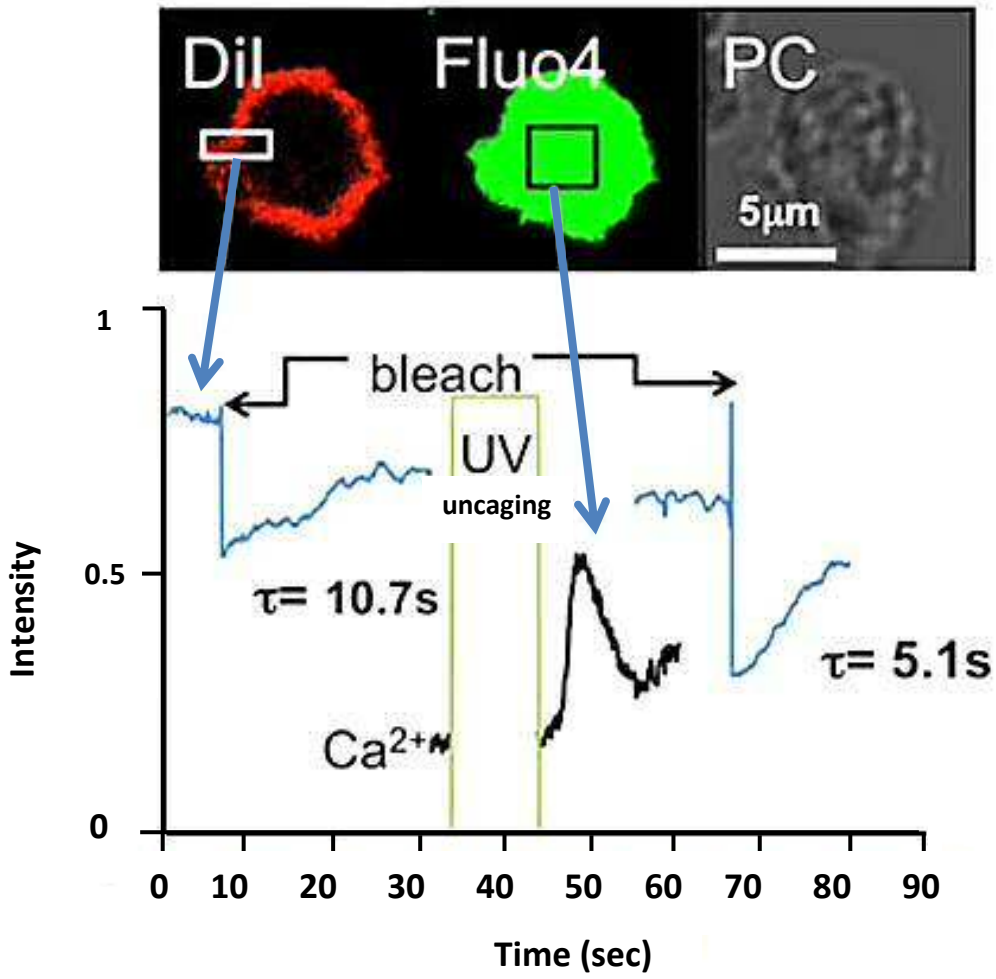

Figure 4.10 Uncaging cytosolic caged IP_3 on cytosolic Ca^{2+} and cell surface topography. An example of a neutrophil loaded with the cytosolic Ca^{2+} indicator fluo4, cytosolic caged IP_3 and membrane DiI, sedimented onto a plastic film coated coverslip on which spreading cannot occur. The images show the DiI image (DiI) showing its location at the cell periphery, fluo4 shows its cytosolic location (fluo4) and the phase contrast image (PC). The graphs show the time courses of DiI fluorescence (blue) and fluo4 intensity (black). IP_3 was uncaged by transient illumination with the 404nm laser as shown (UV uncaging) while fluo4 intensity, as a marker of cytosolic Ca^{2+} was monitored. DiI was photo-bleached both before and after the IP_3–induced Ca^{2+} signal in the zone shown and the characteristic times, τ, for sdFRAP are shown. This was typical of at least 4 experiments and neutrophils were sourced from four separate donors.

In order to discover whether this effect was the result of IP_3 driven Ca^{2+} influx or the global elevation of cytosolic Ca^{2+}, cytosolic Ca^{2+} was elevated using a Ca^{2+} ionophore, ionomycin. Ionophores have the effect of increasing the inward leak of Ca^{2+} into the cell (by acting as a cryptating ion carrier across the plasma membrane). This method of elevating cytosolic Ca^{2+} to a similar level to the peak of the IP_3-induced Ca^{2+} signal had no effect on the cell surface topography (fig 4.11). In three similar experiments there was no significant change in the sdFRAP signal (paired *t*-test $p>0.6$). This demonstrates that the physiological route of elevating Ca^{2+} via IP_3 and Ca^{2+} channel opening and not the elevation of cytosolic Ca^{2+} itself was responsible for triggering the change in cell surface topography. This result was therefore consistent with the requirement for the opening of physiological Ca^{2+} channels. These data point to Ca^{2+} influx alone as being responsible for controlling the wrinkled morphology of the cell surface.

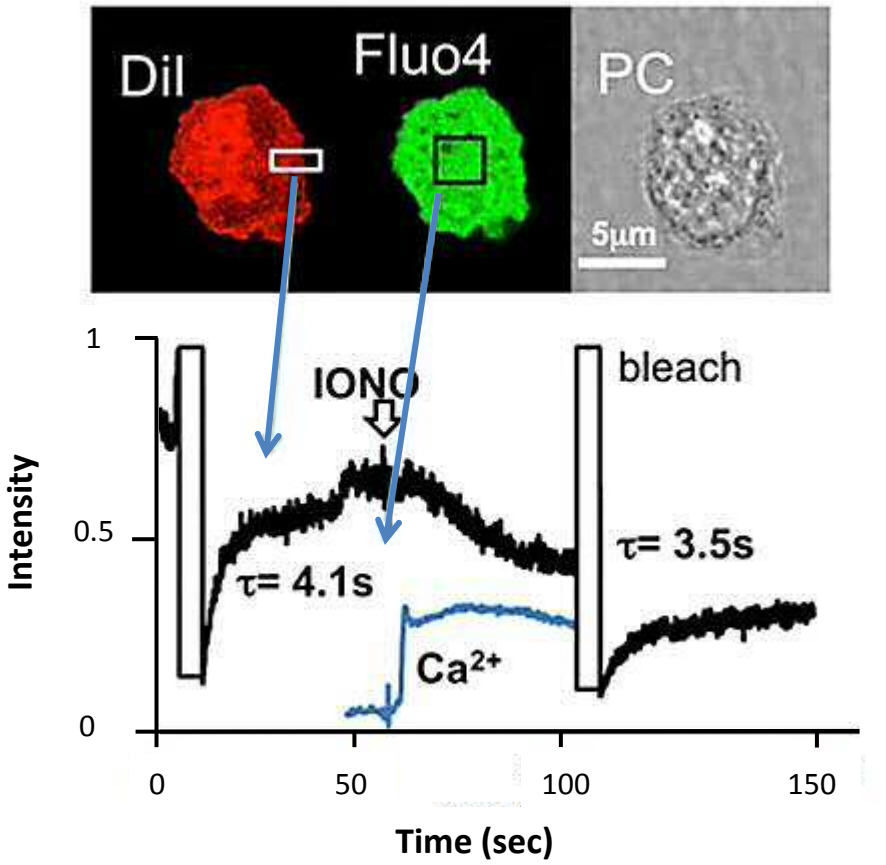

Figure 4.11 The effect of elevating cytosolic Ca^{2+} using ionomycin on the cell surface topography. An example of a neutrophil loaded with the cytosolic Ca^{2+} indicator fluo4 and membrane DiI, sedimented onto a plastic film coated coverslip to which it cannot spread. The images show the DiI image (DiI) showing its location at the cell periphery, the cytosolic location of fluo4 (fluo4) and the phase contrast image (PC). The graphs below show the time courses of DiI fluorescence (black) and fluo4 intensity (blue). Ionomycin (4µM) was added (IONO) while fluo4 intensity, as a marker of cytosolic Ca^{2+}, was monitored. DiI was photo-bleached both before and after the ionomycin-induced Ca^{2+} signal and characteristic times, τ, for sdFRAP are shown. These data were typical of 3 experiments undertaken on three separate days and neutrophils were sourced from three separate donors.

4.4 Discussion

The novel approach developed in Chapter 3 depends simply on the incorporation of a fluorescent probe into the plasma membrane and monitoring recovery of fluorescence at a defined distance from the photo-bleach front (sdFRAP). This method clearly showed that the plasma membrane of neutrophils was significantly wrinkled (Chapter 3), but that globally during cell spreading or locally in the neutrophil tail, this wrinkling is lost. In this chapter, it is shown that during phagocytic cup formation and phagosome formation, the wrinkled plasma membrane becomes a smooth surface. These novel results are therefore consistent with the unwrinkling of the plasma membrane as being the reservoir of membrane in neutrophil shape change. This would explain the finding that ruffling of the neutrophil surface is inhibited if the cell is forced to adopt an extremely elongated morphology and resumes when the cell is severed to form two non-elongated forms (Houk *et al*., 2012). Our data suggest that the extremely elongated form takes up all the slack provided by the wrinkled topography, such that further deformation of the surface to form ruffles is prevented. On severing the cell, relaxation of the two cell fragments into non-elongated form would permit the slack in the membrane to become available again and the neutrophil would then resume surface ruffling. In that paper, the discussion was in terms of membrane tension. Membrane tension has also been implicated in both cell spreading (Gauthier *et al*., 2011) and phagocytosis (Masters *et al.,* 2013). However, as ezrin is both a regulator of membrane tension (Brueckner *et al.,* 2015) and the maintenance of non-smooth cell topographies such as microvilli and microridges (Bretscher *et al.,* 1997; Lamb *et al.,* 1997), membrane tension may be controlled by the

ability to form these surface structures (Brueckner *et al.,* 2015) and so be intrinsically linked.

It is obvious that there is an apparent increase in the cell surface membrane after internalisation of a phagocytotic target, which is sufficient to enclose the phagocytic target. It has been suggested that the additional membrane may come from the addition of extra membrane by fusion of membrane vesicles within the cell with the plasma membrane. However, it is difficult to arithmetically account for the extra membrane from this source (Hallett and Dewitt, 2007). An alternative proposal is that the "additional" membrane is held in a reservoir of membrane held within wrinkles at the cell surface. However, this has never been tested as there has been no methodology available to demonstrate a change in cell surface topography in living cells. There are also questions about how spatially restricted such unwrinkling might be. SEM images have been used but are difficult to quantify and could be criticised as they are images of fixed dehydrated cells, which may consequently have altered surface topography. The work presented in this chapter has therefore employed the technique which I developed in the earlier chapter (Chapter 3) aimed at quantifying changes in cell surface topography in living cells, subdomain FRAP. In this work here, I have extended sdFRAP to compare the topography of subregions of the membrane in neutrophils which were undergoing phagocytosis. In this way, I sought to answer the question of whether unwrinkling of the cell surface could be observed and if so whether the effect was global or localised to the region of the cell undergoing phagocytosis.

It was found that there was a striking difference on the smoothness of the topography of membrane in closed phagosomes and the nearby plasma membrane (section 4.3.1). The lack of wrinkles in the phagosome was consistent with localised unwrinkling of the plasma membrane. The degree of wrinkling of the plasma membrane in neutrophils with phagosomes was not significantly different from inactive (non-phagocytic) neutrophils. This suggested that only a small fraction of the membrane reservoir had been used to form the phagosome. Of course, the wrinkles at the cell surface may have been globally released during phagocytosis and reformed before the sdFRAP measurements were taken. In order to investigate this, neutrophils were chosen which were in the process of phagocytosis and had forming phagocytic cups, but were yet to completed phagocytosis. Again it was found the phagocytic cup membrane was significantly smoother than the rest of the cell body and again that the cell body was wrinkled to a similar degree as in non-phagocytic cells.

By monitoring cytosolic Ca^{2+} changes during phagocytosis, it is known that the cells which had paused at the phagocytic cup stage had not yet fired a Ca^{2+} signal. Once the Ca^{2+} signal had fired, completion of phagocytosis was too quick to allow sdFRAP to be performed. The role of cytosolic Ca^{2+} was therefore addressed separately in cells in which the Ca^{2+} signal could be controlled experimentally. It was found that the cell surface topography was modified simply by uncaging cytosolic IP_3, which releases stored Ca^{2+} and opens Ca^{2+} influx channels at the plasma membrane. This experimental procedure reduced the wrinkledness of the cell surface significantly even in cells which are prevented from spreading onto a glass surface. This finding would explain why Ca^{2+} influx permits an

increase in the rate of both neutrophil spreading and phagocytosis, as it makes wrinkled surface membrane available for the increase in surface area required. It is therefore proposed that cell surface topography, while previously little considered, is a controlled feature of cells, which is a key element in maintaining cell surface tension and permitting the apparent membrane expansion required for spreading and phagocytosis.

The possibility exists that 'slack' in the wrinkles would allow them to un-wrinkle a little without the need for a Ca^{2+} signal. Herant *et al* (2002) have shown that using a micropipette to aspirate the cell surface of neutrophils, that only a small suction force need be applied locally to cause a small deformation of membrane into the mouth of the pipette (local membrane expansion) but that a considerably higher force must be applied to unwrinkle the membrane further. These authors suggested that the wrinkles are held together by a molecular "velcro" and modelled the slack as occurring at the wider base of the wrinkles and the tighter adhesion along the length of the narrow projection (as with the strength of macro-velcro). Ca^{2+} activated calpain may be able to cleave this molecular "Velcro" composed of cross-linking proteins, such as ezrin (cytovillin) and so may account for the acceleration phase. It has previously been proposed that a localised elevation of cytosolic Ca^{2+} (perhaps restricted to the wrinkles) would be sufficient to activate the Ca^{2+} activated protease calpain-1 to cleave ezrin specifically within the wrinkles. Mathematical modelling has shown that within wrinkles, Ca^{2+} influx could transiently elevate the Ca^{2+} concentration to 30-80μM (Brasen *et al.,* 2010). Before the Ca^{2+} signal was induced, i.e. early phagocytic cup formation, the data presented here suggest that there was sufficient extra membrane in the wrinkle "slack" such that complete unwrinkling was not required for this initial stage

(section 4.3.3). Under these conditions where multiple phagocytotic events were occurring, if all the slack were used by the multiple cups, the membrane remote from the phagocytic cups may be stretched and its slack also utilised. However, it was found that even with multiple phagocytotic cups, there was sufficient localised unwrinkling in the forming cup and that no change in surface topography at sites away from the phagocytic cup was required. This underlined the scale of the membrane reservoir within the cell surface wrinkles.

4.5 Summary

In this chapter I have presented work using the novel technique that I developed in Chapter 3 to investigate neutrophil cell surface topography during phagocytosis. I discovered that the membrane of the closed phagosome is virtually smooth, showing that unwrinkling of the plasma membrane had occurred. In addition, the unwrinkling preceded phagosome closures as phagocytic cups were similarly unwrinkled. The time of unwrinkling was pinpointed to between adhesion and phagocytic cup formation.

Chapter 5

Hyper-wrinkled neutrophils:

Effects on cell spreading, chemotaxis and phagocytosis

5.1 Introduction

In a previous chapter (Chapter 3), I have developed a methodology that allows changes in the cell surface topography to be monitored in living cells. This work showed that there was sufficient "additional" membrane within the cell surface "wrinkles" to account for the additional membrane required for phagocytosis and cell spreading. In addition, the work in Chapter 4 showed that during neutrophil shape change (phagocytosis and spreading), the degree of wrinkling was reduced and was totally lost in the phagocytic cup. It was thus hypothesised that the cell surface topography of neutrophils is important in providing a reservoir of membrane which is required for cell spreading and phagocytosis (see also Chapter 1). Although this hypothesis had been difficult to test directly, the work presented in Chapter 3 using sdFRAP to report on changes in the cell topography, showed that the cell surface topography of neutrophils could be altered experimentally by osmotic shrinking or swelling and also chemically by the addition of the membrane "expander", deoxycholate. This opens the possibility of establishing the effect on the ability of neutrophils to change shape by experimentally changing the surface topography osmotically and chemically by the use of membrane expanders, such as deoxycholate, on these neutrophil functions.

The effect of these experimental manipulations may be anticipated. For example, osmotic shrinking, which I have shown increases the wrinkledness of the cell surface, may inhibit cell shape changes. The osmotically formed wrinkles would remain, even after triggering the release of the constraints holding the "physiological wrinkles" in place. This

would so prevent the expansion of the cell (fig 5.1 b). In contrast, adding extra cell surface area chemically with membrane expanders, which I have shown also increases the cell surface “wrinkledness”, may not be expected to inhibit the normal expansion of membrane. Under these conditions, the release of the constraints holding the “physiological wrinkles” in place would still be able to add available additional membrane for spreading (fig 5.1 a). It is unclear what cell swelling would do. If swelling was sufficient to take up the “slack” within the wrinkles, with the constraints still holding the “physiological wrinkles” in place remaining, there would be little effect. However, if swelling was sufficient to break apart the “molecular velcro” holding the “physiological wrinkles” in place, no further membrane expansion would be possible (fig 5.1 c).

These are testable predictions from the hypothesis that the cell surface topography controls the ability of neutrophils to expand their apparent cell surface area. These will therefore be addressed in this chapter.

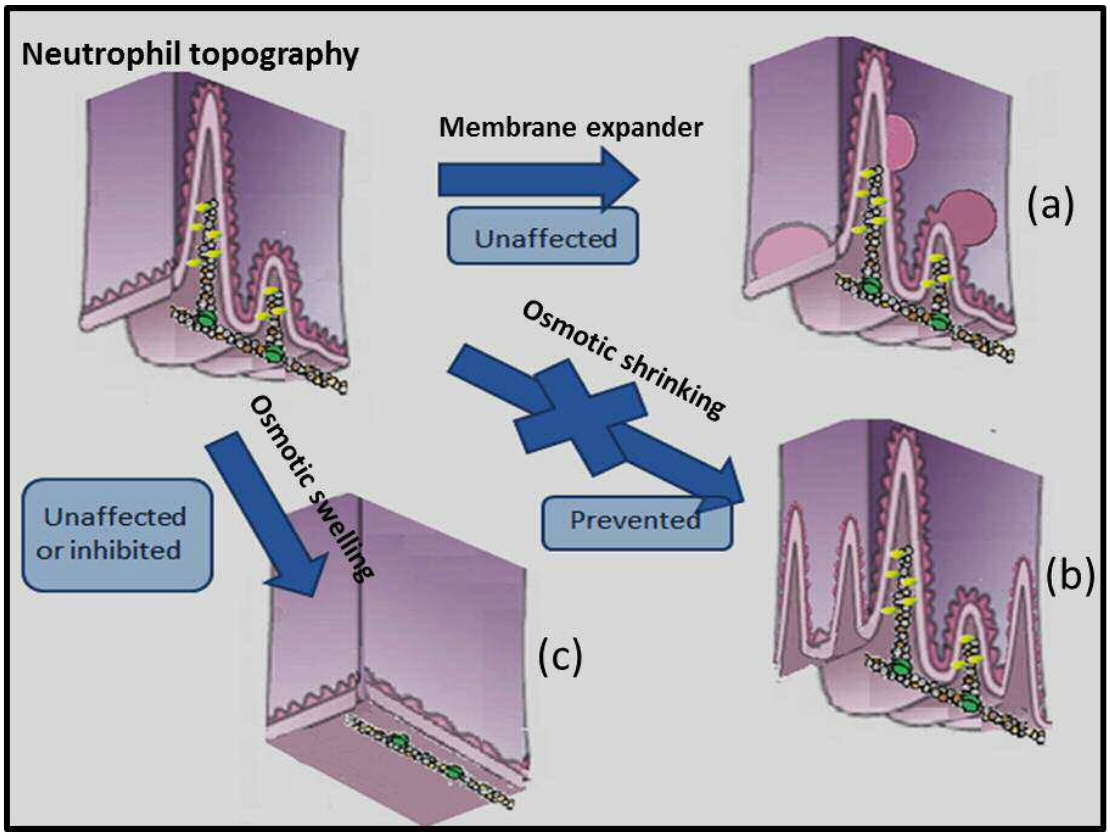

Figure 5.1 Summary of anticipated effects of experimental manipulation of neutrophil surface topography. The figure shows the effect of experimental manipulations on the neutrophil surface topography and its expected effect on the ability to expand in response to three different conditions. The upper left figure shows the normal neutrophil topographical architecture. The surface folds are held in place by cross-linking elements between the plasma membrane and the cortical polymerised actin. The arrow pointing to (a) indicates the effect of expanding the surface area by deoxycholate and the anticipated effect on neutrophil shape change behaviour is shown beneath the arrow. The arrow pointing to (b) shows the effect of hyperosmolarity, where surface wrinkles are formed via osmotic wrinkling of the cell. The arrow pointing to (c) displays the effect of hypo-osmolarity, which forces the physiological wrinkles to unwrinkle by mechanical stress.

5.2 Aim of the Chapter

The aims of the work in this chapter are to establish whether events which require neutrophil membrane expansion, such as phagocytosis and cell spreading, can be influenced by osmotic change and by chemical membrane expanders. The objectives of the work presented in this chapter, therefore, were to

1. Test whether experimental alteration of the cell surface topography had an effect on the ability of neutrophils to change shape and undertake spreading, chemotaxis or phagocytosis consistent with the membrane reservoir hypothesis outlined above.

2. If inhibition was observed, to establish whether the effect was explicable solely by the effects on cell surface topography or whether an inhibition of Ca^{2+} signalling events (the obligatory trigger) was also affected.

5.3 Results

5.3.1 Experimental manipulation of the cell topography

In Chapter 3, the effect of 3 experimental conditions (osmotic cell swelling, shrinking and the use of chemical plasma membrane expanders) were shown to affect of the sdRAP signal consistent with a change in the cell surface topography. This opens the possibility of using these experimental manipulations to investigate changes in cell surface topography on cell behaviour. It was, however, important to confirm the sdFRAP-derived conclusions by direct visualisation of the cell surface topography. As scanning electronic microscopy has sufficient resolution to visualise the cell surface in fixed cells, this was employed. Neutrophils were subjected to the three conditions found to affect the sdFRAP signal. Samples of the cells were examined by light microscopy and by sdFRAP and when the sdFRAP change had been confirmed, cell samples were immediately glutaraldehyde fixed in suspension to maintain the cell surface on the cells before adhesion. The fixed cells were sedimented onto the matrix of an SEM imaging “stud” by filtration and then gold coated (see section 2.9). In this way, the morphological alterations made to the normal topography of the neutrophils could be seen (fig 5.2). In the untreated neutrophils, the normal microridges and wrinkles were observed (fig 5.2 i). After osmotic swelling, the neutrophils were enlarged and more smooth with fewer wrinkles (fig 5.2 ii), as predicted from the sdFRAP measurements. Osmotic shrinking caused a dramatic increase in the appearance of wrinkles and increased the wrinkle coverage of the cell surface (fig 5.2 iii). Pre-treating the cells with the membrane expander Doc produced slightly enlarged cells with distorted microridges

decorated with microbleb-like structures (fig 5.2iv). Thus, SEM imaging confirmed visually the conclusion reached by sdFRAP measurements. It was therefore concluded that these three experimental manipulations could be used with confidence in the nature of changes in the cell surface topography which they generated.

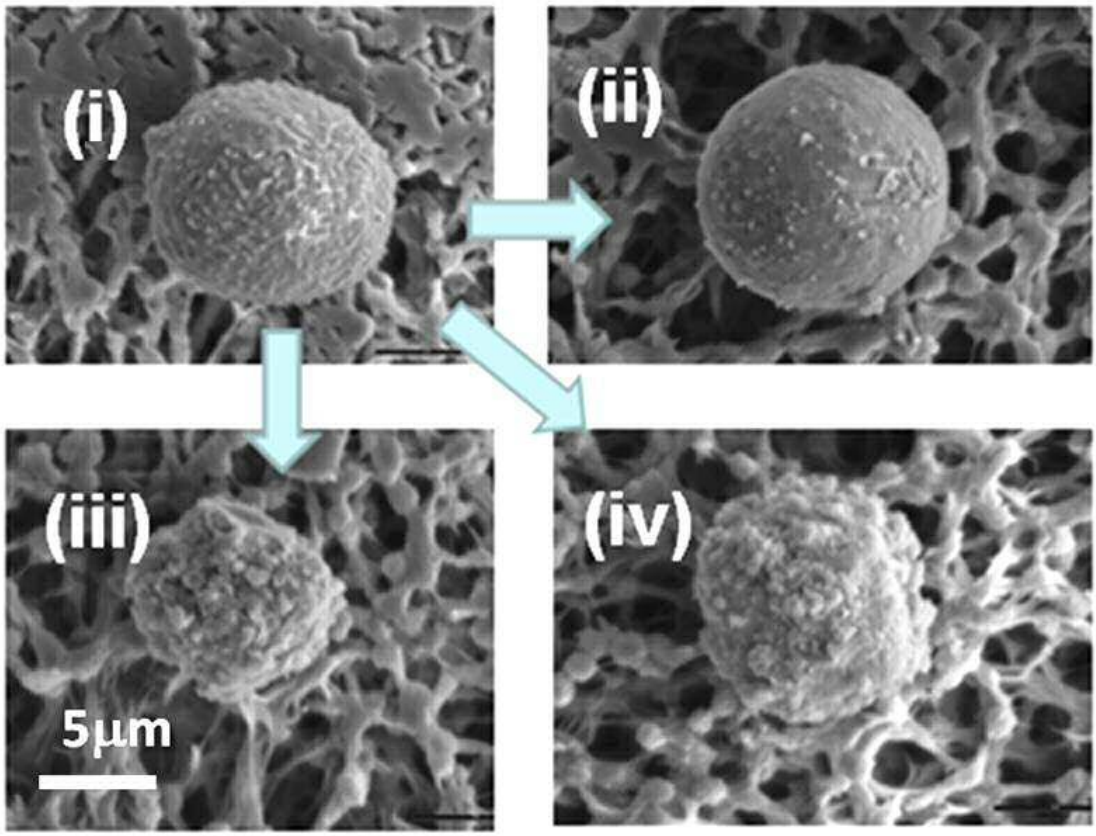

Figure 5.2 Scanning electron micrographs of neutrophils treated as in the live cell experiments. (i) An untreated cell with numerous surface microridges (wrinkles), (ii) a cell after hypo- osmotic swelling with fewer surface wrinkles and increased cell volume, (iii) a cell after hyperosmotic treatment with a smaller cell volume and numerous additional cell surface features and (iv) a cell after treatment with deoxycholate showing additional cell surface features but a similar cell diameter. The micrographs were typical of similarly treated cells in the same microscopic field (n>50). Two separate experimental runs with neutrophils from two sources confirmed these observations.

5.3.2 Effect of chemical "membrane expanders" on neutrophil cell spreading

The effects of two membrane expanders, deoxycholate and octanol, on the ability of cells to spread were tested. Neutrophils pre-treated with deoxycholate showed a typical transition from spherical to spread morphology (fig 5.3) with the kinetics not significantly different from untreated control cells (fig 5.1). The mean sizes of the contact area of the cells before and after treatment with deoxycholate (0.4mM, 15 mins) were: initial area control 72.2 ± 1.8μm^2, treated 74.5 ± 1.4μm^2 and after spreading the contact areas were 126.7 ± 11.3μm^2 and 142.4 ± 17.4μm^2 respectively. The times taken for spreading were 177 ± 18.5 sec and 124 ± 24.0s. It should be noted that these times are slower than in untreated cells because all cells, including the controls, were maintained at 37^oC for 15 mins before the experiment. However, the times required for spreading were not significantly different between the deoxycholate-treated and control (fig 5.4). Neutrophils pre-treated with octanol were also able to spread and achieved spread areas similar to the untreated or the deoxycholate -treated cells (fig 5.4). However, they were significantly slower in the time required to reach their final spread size. The mean sizes of the contact area of the cells before and after treatment with octanol (0.4mM, 15 mins) were: initial area control 72.2 ± 1.8μm^2, treated 71.7 ± 1.5μm^2 and after spreading the contact areas were 126.3 ± 11.3 and 133.1 ± 9.6μm^2 respectively. These were not significantly different (fig 5.4). The times taken for spreading, however, were 177 ± 18.5s and 287.5 ± 56.3s. This latter difference was significantly different at p<0.1. It was possible that Octanol had an additional toxic effect in addition to the effect on cell surface topography which slowed the spreading process. However, as DOC-treated cells with a demonstrably increased surface wrinkledness (see

section 3.3.7) could spread in a similar manner to control, this eliminated the possibility that the membrane expander-induced change in topography, by itself, was sufficient to prevent spreading.

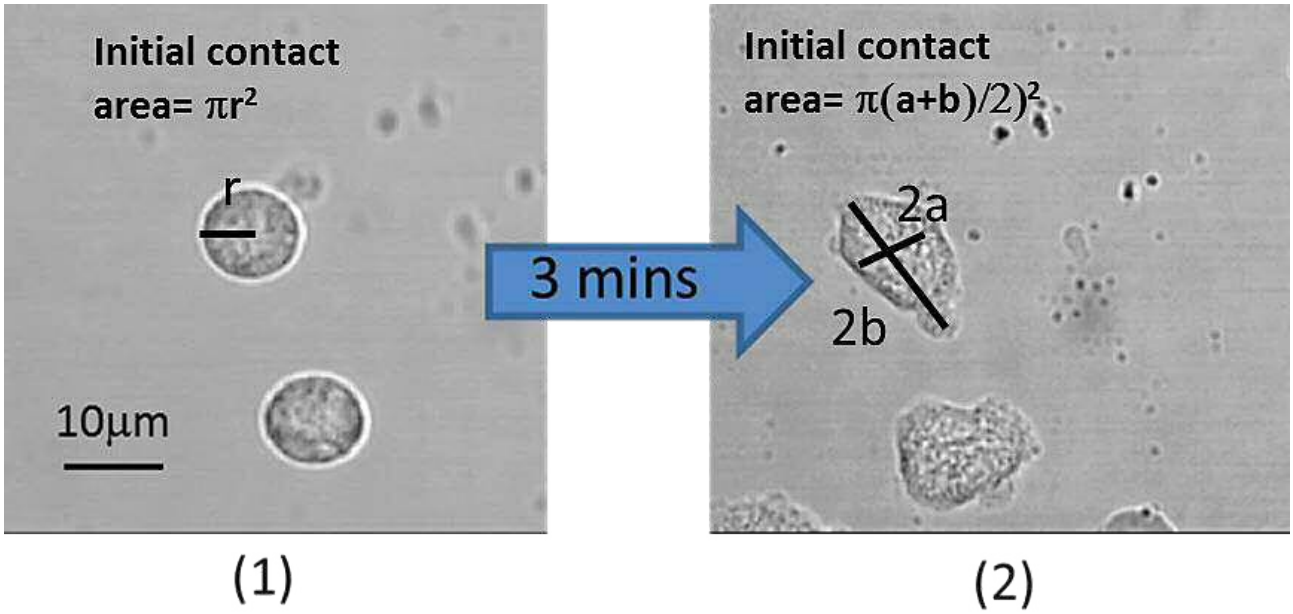

Figure 5.3 Spontaneous spreading of deoxycholate-treated neutrophils. (1) Neutrophils pre-incubated with Doc (0.4mM) showing "spherical morphology". (2) The same microscopic field is shown three minutes later, showing the same neutrophils now with typical spread morphology. The initial and final contact areas of the cells were calculated from measurement of the radius of the spherical cell and the longest and short lengths of the spread cell as shown. This result was typical of at least 30 other cells that were recorded before and after spontaneous spreading over seven different days, with four blood donors.

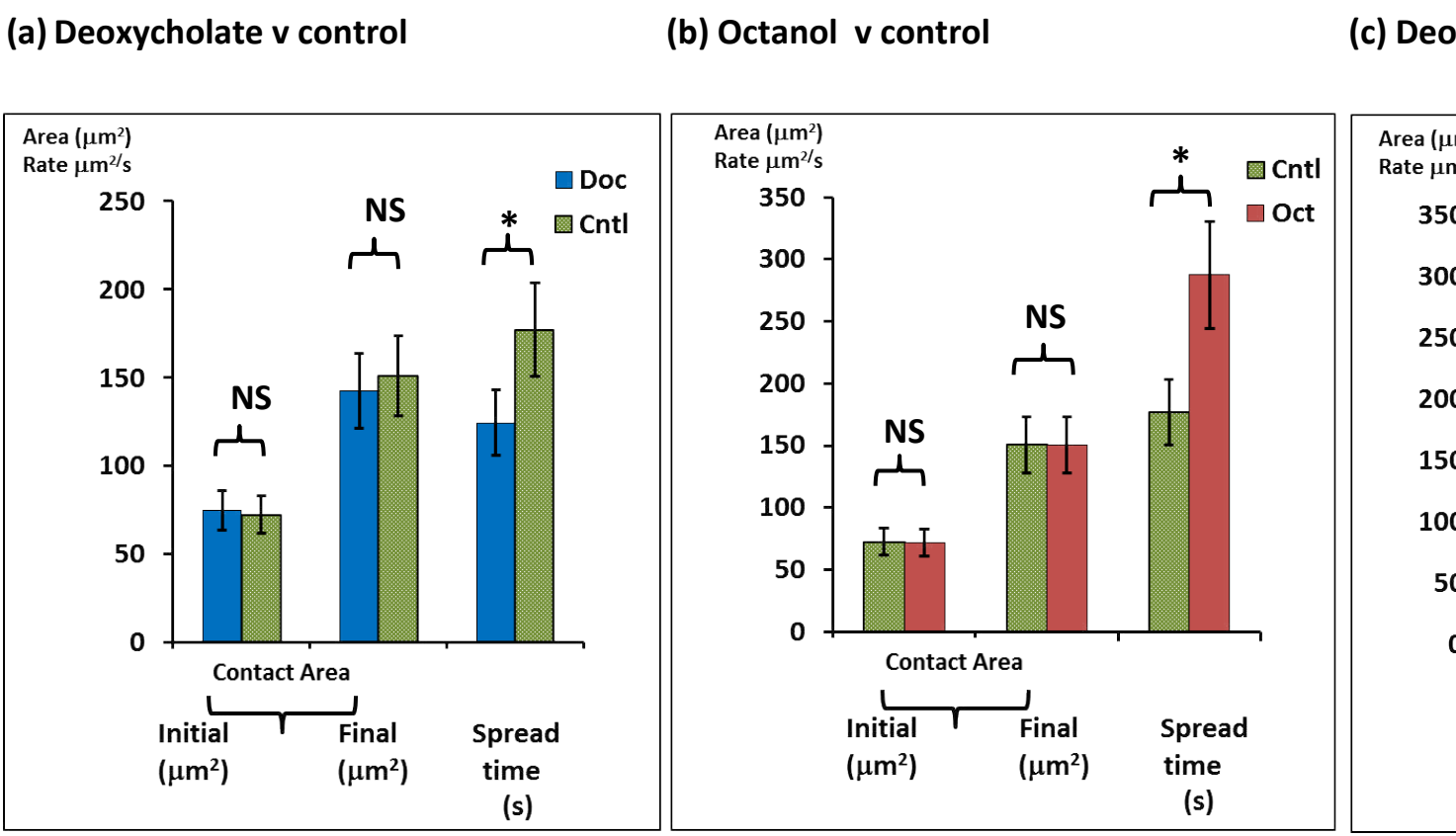

Figure 5.4 The effect of pretreatment with membrane expanders deoxycholate and octanol on neutrop neutrophils was captured microscopically and three parameters measured, the initial and spread conta the time required to transition from the initial area to the final area. (a) Compares the pretreatment (0.4mM) with sham treatment (15 min preincubation), (b) compares pretreatment of the cells (15 treatment preincubation and (c) compares pretreatment with the two membrane expanders (deoxych the mean and sd for each condition where n = 8 for deoxycholate, n = 9 for octanol and n = 8 for contr contact area under any of the parameters (i.e. Doc/control, Oct/control or Doc/Oct). However, Oct spread than either control or deoxycholate treated cells (p<0.05 (t-test).

5.3.2 Effect of osmotically induced changes in cell surface topography on neutrophil cell spreading

The effects of two osmotic conditions, hypo-osmolarity and hyperosmolarity on the ability of cells to spread were tested. It was shown in Chapter 3 (and fig 5.2) that the former condition produces a flattened surface topography whereas the latter increased cell surface wrinkledness. Neutrophils pre-treated with hypo-osmolar medium swelled visibly and often lysed before the experiment. However, approximately 70% of surviving cells which were clearly swollen, showed a typical transition from spherical to spread morphology (fig 5.5 a) but with a slowed kinetics significantly different from untreated control cells (fig 5.6). The mean sizes of the contact area of the cells were: initial area control 74.5 ± 1.7μm^2 and treated 90.3 ± 3.6μm^2. This was significantly different and confirmed that cell swelling had occurred. After spreading the contact areas were 260.0 ± 17.6μm^2 and 204.5 ± 30.49μm^2 respectively. This was not significantly different. The times taken for spreading were 62.4 ± 9.6s and 180.5 ± 29.6s. It should be noted that, unlike the Doc-treated experiments there was no requirement for pre-treatment, the untreated spreading times were faster. However, the time for spreading of hypotonically treated cells were significantly different (t-test $p<0.05$) (fig 5.6). Although they were significantly slower to reach their final spread size, the cells remained able to spread.

These data were in stark contrast to the effect of hyperosmotic shrinking. Neutrophils subjected to hyperwrinkling failed to spread despite being in contact with the surface for up to 25 mins (fig 5.5b). The initial contact area was 60.4 ± 2.1μm^2 significantly smaller than the

control cells consistent with a reduced cell volume (n = 10); in no experiments were any cells observed to increase this area or to spread within 25 mins while in contact with the surface (fig 5.6). This profound inhibitory effect was not the result of irreversible “damage” to the cells, as cells which failed to spread would spread normally when spun and re-suspended in iso-osmotic media. Also, the osmolarity increase was achieved with sucrose, so this was unlikely to be an ionic effect.

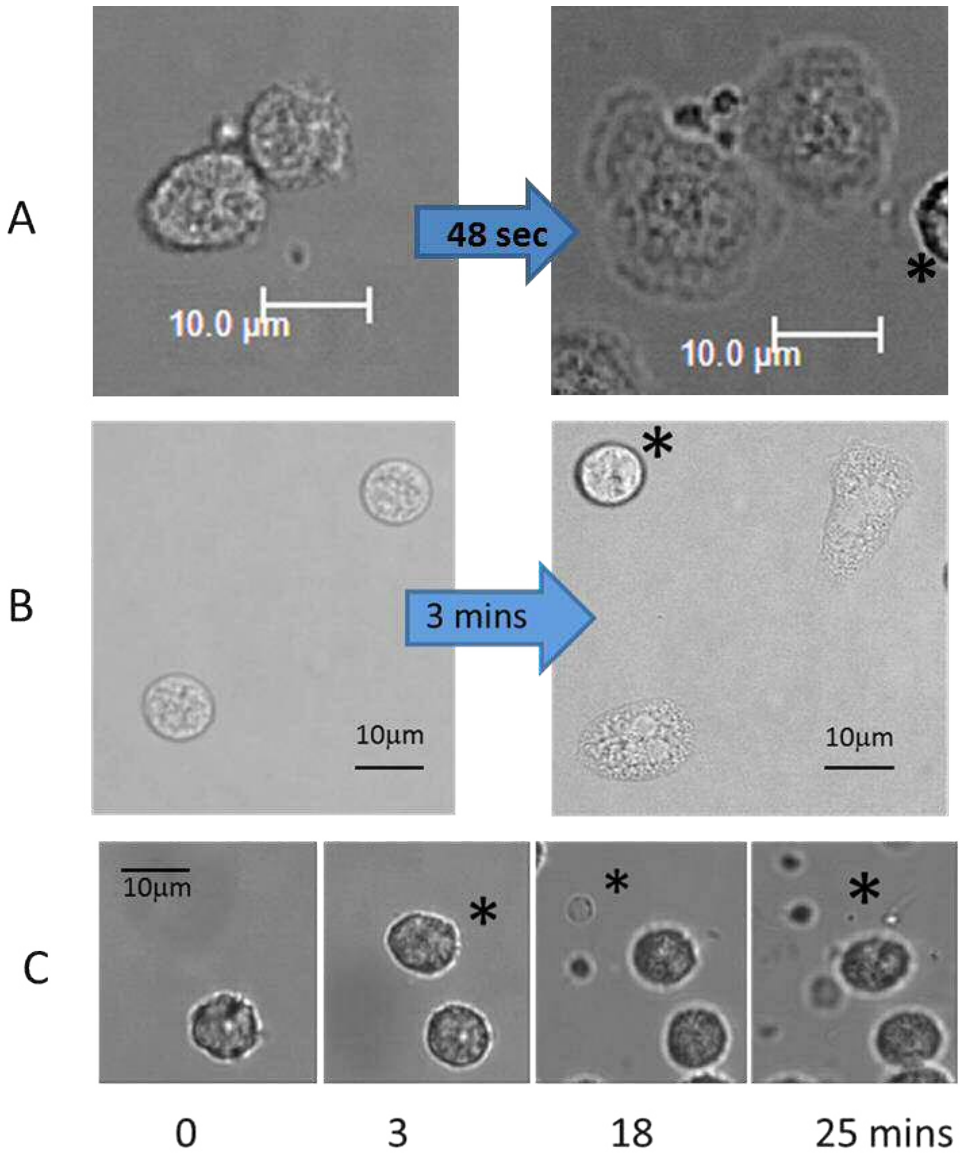

Figure 5.5 Spreading of osmotically treated neutrophils. (A) Shows two normal neutrophils on first contact with the glass coverslip, which are confirmed to be spreading after 48s in the next images and (B) displays two osmotically swollen neutrophils, which are shown on first contact with the glass coverslip as spherical cells. The next image is 3 mins later when both cells have spread onto the glass substrate. The passage of time can be seen by the arrival of another neutrophil sedimenting onto the slide and indicated by asterisk. (C) Shows one osmotically shrunk neutrophil on first contact with the glass coverslip. The shrunk and more wrinkled morphology can be seen. By 3 mins, another shrunk neutrophils had sedimented into the microscopic field (marked with asterisk). By 18 mins, smaller and less dense platelets began to sediment (marked by asterisk) in the field. Cells showed no spreading within the 25 mins recording. These results were typical of at least 12 other experiments undertaken on four separate days with four different blood donors.

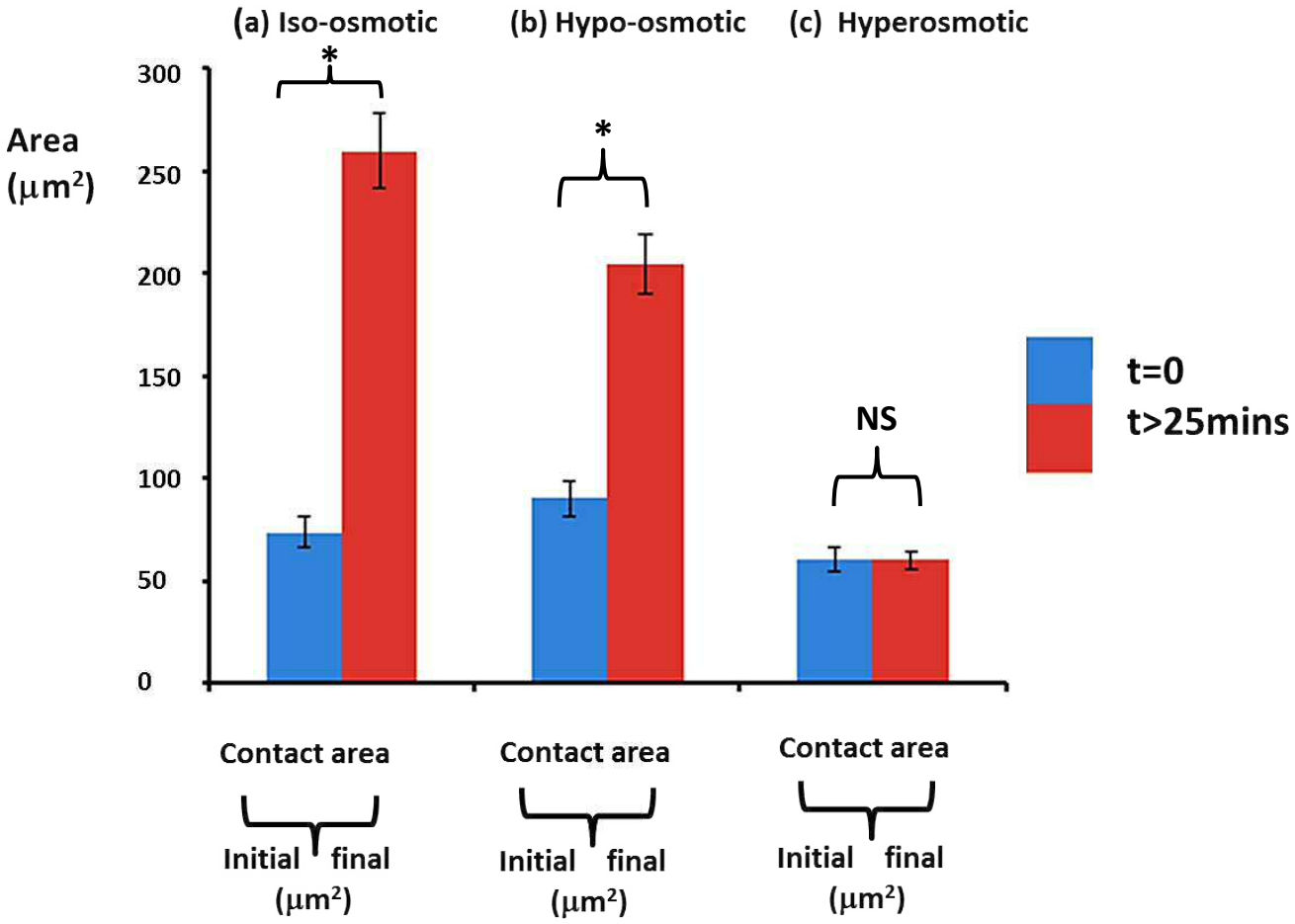

Figure 5.6 Spreading of osmotically treated neutrophils. The spreading of individual neutrophils was captured microscopically and the contact area of the cell measured on first contact (initial) and 25 mins later (final). The first pair of bars (a) shows the mean ± sem of neutrophil area without osmotic manipulation (iso-osmotic (n = 9)); the second pair of bars (b) shows the mean ± sem of neutrophil area in hypo-osmotic medium (150mOsM, n = 10); the third pair of bars (c) shows the data for neutrophils in hyperosmotic media (600mOsM, n = 10). There was a significant differences between the initial and final contact area for the neutrophils in iso-osmotic and hypo-osmotic media ($p<0.05$ (t-test)), but not for cells in hyperosmotic medium.

Furthermore, in cell populations, where no selection of cells for study can be made, the cell diameters of all the cells within the population can be measured objectively using a Cellometer (see methods Chapter 2) and a similar effect was observed. In establishing the Cellometer experimental parameters, cells with diameters less than 7μm were not counted ensuring cell debris, platelets and contaminating lymphocytes were excluded. Cells larger than neutrophils, such a monocytes and cells of similar size e.g. basophils and eosinophils, cannot be excluded by this method. However, as neutrophils were the most numerous cell type (accounting for more than 90% of the cells used), the data mainly reflected neutrophil behaviour.

It was necessary to modify the Cellometer cell counter chamber so that the neutrophils could attach to the glass surface and for the imaging to be achieved at the contact surface. However, such experiments could not be performed at 37^{o}C, but were undertaken at room temperature. This resulted in a far slower spreading time. However, it was helpful to see that the microscopic observations were confirmed in non-subjective cell population measurements. The initial distribution of cell sizes in the population (fig 5.7) showed that the majority of cells had a diameter 8-10μm, as expected for neutrophils in suspension. The skewness of the population distribution with a long tail, with some cells having diameters up to 18μm, may be explained by the presence of large non-neutrophilc cells, such as eosinophils, or some neutrophils which have already spread, or some cells aggregated. However, as the population was mainly of the expected size for neutrophils, the population was simply divided into cells with diameters smaller than and greater than 11μm (i.e. pop1

<11μm>pop2). As neutrophil spreading on the imaging chamber was allowed to proceed, a clear shift in the cell size distribution was observed (fig 5.8). This was used to document the progression of the cell spreading on the slides.

In hypo-osmotic media, it was found that the neutrophils in suspension had increased in diameter, as expected (fig 5.8). The Cellometer would record only intact cells, even though some cells may have bursted by the hypo-osmotic treatment. There was a clear further increase in cell diameter as cells adhered to the glass surface (fig 5.8). By calculating the change in the number of cells which crossed the 11μm diameter cut-off, it can be seen that hypo-osmotically treated cells spread at a reduced rate compared to iso-osmotic cells (fig 5.8c). However, non-lytic swelling of neutrophils sufficient to increase the cell diameter remained able to spread. This degree of osmotic swelling did not prevent the ability of neutrophils to spread. This confirms the single cell observations reported above.

In contrast to the lack of effect of swelling, osmotically shrinking the cells totally inhibited their ability to spread (fig 5.5 b). Initially, osmotic shrinking reduced the cell diameter of approximately 80% of the neutrophils to below 11μm, this percentage did not change substantially over the subsequent 30 mins (fig 5.8). Again, the cell population measurement confirmed the earlier observation made microscopically. The difference between the untreated and hypotonic cells were not significantly (p = 0.18), but between the untreated and hypertonic cells were significantly different (p = 0.006)

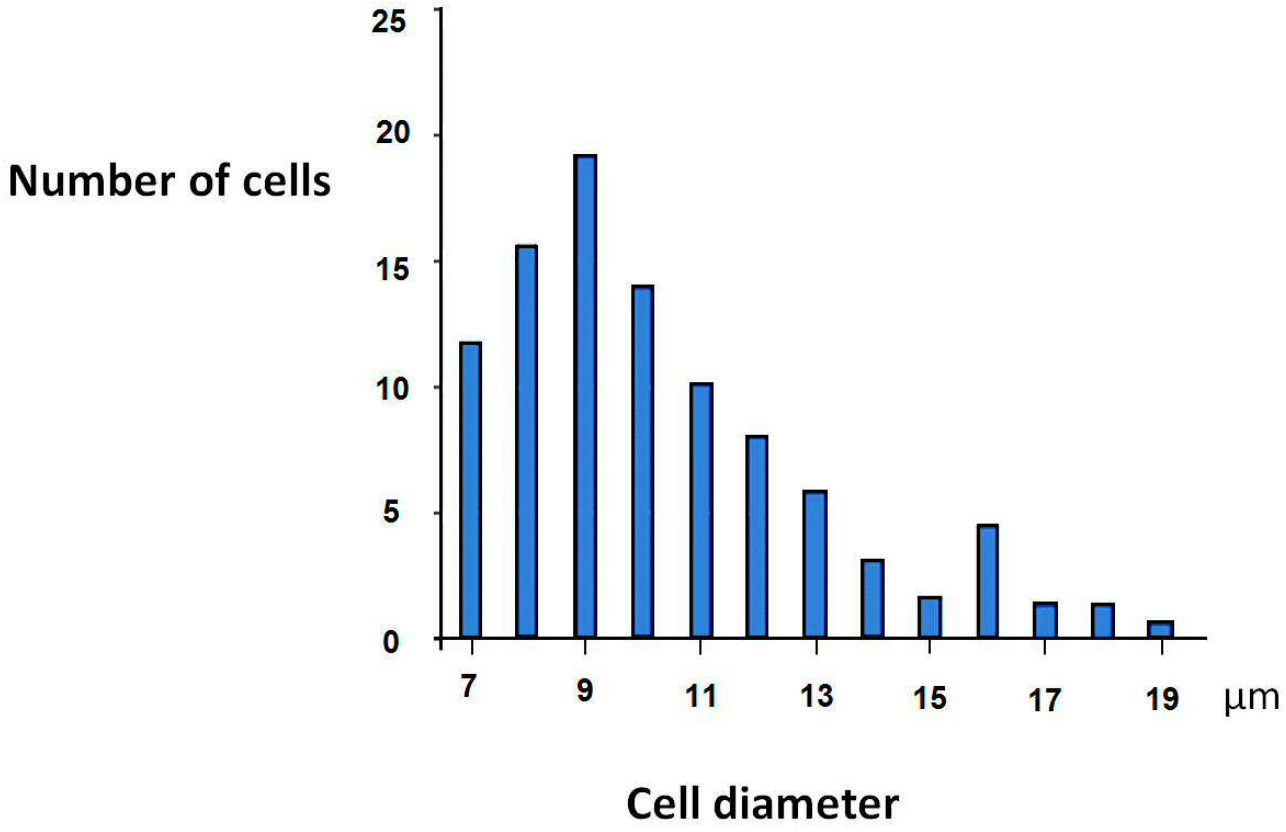

Figure 5.7 The distribution of cells diameters measured by Cellometry. The figure shows the typical distribution determined by Cellometer analysis. It was necessary to exclude objects smaller than 7µm, as this included cell debris and contaminating platelets. The tail of the distribution above 11µm may represent a few eosinophils, or neutrophils that had begun to spread onto the imaging surface, or had small formed aggregates (2 cells).

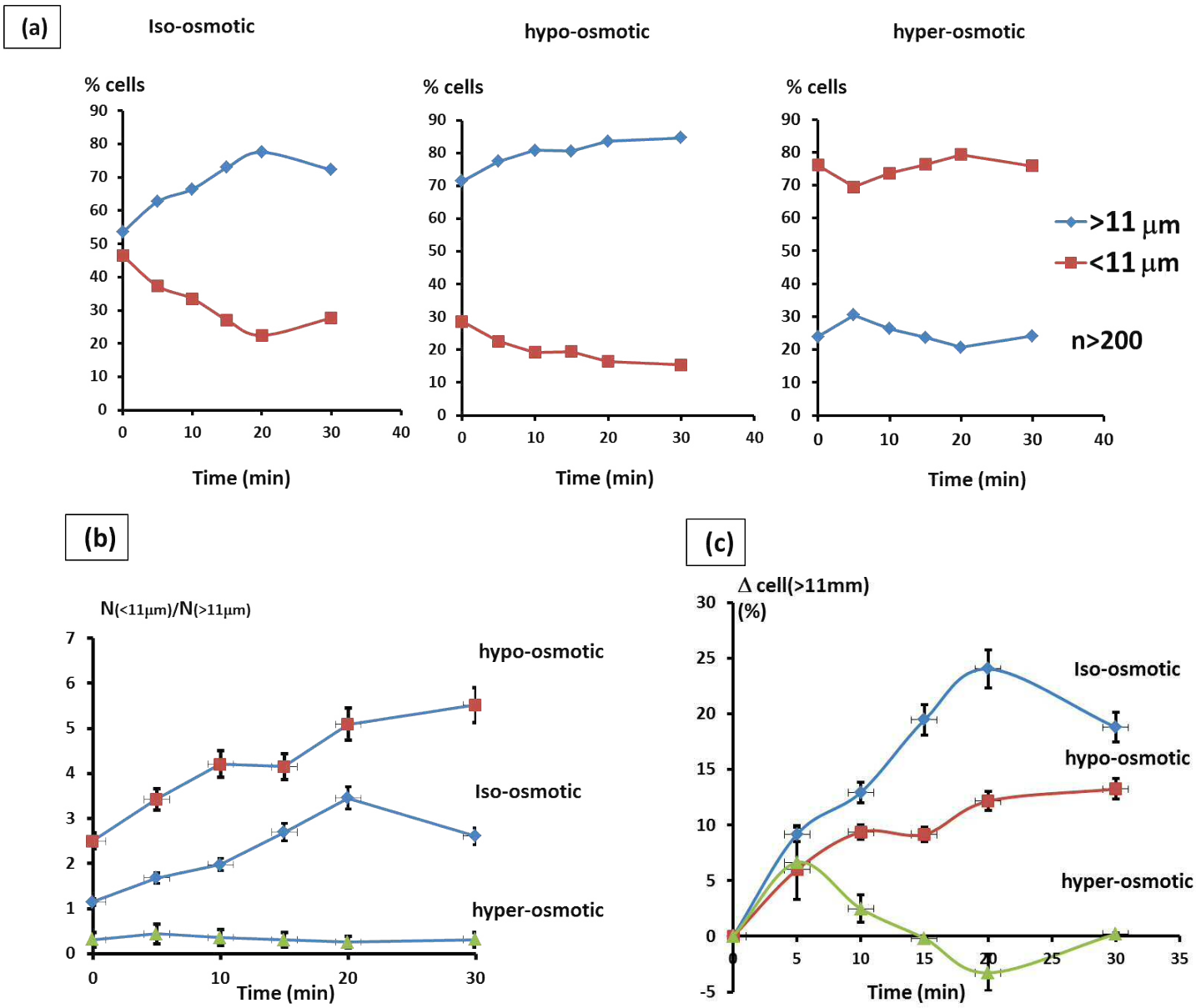

Figure 5.8 The shift in the distribution of neutrophil diameters during spreading. (a) The time course of typical cell spreading assays of cells without osmotic manipulation (iso-osmotic), in hypo-osmotic medium (150mOsM) and in hyperosmotic media (600mOsM) are shown as indicated. The two lines show the percentage of cells analysed which were larger than 7μm but smaller or equal to 11μm (i.e. 7μm > cells ≤ 11μm) and the percentage with diameters above 11mm. (b) shows the ratio of these two measurements to provide a single "population spreading parameter" (N (<11μm)/N (>11μm)) for comparison of the three conditions indicated. (c) Shows an alternative method of comparing spreading, by calculating the number of cells which changed their diameter and exceeded 11μm (Δ cell(>11μm)). This negates the difference in the initial cell size and shows more clearly the comparative rates at which cell spreading occurred. The error bars in (b) and (c) show the means ± sem in the vertical and the time range over which the measurements were taken (horizontal). In all experiments, n>200.

5.3.3 Cytosolic Ca^{2+} signalling in hyperwrinkled neutrophils

The sdFRAP studies showed that the cell surface was considerably more wrinkled under these hyper-osmotic conditions. However, as the spreading of untreated neutrophils onto glass triggers a cytosolic Ca^{2+} signal, which is obligatory to initiate cell spreading, it was important to establish whether shrunk cells were also able to elicit this Ca^{2+} signal. In fluo 4 loaded neutrophils, the cytosolic Ca^{2+} level was recorded in individual neutrophils as they sedimented onto the glass. The interval between them appearing at the glass surface and the Ca^{2+} signal could thus be accurately measured in individual cells.

It was found that untreated neutrophils produced a single large Ca^{2+} peak ("Ca^{2+} flash) between 20s to 60s after contact with the glass (3/3 cells). This was followed by a rapid cell spreading response (fig 5.9). This is in agreement with the reported obligatory requirement for a large Ca^{2+} signal to trigger cell spreading. However, osmotically shrunk neutrophils failed to signal Ca^{2+} after contact with the glass (fig 5.10). After osmotic shrinkage, restoration of osmolarity permitted both cell spreading and the Ca^{2+} signal (fig 5.11). The possibility, therefore, existed that the extremely wrinkled surface did not present sufficient area to the glass to exceed the threshold amount of integrin binding to initiate the Ca^{2+} signal.

It could not therefore be concluded simply that additional surface wrinkling inhibited cell spreading as a result of a restriction of the availability of the surface membrane, as the

Ca^{2+} signal is an absolute requirement for neutrophil spreading. In order to overcome this problem, two approaches were adopted; the first was to allow neutrophils to contact the glass in iso-osmotic conditions and impose an osmotic step-up after cells had elicited a Ca^{2+} signal. The second approach was to load the hyperwrinkled cells with caged IP_3 so that optical uncaging of caged IP_3 could be employed to force a Ca^{2+} signal in wrinkled neutrophils after contact with the glass.

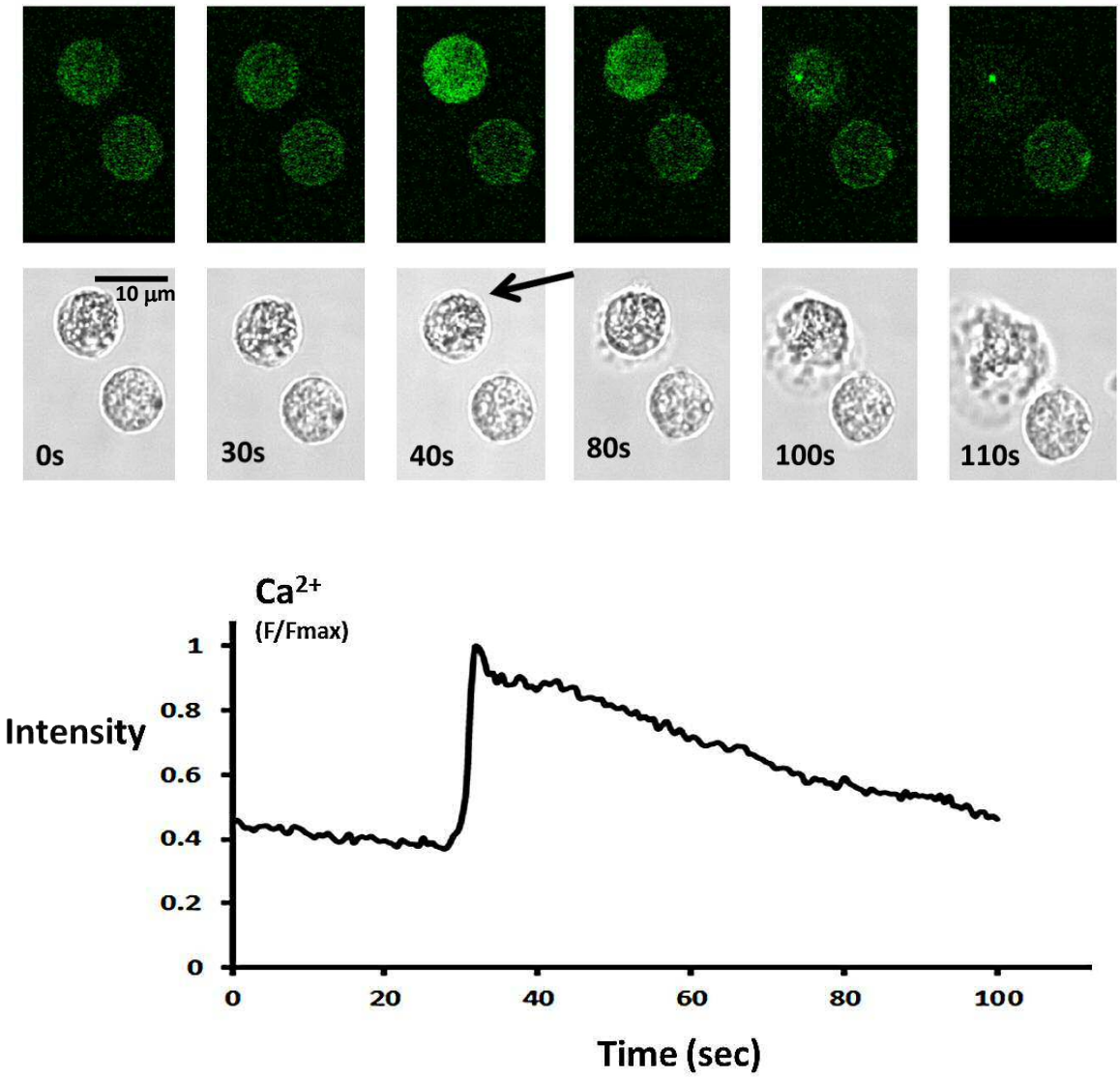

Figure 5.9 The relationship between cytosolic Ca^{2+} and neutrophil spreading. A typical fluo4 intensity trace showing the large transient elevation in cytosolic free Ca^{2+} prior to spreading of untreated neutrophils in the imaging plane. The upper series of images show the phase contrast images with corresponding fluo4 intensity images (Ca^{2+}) at the times indicated. In this example, a pair of cells is shown, only one of which responded by an elevation in cytosolic Ca^{2+} and subsequently spreaded rapidly (Indicated by the arrow). The other cell which failed to generate a Ca^{2+} signal did not subsequently spread. The lower graph shows the time course of the fluo4 intensity changes in the spreading cell as relative intensity (F/F_0) as a monitor of Ca^{2+}. This experiment was typical of similar results obtained in at least three other donors on different days.

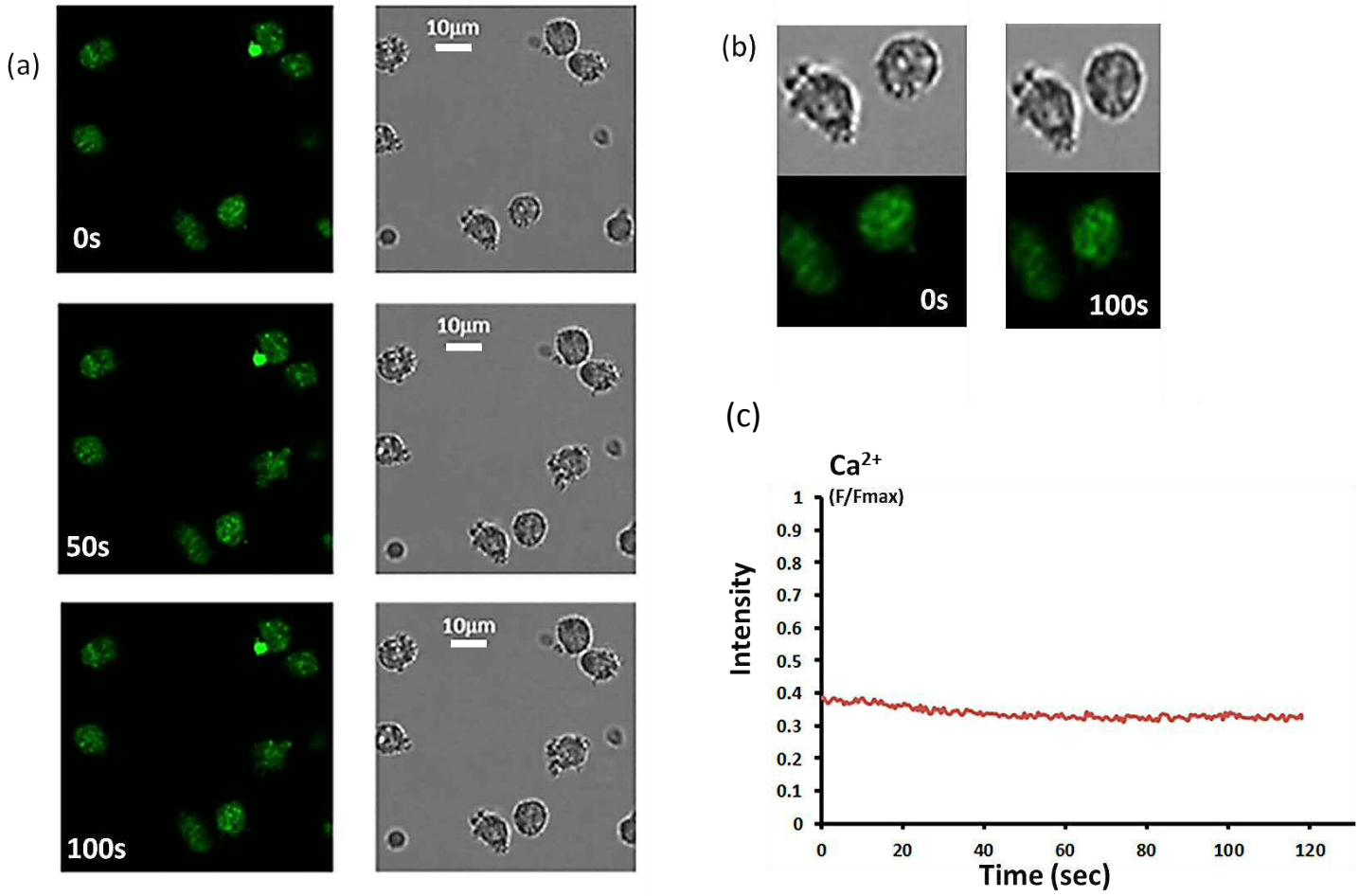

Figure 5.10: Cytosolic Ca^{2+} in non-spreading hyperwrinkled neutrophils. (a) A series of images pairs (fluo4 intensity and phase contrast) of hyperwrinkled neutrophil (hyperosmotic medium 600mOsM) are shown for the times indicated. There were no Ca^{2+} signals or cell spreading during the time of imaging. (b) Images show a more magnified view of the lower pair of cells which show that although the cells changed shape slightly there was no 'spreading response' or Ca^{2+} elevation. (c) Graph shows the time course of relative flou4 intensity (F/F_0) for comparison with the untreated neutrophil response shown in fig 5.8. This experiment was typical of four others from four different blood donors.

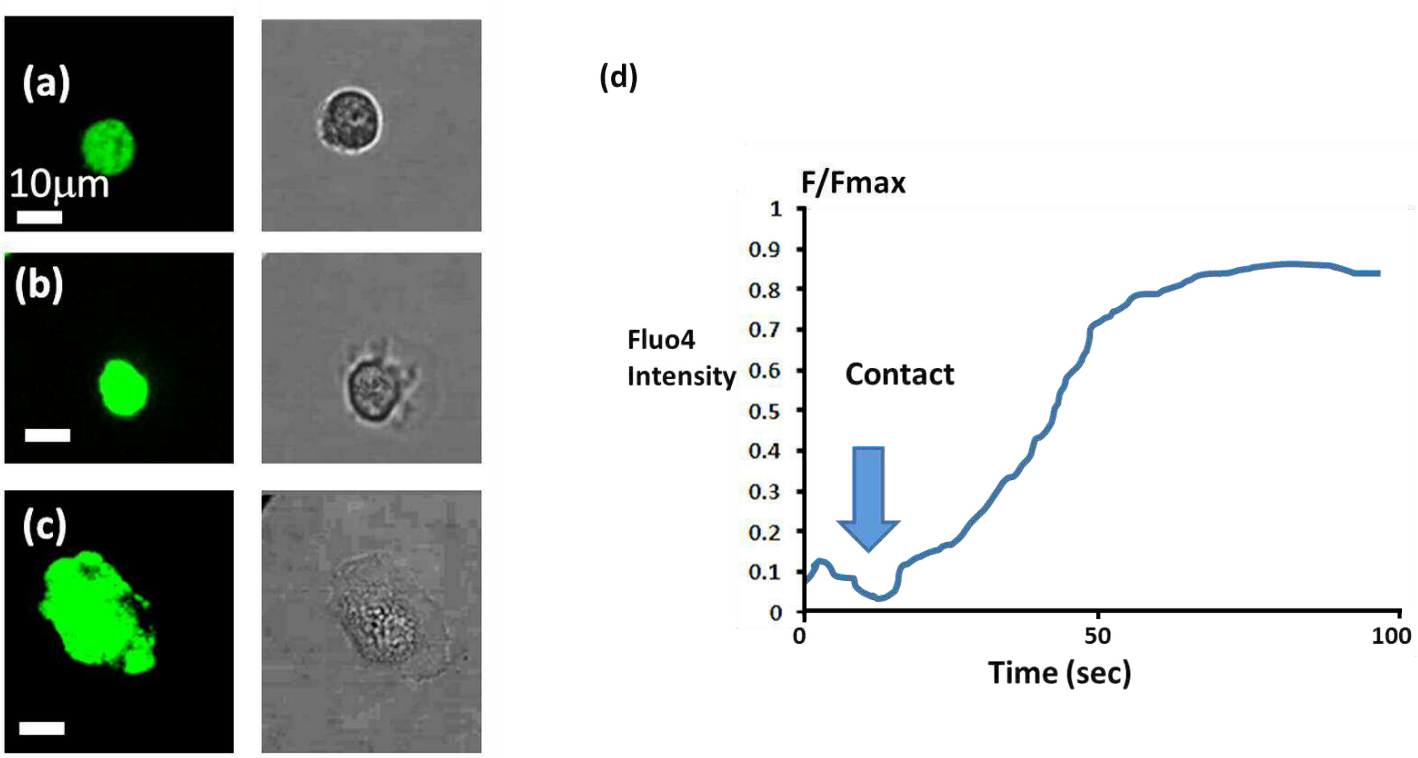

Figure 5.11 Normal spreading responses after osmotic shrinking and restoration of normal osmolarity. The image pairs show the phase contrast and fluo4 intensity images of (a) a neutrophil which had been osmotically shrunk for 15 mins before (b) restoring the osmolarity to normal and (c) the full extent of spreading at 100s. Increase in fluo4 intensity confirmed the Ca^{2+} signal occurred and cell spreading followed. (d) The complete time course of the fluo4 signal is shown with the contact time and onset of Ca^{2+} signalling shown. These data were typical of five other experiments performed on different days with three different donors.

5.3.5 The effect of dynamic osmotic change after Ca^{2+} signalling

By loading neutrophils with fluo4, which is a cytosolic Ca^{2+} probe, changes in cytosolic Ca^{2+} were recorded in real time after neutrophils had contacted the glass surface in isotonic medium. In this series of experiments, neutrophils which had generated a clear Ca^{2+} signal were then challenged by increasing the osmolarity to alter the cell surface wrinkledness. However, the speed at which cell spreading occurred once the Ca^{2+} signal had been generated was faster than it was possible to change the osmolarity and it was thus not possible to establish a clear inhibition of spreading at this stage. However, the cells were clearly arrested after the osmotic step-up and failed to show any subsequent cell shape change behaviour (see section 5.3.7). This was consistent with the inhibitory effect occurring after Ca^{2+} signalling and thus down-stream of the Ca^{2+} signal. However, it was necessary to design a further confirmatory experiment before accepting this conclusion.

5.3.6 The effect of IP_3 induced Ca^{2+} signalling on hyper-wrinkled neutrophils

In order to overcome the problem presented by the failure of hyper-wrinkled neutrophils to elicit a Ca^{2+} signal on contact with the glass surface, neutrophils were loaded with both fluo4 (to monitor cytosolic Ca^{2+}) and caged IP_3. The latter was inert within the cell until photolysed by light of the appropriate wavelength (405nm diode laser), when biologically active IP_3 is liberated within the cytosol and a physiological Ca^{2+} signal is elicited. This tactic has been used previously within our laboratory to trigger neutrophil spreading on demand (Dewitt *et al.,* 2013).

With osmotically hyper-wrinkled neutrophils which had failed to spread, this approach was used to force a cytosolic Ca^{2+} signal within the cells after contact with the surface. It was observed that hyper-wrinkled cells responded to the IP_3-forced elevation of cytosolic Ca^{2+} by extending portions of membrane in an uncoordinated manner (fig 5.12). This uncoordinated spreading was not an irreversible consequence of hyper-osmolarity on the neutrophils, as neutrophils which had been exposed to hyperosmotic solutions and then the osmolality restored to normal, were able to both signal Ca^{2+} and spread normally. This series of experiments showed that the hyper-wrinkled neutrophils retained the ability to elevate cytosolic Ca^{2+} via the IP_3 route, but could not respond with normal spreading, an interpretation of this data was that the unusual response to elevated cytosolic Ca^{2+} was the result of punctured membrane expansion. There would result from the unwrinkling of some physiological wrinkles (ezrin maintained) but not others which were osmotically induced wrinkles (see section 5.5 for further discussion).

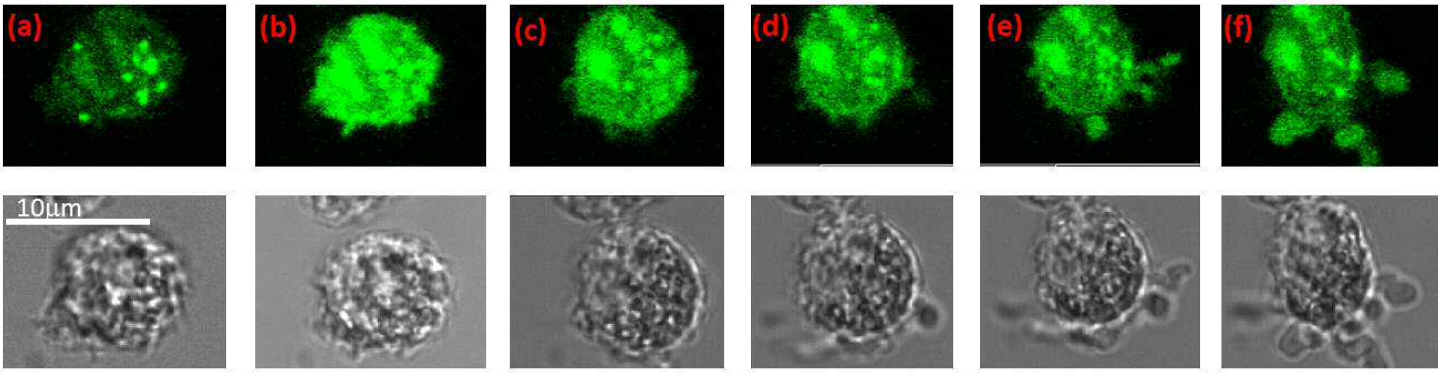

Uncaging pulse

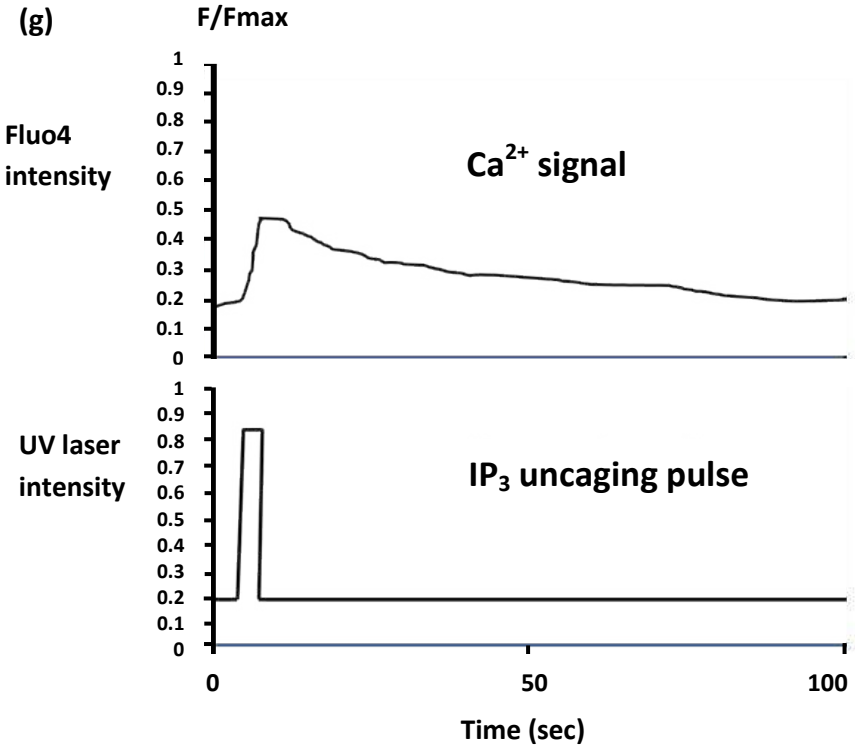

Figure 5.12 The effect of uncaging cytosolic IP_3 to force a Ca^{2+} signal in hyperwrinkled neutrophils. The series of images show a hyper-wrinkled neutrophil loaded with both fluo4 and caged IP_3. The greyscale and fluorescence images in the sequence above (a - f) show the effect of IP_3 uncaging on fluo4 intensity (cytosolic Ca^{2+}) and the cell morphology (phase contrast). (g) Shows the complete time course for fluo4 intensity change (cytosolic Ca^{2+} signal) in the hyperwrinkled shrunk cell (upper trace) and the 405nm laser uncaging pulse (lower trace). This experiment was typical of three other experiments performed on different days with three different donors.

5.3.7 Effects of osmotic shrinking on neutrophil chemokinesis

The effect on cell spreading of inducing additional cell surface wrinkles by osmotic shrinking suggested that this strategy limits the membrane availability for neutrophil shape change. This approach would therefore provide a way of testing the hypothesis that unwrinkling of cell surface wrinkles was required for other neutrophil shape change events such as during chemotaxis and phagocytosis. In order to test this hypothesis, neutrophils were allowed to adhere to glass surface and to undergo spontaneous chemotaxis in isotonic conditions. When a hyperosmotic step up (to 600mOsM) was induced using NaCl, the motile cells did not shrink. Presumably this was because they had already adopted a spread out morphology and the glass substrate prevented visible shrinkage. However, the motile cells immediately stopped moving and remained fixed in a motile conformation (fig 5.13 i). The cells were not lysed as they retained cytosolic dyes (such as fluo4) and no increased Brownian motion of cytosolic granules was observed. A similar result was observed in non-isotonic conditions through hyperosmotic step (up to 600mOsM) using sucrose (fig 5.13 ii).

As it was obvious that the cells were arrested in the process of chemotaxis, but were viable, a series of experiments were performed to establish the effect of restoration of osmolality. As this would allow the osmotically induced wrinkles to become unwrinkled, the cells may have been able to continue their normal chemotaxis. However, a surprising result was that after restoration of cell surface topography, cells were able to move but the polarity of the cell was lost. Pseudopodia formed at right angles to the adherence surface to form a conical (volcano) shape. The original “skirt” around the cells remained attached to

the glass and protrusions were formed at the free edges of the cell (fig 5.14). This phenomenon may have arisen because the polarity cues which maintain the chemotactic direction had been lost during the osmotic arrest period or after arrest and restoration that the Brownian Ratchet assembly of actin was released to form pseudopodia at any site with sufficient available membrane.

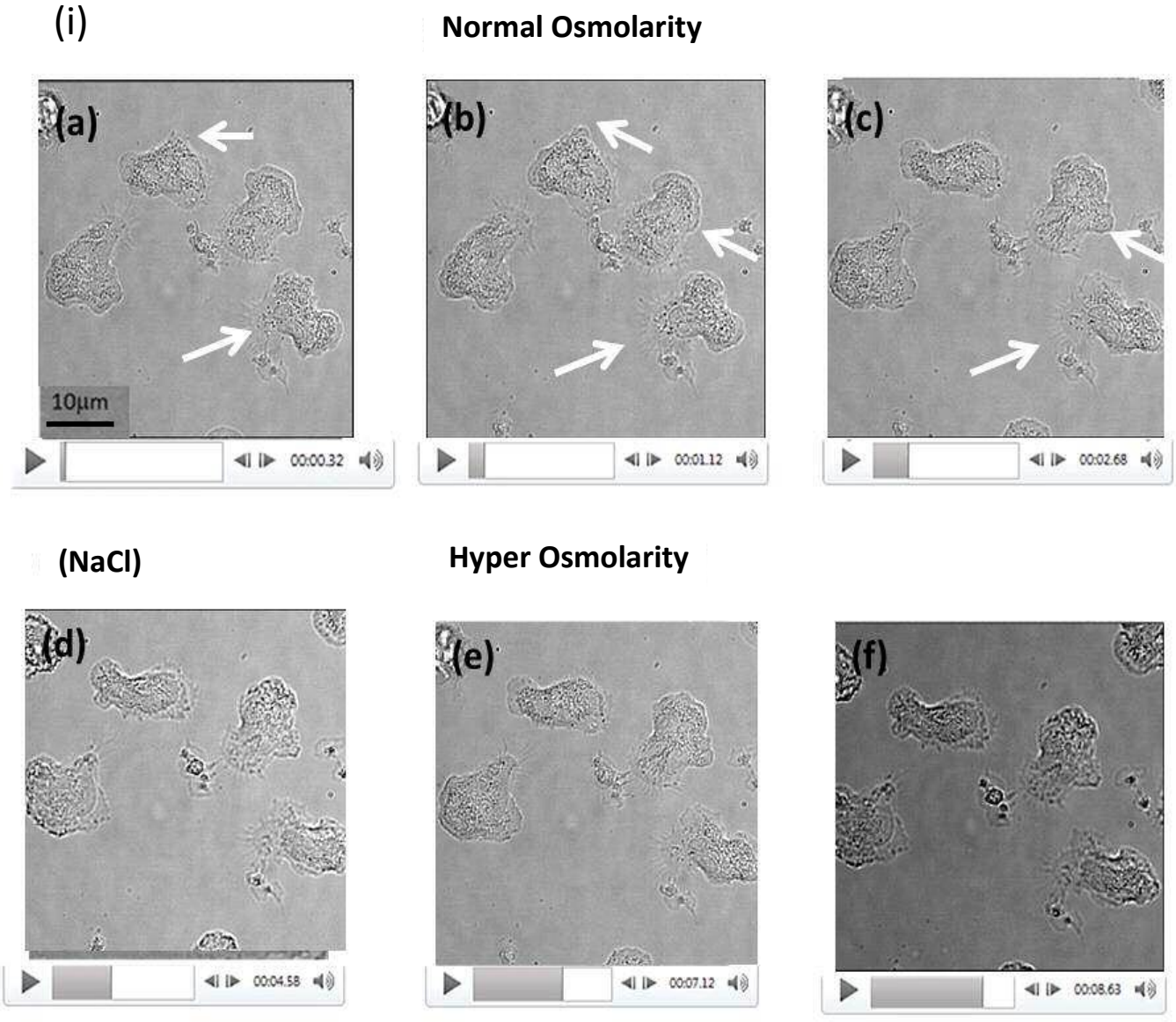

Figure 5.13 (i) The chemokinetic arrest by hyper-wrinkling with hypertonic conditions. Frames from a continuous recording of neutrophils undergoing spontaneous chemokinesis are shown to demonstrate the arrest of chemokinesis after the cells are subjected to a hyperosmotic step up from 300mOsM to 600mOsM using NaCl (150mM increase). In the sequence, the first three images (a - c) show the motility of the cells with arrows highlighting extensions and pseudopodia. The lower three images (d - f) show the arrested nature of cell movement after hyperosmotic step-up. As the cells are stationary after hyperosmotic increase, frames look similar. The time bar below each frame shows the length of time that has elapsed. The time of each frame were as follows (a) 32s, (b) 72s, (c) 188s, (d) 298s, (e) 437s and (f) 943s. This experiment was typical of those performed on at least 5 occasions.

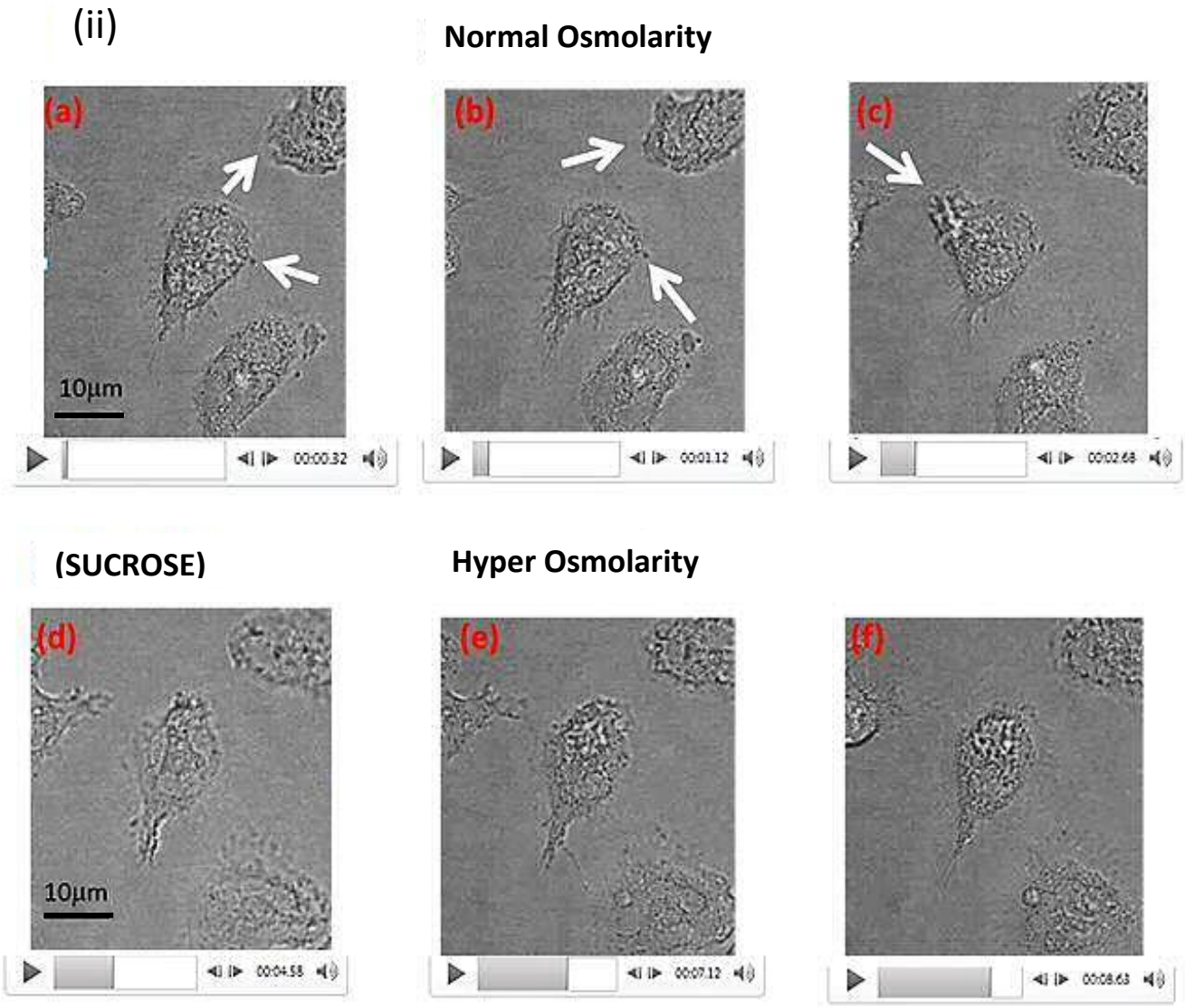

Figure 5.13 (ii) The chemokinetic arrest by hyper-wrinkling with sucrose-induced hypertonic conditions. As above, *frames from a continuous "movie" are shown to demonstrate the arrest of chemokinesis after the cells are subjected to a hyperosmotic step up (300mOsM to 600mOsM) using sucrose (300mM added). In the sequences, the first three images (a-c) show the motility of the cells with arrows highlighting extensions and pseudopodia. The lower three images (d - f) show the arrested nature of cell movement after hyperosmotic step-up. As the cells are stationary after hyperosmotic increase, the positions of the cells look similar. The time bar below each frame shows the length of time that has elapsed. The time of each frame were as follows (a) 32s, (b) 72s, (c) 188s, (d) 298s, (e) 437s and (f) 943s. This experiment was typical of those performed on at least 5 occasions.*

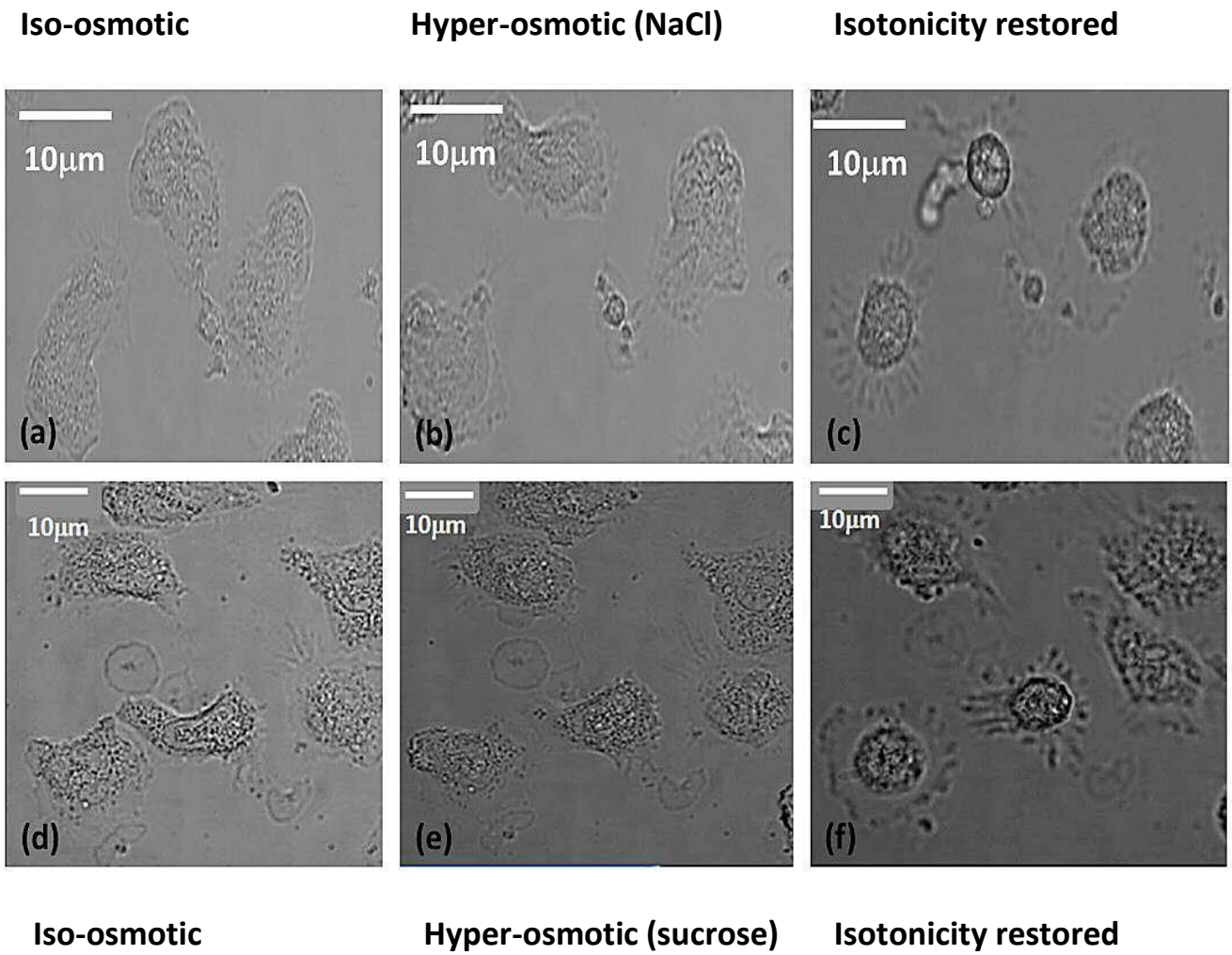

Figure 5.14 The effect of restoring isotonicity to hyperosmotic arrested neutrophils undergoing chemokinesis. The series of images show frames which summarise the effect of restoring isotonicity to neutrophils after arrest of chemokinesis by hyperosmotic medium (600mOsM) as shown in detail in fig 5.12). The upper sequence shows the effect of hyperosmolarity increase using NaCl, and the lower series show the effect of hyperosmolarity increase using sucrose. Both (a) and (d) show fields of neutrophils undergoing spontaneous chemokinesis. (b) and (e) show frames of the same fields of cells after arrest of chemokinesis by stepping up the osmolarity and show the effect of restoring osmolarity to the level that the cells experienced in images (a) and (f) respectively. In images (c) and (f) the retraction of the cell "skirts" can be seen as the cell body pushes upwards. In the recording (from which these frames were taken) the upward movement resembles that of an uprising volcano. The "volcano" effect shown was observed in the majority of cells and the images shown here were typical of at least 5 other experiments and the neutrophils were sourced from different blood donors on different days.

5.3.8 Effects of osmotic shrinking on neutrophil phagocytosis

A similar approach was adapted to test whether phagocytosis was also dependent on the cell surface wrinkled topography. In order to establish the role played by neutrophil surface topography in phagocytosis, the neutrophil surface wrinkledness was either increased or decreased using experimental procedures shown to have these effects (see Chapter 3). The phagocytic ability of neutrophils either osmotically swollen or osmotically shrunk was therefore determined (fig 5.15). Untreated cells challenged with iC3b -opsonised zymosan resulted in multiple internalisation events, with single neutrophils internalising up to 9 zymosan particles within a few minutes (fig 5.15 A). However, no neutrophils which had been osmotically shrunk were able to take up any zymosan (fig 5.15 C). Osmotically swollen neutrophils retained an ability to phagocytose, but the number of particles per neutrophil was greatly reduced; with only 1 or 2 particles taken up. Zymosan particles adherent to the cell surface or within a phagocytic cup were also observed in the swollen neutrophils (fig 5.15 B).

These data are consistent with the physiological surface topography being important for providing a membrane reservoir for phagocytosis. After shrinking, the additional wrinkles which formed were unable to contribute to phagocytosis and hence phagocytosis could not occur. With swollen cells, the wrinkled surface tends to be smoothed out by the increased cell volume. However, it is difficult to swell neutrophils without them bursting. The reduced uptake suggested that most of the wrinkled surface was removed in the surviving cells, which consequently reduced the capacity for phagocytosis.

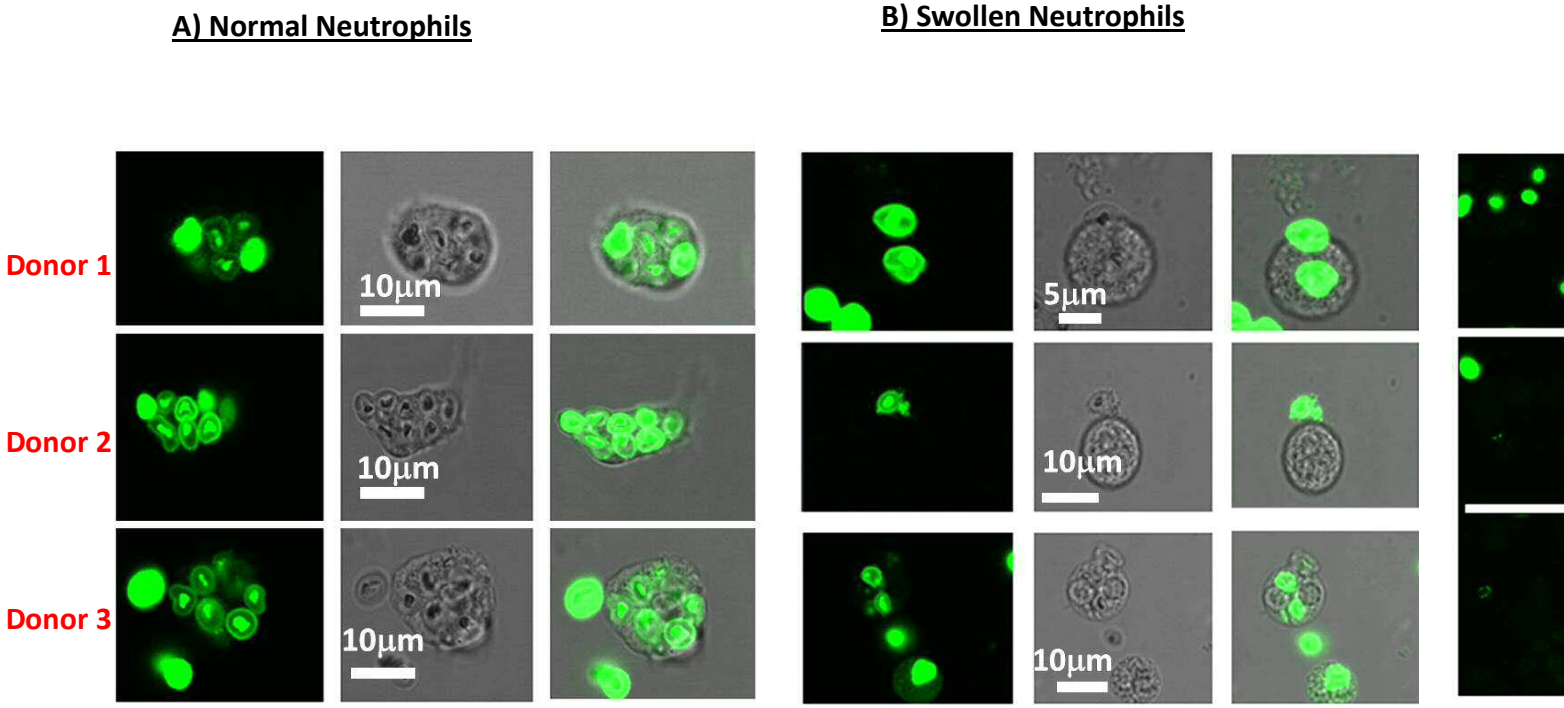

Figure 5.15 Phagocytosis by osmotically treated neutrophils. The triple images show the fluorescence f phase contrast to show the cell and the overlay of the first two images to show the internalisat representative images of neutrophils from different donors. (A) Untreated neutrophils, (B) osmotically osmotically shrunk neutrophils (600mOsM). Fluorescently labelled zymosan particles were imaged usin that their intracellular location was confirmed. As no particles were found within the "shrunk neutrop that the presence of zymosan particles in the microscopic field can be confirmed but none are evident w

5.3.9 Effect of dynamically hyperwrinkling neutrophils during phagocytosis

In order to investigate the dynamic effects of hyperwrinkling, neutrophils were permitted to undergo phagocytosis on the glass surface whilst imaging. Here, non-opsonised zymosan particles were attached to the glass, neutrophils were subsequently allowed to sediment and attach, then human serum was added while imaging. The surface of zymosan activated complement and both diffusible C5a is generated (which signals chemotaxis towards the particle) and the zymosan is iC3b-opsonised. Thus, the progress of movement towards the particle and its contact with the particle can be monitored. When a phagocytic cup had formed, the hyperosmotic step was imposed. In all cases studied, phagocytosis was arrested at that stage. The phagocytic cup failed to progress to full phagosome formation (fig 5.16). This suggested that the wrinkled cell surface membrane reservoir was required for the progression from the formation of the cup, to completion of the phagosome.

When the osmolarity was restored, a few cells that arrested at cup formation continued and completed phagocytosis (fig 5.16). This suggested that signals from attachment to the zymosan particle had persisted and that once released from the osmotic tension holding back the unwrinkling process, the cell was free to complete the task. The reversibility presented a strong evidence that phagocytosis depended on the availability of membrane held on the cell surface. However, in the majority of cells, restoration of isotonicity released the cells from motion arrest, but direction finding was lost and, as with the chemokinesis experiments (section 5.3.7), cells often underwent the “volcano” response

pushing membrane away from the glass surface and failing to complete phagocytosis (5/7 cells).

As it was found that osmotically shrunk neutrophils failed to signal Ca^{2+} when in contact with the glass surface, it was possible that the failure of phagocytic cups to progress was because the osmotic shrinking prevented Ca^{2+} signalling (an essential triggered for phagocytosis, see Chapter 1). This would occur if the shrinking step was imposed before integrin was fully engaged and the Ca^{2+} signal had not been evoked. As with the spreading experiments, the wrinkled membrane would present fewer intergins to bind to the zymosan and may be less than that required to trigger a Ca^{2+} signal. Both these possibilities were excluded by measuring cytosolic Ca^{2+} in the neutrophils undergoing phagocytosis. In order to eliminate these possibilities, neutrophils which had elicited a clear zymosan binding Ca^{2+} signal during phagocytic cup formation were examined (fig 5.17). This signal resulted in the rapid closure of the phagosome in untreated cells. However, at this stage, the osmotic step was imposed. Despite a previous Ca^{2+} signal, showing the interaction between the opsonised zymosan and the neutrophil had reached the critical stage for phagocytosis, stepping up the osmolarity after the Ca^{2+} signal still prevented completion of phagocytosis (fig 5.17). This placed the inhibitory effect of the osmotic step after Ca^{2+} signalling but before full release of additional membrane for completion of phagocytosis.

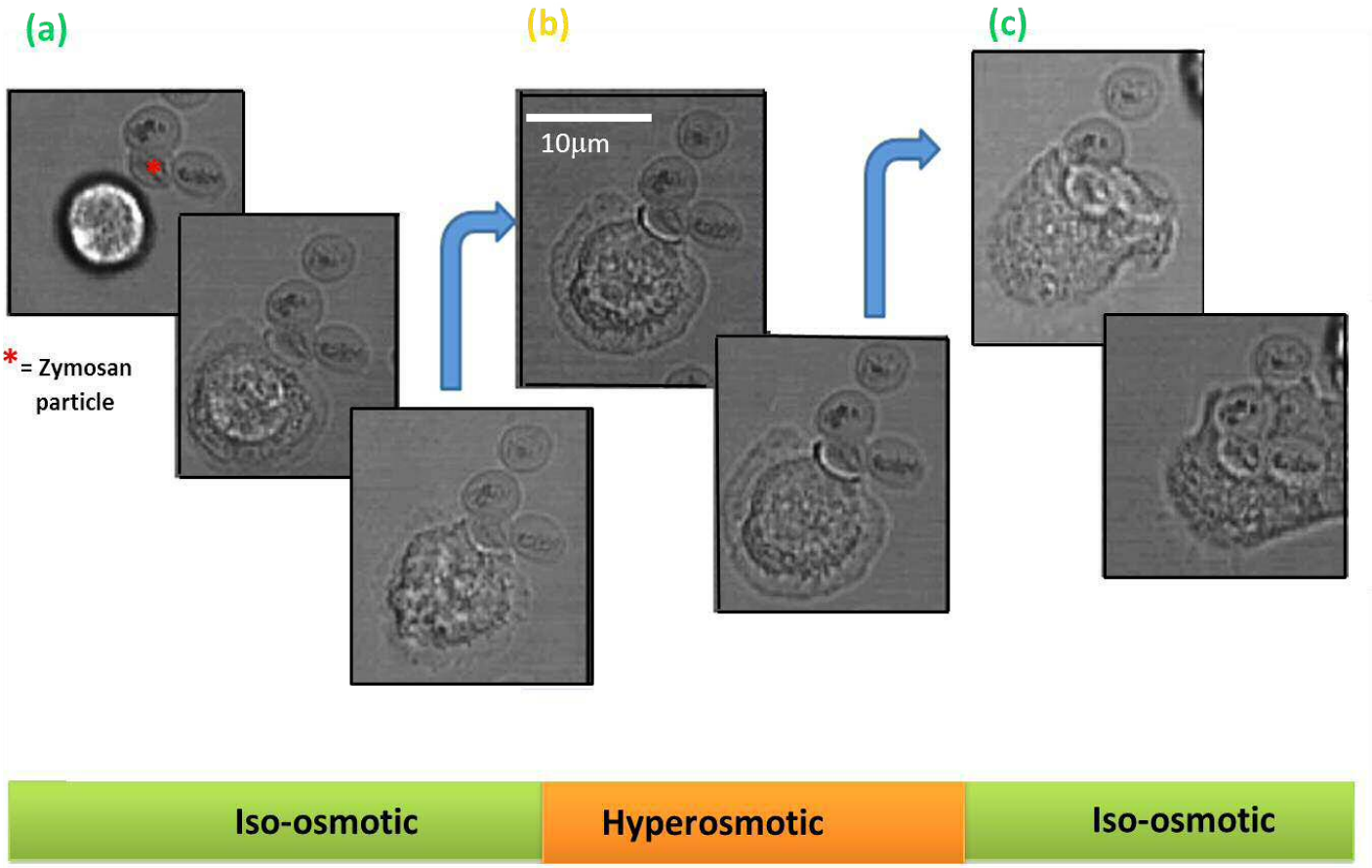

Figure 5.16 Effect of hyperwrinkling on phagocytosis arrest. (a) The first three images show the formation of a phagocytic cup around a zymosan particle in iso-osmotic medium (images at time zero, 50s and 70s). (b) At that point, the osmolarity was stepped up (to 600mOsM). The subsequent two images are at 100s and 200s. (c) Osmolarity was restored to normal at 210s and the subsequent images show progression of phagocytosis at times 240s and 300s. The arrest of phagocytosis was typical of all experiments performed (7/7) but the recovery was not typical (2/7). A more typical lack of progression of phagocytosis is shown in the next figure.

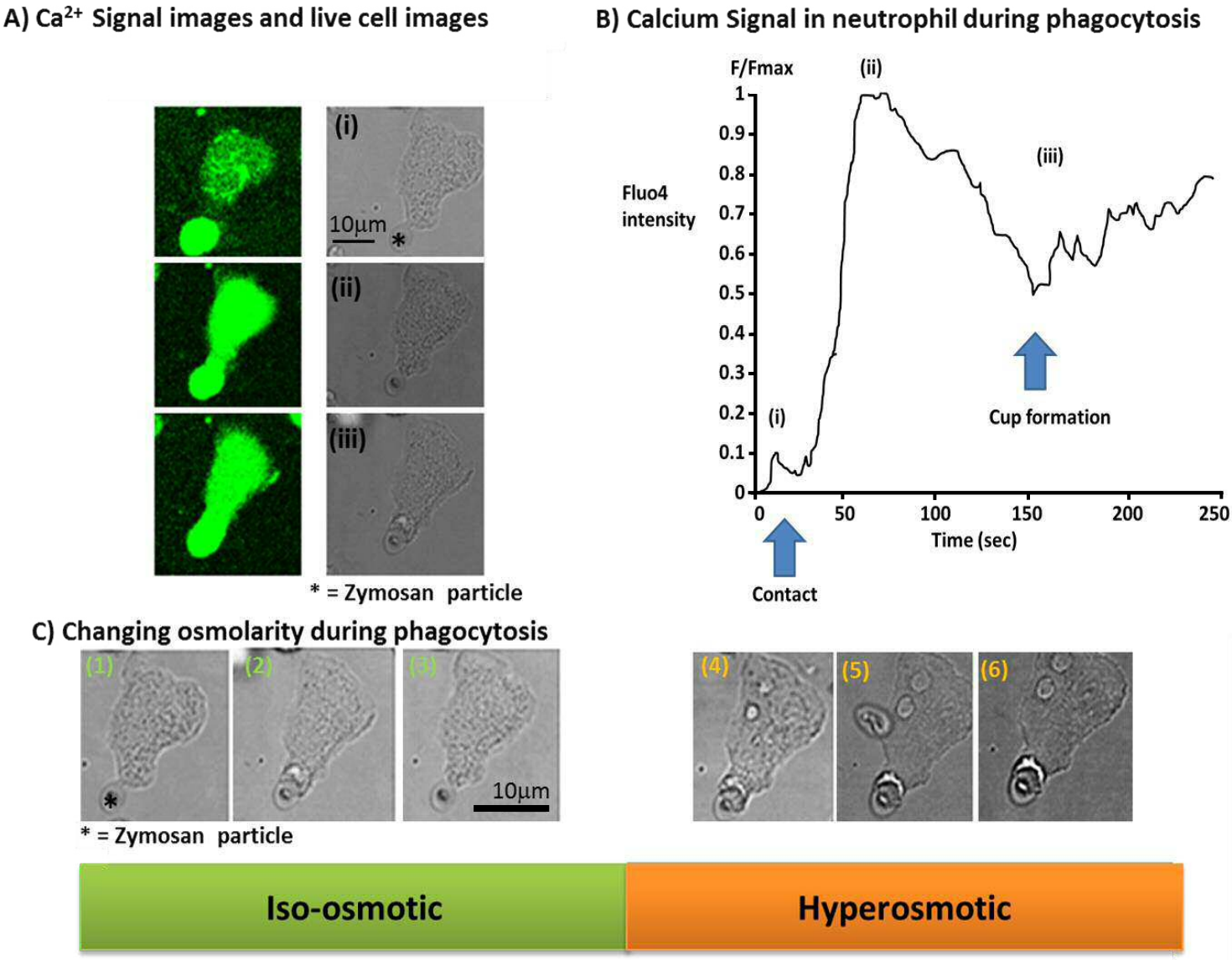

Figure 5.17 Effect of increasing osmolarity during phagocytic cup formation and whilst measuring cytosolic Ca^{2+}. (A) The Images represent the cytosolic Ca^{2+} concentration within a fluo4 loaded neutrophil on contact with a zymosan particle as the phagocytic cup forms where (i) is before contact, the neutrophil having low cytosolic Ca^{2+} (ii) at contact when the neutrophil Ca^{2+} is elevated and (iii) phagocytic cup formation. (B) Shows the time course of the cytosolic Ca^{2+} change with contact and phagocytic cup formation indicated. The point at which images (i), (ii) and (iii) were taken is also indicated. (c) Shows the effect of stepping up the osmolarity after phagocytic cup formation and the elevation of cytosolic Ca^{2+} (images 1, 2 and 3) and the resulting arrest of phagocytosis after hyperosmotic step up (images 4, 5 and 6 at 160s, 200s, 250s). Similar results were obtained in similar experiments with neutrophils from three other donors on different days.

5.5 Discussion

In this chapter it has been demonstrated that changes in the cell surface topography induced by hyperosmolarity have a physiologically significant impact on human neutrophil function. The data presented in this chapter suggest that the wrinkled surface topography is required as a membrane reservoir for cell surface area expansion during spreading, chemokinesis and phagocytosis. The dramatic effects of cell shrinkage were interpreted as resulting from additional wrinkles being formed which were not controllable. The possibility that any means of disrupting the cell surface topography by increased wrinkledness were excluded by the use of membrane expanders. It was shown in Chapter 3, that membrane expanders increased the diffusion path-length for DiI and that this was due to the addition of artificial contours (see fig 5.1). These agents were predicted to make the membrane more "baggy" (lower membrane tension), but it was unclear whether this would affect the ability of the cell to change shape. However, it was found to have minimal impact on neutrophil shape change.

Since my work had shown that osmotic shrinking had a significant impact on the cell surface topography of neutrophil (using sdFRAP), I sought to establish whether this could be used to investigate the relationship of surface topography to neutrophil function. It was predicted that experimentally induced changes in the surface topography would impact on neutrophil behaviour. I found that osmotically swollen neutrophils either burst or were able to spread rapidly on to glass coverslips. From measurement of the swollen cell radius, it was

calculated from volume increase that only 5% of the wrinkles or 5% of the surface area of each wrinkle was lost (see section 2.5.11.6).

This suggested that cell surface wrinkles still existed and that these could participate in the spreading response. Scanning electron microscopy of the cell surface of swollen neutrophils confirmed this (fig 5.2). I therefore investigated the effects of osmotic shrinking. I found that osmotically increasing the wrinkled state of the cell surface had a profound inhibitory effect on the ability of neutrophils to spread onto glass and to undergo phagocytosis. This indicated that the osmotic shrinking caused a lethal effect and so inhibited cell spreading and phagocytosis in that way. This was tested by restoring normal osmolarity of neutrophils which had been arrested at the phagocytic cup stage by shrinking. In the majority of cells, this procedure released the stasis of the neutrophil but they subsequently moved randomly (as was also seen with cells arrested during chemokinesis). In some cells, restoration of osmolarity caused the neutrophil to continue phagocytosis and complete phagocytosis in an apparently physiological manner (fig 5.16). It was clear that osmotic shrinking had not irreversibly impaired the ability of neutrophils to phagocytose.

In a series of experiments observing over 50 individual cells, no cell was found to spread following osmotic shrinkage. The Ca^{2+} signalling ability of these cells remained intact. When cells were allowed to adhere to glass first and then they were wrinkled osmotically, it was found that cell movement, pseudopod formation and ruffling were all inhibited dramatically. Restoring the osmolarity to normal allowed the cells to return to a motile state. I found that the same effect was observed regardless of whether osmotic shrinking was achieved

ionically (NaCl) or non-ionically (sucrose). Using this approach, I examined the role of wrinkling during phagocytosis. Again it was possible to arrest the progression of phagocytosis by changing the wrinkled state. If a cell was arrested during phagocytic cup formation but before completion of phagocytosis, completion would resume after returning the osmolarity to normal. A surprising result was that after restoration of cell surface topography, the polarity of the cell was lost. Cells migrating along the glass slide were often seen to form pseudopodia at right angles to the adherence surface to form a conical (volcano) shape. This suggests that cell polarity is maintained in some way by the established surface topography.

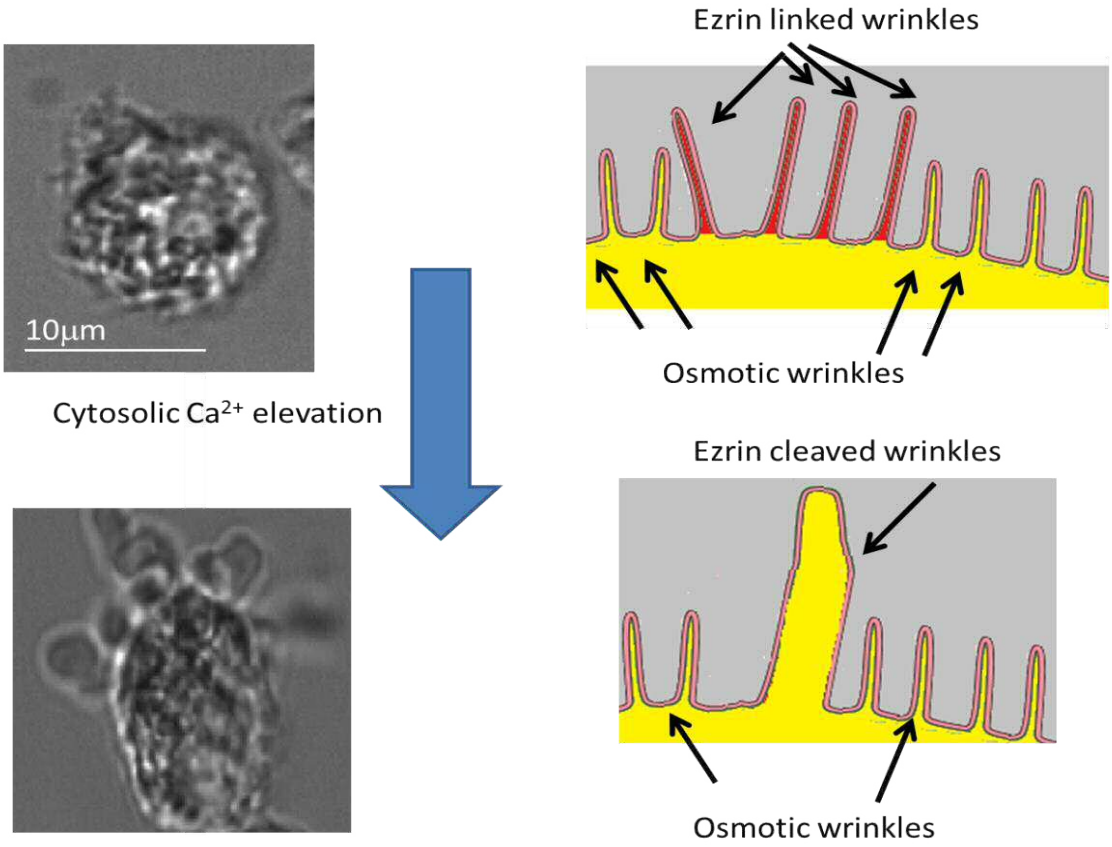

Figure 5.18 Proposed mechanism underlying the Ca^{2+} induced elongated bleb formation in hyper-wrinkled neutrophil. The cartoon on the right attempts to illustrate the hypothesis proposed to explain the abnormal cell shape change observed following Ca^{2+} signalling in osmotically shrunk neutrophils (left). The proposal rests on there being two sorts of wrinkle at the cell surface after osmotic shrinkage; physiological wrinkles held in place by membrane cross-linking proteins such as ezrin (shown in red), and the other is simply the result of the osmotically reduced cell volume (shown in yellow). After the forced elevation of cytosolic Ca^{2+}, calpain is activated and ezrin is cleaved. Normally this permits a symmetrical expansion of cell surface area and permits uniform spreading of the cell. However, under the hyperwrinkled conditions imposed by the hyperosmolarity, the release of membrane only occurs in the ezrin-maintained wrinkles and expansion is thus limited by the non-ezrin wrinkles (as shown in the lower cartoon).

In an attempt to force spreading of hyperwrinkled neutrophils, an interesting discovery was made that may be relevant to the understanding of the inhibition mechanism by osmotic shrinkage. I found that hyperwrinkled neutrophils were unable to signal Ca^{2+} on contact with the glass surface. These experiments thus pointed strongly to an inhibitory effect of hyper-wrinkling in reducing the availability of addition surface area required for effective neutrophil spreading. Caged IP_3 was therefore used to elevate cytosolic Ca^{2+} within the hyperwrinkled cells. It was found that unusual surface structures were formed (see fig 5.14). The most likely interpretation of this data was that elevated cytosolic Ca^{2+} acted through the physiological route of calpain activation and ezrin cleavage (see Chapter 1), but the result was punctated membrane expansion because other wrinkles were not maintained by ezrin, but by the osmotic effect (fig 5.18). Therefore, unwrinkling of some physiological ezrin-maintained wrinkles would occur but be prevented from extending in the usual way, because other membrane folds (which were osmotically induced wrinkles) remained and prevented full expansion, this is shown in fig 5.18. Interestingly, elongated bleb like structures have also been observed in neutrophils in which calpain has been partially inhibited (Dewitt *et al.,* 2013). Although the route to achieve the generation of elongated bleb like structures was different, the underlying cause would be the same; namely partial release of wrinkles resulting in punctated release of membrane. It was suggested in these previous experiments that some wrinkles may have been released in advance of others as a result of inhibition of some calpain (which is activated by the Ca^{2+} signal). In the osmotically wrinkled cells, a similar effect may have occurred as the physiological wrinkles were forced to be released by uncaging IP_3, but the osmotic wrinkles were retained (see fig 5.18).

The inhibition of chemokinesis and phagocytosis may have a physiological relevance. Most types of cells are located in particular places within the body and do not experience changes in osmolarity. However, neutrophils migrate from the blood stream to the extravascular space in many different parts of the body, including the kidneys, lung and gut. At these sites, neutrophils may be exposed to large changes in osmotic conditions (Bryant *et al.,* 1972). For example, the osmolarity in the renal medulla of the kidney may be as high as 1400 mosmol. Similarly, the osmolarity in the interstitial fluid of enclosed inflammatory spaces is increased by the hydrolysis of macromolecules into smaller (osmotically active) fragments (Leak and Burke, 1974). Previous studies have also reported that osmotic conditions have an impact on neutrophil exocytosis (Kazilek *et al.,* 1988), chemotaxis (Bryant *et al.,* 1972) and even oxidase activation (Hampton *et al.,* 1994). Nevertheless, the mechanism behind affecting these behaviours is not yet fully recognised. It is possible that changing the cells volume and hence their surface topography, which I have found here, is the underlying explanation for the changes to the usual behaviour of the neutrophil reported previously and in this chapter.

5.6 Summary

The results in this chapter have demonstrated;

1. That hyper-wrinkling the neutrophil cell surface has an inhibitory effect on phagocytosis, cell spreading and chemokinesis.
2. And that this effect is partially the result of reduced receptor engagement, however, when signalling is intact, the inhibition results from a step between Ca^{2+} elevation and membrane expansion.
3. These data are consistent with the hypothesis that the cell surface wrinkles provide a necessary reservoir of additional membrane to permit phagocytosis and cell spreading.

Chapter 6

General Discussion

6.1 Overview

In this thesis, work has been presented which tested the proposal that when neutrophils undergo an apparent increase in cell surface area, such as during cell spreading and phagocytosis, there is a change in cell surface wrinkling, the unwrinkling of micro-ridges at the surface providing the additional membrane required. This proposal has been based on previous work, which has indirectly suggested this to be true. However, it has not been possible to directly test this proposal. The aim of the work in this thesis could only be achieved by developing a new approach to investigate the micro-ridges at the cell surface in living cells, preferably undergoing cell shape change. The earliest results chapter presents the development of subdomain FRAP as a way of establishing sub-microscopic changes in the neutrophil surface topography (Chapter 1). The approach was validated by changing the cell surface topography by experimental manipulation. In the subsequent chapters, this novel experimental approach was used to investigate whether changes in neutrophil topography occurred physiologically and could thus provide the explanation for increasing surface membrane availability. This work showed that an adaptation of manipulation was able to clearly demonstrate that large changes in the cell surface occurred and could be monitored by sdFRAP (Chapter 4). The last results chapter (Chapter 5), sought to establish whether these changes were necessary for neutrophil shape change. As it was shown that osmotic shrinking induced additional (non-physiological controlled) wrinkles, this simple approached showed that such a tactic could arrest neutrophils in the act of phagocytosis or chemotaxis and that this could be revered by simply restoring the osmolarity. Since other events within in the cell, such as Ca^{2+} signalling were not impeded, this was consistent with

the cell surface topography having an important role to play in controlling neutrophil behaviour.

6.2 Summary of the results presented in this thesis

6.2.1. Development of sdFRAP to monitor cell surface topography

It had not been possible previously to monitor changes in the cell surface topography of neutrophils (or any other cell type) undergoing cell shape change. Here, I have developed a method which allows monitoring of such changes. Chapter 3 presents the work which led to the use of sdFRAP and its validation. Obviously, the discoveries made in the work presented in this thesis depended on the success of producing such method. The theoretical basis for the method was that diffusion over a defined distance in the plane of the membrane was constant, so the time taken for diffusion would provide a measure of the path that had to be taken. If the surface was flat, diffusion followed the expected time course. This was shown by monitoring diffusion of DiI in flat region of the neutrophil membrane, such as the extended 'tail' of neutrophils, or by experimentally stretching the membrane osmotically to give a flat surface. In the first experiments undertaken with neutrophils in a 'spherical' configuration or in regions of neutrophils other than the flat 'tail', it was obvious that the diffusion time was significantly longer. This was the first time that a direct measurement of the wrinkledness of the cell surface has been made. The validity of this approach was tested by increasing the wrinkledness further by osmotic shrinking or by the addition of membrane expanders. In all measurements, these conditions increased the diffusion time still further. The method was therefore responsive to measurement of wrinkledness over the extremes

that may be expected (i.e. from absolutely flat to highly wrinkled) and could be used in the work presented here. As the method relied only on introducing a fluorescent marker to the plasma membrane and the equipment to photobleach and to spatially record fluorescence recoveries, it was relatively easy and robust and could be extended to other living cell types.

6.2.2. Using sdFRAP to measure wrinkledness during neutrophil activity

The purpose of developing the sdFRAP methodology was to study the cell surface topography in living neutrophils, especially as they change shape during spreading and locally during phagocytosis. The method was clearly able to detect differences in the wrinkledness during these activities. For example, during phagocytosis, the membrane around the developing phagosome or the phagocytic cup which was initially wrinkled was transformed to a smooth (non-wrinkled) surface. This was consistent with localised surface unwrinkling providing the additional membrane required to form the phagocytic cup and the complete phagosome. Likewise, neutrophils which had spread onto glass surface were significantly less wrinkled that spherical cells. The reduction in wrinkledness was not confined to any part of the cell body. Again, this was consistent with global surface unwrinkling providing the additional membrane required to transition from spherical to flattened (spread).

6.2.3 Requirement of unwrinkling for neutrophil behaviour

The sdFRAP provided an observation of unwrinkling within certain neutrophil responses. This, of course, led to the hypothesis that unwrinkling caused or was permissive

for the neutrophil behaviour. As I had found that it was possible to alter the wrinkledness experimentally, these conditions were applied to neutrophils undergoing spreading/chemotaxis or phagocytosis. This data is presented in Chapter 5. In essence, simply by wrinkling the membrane osmotically, it was possible to freeze the neutrophil behaviour at the point of phagocytic cup formation or chemotaxis. Ca^{2+} signalling was unaffected by this wrinkling event and a cell could be chosen which had already signalled Ca^{2+} under normal conditions and still the osmotic wrinkling prevented the shape change response. This was strong evidence that the control of the wrinkled surface was important for neutrophil responses.

A remarkable finding was that after arresting neutrophils in the process of phagocytosis by osmotic wrinkling, restoration of isotonicity permitted some cells to continue in a co-ordinated manner. In other cells the directionality was lost. After the arrest of chemotaxis, restoration of isotonicity resulted in an uncoordinated attempt to continue to migrate. In no cell could a restoration of migration be observed and cell pushed out pseudopodia randomly, especially away from the adherence surface. It was not clear what the mechanism for this was, but it was clear that during the period of arrest, actin within the cell remained able to exert a force, but that key signals from the underlying substrate were lost.

It was interesting that adding artificial membrane expanders (deoxycholate), which increased the diffusion path-length as measured by sdFRAP, had little effect on the

behaviour of neutrophils. Although SEM imaging showed that the cells were 'flabby' with additional membrane, the phagocytic behaviour of the expanded cells was completely normally. Presumably, the actin- membrane linkage within physiological wrinkles was still controlled physiologically and additional deoxycholate wrinkles were not. The large physiological reservoir of wrinkled membrane which was required to unwrinkled during spreading on phagocytosis remained.

6.3 New advances in cell membrane topography since the start of this work

The work presented in this thesis can be put into the context of recent developments published during the course of this work. At the onset of this work, the relationship between membrane tension and cell surface topography was little considered (Hallett and Dewitt, 2007). However, during the course of the work reported in this thesis, this link between ezrin (which hold wrinkles in place) and membrane tension has also been reported (Brueckner *et al.,* 2015). These workers showed that MDCK II cells either depleted of ezrin by siRNA technology or over expressing ezrin had different mechanical properties, when assessed by force indentation experiments. There was a substantial increase in membrane tension (stiffening) with increased cytoplasmic ezrin and a decrease in membrane tension in ezrin-depleted cells. Interestingly, ezrin depletion also caused the loss of excess surface area, which would be indicative of reduced cell surface wrinkling (Brueckner *et al.,* 2015).

While this work was not undertaken on cells which rapidly change shape and regulate their surface area, this work on a model cell type was in agreement with the topographical

surface changes found in neutrophils using the newly developed sdFRAP technique. There is considerable interest in how the tension within the membrane is regulated and its consequences. Essentially, the relationship to ezrin shows that membrane tension is the outcome of how tightly linked the membrane wrinkles are. The more tightly linked the wrinkles are, the greater the force is required to distort the membrane experimentally. The work in this thesis has shown that the cell surface wrinkles can become flattened physiologically (Chapter 4) and that changing the degree of wrinkling has an effect on cell behaviour (Chapter 5). This work thus provides the experimental link between measured "membrane tension" and the actual cell surface topography.

Apart from changes in membrane tension allowing membrane expansion, there is an increasing number of reports that membrane tension can have effect on other properties of the cell. For example, the two stage process of phagocytosis reported here and elsewhere (Dewitt and Hallett, 2002) are reported to correlate with membrane tension as follows. The first phase of phagocytosis results from pseudopods extending rapidly by actin polymerization, pushing the plasma membrane forward, but the second phase occurs after the membrane area from available reservoirs is depleted (i.e. the slack in the wrinkles is taken up). This point is "sensed" by the cell as an increased membrane tension (Masters *et al.,* 2013). They also report that the increased tension directly altered the small Rho GTPase Rac1, 3'-phosphoinositide and cytoskeletal organization. These authors propose that, during phagocytosis, biochemical signalling is "orchestrated by the mechanical signal of membrane tension" and that this puts "a simple mechanical signal at the heart of understanding immunological responses" (Masters *et al.,* 2013). Unfortunately, Ca^{2+} signalling was not

looked at in this study and may have been responsible for some of the biochemical changes reported. However, the membrane tension alone could influence these biochemical events directly, as it was recently shown that a reduction in membrane tension has an influence on membrane protein density, presumably as a consequence of insertion and lateral diffusion (Shi and Baumgart, 2015). Although, membrane tension of the plasma membrane may be thought of as a whole cell mechanical property, the authors showed that it can be localised and involved in controlling cell polarity during cell migration (Tsujita *et al.,* 2015). The authors showed that FBP17 (marker of "membrane bending") in migrating cells is at the leading edge, but that reduction of the global plasma membrane tension, results in a random distribution throughout the cell. This would indicate that although "membrane bending" as indicated by FBP17 occurred globally when global membrane tension was reduced, in the migrating cell and its location only at the leading edge showed that membrane tension was reduced only at these loci. These locations also correlated with actin polymerisation (marked by WASP/N-WASP) and it was suggested that this acts as a feedback loop that regulates cell migration. Of course, the actin polymerisation ratchet (Grebecki, 1994, see section 4.1.4) would also only operate in regions of the cell with locally reduced membrane tension. The mechanism by which localised membrane tension is reduced was not addressed by Grebecki (1994), but the work in this thesis supports the proposal that local unwrinkling of cell surface wrinkles releases additional membrane and so reduces membrane tension. This effect was extremely localised in phagocytosis (see Chapter 4). It has been proposed that localised Ca^{2+} influx triggered by localised receptor binding was the initiator of these events, but there is new evidence that some cells have a membrane-tension gated Ca^{2+} channel (He *et al.,* 2017). It is known that neutrophils respond

to a mechanical stimulus by an increase in cytosolic Ca^{2+} (Laffafian and Hallett, 1995), so such a channel, if it exists on neutrophils, could be an initiator of Ca^{2+} influx in the absence of receptor ligation, since any contact with a solid object sufficient to stretch the membrane (i.e. increase local membrane tension) could trigger Ca^{2+} influx and unwrinkling to restore the tension to the lower level.

6.4 Proposed Model

From the work in this thesis, a model can be proposed (fig 6.1). This shows the effects of experimental manipulations on cell surface topography and the expected consequence on neutrophil behaviour. The upper part of the figure explains why simply expanding the surface area by DOC had an effect on sdFRAP, which shows how the surface topography has been changed (is reported by sdFRAP as extra path length for diffusion), but that there was no effect on the ability of the cells to spread or undergo phagocytosis. This was because the physiological wrinkles were held in place by linkage to cortical actin via ezrin. When stimulated, these links are broken by Ca^{2+} activation of calpain and spreading occurs. This is in contrast to the second condition, osmotic wrinkling. In this condition, additional wrinkles are formed, as reported by sdFRAP, but these are not maintain by physiological molecular linkage to actin and cannot be released by Ca^{2+} activated calpain. Even after actin-linkage cleavage, the wrinkles are held in place by the osmotic effect. Once isotonicity is restored, the wrinkles are free to unwrinkle and spreading and shape change can occur. The last condition is osmotic swelling, which forces the physiological wrinkles to unwrinkle by mechanical stress. The surface topography is flat, as reported by sdFRAP. The resulting effect on neutrophil behaviour could be inhibition, because the cell is so swollen that there is no

slack in the membrane and actin cannot push against this force. This effect has been shown in neutrophils which were stretched to a point where pseudopodia formation could not occur (Houk *et al.,* 2012). However, when the stretch part of the cell was severed by laser cutting, pseudopodia formation was restored. This effect was explained by the membrane tension effect. In the experiments reported here, if the tension was insufficient to pull apart the wrinkles, but only take up the slack in them, there would be no inhibition, as was seen. The problem with osmotic swelling is that once a cell swells to the point at which the cortical actin has been removed from the membrane, the membrane forms a geometrical shape (usually a semi-sphere) and the cell bursts. Cells which have not bursted during osmotic swelling thus probably still have some cortical actin to counteract the swelling effect and thus still have some wrinkles in place.

This model explains all the results reported here. Of course, there are other features, such as the loss of cell polarity which occurs when restoring isotoncity to osmotically hyperwrinkled neutrophils which are yet to be fully explained.

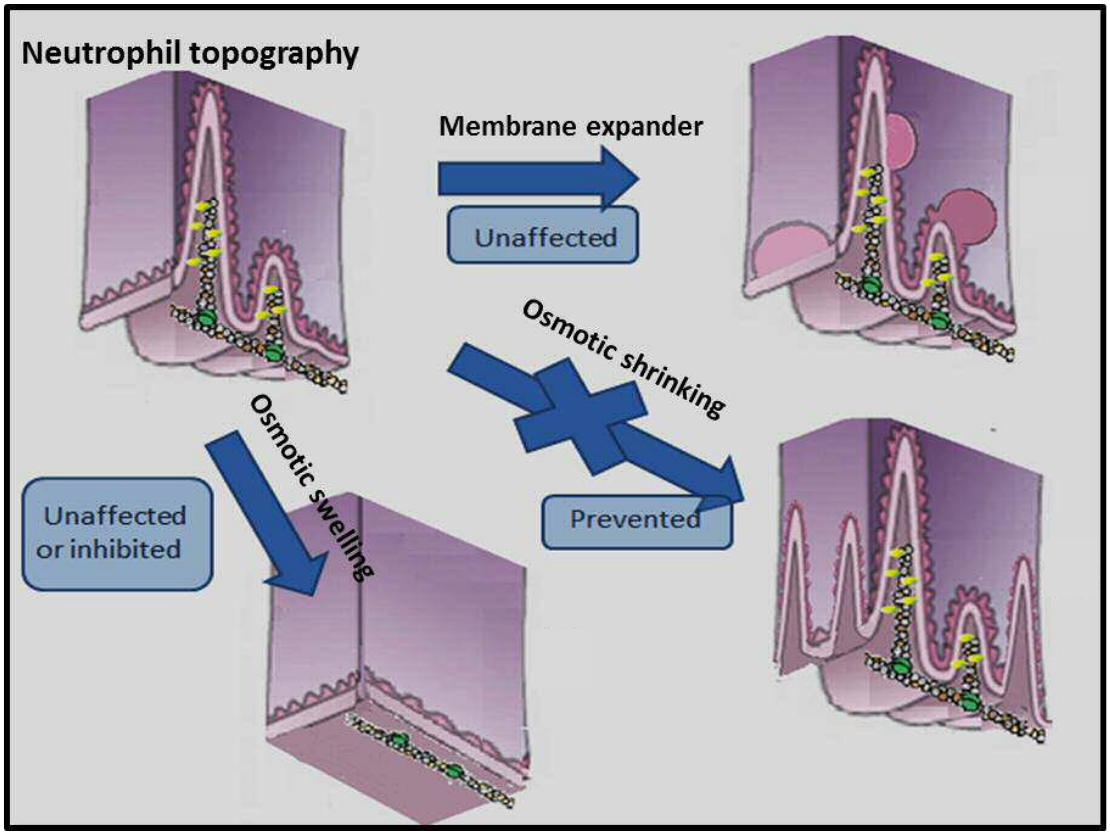

Figure 6.1 The effect of experimental manipulation of the neutrophil topography and its expected effect on the ability to expand in response to physiology demand.

6.5 Future Prospects

The work presented in this thesis opens a possibility of answering some significant questions which underlie cell behaviour. In the future, I envisage that sdFRAP will be used in a number of cell types and thus extend the findings here into other areas. For example, a lot of work has been done using fibroblast and similar cell types. Although these cell are not phagocytic and cell spreading is considerably slower that neutrophils (hours rather than minutes), they have the advantage that molecular biological manipulations, such as expressing fluorescent proteins and knocking down specific proteins, can be achieved. The hypothesis generated here makes some specific predictions about the cell surface topography in these experimentally produced genetically manipulated cells. It would thus be interesting and very useful to utilise sdFRAP in these cells.

There is a considerable amount of work to be done on neutrophils. It would be useful to investigate the effect of inhibition of calpain (calpain inhibitors) on sdFRAP. It has been shown that inhibition of calpain has no effect on Ca^{2+} signalling but causes total inhibition of neutrophil spreading. Although this is consistent with the proposed role of calpain activation by a rise in cytosolic Ca^{2+}, there is no direct evidence for a causal link with changes in cell surface topography. Obviously, sdFRAP could provide evidence for this link. It would also be instructive to investigate the role played by actin polymerisation. Inhibitors of actin polymerisation, such as cytochalasins, can also totally inhibit neutrophil cell shape change. This is not surprising, as it is the Brownian Ratchet effect (see Chapter 1 and section 4.1.4) of actin polymerisation near the plasma membrane which “pushes” the membrane and provides the force required to “expand “the membrane. It is predicted that in the absence

of this actin-mediated pushing the membrane out, non-spreading cells would still have a topographical change (as Ca^{2+} activated calpain activity would have occurred). These future studies would lead to a fuller understanding of the relationship between neutrophil cell surface topography and the ability to undergo rapid cell shape changes.

Another possibility for future work is that sdFRAP could be used in combination with other imaging techniques. For example, TIRF (total internal reflection microscopy) can image the wrinkles very near to the glass substrate (within 10nm) and can detect microridges as neutrophils roll (Prithu *et al.,* 2010). This could be used to confirm and extend the findings here. Moreover, imaging surface topography (non-quantitatively) together with sdFRAP (quantitatively) may give a further insight into the timing and loci at which membrane unwrinkling occurs. Also, it might be beneficial to monitor wrinkles in living cells simultaneously with monitoring elevated cytosolic Ca^{2+} changes and near membrane Ca^{2+} using TIRF microscopy.

6.6 Relevance of the work presented here

Neutrophils are the major cell type and first type to be recruited from the blood to sites of inflammation. In order to achieve this, neutrophils have to change their shape and then move through the blood vessels walls before undergoing chemotaxis to the area of inflammation. Activated neutrophils on the blood vessel endothelium roll and bind, assisted by selectins and ICAM-1 (Dewitt and Hallett, 2007). They then extravasate from the blood vessel to the tissue. However before they undergo this phase, they have to adhere and

spread out (Theler *et al.,* 1995). These same processes occur during pathological or chronic inflammation, where neutrophils continually accumulate at the inflamed site and cause localised damage to the tissues. When neutrophils are attracted to an enclosed space, such as the joint space, they can accumulate to high cell densities. The essential step in the process of extravasation is cell spreading, without which neutrophils are unable to leave the bloodstream (Dewitt and Hallett, 2007). This then would provide a therapeutic target for the treatment of inflammatory diseases and knowledge of the mechanism controlling neutrophil shape change may lead to useful therapeutic drugs.

Neutrophils undergo a number of steps during extravasation, including spreading, adhesion and chemotaxis migration. Some theories and analyses have shown that large changes in the available surface area must occur. It has been established that intracellular Ca^{2+} in the neutrophils either during spreading or phagocytosis, are required for the membrane expansion (Davies and Hallett, 1998; Hillson *et al*., 2006; Hillson and Hallett, 2007; Pettit and Hallett, 1997, 1998). In addition, activation of calpain, a Ca^{2+} activated protease in neutrophils, has been shown to be essential. The work in this thesis is consistent with the proposal that during neutrophil spreading, the apparent increase in the area of cell surface membrane arises from a reservoir of extra membrane within surface wrinkles and that 'un-wrinkling' of the neutrophil membrane permits the cell to spread out (Dewitt and Hallett, 2007). Therapeutic inhibition of plasma membrane unwrinkling would prevent excessive extravasation of neutrophils at pathological and chronic inflammatory sites.

6.7 Conclusion

In summary, the aim of the work in this thesis was to investigate the surface topography of neutrophils by developing a novel technique to image the diffusion rates of a fluorescent molecule, DiI, incorporated into the cell surface during phagocytosis, spreading and chemotaxis. This was achieved by photobleaching and monitoring recovery at a defined distance within the zone (a subdomain) and hence was called sdFRAP subdomain fluorescence recovery after photobleaching. Experimentation noted that differences in cell membrane surface topography were apparent during phagocytosis and shrinking, which were indicated by apparent differences in the diffusion. As sdFRAP reflects the cell surface topography at defined loci on the cell, this methodology opened a novel way of monitoring an important cell characteristic which has not been possible to study previously. These results are important as they not only validate the notion of topographic changes during biological activation of neutrophils, but also support the role of confocal microscopy in exploring these changes through the FRAP design. As such, future experiments should aim to replicate and develop these findings in order to provide a detailed overview of cell surface changes during neutrophil spreading and chemotaxis.

Chapter 7

References

A

Abercrombie M. (1980) The Croonian Lecture, 1978: The Crawling Movement of Metazoan Cells. *Proc Roy Soc Lond B* 207, 129-147.

Abercrombie M. (1980) The Croonian Lecture, 1978: The Crawling Movement of Metazoan Cells. *Proc Roy Soc Lond B* 207, 129-147.

Abramson JS, Wheeler JG. (1993) The natural immune system: The neutrophil. Oxford University Press, New York, USA.

Abul KA andrew HL, Shiv P.(2014) Basic Immunology: Functions and Disorders of the Immune System. *Elsevier*, Fourth Edition.

Aderem A, Underhill DM. (1999) Mechanisms of phagocytosis in macrophages. *Annu Rev Immunol* 17, 593-623.

Aderem, A. and D.M. Underhill. (1999) Mechanisms of phagocytosis in macrophages. *Annu Rev Immunol* 17, 593-623.

Afonso P, Parent C. (2012) Neutrophil under tension.*Dev Cell*. 22(2), 236–238.

Alberts B, Johnson A, Lewis J, et al. (2002) Molecular Biology of the Cell, 4e. *Garland Science*.

Alberts B, Johnson A, Lewis J. (2002) Molecular Biology of the Cell, 4e. *Garland Science*.

Allen LH, Aderem A. (1996b) Molecular definition of distinct cytoskeletal structures involved in complement and Fc receptor mediated phagocytosis in macrophages. *J Exp Med* 184, 627-637.

Al Jumaa, M.A., Dewitt, S. Hallett, MB. (2017) Topographical interrogation of the living cell surface reveals its role in rapid cell shape changes during phagocytosis and spreading. *Scientific Reports* 7, 9790.

Allingham, M. J., Van Buul, J. D. & Burridge, K. (2007) ICAM-1-mediated, Src- and Pyk2-dependent vascular endothelial cadherin tyrosine phosphorylation is required for leukocyte transendothelial migration. *J Immunol* 179**,** 4053-64.

Al-Mohanna FA, Hallett MB. (1988) The use of fura 2 to determine the relationship between intracellular free Ca^{2+} and oxidase activation in rat neutrophils. *Cell Calcium* 8, 17-26.

Al-Mohanna FA, Hallett MB. (1987). Actin polymerization modifies stimulus - oxidase coupling in rat neutrophils. *Biochim Biophys Acta* 927, 366-371.

Al-Mohanna FA, Hallett MB. (1990) Actin polymerisation in neutrophils is triggered without a requirement for a rise in cytosolic free Ca^{2+}. *Biochem J* 266,669-674.

Alteraifi MA, Zhelev DV. (1997) Transient increase of free cytosolic calcium during neutrophil motility responses. *J Cell Sci* 110, 1967-1977.

Anderson CL, Shen L, Eicher DM, Wewers MD, Gill JK. (1990) Phagocytosis by three distinct Fcγ receptor classes on human leukocytes. *J exp Med* 171, 1333-1345.

Anderson DC, Springer, TA. (1987) Leukocyte adhesion deficiency: an inherited defect in the Mac-1, LFA-1 and gp150,95 glycoproteins. *Annu Rev Med* 38, 175-94.

Anderson et al. (2000). Role of the cytoskeleton in rapid activation of CD11b/CD18 function and its subsequent downregulation in neutrophils. *J Cell Sci* 113, 2737-2745.

Anderson SI, Hotchin NA, Nash GB. (2000) Role of the cytoskeleton in rapid activation of CD11b/CD18 function and its subsequent downregulation in neutrophils. *J Cell Sci* 113(15), 2737-2745.

Araki N, Johnson MT, Swanson JA. (1996) A role for phosphoinositide 3-kinase in the completion of macropinocytosis and phagocytosis by macrophages. *J Cell Biol* 135(5), 1249-1260.

Arsenault J and O'Brien JA. (2013) Optimized mheterologousm transfection of viable adultorganotypic brain slices using an enhanced genegun. *BMC Res. Notes* 6, 544.

Aspenstrom P. (1999) The Rho GTPases have multiple effects on the actin cytoskeleton. *Exp Cell Res* 246, 20-25.

Aurrand-Lions, M., Lamagna, C., Dangerfield, J. P., Wang, S., Herrera, p., Nourshargh, S. & Imhof, B. A. (2005) Junctional adhesion molecule-C regulates the early influx of leukocytes into tissues during inflammation. *J Immunol* 174**,** 6406-15.

Axelsson L, Hellberg C, Melander F, Smith D, Zheng L andersson T. (2000) Clustering of beta(2)-integrins on human neutrophils activates dual signalling pathways to PtdIns 3-kinase. *Exp Cell Res 256*(1), 257-263.

B

Bag N, Yap DHX and Wohland T. (2014) Temperature dependence of diffusion in model and live cell membranes characterized by imaging fluorescence correlation spectroscopy. Biochimica et Biophysica Acta (BBA) - Biomembranes 1838, 802–813.

Bainton, D. F. (1973) "Sequential degranulation of the two types of polymorph nuclear leukocyte granules during phagocytosis of microorganisms" *J.Cell Biol* 58, 249-264.

Bainton DF, Ullyot JL, Farquhar MG. (1971) The development of neutrophilic polymorphonuclear leukocytes in human bone marrow. *J Exp Med* 134, 907.

Bainton F. (1973) Sequential degranulation of the two types of polymorphonuclear leukocyte granules during phagocytosis of microorganisms. *J.Cell Biol* 58, 249-264.
Bajno L, Peng XR, Schreiber AD, Moore HP, Trimble WS, Grinstein S. (2000) Focal exocytosis of VAMP3-containing vesicles at sites of phagosome formation. *J Cell Biol* 149(3), 697-706.

Bajt ML, Goodman T, McGuire SL. (1995) Beta 2 (CD18) mutations abolish ligand recognition by I domain integrins LFA-1 (alpha L beta 2, CD11a/CD18) and MAC-1 (alpha M beta 2, CD11b/CD18). *J Biol Chem* 270, 94-98.

Bartus RT, Hayward NJ, Elliot PJ, Sawyer SD, Baker KL, Dean RL, Akiyama A, Straub JA, Harbeson SL, Li Z, Powers J. (1994) Calpain inhibitor AK295 protects neurons from focal brain ischemia. Effects of postocclusion intra-arterial administration. *Stroke* 25, 2265-2270.

Bellis SL, Perotta JA, Curtis MS, Turner CE. (1997) Adhesion of fibroblasts to fibronectin stimulates both serine and tyrosine phosphorylation of paxillin. *Biochem J* 325, 375-381.

Bengtsson T, Jaconi ME, Gustfson M, Magnusson KE, Theler JM, Lew DP, Stendahl O. (1993) Actin dynamics in human neutrophils during adhesion and phagocytosis is controlled by changes in intracellular free calcium. Eur J Cell Biol 62, 49-58.

Benjamin E, Coico R, Sunshine G. (2000) Immunology: Ed 4 Wiley-Liss, Canada.

Berg, H. C. (1977) Random Walks in Biology. Princeton.

Berg JS, Derfler BH, Pennisi CM, Corey DP, Cheney RE. (2000) Myosin-X, a novel myosin with pleckstrin homology domains, associates with regions of dynamic actin. *J Cell Sci* 113(19), 3439-3451.

Beron W, Colombo MI, Mayorga LS, Stahl PD. (1995) In vitro reconstruction of phagosome-endosome fusion: evidence for regulation by heterotrimeric GTPases. *Arch Biochem Biophys* 317, 337-342.

Berridge MJ, Irvine RF. (1984) Inositol 1,4,5-triphosphate, a novel second messenger in cellular signal transduction. *Nature* 312, 315-321.

Berridge MJ, Irvine RF. (1989) Inositol 1,4,5-triphosphate and cell signalling. *Nature* 341, 197-205.

Berton G, Fumagalli L, Laudanna C, Sorio C. (1994) Beta 2 integrin-dependent protein tyrosine phosphorylation and activation of the FGR protein tyrosine kinase in human neutrophils. *J Cell Biol* 126, 1111-1121.

Bevilacqua M, Butcher E, Furie B, Gallatin M, Gimbrone M, Harlan J, Kishimoto K, Lasky L, McEver R, et al. (1991) Selectins: a family of adhesion receptors. *Cell* 67, 233-234.

Blanchard H, Grochulski P, Yunge L, Arthur SC, Davies PL, Elce JS, Cygler M. (1997) Structure of calpain Ca^{2+}-binding domain reveals novel EF-hand and Ca^{2+}-inuced conformational changes. *Nat Struct Biol* 4(7), 532-538.

Bogen S., Pak J., Garifallou M., Deng X, Muller WA. (1994) Monoclonal antibody to murine PECAM-1 (CD31) blocks acute inflammation in vivo. *J Exp Med* 179**,** 105964.

Bokoch GM, Quilliam LA. (1990) Guanine nucleotide binding properties of rap1 purified from human neutrophils. Biochem J 267(2), 407-411.

Bokoch GM. (1990) Signal transduction by GTP binding proteins during leukocyte activation: phagocytic cells. *Curr Top Membr Transp* 35, 65-101.

Bokor M, Csizmok V, Kovacs D , Banki P, Friedrich P,Tompa P, Tompa K. (2005) NMR relaxation studies on the hydrate layer of intrinsically unstructured proteins. Biophys. J. 88, 2030–2037.

Bokshtein, B. S., Mendelev, M. I. Srolovitz, D. J. (2005).Thermodynamics and Kinetics in Materials Science: A Short Course. *Oxford University Press* 167–171.

Bommakanti RK, Dratz EA, Siemsen DW, Jesaitis AJ. (1995) Extensive contact between Gi2 and N-formyl peptide receptor of human neutrophils: mapping of binding sites using receptor-mimetic peptides. *Biochemistry* 34, 6720-6728.

Booth JW, Trimble WS, Grinstein S. (2001) Membrane dynamics in phagocytosis. *Semin Immunol* 13(6), 357-364.

Borregaard N, Cowland JB (1997). Granules of the human neutrophilic polymorphonuclear leukocyte. *Blood* 89, 3503–21.

Borregaard N, Heiple JM, Simons ER, Clark RA. (1983) Subcellular localisation of the b-type cytochrome component of the human neutrophil microbial oxidase: translocation during activation. *J Cell Biol* 97, 52-61.

Borregaard N, Kjeldsen L, Sengelov H, Diamond MS, Springer TA anderson HC, Kishmoto TK, Bainton DF. (1994) Changes in subcellular localization and surface expression of L-selectin, alkaline phosphatase and Mac-1 in human neutrophils during stimulation with inflammatory mediators. *J Leukoc Biol,* 56**,** 80-7.

Borregaard N, Sehested M, Nielsen BS, Sengeløv H, Kjeldsen L. (1995). Biosynthesis of granule proteins in normal human bone marrow cells. Gelatinase is a marker of terminal neutrophil differentiation. *Blood* 85, 812–7.

Borregaard, N. et al. (1996). Granules and secretory vesicles of the human neutrophil. *International Journal of Pediatric Hematology/Oncology* 3(5), pp. 307-319.

Borregaard, N and Cowland, J. (1996) Granules of the Human Neutrophilic Polymorphonuclear Leukocyte. *Blood* 89, 3503-3521.

Botelho RJ, Tapper H, Furuya W, Mojdami D, Grinstein S. (2002) Fc gamma R-mediated phagocytosis stimulates localized pinocytosis in human neutrophils. *J Immunol* 169 (8), 4423-9.

Botelho RJ, Teruel M, Dierckman R anderson R, Wells A, York JD, Meyer T, Grinstein S. (2000) Localised biphasic changes in phosphatidylinositol-4,5-bisphosphate at sites of phagocytosis. *J Cell Biol* 151(7), 1353-1368.

Boulay F, Tardif M, Brouchon L, Vignais P. (1990) The human N-formylpeptide receptor. Characterization of two cDNA isolates and evidence for a new subfamily of G-protein-coupled receptors. *Biochemistry* 29, 11123-11133.

Bradfield PF, Nourshargh OS, Aurrand-Lions M, Imhof BA. (2007) JAM family and related proteins in leukocyte migration (Vestweber series). *Arterioscler Thromb Vasc Biol* 27**,** 2104-12.

Brandman O, Meyer T. (2008) Feedback Loops Shape Cellular Signals in Space and Time. *Science*. 322, 390–395.

Brasen, J. et al. (2010) Cell surface topology creates high Ca2+signalling microdomains. *Cell Calcium* 47, *339-349*.

Brini M, Di Giorgo F, Murgia M, Marsault R, Massimo ML, Cantini M, Rizzuto R, Pozzan T. (1997) Subcellular analysis of Ca^{2+} homeostasis in primary cultures of skeletal myotubules. *Mol Cell Biol* 8, 129-143.

Brown EJ. (1986) The role of extracellular matrix proteins in the control of phagocytosis. *J Leuk Biol* 39, 579-591.

Brown EJ. (1995) Phagocytosis. *BioEssays*. 17(2), 109-117.

Brueckner, BR, Pietuch, A, Nehls, S, Rother, J, Janshoff, A. (2015). Ezrin is a major regulator of membrane tension in epithelial cells. *Scientific Reports* 5, 14700.

Bryant RE, Sutclije MC, McGee ZA. (1972) Eject of osmolarities comparable to those of the renal medulla on function of human polymorph nuclear leukocytes. *J.Infect. Dis* 126, 1-10.

Bryant, R.E., M.C. Sutclije, Z.A. McGee. (1972) "Eject of osmolarities comparable to those of the renal medulla on function of human polymorph nuclear leukocytes" *J. Infect. Dis* 126, 1-10.

C

Calderwood DA, Shattil SJ, Ginsberg MH.(2000) Integrins and actin filaments: reciprocal regulation of cell adhesion and signaling. *J Biol Chem* 275(30), 22607-22610.

Calderwood DA, Zent R, Grant R, Rees DJ, Hynes RO, Ginsberg MH. (1999) The Talin head domain binds to integrin beta subunit cytoplasmic tails and regulates integrin activation. *J Biol Chem* 274(40), 28071-28074.

Carafoli E, Molinari M. (1998) Affinity purification of mu-calpain from erythrocytes on an immobilized peptide from the plasma membrane calcium pump. Some studies on erythrocyte mu-calpain. *Biochem Biophys Res Commun* 247, 193-203.

Carlsson AE. (2003) “Growth velocities of branched actin networks” *Biophys J* 84 (5), 2907-18.
Carlsson AE. (2003) Growth velocities of branched actin networks. *Biophys J* 84, (5), 2907-18.
Caron E, Hall A. (1998) Identification of two distinct mechanisms of phagocytosis controlled by different Rho GTPses. *Science* 282, 1717-1721.

Caron E, Self AJ, Hall A. (2000) The GTPase Rap1 controls functional activation of macrophage integrin alphaMbeta2 by LPS and other inflammatory mediators. *Curr Biol* 10, 974-978.

Cassatella MA, Anegon I, Cuturi MC, Griskey P, Trinchiere G, Perussia B. (1989) FcγR (CD16) interaction with ligand induces Ca^{2+} mobilisation and phosphoinositide turnover in human natural killer cells. *J Exp Med* 171, 1239-1255.

Castellano F, Chavrier P, Caron E. (2001) Actin dynamics during phagocytosis. *Semin Immunol* 13(6), 347-355.

Chatterjee et al (2005) Inhibitors of calpain activation (PD150606 and E-64) and renal ischemia-reperfusion injury. *Biochem Pharmacol* 69, 1121-1131.

Cheah FC, Hampton MB, Darlow BA, Winterbourn CC, Vissers MC (2005) Detection of apoptosis by caspase-3 activation in tracheal aspirate neutrophils from premature infants: relationship with NF-kappaB activation. *J Leukoc Biol.* 77, 432-7.

Cheek TR, Berridge MJ, Moreton RB, Stauderman KA, Murawsky MM, Bootman MD. (1994) Quantal Ca^{2+} mobilisation by ryanodine receptors is due to all-or-none release from functionally discrete intracellular stores. *Biochem J* 301, 879-833.

Chen Y, Corriden R, Inoue Y, Yip L, Hashiguchi N, Zinkernagel A, Nizet V, Insel PA, Junger WG. (2006) ATP release guides neutrophil chemotaxis via P2Y2 and A3 receptors .*Science* 314, 1792–1795.

Cockroft S, Gomperts BD. (1985) Role of guanidine nucleotide binding protein in the activation of polyphosphoinositide phosphodiesterase. *Nature* 314, 534-536.

Cohen, Stephen; Burns, Richard C. (2002) Pathways of the Pulp *(8th ed.). St. Louis: Mosby. p. 465.*

Cohnheim J. (1867a) Uber. Enteundung und Eitung. Virchow's Arch Pathol Anat 40, 1-25.

Cohnheim J. (1867b) Inflammation in Lectures in General Pathology. *Syndenham Society of London* 1, 242-254.

Collier NC, Wang K. (1982) Purification and properties of human platelet P235. A high molecular weight protein substrate of endogenous calcium-activated protease(s). *J Biol Chem* 257, 6937-6943.

Connelly PA, Farrell CA, Merenda JM, Conklyn MJ, Showell HJ. (1991) Tyrosine phosphorylation is an early signalling event common to Fc receptor crosslinking in human neutrophils and rat basophilic leukaemia cells (RBL-2H3). *Biochem Biophys Res Commun* 177, 192-201.

Cooke E Hallett MB. (1985) The role of c-kinase in the physiological activation of neutrophil oxidase; evidence using pharmacological manipulation of c-kinase activity in intact cells. *Biochem J* 232, 323-327.

Coppolino MG, Krause M, Hagendorff P, Monner DA, Trimble W, Grinstein S, Wehland J, Sechi AS. (2001) Evidence for a molecular complex consisting of Fyb/SLAP, SLP-76, Nck, VASP and WASP that links the actin cytoskeleton to Fcgamma receptor signalling during phagocytosis. *J Cell Sci* 114(23), 4307-4318.

Cox D, Berg JS, Cammer M, Chinegwundoh JO, Dale BM, Cheney RE Greenberg S. (2002) Myosin X is a downstream effector of PI(3)K during phagocytosis. *Nat Cell Biol* 4, 469-477.

Cox D, Dale BM, Kashiwada M, Helgason CD, Greenberg S. (2001) A regulatory role for Src homology 2 domain-containing inositol 5'-phosphatase (SHIP) in phagocytosis mediated by Fc gamma receptors and complement receptor 3 (alpha(M)beta(2); CD11b/CD18). *J Exp Med* 193(1), 61-71.

Cox D, Tseng CC, Bjekic G, Greenberg S. (1999) A requirement for phosphatidylinositol 3-kinase in pseudopod extension. *J Biol Chem* 274, 1240-1247.

Cox, D., P. Chang, T. Kurosaki and S. Greenberg. (1996) "Syk tyrosine kinase is required for immunoreceptor tyrosine activation motif-dependent actin assembly" *J Biol Chem* 271, 16597-16602.

Cramer EB, Gallin JI. (1979) Localisation of submembranous cations to the leading edge of human neutrophils during chemotaxis. *J Cell Biol* 82, 369-375.

Crank, J. (1980)The Mathematics of Diffusion. *Oxford University Press*.
Critchley DR. (2000) Focal adhesions – the cytoskeletal connection. *Curr Opin Cell Biol* ,12, 133-139.

Croce et al (1999) Inhibition of calpain blocks platelet secretion, aggregation and spreading *J Biol Chem*, 274 , 36321-36327.

Cuerrier, D et al (2007) Development of calpain-specific inactivators by screening of positional scanning epoxide libraries *J. Biol. Chem*. 282, 9600-9611.

Cuzzocrea et al. (2000) Calpain inhibitor I reduces the development of acute and chronic inflammation. *Am J Pathol.* 157:2065-79.

D

Dace JV, Lewis SM. (1995) Practical Haematology. Ed 8. Churchill Livingstone, New York.

Davies EV, Blanchfield H, Hallet MB. (1997). Use of fluorescent dyes for measurement and localisation of organelles associated with Ca^{2+} store release in human neutrophils. *Cell Biology International* 21, 655-663.

Davies EV, Cambell AK, Hallet MB. (1994). Ca^{2+} oscillations in neutrophils triggered by immune complexes result from Ca^{2+} influx*. Immunology* 82, 57-62.

Davies EV, Hallett MB, Cambell AK. (1991). Localised superoxide release by neutrophils can be provoked by a cytosolic calcium cloud. *Immunology* 73, 228-234.

Davies EV, Hallett MB. (1995) A soluble factor directly stimulates Ca^{2+} entry in neutrophils. Biochem Biophys Res Commun 206, 348-354.

Davies EV, Hallett MB. (1995b) A novel pathway for Ca^{2+} signalling in neutrophils by immune complexes. *Immunology* 85, 538-543.

Davies EV, Hallett MB. (1996) Near membrane Ca^{2+} changes resulting from store release in neutrophils: detection by FFP-18. *Cell Calcium* 19, 255-362.

Davies EV, Hallett MB. (1998) High micromolar Ca^{2+} beneath the plasma membrane in stimulated neutrophils. *Biochem. Biophys. Res. Commun* 248, 679-683.

Davies, E. V. and Hallett M. B. (1998) "High micromolar Ca^{2+} beneath the plasma membrane in stimulated neutrophils. *Biochemical & Biophysical Research Communications*, 248 , 679-83.
Davies, E. V. and M. B. Hallett (1998). High micromolar Ca^{2+} beneath the plasma membrane in stimulated neutrophils. *Biochemical & Biophysical Research Communications*, 248 (3), 679-83.

Davies-Cox EV, Laffafian I, Hallett MB. (2001) Control of Ca^{2+} influx in human neutrophils by inositol 1,4,5-trisphosphate (IP_3) binding: Differential effects of micro-injected IP_3 receptor antagonists. *Biochem J* 355, 139-143.

De Lozanne A, Spudich JA. (1987) Disruption of the Dictyostelium myosin heavy chain gene by homologous recombination. *Science* 236, 1086-1091.

Della Bianca V, Grzeskowiak M, Dusi S, Rossi F. (1993) Transmembrane signalling pathways involved in phagocytosis and associated activation of NADPH oxidase mediated by Fc gamma Rs in human neutrophils. *J Leuk Biol* 63, 427-438.

Della Bianca V, Grzeskowiak M, Rossi F. (1990) Studies on molecular recognition of phagocytosis and activation of the NADPH oxidase in neutrophils. IgG- and C3b-mediated ingestion and associated respiratory burst independent of phosphoinositide turnover and Ca^{2+} transients. *J Immunol* 144, 1411-1417.

Demareux N, Monod A, Lew DP, Krause KH. (1994) Characterisation of receptor-mediated and store regulated calcium influx in human neutrophils. *Biochem J* 297, 595-601.
Demaurex N, Lew DP, Krause K-H. (1992) Cyclopiazonic acid depletes intracellular Ca^{2+} stores and activates an influx pathway for divalent cations in HL-60 cells. *J Biol Chem* 267, 2318-2324.

Desjardins M, Celis JE, van Meer G, Dieplinger H, Jahraus A, Griffiths G, Huber LA. (1994) Molecular characterisation of phagosomes. *J Biol Chem* 269, 32194-32200.

Desjardins M, Huber LA, Parton RG, Griffiths G. (1994b) Biogenesis of phagolysosomes proceeds through a sequential series of interactions with the endocytic apparatus. *J Cell Biol* 134, 677-688.

Desjardins M. (1995) Biogenesis of phagolysosomes: the 'kiss and run' hypothesis. *Trends Cel Biol* 5, 183-186.

Detmers PA, Wright SD, Olsen E, Kimball B and Cohn ZA. (1987) Aggregation of complement receptors on human neutrophils in the absence of ligand. *J Cell Biol* 105, 1137-1145.

Devitt A, Marshall LJ. (2011) The innate immune system and the clearance of apoptotic cells. *J Leukoc Biol* 90, 447-457.

Devreotes P, Janetopoulos C. (2003) Eukaryotic chemotaxis: distinctions between directional sensing and polarization. *J. Biol. Chem.* 278, 20445–20448.

Dewitt , S, Darley , RL , Hallett MB. (2009) Translocation or just location? Pseudopodia affect fluorescent signals *J. Cell Biol* 184, 197–203.

Dewitt S, Laffafian I, Hallett MB. (2002) Does neutrophil CD38 have a role in Ca^{++} signaling triggered by β_2 integrin? *Nat Med* 8(4), 307.

Dewitt S, Hallett MB. (2002) Cytosolic free Ca2+ changes and calpain activation are required for β integrin–accelerated phagocytosis by human neutrophils. *The Journal of Cell Biology* 159(1), 181-189.

Dewitt S, Hallett MB. (2007) Leukocyte membrane expansion: a central mechanism for leukocyte extravasation. *J Leukoc Biol* 81**,** 1160-4.

Di Rosa G, Odrijin T, Nixon RA, Arancio O. (2002) Calpain inhibitors: a treatment for Alzheimer's disease. *J Mol Neurosci* 19(1-2), 135-141.

Diacovo TG, Roth SJ, Buccola JM, Bainton DF, Springer TA. (1996) Neutrophil rolling, arrest and transmigration across activated, surface-adherent platelets via sequential action of P-selectin and the β2-integrin CD11b/CD18. *Blood* 88, 146-157.

Diamond MS. (1991) Binding of the integrin Mac-1 (CD11b/CD18) to the third immunoglobulin-like domain of ICAM-1 (CD54) and its regulation by glycosylation. *Cell* 65, 961-71.

Ding ZM, Babensee JE, Simon SI, Lu H, Perrard JL, Bullard DC, Dai XY, Bromiley SK, Dustin ML, Entman ML, Smith CW, Ballantyne CM. (1999) Relative contribution of LFA-1 and Mac-1 to neutrophil adhesion and migration. *J Immunol* 163**,** 5029-38.

Dittrich PS, Schwille P. (2001) Photobleaching and stabilization of fluorophores used for single-molecule analysis with one- and two-photonexcitation. *Appl. Phys.* B 73, 829–837.

Dunne JL, Ballantyne CM, Beaudet A L, Ley K. (2002) Control of leukocyte rolling velocity in TNF-alpha-induced inflammation by LFA-1 and Mac-1. *Blood* 99, 336-41.

Du J, Xie J, Yue L. (2009) Intracellular calcium activates TRPM2 and its alternative spliced isoforms. *Proc Natl Acad Sci U S A* 106**,** 7239-44.

Dusi S, Della Bianca V, Donini M, Nadalini KA, Rossi F. (1996) Mechanisms of stimulation of the respiratory burst by TNF in nonadherent neutrophils: its dependence of lipidic transmembrane signalling and dependence on protein tyrosine phosphorylation and cytoskeleton. *J Immunol* 157(10), 4615-4623.

E

Ehrengruber, MU, , Coates, TD, Deranleau, DA. (1995) Shape Oscillations- A fundamental response of humn neutrophils stimulated by chemotactic peptides. *FEBS LETTERS* 359, 229-232.

Ehrengruber, MU, Deranleau, DA, Coates, TD. (1996) Shape oscillations of human neutrophil leukocytes: Characterization and relationship to cell motility. *J Exp Biol* 199, 741-747.
Ellett, F. et al. (2011) mpeg1 promoter transgenes direct macrophage-lineage expression in zebrafish. *Blood*. 117, 49-56.

Ellson CD anderson KE, Morgan G, Chilvers ER, Lipp P, Stephens LR, Hawkins PT. (2001b) PI(3)P is generated in phagosomal membranes. *Current Biol* 11, 1631-1635.

Ellson CS, Gobert-Gosse S andersen KE, Davidson K, Erdjument-Bromage H, Thuring JW, Cooper MA, Lim Z-Y, Holmes AB, Gaffney PRJ, CoadwellJ, ChilversER, HawkinsPT, StephensLR. (2001) PtdIns(3)P regulates the neutrophil oxidase complex by binding to the PX domain of p40phox. *Nature Cell Biol* 3, 679-682.

Elomaa O, Kangas M, Sahlberg C, Tuukkanen J, Sormunen R, Liakka A, Thesleff I, Kraal G, Tryggvason K. (1995) Cloning of a novel bacteria binding receptor structurally related to scavenger receptors and expressed in a subset of macrophages. *Cell* 80, 603-609.

Erwig, L. P. and P. M. Henson. (2007) Immunological consequences of apoptotic cell phagocytosis. *Am. J. Pathol.* 171, 2–8.

Evans E, Leung A, Zhelev D. (1993) Synchrony of cell spreading and contraction force as phagocytes engulf large pathogens. *J Cell Biol* 122(6), 1295-1300.

F

Fadeel B, Åhiln A, Henter JI, Orrenius S, Hampton MB. (1998) Involvement of caspases in neutrophil apoptosis: regulation by reactive oxygen species. *Blood* 92, 4808-4818.

Fällman M andersson R andersson T. (1993) Signaling properties of CR3 (CD11b/CD18) and CR1 (CD35) in relation to phagocytosis of complement-opsonised particles. *J. Immunol*. 151, 330-338.

Fällman M, Gullberg M, Hellberg C and Andersson T. (1992) Complement receptor mediated phagocytosis is associated with accumulation of phosphatidylcholine-derived diglyceride in human neutrophils. Involvement of phospholipase D and direct evidence for a positive feedback signal of protein kinase. *J Biol Chem* 267, 2656-2663.

Fällman M, Lew DP, Stendahl O andersson T. (1989) Receptor-mediated phagocytosis in human neutrophils is associated with increased formation of inositol phosphates and diacylglycerol. Elevation in cytosolic free calcium and formation of inositol phosphates can be dissociated from accumulation of diacylglycerol. *J Clin Invest* 84(3), 886-891.

Favre CJ, Jerström P, Foti M, Stendhal O, Huggler E, Lew DP, Krause KH. (1996) Organisation of Ca^{2+} stores in myeloid cells: association of SERCA2b and the type-1 inositol-1,4,5-trisphosphate receptor. *Biochem J* 316, 137-142.

FENG, D., NAGY, J. A., PYNE, K., DVORAK, H. F. & DVORAK, A. M. (1998) Neutrophils emigrate from venules by a transendothelial cell pathway in response to FMLP. *J Exp Med* 187**,** 903-15.

Fernandez R, Suchard SJ. (1998) Syk activation is required for spreading and H_2O_2 release in adherent human neutrophils. *J Immunol* 160, 5154-5162.

Foder B, Scharff O, Thastrup O. (1989) Ca^{2+} transients and Mn^{2+} entry in human neutrophils induced by thapsigargin. *Cell Calcium* 10, 477-490.

Fratti RA, Backer JM, Gruenberg J, Corvera S, Deretic V. (2001) Role of phosphatidylinositol 3-kinase and Rab5 effectors in phagosomal biogenesis and mycobacterial phagosome maturation arrest. *J Cell Biol* 154, 631-644.

Fratti, R.A., J.M. Backer, J. Gruenberg, S. Corvera and V. Deretic. (2001) “Role of phosphatidylinositol 3-kinase and Rab5 effectors in phagosomal biogenesis and mycobacterial phagosome maturation arrest” *J Cell Biol* 154, 631-644.

Frank, M. M. and Fries L. F. (1991) The role of complement in inflammation and phagocytosis. *Immunol Today* 12(9), 322-6.

Fuortes M, Jin WW, Nathan C. (1993) Adhesion-dependent protein tyrosine phosphorylation in neutrophils treated with tumour necrosis factor. *J Cell Biol* 120, 777-784.

G

Gagnon E, Duclos S, Rondeau C, Chevet E, Cameron PH, Steele-Mortimer O, Paiement J, Bergeron JJM, Desjardins M. (2002) Endoplasmic reticulum-mediated phagocytosis is a mechanism of entry into macrophages. *Cell* 110, 119-131.

Gan WB ,Bishop DL ,Turney SG, Lichtman JW.(1999) Vitalimaging and ultra-structural analysis of individual axon terminals labelled by iontophoretic application of lipophilic dye. *J. Neurosci. Methods* 93, 13–20.

Gan WB, Grutzendler J, Wong WT, Wong RO, Lichtman JW. (2000). Multicolor "DiOlistic" labelling of the nervous system using lipophilic dye combinations. *Neuron* 27, 219–225.

Gao JX, Wilkins J, Issekutz AC. (1995) Migration of human polymorphonuclear leukocytes through a synovial fibroblast barrier is mediated by both beta 2 and (CD11/18) integrins and the beta1 (CD29) integrins VLA-5 and VLA-6. *Cell Immunol* 163, 178-186.

GARRIDO-URBANI, S., BRADFIELD, P. F., LEE, B. P. & IMHOF, B. A. (2008) Vascular and epithelial junctions: a barrier for leucocyte migration. *Biochem Soc Trans,* 36**,** 203-11.

Geering B, Simon HU. (2011) Pecularities of cell death mechanism in neutrophils. *Cell Death Diff* 18, 1457 - 1469.

Gennaro R, Pozzan T, Romeo D. (1984) Monitoring of cytosolic free Ca^{2+} in C5a-stimulated neutrophils: Loss of receptor-modulated Ca^{2+} stores and Ca^{2+} uptake in granule-free cytoplasts. Proc Natl Acad Sci USA 81, 1416-1420.

Glitsch MD, Bakowsi D, Parekh AB. (2002) Store-operated Ca^{2+} entry depends on mitochondrial Ca^{2+} uptake. *EMBO J* 21(24), 6744-6754.

Gold ES, Underhill DM, Morrissette NG, Guo J, McNiven MA, Aderem A. (1999) Dynamin 2 is required for phagocytosis in macrophages. *J Exp Med* 190, 1849-1856.

Goll et al (2003) The calpain system *Physiol Rev* 83, 731-801.
Gonzalez-Amaro R, Sanchez-Madrid F. (1999) Cell adhesion molecules: selectins and integrins. *Crit Rev Immunol* 19(5-6), 389-429

Goodman TG, Bajt ML. (1996) Identifying the putative metal ion-dependent adhesion site in the beta2 (CD18) subunit required for alphaLbeta2 and alphaMbeta2 ligand interactions. *J Biol Chem* 271, 23729-23736.

Gotsch U, Borges E, Bosse R, Boggemeyer E., Simon M, Mossmann H, Vestweber D. (1997) VE-cadherin antibody accelerates neutrophil recruitment in vivo. *J Cell Sci,* 110 (Pt 5)**,** 583-8.

Graham IL, Brown EJ. (1991) Extracellular calcium results in a conformational change in Mac-1 (CD11b/CD18) on neutrophils. Differentiation of adhesion and phagocytosis functions of Mac-1. *J Immunol* 146, 685-691.

Grebecki, A. (1994) “Membrane and cytoskeletal flow in motile cells with emphasis on the contribution of free-living amoeba” *Int. Rev. Cytol* 148, 37–79.
Gregory J S . (2009). The Immune System. US. *Infobase.*

Greenberg S, Burridge K, Silverstein SC. (1990) Colocalisation of F-actin during Fc receptor-mediated phagocytosis in mouse macrophages. *J Exp Med* 172, 1853-1856.

Greenberg S. (1995) Signal transduction of phagocytosis. Trends Cell Biol 5, 93-99.

Greenberg S. (2001) Diversity in phagocytic signalling. *J Cell Sci* 114(6), 1039-1040.

Gresham HD, Graham IL anderson DC, Brown EJ. (1991) Leukocyte adhesion-deficient neutrophils fail to amplify phagocytic function in response to stimulation. Evidence for CD11b/CD18-dependent and independent mechanisms of phagocytosis. *J Clin Invest* 88, 588-597.

Griffin FM, Griffin JA, Leider JE, Silverstein SC. (1975) Studies on the mechanism of phagocytosis. I. Requirements for circumferential attachment of particle-bound ligands to specific receptors on the macrophage plasma membrane. *J Exp Med* 142(5) 1263-1282.

Griffin FM, Griffin JA, Silverstein SC. (1976) Studies on the mechanism of phagocytosis. II. The interaction of macrophages with anti-immunoglobulin IgI-coated bone marrow derived lymphocytes. *J Exp Med* 144(3), 788-809.

Gullapalli RR, Demirel MC, Butler PJ. (2008) Molecular dynamics simulations of DiI-C18(3) in a DPPC lipid bilayer. *Phys Chem Chem Phys*. 10, 3548-60.

H

Hackman DJ, Rotstein OD, Sjolin C, Schreiber AD, Trimble WS, Grinstein S. (1998) v-SNARE – dependent secretion is required for phagocytosis. Proc Natl Acad Sci USA 95, 11691-11696.
Hallett MB, Campbell AK. (1984) Is intracellular Ca^{2+} the trigger for oxygen radical production by polymorphonuclear leukocytes?. *Cell Calcium* 5, 1-19.

Hallett MB, Davies EV, Campbell AK. (1990) Oxidase activation in individual neutrophils is dependent on the onset and magnitude of the Ca^{2+} signal. *Cell Calcium* 11, 655-663.

Hallett MB, Dewitt S. (2007) Ironing out the wrinkles of neutrophil phagocytosis. *Trends in Cell Biology* 17(5),209-14.

Hallett MB, Lloyds D. (1995) Neutrophil priming: the cellular signals that say 'amber' but not 'green'. *Immunol Today,* 16**,** 264-8.

Hallett MB, Hodges R, Cadman M, Blanchfield H, Dewitt S, Pettit E, Laffafian I, Davies EV. (1999) Techniques for measuring and manipulating free Ca^{2+} in the cytosol and organelles of neutrophils. *J Immunol Meth* 232, 77-88.

Hallett MB, Lloyds D. (1997) Molecular and Ionic signalling of neutrophils. Springer-Verlag, New York. Landes Bioscience Pub., TX

Hallett MB, Pettit EJ, Davies EV. (1996a) Capacitative Ca^{2+} influx and a diffusible influx factor. *Biochem J* 314, 1054-1055.

Hallett MB, Pettit EJ. (1997) Stochastic events underlie Ca^{2+} signalling in neutrophils. *J Theor Biol* 186(1), 1-6.

Hallett MB. (1989). The significance of stimulus-response coupling in the neutrophil for physiology and pathology. In: The neutrophil: cellular biochemistry and physiology. Hallett, MB. *CR Press.* pp 1-22.

Hamilton RF, Thakur SA, Mayfair JK, Holian A. (2006) MARCO mediates silica uptake and toxicity in alveolar macrophages from C57BL/6 mice. *J Biol Chem* 281, 34218-34226.

Hamilton, R.F., Jr., S.A. Thakur, J.K. Mayfair and A. Holian. (2006) “MARCO mediates silica uptake and toxicity in alveolar macrophages from C57BL/6 mice” *J Biol Chem* 281, 34218-34226.

Hammer JA. (1994) The structure and function of unconventional myosins: a review. *J Musc Res Cell Motil* 15, 1-10.

Hampton MB, Chambers ST, Vissers M, Winterbourn CC. (1994) Bacterial killing by neutrophils in hypertonic environments." *J. Infect. Dis,* 169, 839-846.

Hampton, M.B., S.T. Chambers, M.C.M. Vissers, C.C. Winterbourn. (1994) "Bacterial killing by neutrophils in hypertonic environments." *J. Infect*. Dis, 169, 839-846.

Harris ES, McIntyre TM, Prescott SM, Zimmerman GA. (2000) The leukocyte integrins. *J Biol Chem* 275(31), 23409-23412.

Hartwig JH, Thelen M, Rosen A, Janmey PA, Nairn AC, Aderem A. (1992) MARCKS is an actin filament crosslinking protein regulated by protein kinase C and calcium-calmodulin. *Nature* 356, 618-622

Haslett C. (1992) Resolution of acute inflammation and the role of apoptosis in the tissue fate of granulocytes. *Clin Sci* (Lond) 83(6), 639-48.

Haslett, C. (1997) Granulocyte apoptosis and inflammatory disease. *Br. Med. Bull.* 53,669–683.

Hata S, Sorimachi H, Nakagawa K, Maeda T, Abe K, Suzuki K. (2001) Domain II of m-calpain is a Ca($^{2+}$)-dependent cysteine protease. *FEBS Lett* 501(2-3), 111-114.

Hato T, Pampori N, Shattil SJ. (1998). Complementary roles for receptor clustering and conformational change in the adhesive and signaling functions of integrin alpha(IIb)beta(3). *J.Cell Biol* 14, 1685-1695.

He, L, Tao, J, Si F, Wu Y, Wu T, Prasath V and Wirtz D. (2017) Role of membrane-tension gated Ca^{2+} flux in cell mechanosensation. BioRxiv preprint Cold Spring Harbour Labs https://doi.org/10.1101/134395.

Heimstra PS, Annema A, Schippers EF, van Furth R. (1992) Pertussis toxin partially inhibits phagocytosis of immunoglobulin G-opsonised Staphylococcus aureus by human granulocytes but does not affect intracellular killing. *Infect Immun* 60, 202-205.

Hellberg K, Molony L, Zeng L andersson T. (1996). Ca^{2+} signalling mechanisms of the β2 integrin on neutrophils: involvement of phospholipase Cγ2 and Ins (1,4,5)P3. *Biochem J* 317, 403-409.

Hemmings L, Rees DJ, Ohanian V, Bolton SJ, Gilmore AP, Patel B, Priddle H, Trevithick JE, Hynes RO, Critchley DR. (1996) Talin contains three actin-binding sites each of which is adjacent to a vinculin-binding site. *J Cell Sci* 109, 2715-2726.

Hendey & Maxfield FR (1993). Regulation of neutrophil motility and adhesion by intracellular calcium transients. *Blood Cells* 19, 143-164.

Herant, M., Heinrich, V. & Dembo , M. (2006) Mechanics of neutrophil phagocytosis: experiments and quantitative models. *J Cell Sci* 119**,** 1903-13.

Herant, M., Heinrich, V. & Dembo, M. (2005) Mechanics of neutrophil phagocytosis: behaviour of the cortical tension. *J Cell Sci* 118, 1789-97.

Hillson, E. J. and M. B. Hallett (2007). "Localised and rapid Ca^{2+} micro-events in human neutrophils: conventional Ca^{2+} puffs and global waves without peripheral-restriction or wave cycling." *Cell Calcium* 41 (6), 525-36.

Hillson, E. J. and M. B. Hallett (2007). Localised and rapid Ca^{2+} micro-events in human neutrophils: conventional Ca^{2+} puffs and global waves without peripheral-restriction or wave cycling. *Cell Calcium* 41 (6), 525-36.

Hillson, E. J., S. Dewitt and M. B. Hallett (2006). "IP3-induced cell spreading of human neutrophils requires Ca2+ influx." *Molecular & Cellular Biology* 17.

Hillson, E. J., S. Dewitt and M. B. Hallett (2006). "IP3-induced cell spreading of human neutrophils requires Ca2+ influx." *Molecular & Cellular Biology* 17.

Hirsch E, Katanaev VL, Garlanda C, Azzolino O, Pirola L, Silengo L, Sozzani S, Mantovani A, Altruda F, Wymann MP. (2000) Central ole for G protein-coupled phosphoinosiide 3-kinase gamma in inflammation. *Science* 287(5455), 1049-1053.

Hirsch JG, Cohn ZA. (1960) Degranulation of polymorphonuclear leukocytes following phagocytosis of microorganisms. *J Exp Med* 112, 1005.

Hoffstein ST. (1979) Ultrastructural demonstration of calcium loss from local regions of the plasma membrane of surface-stimulated human granulocytes. *J Immunol* 123**,** 1395-402.

Hofmann MH, Bleckmann H. (1999) Effect of temperature and calcium on transneuronal diffusion of DiI in fixed brain preparations. *J Neurosci Methods* 88, 27–31.

Hogg JC. (1987) Neutrophil kinetics and lung injury. Physiological Reviews 67(4), 1249-1295.

Hogg N, Leitinger B. (2001) Shape and shift changes related to the function of leukocyte integrins LFA-1 and Mac-1. *J. Leukocyte Biol* 69, 893-898.

Holmes WE, Lee J, Kuang W-J, Rice GC, Wood WI. (1991) Structure and functional expression of a human interleukin-8 receptor. *Science* 253, 1278-1280.

Honig, MG, Hume RI. (1986) Fluorescent carbocyanine dyes allow living neurons of identified origin to be studied in long-term cultures. *J Cell Biol* 103, 171–87.

Hoppe A, Wertheim D, Jiang WG, Williams R, Harding K. (1999) An interactive image processing system for assessment of cell movement. Medical & Biological Engineering & Computing 37(4), 419-423.

Hosfield CM, Elce JS, Davies PL, Jia Z. (1999) Crystal structure of calpain reveals the structural basis for Ca($^{2+}$)-dependent protease activity and a novel mode of enzyme activation. *EMBO J* 18(24), 6880-6889.

Houk andrew R.; Jilkine, Alexandra; Mejean, Cecile O. (2012) Membrane Tension Maintains Cell Polarity by Confining Signals to the Leading Edge during Neutrophil Migration Cell 148, 175-188.

Hughes PE, Diaz-Gonzalez F, Leong L, Wu C, McDonald JA, Shattil SJ, Ginsberg MH. (1996) Breaking the integrin hinge. A defined structural constraint regulates integrin signaling. *J Biol Chem* 271, 6571-6574.

Humphries MJ. (2000) Integrin structure. *Biochem Soc Trans* 28(4), 311-339.

Hynes RO. (1992) Integrins: versatility, modulation and signaling in cell adhesion. *Cell* 69(1), 11-25.

I –K

Ikeda et al (2002) Attenuation of neutrophil-mediated myocardial ischemia-reperfusion injury by a calpain inhibitor Am *J Physiol Heart Circ Physiol* 282: H1421-H1426.

Indik Z, Kelly C, Chien P, Levinson AI, Schreiber AD. (1991) Human Fc gamma RII, in the absence of other Fc gamma receptors, mediates a phagocytic signal. *J Clin Invest* 88(5), 1766-1771.

Inomata M, Hayashi M, Ohno-Iwashita Y, Tsubuki S, Saido TC, Kawashima S. (1996) Involvement of calpain in integrin-mediated signal transduction. *Arch Biochem Biophys* 328, 129-134.

Isakoff SJ, Cardozo T andreev J, Li Z, Ferguson KM, Abagyan R, Lemmon MA, Aronheim A, Skolnik EY. (1998) Identification and analysis of PH domain-containing targets of phosphatidylinositol 3-kinase using a novel in vivo assay in yeast. *EMBO J* 17(18), 5374-5387.

Ivetic A, Deka J, Ridley A, AGER A. (2002) The cytoplasmic tail of L-selectin interacts with members of the Ezrin-Radixin-Moesin (ERM) family of proteins: cell activation-dependent binding of Moesin but not Ezrin. *J Biol Chem,* 277**,** 2321-9.

Iyer GYN, Islam MF, Quastel JH. (1961) Biochemical aspects of phagocytosis. *Nature* 192, 535.

Jaconi MEE, Lew DP, Carpentier JL, Magnusson KE, Sjogren KE, Stendahl O. (1990) Cytosolic free calcium elevation mediates phagosome-lysosome fusion during phagocytosis in human neutrophils. *J Cell Biol* 110, 1555-1564.

Jaconi MEE, Theler JM, Schlegel W, Appel RD, Wright SD, Lew PD. (1991). Multiple elevations of cytosolic free Ca^{2+} in human neutrophils: initiation by adherence to receptors of the integrin family. *J Cell Biol* 112, 1249-1257.

Janeway C. (2005) Immunobiology : the immune system in health and disease (pp. 55-75). Garland Science, New York.

Jilkine A, Edelstein-Keshet L. (2011). A comparison of mathematical models for polarization of single eukaryotic cells in response to guided cues.*PLoS Comput. Biol*. 7, e1001121.

Kamada S, Kikkawa U, Tsujimoto Y, Hunter T. (2005) Nuclear translocation of caspase-3 is dependent on its proteolytic activation and recognition of a substrate-like protein(s). *J Biol Chem* 280, 857-860.

Kamakura K, Ishura S, Sugita H, Toyokura Y. (1983) Identification of Ca^{2+} activated neutral protease in the peripheral nerve and its effects on neurofilament degradation. *J Neurochem* 40, 908-913.

Kanai F, Liu H, Field SJ, Akbary H, MatsuT, BrownGE, Cantley LC Yaffe MB. (2001) The PX domains of p47phox and p40phox bind to lipids products of PI(3)kinase. *Nature Cell Biol* 3, 675-678.

Kanno S, Furuyama A, Hirano S. (2007) A murine scavenger receptor MARCO recognizes polystyrene nanoparticles. *Toxicol Sci* 97, 398-406.

Kanno, S., A. Furuyama and S. Hirano. (2007) A murine scavenger receptor MARCO recognizes polystyrene nanoparticles. *Toxicol Sci* 97, 398-406.

Kanwar VS, Cairo MS. (1993) Neonatal neutrophil maturation, kinetics and function. In The natural immune system: The neutrophil, Abramson JS, Wheeler JG, Oxford University Press, 1993 New York, USA. Pg2-21.

Kaplan M. (2013) role of neutrophils in systemic autoimmune diseases. *Arthritis research & therapy* 15, 219.

Kazilek CJ, Merkle CJ, Chandler DE.(1988) Hyperosmotic inhibition of calcium signals and exocytosis in rabbit neutrophils. *Am. J. Physiol* 254, C709-718.

Keller HU, Fedier A, Rohner R (1996) Relationship between light scattering in flow cytometry and changes in sh[pae, volume and actin polymerization in human polymorphonuclear leukocytes ***J. Leukocyte Biol*** 58 : 519-525.

Kernan P, Wymann, MP, Vontscharner V, Deanleau DA, Tai PC, Spry CJ, Dahinden CA, Baggiolini M. (1991) Shape changes, exocytosis and cytsosolic free calcium changes in stimulated eosinophils. ***J Clin Invest*** 87, 2012-2017.

Kimberly RP, Ahlstrom JW, Click ME, Edberg JC. (1990) The glycosyl phosphatidylinositol-linked FcγRIII$_{PMN}$ mediates transmembrane signalling events distinct from FcγRII. *J Exp Med* 171, 1239-1255.

King JS, Insall RH.(2009) Chemotaxis: finding the way forward with Dictyostelium.
Trends Cell Biol 19, 523–530.

Klaus D. Elgert.(2009) Immunology: Understanding The Immune System. *Wiley Blackwell*, US.Second Edition.

Klebanoff SJ, Vadas MA, Harlam JM, Sparks LH, Gamble JR, Agosti JM, Waldersdorph AM. (1986) Stimulation of neutrophils by tumour necrosis factor. *J Immunol* 136, 4220-4225.

Knecht DA, Loomis WF. (1987) Antisence RNA inactivation of myosin heavy chain gene expression in Dictyostelium discoideum. *Science* 236, 1081-1086.

Kobayashi K, Takahashi K, Nagasawa S. (1995) The role of tyrosine phosphorylation and Ca^{2+} accumulation in Fcγ-receptor-mediated phagocytosis of human neutrophils. *J Biochem* 117, 1156-1161.

Kobayashi, S. et al.(2005) Neutrophils in the innate immune response *Arch Immunol* Ther Exp. 53, 505–517.

Kobbert, C. Apps R, Bechmann I, Lanciego JL, Mey J, Thanos S. (2000) Currewnt concepts of neuroanatomical racing. *Progress in Nuerobiology* 62 (4), 327-351.

Kolaczkowska E, Kubes P (2013). Neutrophil recruitment and function in health and inflammation. *Nat Rev Immunol.* 13,159-75.

Kolanus W, Nagel W, Schiller B, Zeitlmann L, Godar S, Stockinger H, Seed B. (1996) Alpha L beta 2 integrin/LFA-1 binding to ICAM-1 induced by cytohesin-1, a cytoplasmic regulatory molecule. *Cell* 86, 233-242.

Krause KH, Schlegel W, Wollheim CB andersson T, Waldvogel FA., Lew PD. (1985). Chemotactic Peptide Activation of Human Neutrophils and HL-60 Cells. *J Clin Invest* 76, 1348-1354.

Kruskal BA, Maxfield FR. (1987). Cytosolic free calcium increases before and oscillates during frustrated phagocytosis in macrophages*. J Cell Biol* 105, 2684-2693.

Kruskal BA, Shak S, Maxfield FR. (1986). Spreading of neutrophils is immediately preceded by a large increase in cytosolic free calcium*. Proc Natl Acad Sci* USA 83, 2919-2923.

Kucik DF, Dustin ML, Miller JM, Brown EJ. (1996) Adhesion-activating phorbol ester increases the mobility of leukocyte integrin LFA-1 in cultured lymphocytes. *J Clin Invest* 97, 2139-2144.

Kuijpers TW, Van Lier RA, Hamann D, de Boer M, Thung LY, Weening RS, Verhoeven AJ, Roos D. (1997) Leukocyte adhesion deficiency type I (LAD-1)/variant. A novel immunodeficiency syndrome characterised by dysfunctional beta2 integrins. *J Clin Invest* 100, 1725-1733.

L

Lad PM, Olson CV, Grewal IS. (1986) A step sensitive to pertussis toxin and phorbol ester in human neutrophils regulates chemotaxis and capping but not phagocytosis. *FEBS Lett* 200(1), 91-96.

Laffafian I, Hallett MB. (1995) Does cytosolic free Ca^{2+} signal neutrophil chemotaxis? *J Cell Sci* 108, 3199- 3205.

Laffafian I, Hallett MB. (1998) Lipid-assisted microinjection: introducing material into the cytosol and membranes of small cells. *Biophys J* 75, 2558-2563.

Lanciego JL, Wouterlood FG. (2011) Ahalfcenturyofexperi- mental neuroanatomicaltracing. *J. Chem.Neuroanat* 42, 157–183.

Laffian I, Hallett MB. (1995) Does cytosolic free $Ca2^{+}$ signal neutrophil chemotaxis in response to formylated chemotactic peptide. *Cell Sci* 108, 3199-3205.

Laudanna C, Campbell JJ, Butcher EC. (1996) Role of Rho in chemoattractant-activated leukocyte adhesion through integrins. *Science* 271, 981-983.

Laudanna C, Campbell JJ, Butcher EC. (1997) Elevation of intracellular cAMP inhibits RhoA activation and integrin-dependent leukocyte adhesion induced by chemoattractants. *J Biol Chem* 272, 24141-24144.

Lawrence MB, Springer TA. (1991) Leukocytes roll on a selectin at physiological flow rates: distinction from and prerequisite for adhesion through integrins. *Cell* 65, 859-873.

Lawson MA, Maxfield FR. (1995). Ca^{2+} - and calreticulin-dependent recycling of an integrin to the front of migrating neutrophils. *Nature* 377, 75-79.

Leak, L.V. and J.F. Burke.(1974) "Early events of tissue injury and the role of the lymphatic system in early inflammation, in: B.W. Zweifach, L. Grant, R.T. McCluskey (Eds.), The Inflammatory Process, Academic Press, New York/London.

Leblanc V, Tocque B, Delumeau I. (1998) Ras-GAP controls Rho-mediated cytoskeletal reorganization through its SH3 domain. *Mol Cell Biol* 18(9), 5567-5578.

Lee JO, Rieu P, Arnaout MA, Liddington R. (1995) Crystal structure of the A domain from the alpha subunit of integrin CR3 (CD11b/CD18). *Cell* 80, 631-638.

Lee, W. L., Harrison R. E. and Grinstein S. (2003). Phagocytosis by neutrophils. *Microbes & Infection* 5(14), 1299-306.

Lehrer RI, Ganz T. (1990) Antimicrobial polypeptides of human neutrophils. *Blood* 76, 2169.

Leitinger B, McDowall A, Stanley P, Hogg N. (2000) The regulation of integrin function by Ca^{2+}. *Biochim Biophys Acta* 1498, 91-98.

Lew DP andersson T, Hed J, Di Virgilio F, Pozzan T, Stendahl O. (1985). Ca^{2+} dependent and Ca^{2+} independent phagocytosis in human neutrophils. *Nature* 315, 509-511.

Lew DP, Monad A, Waldvogel FA, Dewald B, Baggiolin M, Pozzan T. (1986) Quantitative analysis of the cytosolic free Ca^{2+} dependency of exocytosis from three subcellular compartments in intact human neutrophils. *J Cell Biol* 102, 2197-2204.

Lew PD, Wollheim CB, Waldvogel FA, Pozzan T. (1984) Modulation of cytosolic-free calcium transients by changes in intracellular calcium-buffering capacity: correlation with exocytosis and O2-production in human neutrophils. *J Cell Biol* 99, 1212-1220.

Lewis, Bain & Bates (2006) Dacie and Lewis Practical Haematology, Churchill Livingstone *Elsevier*.

Li R, Rieu P, Griffith DL, Scott D, Arnaout MA. (1998). Two functional states of the CD11b A-domain: Correlations with key features of two Mn^{2+}-complexed crystal structures. *J. Cell Biol* 143, 1523-1534.

Li Z, Jiang H, Xie W, Zhang Z, Smrcka AV, Wu D. (2000) Roles of PLC-β2 and - β3 and PI3Kγ in chemoattractant mediated signal transduction. *Science* 287, 1046-1049.

Lin G, Chattopadhay D, Maki M, Wang KKW, Carson M, Jin L, Yuen P, Takano, Hatanaka M, DeLucas LJ, Narayana SVL. (1997) Crystal structure of calcium bound domain VI of calpain at 1.9Å resolution and its role in enzyme assembly, regulation and inhibitor binding. *Nature Struct Biol* 4, 539-547.

Lo DC, McAllister AK, Katz LC. (1994) Neuronal transfection in brain slices using particle-mediated gene transfer. *Neuron* 13, 1263–1268.

Loftus JC, Liddington RC. (1997) Cell adhesion in vascular biology. New insights into integrin-ligand interaction. *J Clin Invest* 99(10):2302-2306.

Lorant DE, Patel KD, McIntyre TM, McEver RP, Prescott SM, Zymmerman GA. (1991) Coexpression of GMP-140 and PAF by endothelial stimulated by histamine or thrombin: a juxtacrine system for adhesion and activation of neutrophils. *J Cell Biol* 115, 223-234.

Lowry MB, Duchemin AM, Coggeshall KM, Robinson JM anderson CL. (1998b) Chimeric receptors composed of phosphoinositide 3-kinase domains mediate phagocytosis in COS fibroblasts. *J Biol Chem* 273(38), 24513-24520.

Lowry MB, Duchemin AM, Robinson JM anderson CL. (1998) Functional separation of pseudopod extension and particle internalisation during Fc gamma receptor-mediated phagocytosis. *J Exp Med* 187(2), 161-176.

Lu CF, Oxvig C, Springer TA. (1998) The structure of the beta-propeller domain and C-terminal region of the integrin alphaM subunit. Dependence on beta subunit association and prediction of domains. *J Biol Chem* 273, 15138-15147.

Lu CF, Springer TA. (1997). The alpha subunit cytoplasmic domain regulates the assembly and adhesiveness of integrin lymphocyte function-associated antigen-1. *J Immunol* 159, 268-278.

Lub M, van Kooyk Y, van Vliet S, Figdor C. (1997) Dual role of the actin cytoskeleton in regulating cell adhesion mediated by the integrin Lymphocyte Function-associated Molecule-1. *Mol Biol Cell* 8, 341-351.

Lundqvist-Gustafsson H, Gustafsson M Dahlgren C. (2000) Dynamic Ca^{2+} changes in neutrophil phagosomes - A source for intracellular Ca^{2+} during phagolysosome formation? *Cell Calcium* 27, 353-362.

Lupher ML Jr, Harris EA, Beals CR, Sui LM, Liddington RC, Staunton DE. (2001) Cellular activation of leukocyte function-associated antigen-1 and its affinity are regulated at the I domain allosteric site. *J Immunol* 167(3), 1431-1439.

M

Ma AD, Metzian A, Bagrodia S, Taylor S, Abrams CS. (1998) Cytoskeletal reorganisation by G protein-coupled receptors is dependent on phosphoinositide 3-kinaseg, a Rac guanosine exchange factor and Rac. *Mol Cell Biol* 18, 4744-4751.

Macintyre EA, Roberts PJ, Abdul-Gaffer R, O'Flynn K, Pilkington GR, Farace F, Morgrn J, Linch DC. (1988) Mechanism of human monocyte activaton via the 40-kDa Fc receptor for IgG. *J Immunol* 141, 4333-4343.

Macramé E. K., Pryzwansky K. E., Cooney M. H. and Spitznagel J. K. (1980) Scanning electron microscopic observations of early stages of phagocytosis of E. coli by human neutrophils.*Cell & Tissue Research* 209(1),65-70.

Maher J, Martell JV, Brantley BA, Cox EB, Niedel JE, Rosse WF. (1984) the response of human-neutrophils to a chemotactic tripeptide (n-formyl-methionyl-leucyl-phenylalanine) studied by microcinematography. *Blood* 64 (1), 221-228.

Majeed M , Caveggion E, Lowell CA, Berton G. (2001) Role of Src kinases and Syk in Fcgamma receptor-mediated phagocytosis and phagosome lysosome fusion. *J Leukoc Biol* 70, 801-811.

Majeed, M., E. Caveggion, C.A. Lowell and G. Berton. (2001) "Role of Src kinases and Syk in Fcgamma receptor-mediated phagocytosis and phagosome lysosome fusion" *J Leukoc Biol* 70, 801-811.

Mandeville JTH, Ghosh RN, Maxfield FR. (1995) Intracellular calcium levels correlate with speed and persistent forward motion in migrating neutrophils. *Biophys J* 68(4), 1207-1217.

Mandeville JTH, Maxfield FR. (1997) Effects of buffering intracellular free calcium on neutrophil migration through three-dimensional matrices. *J Cell Physiol* 171(2), 168-178.

Manish MI ,Mohammad RI, Siddiqui, Khiem TR ,Sekhar RE and Asrar MA. (2014) Reactive Oxygen Species in Inflammation and Tissue Injury Antioxid. *Redox Signal*. 20, 1126–1167

Marks PW, Maxfield FR. (1990a). Transient increases in cytosolic free calcium appear to be required for the migration of adherent human neutrophils. *J Cell Biol* 110, 43-52.

Marks PW, Maxfield FR. (1990b). Local and global changes in cytosolic free calcium in neutrophils during chemotaxis and phagocytosis. *Cell Calcium* 11, 181-190.

Marshall JG, Booth JW, Stambolic V, Mak T, Balla T, Schreiber AD, Meyer T, Grinstein S. (2001) Restricted accumulation of phoshatidylinositol 3-kinase products in a plasmalemmal subdomain during Fc gamma receptor-mediated phagocytosis. *J Cell Biol* 153(7), 1369-1380.
Marzocco et al (2004). Calpain inhibitor I reduces ischemia-reperfusion injury in the rat. *Shock* 21, 38-44.

Masters TA, Pontes B, Viasnoff V, Li Y and Gauthier NC (2013) Plasma membrane tension orchestrates membrane trafficking, cytoskeletal remodeling and biochemical signaling during phagocytosis. *Proc Natl Acad Sci (USA)* 110, 11875–11880.

Matsushita M, Fujita T. (1992) Activation of the classical complement pathway by mannose-binding protein in association with a novel C1s-like serine protease. *J Exp Med* 176, 1497-1502.

May RC Machesky LM (2001) Phagocytosis and the actin cytoskeleton. *J. Cell Sci* 114, 1061-1077.

McDowall A, Leitinger B, Stanley P, Bates PA, Randi AM, Hogg N. (1998) The I domain of integrin leukocyte function associated antigen-1 is involved in a conformational change leading to high affinity binding to ligand intercellular adhesion molecule-1 (ICAM-1). *J Biol Chem* 273, 27396-27403.

McEver RP, Cummings RD. (1997) Perspectives series: cell adhesion in vascular biology: Role of PSGL-1 binding to selectins in leukocyte recruitment. *J Clin Invest* 100, 485-491.

McEver RP. (1991) Selectins: novel receptors that mediate leukocyte adhesion during inflammation. *Throm Haemostas* 65, 223-228.

McPhail LC, Harvath L. (1993) Signal transduction in neutrophil oxidative metabolism and chemotaxis. In The natural immune system: The neutrophil. Ed. Abramson JS, Wheeler JG, Oxford University Press, 1993 New York, USA. Pg 63-107.

Metchnikoff (1905) *Immunity in Infectious Disease*, Cambridge University: London.

Metchnikoff E. (1893) Lecon sur la pathologie comparee de inflammation. *Ann l'Institute Pasteur* 7, 348-357.

Metchnikoff E. (1901) Lectures on the comparative physiology of inflammation. Kegan Paul: London.

Metchnikoff E. (1905) Immunity in Infective Diseases. Cambridge University: London.

Metzner B, Heger M, Hofmann C, Czech W, Norgauer J. (1997) Evidence for the involvement of phosphatidylinositol 4,5-bisphosphate 3-kinase in CD18-mediated adhesion of human neutrophils to fibrinogen. *Biochem Biophys Res Commun* 232(3), 719-723.

Meyer R.A. (1979) Light scattering from biological cells: dependence of backscatter radiation on membrane thickness and refractive index. *Appl. Opt*. 18, 585–588.

Michael W. Davidson and The Florida State University. (2015) Molecular expressions exploring the world of optics and microscopy [online] available at http://micro.magnet.fsu.edu/index.htmlb. [Accessed on 19 February 2016].

Michelle CM, Fox E. (2007) Anterograde Tracing Method using DiI to Label Vagal Innervation of the Embryonic and Early Postnatal Mouse Gastrointestinal Tract. *J Neurosci Methods* 163(2), 213–225.

Michetti M, Salamino F, Minafra R, Melloni E, Pontremoli S.(1997) Calcium-binding properties of human erythrocyte calpain. *Biochem J* 325, 721-726.

Michishita M, Videm V, Arnaout MA. (1993) A novel divalent cation binding site in the A domain of the beta 2 integrin CR3 (CD11b/CD18) is essential for ligand binding. *Cell* 72, 857-867.

Mie G. (1908) Contributions to the optics of turbid media particularly of colloidal metal solutions. *Ann.Phys*. 330, 377–445 (Englishtranslation http://diogenes.iwt.uni-bremen.de/vt/laser/papers/RAE-LT1873-1976-Mie-1908-translation.pdf).

Millan J, Hewlett L., Glyn M, Toomre D., Clark P, Ridley AJ. (2006) Lymphocyte transcellular migration occurs through recruitment of endothelial ICAM-1 to caveola- and F-actin-rich domains. *Nat Cell Biol* 8**,** 113-23.

Miller LS, O'Connell RM, Gutierrez MA, et al (2006) MyD88 mediates neutrophil recruitment initiated by IL-1R but not TLR2 activation in immunity against *Staphylococcus aureus* . *Immunity* 24, 79–91.

Minsky M. (1988) Memoir on Inventing the Confocal Scanning Microscopy, *Scanning* 10: 128-138.

Mogilner A and Oster G. (1996) Cell motility driven by actin polymerization. *Biophys. J* 71, 3030-3045.

Mogilner A and Oster G. (2003) Force generation by actin polymerization II: the elastic ratchet and tethered filaments. *Biophys. J* 84, 1591-1605.

Mogilner A, Oster G. (1996) Cell motility driven by actin polymerization. *Biophys J* 71, 3030-3045.

Mogilner A, Oster G. (2003) Force generation by actin polymerization II: the elastic ratchet and tethered filaments. *Biophys. J* 84, 1591-1605.

Molinari M, Carafoli E. (1997) Calpain: A Cytosolic Proteinase Active at the Membranes. *Journal of Membrane Biology* 156(1), pp. 1-8.

Moldoveanu T, Hosfield CM, Lim D, Elce JS, Jia Z, Davies PL. (2002) A $Ca(^{2+})$ switch aligns the active site of calpain. *Cell* 108(5), 649-660.

Molinari M, Anagli J, Carafoli E. (1995) Purification of μ-calpain by a novel affinity chromatography approach. *J Biol Chem* 270, 2032-2035.

Morgan BP, van der Berg CW, Davies EV, Hallett MB, Horejsi V. (1993) Cross-linking of CD59 and of other glycosyl phosphatidylinositol-anchored molecules on neutrophils triggers cell activation via tyrosine kinase. *Eur J Immunol* 23(11), 2841-50.

Morgan BP. (1990) Complement. Clinical aspects and relevance to disease. Academic Press Ltd, London.

Mukherjee S , Ghosh RN, Maxfield FR. (1997) Endocytosis. *Physiol Rev* 77, 759-803.

Müller-Taubenberger A, Lupas AN, Li H, Ecke M, Simmeth E, Gerisch G. (2001) Calreticulin and calnexin in the endoplasmic reticulum are important for phagocytosis. *EMBO J* 20, 6772-6782.

Murata T, Sullivan JA, Sawyer DW Mandell GL. (1987) Influence of type and opsonization of ingested particle on intracellular free calcium distributuon and superoxide production by human neutrophils. *Infection Immun* 55, 1784,1791.

MyonesBL, Dalzell JG, Hogg N, Ross GD. (1988) Neutrophils and monocyte cell surface p150,95 has iC3b-receptor (CR4) activity resembling CR3. *J Clin Invest* 82, 640-51.

N

Nagarajan S, Chesla S, Cobern L anderson P, Zhu C, Selvaraj P. (1995) Ligand binding and phagocytosis by CD16 (Fc gamma receptor III) isoforms. Phagocytic signaling by associated zeta and gamma subunits in Chinese hamster ovary cells. *J Biol Chem* 270, 25762–25770.

Naji A, Brown F. (2007) Diffusion on Ruffled Membrane Surfaces*. J. Chem. Phys* 126, 1-18.

Nakada MT, Amin K, Christofidou-Solomidou M, O'brien CD, Sun J, Gurubhagavatula I, Heavner GA, Taylor AH, Paddock C, Sun QH, Zehnder JL, Newman PJ, Albelda SM, Delisser HM. (2000) Antibodies against the first Ig-like domain of human platelet endothelial cell adhesion molecule-1 (PECAM-1) that inhibit PECAM-1-dependent homophilic adhesion block in vivo neutrophil recruitment. *J Immunol,* 164**,** 452-62.

Nakagawa K, Masumoto H, Sorimachi H, Suzuki K. (2001) Dissociation of m-calpain subunits occurs after autolysis of the N-terminus of the catalytic subunit and is not required for activation. *J Biochem* 130(5), 605-611

Nathan CF. (1987) Neutrophil activation on biological surfaces. Massive secretion of hydrogen peroxide in response to products of macrophages and lymphocytes *J Clin Invest* 80, 1550-1560.

Ng-Sikorski J andersson R, Patarroyo M andersson T. (1991) Calcium signalling capacity of the CD11b/CD18 integrin on human neutrophils. Exptl. *Cell Res* 195, 504-508.

Ninomiya N, Hazeki K, Fukui Y, Seya T, Okada T, Hazeki O, Ui M. (1994) Involvement of phosphatidyl inositol 3-kinase in Fcγ receptor signalling. *J Biol Chem* 269, 22732-22737.

Noble et al. (1998) Neutrophil transendothelial migration is regulated by the calcium dependent protease calpain. *Blood* 92, 2198 Suppl. 1

Nüsse O, Serrander L, Lew DP Krause K-H. (1998) Ca^{2+}-induced exocytosis in individual human neutrophils: high and low-affinity granule populations and submaximal responses. *EMBO J* 17, 1279-1288.

O

O'Brien JA, Lummis R. (2006) Diolistic labelling of neuronal cultures and intact tissue using a hand-heldgenegun. *Nat.Protoc* 1, 1517–1521.

O'Toole TE, Ylanne J, Culley BM. (1995) Regulation of integrin affinity states through an NPXY motif in the beta subunit cytoplasmic domain. J Biol Chem 270, 8553-8558.

Odin JA, Edberg JC, Painter CJ, Kimberly RP, Unkeless JC. (1991) Regulation of phagocytosis and $[Ca^{2+}]i$ flux by distinct regions of an Fc receptor. *Science* 254, 1785-1788.

Okuda K, Sanghera JS, Pelech SL, Kanakura Y, Hallek M, Griffin JD, Druker BJ. (1992) Granulocyte-macrophage colony-stimulating factor, interleukin-3 and steel factorm induce rapid tyrosine phosphorylation of p42 and p44 MAP kinase. *Blood* 79, 2880-2887.

Onji T, Takagi M, Shibata N. (1987) Calpain abolishes the effect of filamin on the actomyosin system in platelets. *Biochim Biophys Acta* 912(2), 283-286.

Oxvig C, Lu C, Springer TA. (1999) Conformational changes in tertiary structure near the ligand binding site of an integrin I domain. *Proc Natl Acad Sci USA* 96, 2215-2220.

Oxvig C, Springer TA. (1998) Experimental support for a beta-propeller domain in integrin alpha-subunits and a calcium binding site on its lower surface. *Proc Natl Acad Sci USA* 95, 4870-4875.

P

Palecanda A, Paulauskis J, Al-Mutairi E, Imrich A, Qin G, Suzuki H, Kodama T Palecanda, A., J. Paulauskis, E. Al-Mutairi, A. Imrich, G. Qin, H. Suzuki, T. Kodama, K. Tryggvason, H. Koziel and L. Kobzik. (1999) Role of the scavenger receptor MARCO in alveolar macrophage binding of unopsonized environmental particles. *J Exp Med* 189,1497-1506.

Palmeri D, Vanzante A, Huang CC, Hemmerich S, Rosen SD. (2000) Vascular endothelial junction-associated molecule, a novel member of the immunoglobulin superfamily, is localized to intercellular boundaries of endothelial cells. *J Biol Chem* 275**,** 19139-45.

Parekh AB, Terlau H, Stuhmer W. (1993) Depletion of InsP3 stores activates a Ca^{2+} and K^{+} current by means of a phosphatase and a diffusible messenger. *Nature* 364(6440), 814-818.

Parent CA, Blacklock BJ, Froehlich WM, Murphy DB, Devreotes PN. (1998) G protein signalling are activated at the leading edge of chemotactic cells. *Cell* 95, 81-91.

Partida-Sanchez S, Cocayne DA, Monad S, Jacobson EL, Oppenheimer N, Garvy B, Kusser K, Goodrich S, Howard M, Harsmen A, Russell TD, Lund F. (2001) Cyclic ADP-ribose production by CD38 regulates intracellular calcium release, extracellular calcium influx and chemotaxis in neutrophils and is required for bacterial clearance *in vivo*. *Nature Med* 7, 1209-1216.

Pavalko FM, LaRoche SM. (1993) Activation of human neutrophils induces an interaction between the integrin beta 2-subunit (CD18) and the actin binding protein alpha-actinin. *J Immunol* 151(7), 3795-807.

Pavalko FM, Walker DM, Graham L, Goheen M, Doerschuk CM, Kansas GS. (1995) The cytoplasmic domain of L-selectin interacts with cytoskeletal proteins via alpha-actinin: receptor positioning in microvilli does not require interaction with alpha-actinin. *J Cell Biol* 129**,** 1155-64.

Pawley JB. (1995) (ed.), Handbook of Biological Confocal Microscopy, New York: *Plenum Press*.

Pearson AM. (1996) Scavenger receptors in innate immunity. *Curr Opin Immunol* 8, 20-28.
Petersen M, Williams JD, Hallett MB. (1993) Cross-linking of CD11b or CD18 signals release of localised Ca^{2+} from intracellular stores in neutrophils. Immunology 80, 157-159.

Pettit EJ, Davies EV, Hallett MB. (1997) The microanatomy of calcium stores in human neutrophils: Relationship of structure to function. *Histol Histopathol* 12, 479-490.

Pettit EJ, Hallett MB. (1995) Early Ca^{2+} signalling event in neutrophils, detected by confocal laser scanning. *Biochem J* 310, 445-448.

Pettit EJ, Hallett MB. (1996) Temporal and spatial resolution of Ca^{2+} release and influx in human neutrophils using a novel confocal laser scanning mode. *Biochem and Biophys Res Commun* 229, 109-113.

Pettit EJ, Hallett MB. (1996) Localised and global cytosolic Ca^{2+} changes in neutrophils during engagement of CD11b/CD18 integrin visualised using confocal laser scanning reconstruction. *J of Cell Sci* 109, 1689-1694.

Pettit EJ, Hallett MB. (1998b) Two distinct Ca^{2+} storage and release sites in human neutrophils. *J Leuk Biol* 63, 225-232.

Pettit EJ, Hallett MB. (1998) Release of 'caged' cytosolic Ca^{2+} triggers rapid spreading of human neutrophils adherent via integrin engagement. *J Cell Sci* 111, 2209-2215.

Pettit, E. J. and Hallett M. B. (1997).Pulsatile Ca2+ influx in human neutrophils undergoing CD11b/CD18 integrin engagement. *Biochemical & Biophysical Research Communications* 230 , 258-61.

Pettit, E. J. and Hallett M. B. (1998) "Release of 'caged' cytosolic Ca2+ triggers rapid spreading of human neutrophils adherent via integrin engagement." *Journal of Cell Science* 111, 2209-15.

Petty HR, Hafemann, McConnell (1981) Disappearance of macrophage surface folds after antibody-dependent phagocytosis. *J Cell Biol* 89: 223-229.

Pillemer L, Ecker E. (1941) anticomplementary factor in fresh yeast. *J. Biol. Chem* 137, 139-142.

Polakis PG, Evans T, Snyderman R. (1989) Multiple chromatographic forms of the formyl peptide chemoattractant receptor and their relationship to GTP-binding proteins. *Biochem Biophys Res Commun* 161, 276-283.

Pollard TD and Borisy G. (2003) Cellular motility driven by assembly and disassembly of actin filaments. *Cell* 112 (4): 453-465.

Prahl S. (2007). Mie Scattering calculator. http://omlc.ogi.edu/calc/mie_calc.html.
Prithu, S, Gutierrez, E, Pospieszalska, MK. (2010) Quantitative dynamic footprinting microscopy reveals mechanisms of neutrophil rolling. *NATURE METHODS* 7, 821-U73.

Pryzwansky KB, Rausch PG, Spitznagel JK, Herion JC.(1979) Immunocytochemical distinction between primary and secondary granule formation in developing human neutrophils: correlations with Romanowsky stains. *Blood* 53, 179-185.

Pryzwansky KB, MacRae EK, Spritznagel JK, Cooney MH. (1979) Early degranulation of human neutrophils: immunochemical studies of surface and intracellular phagocytic events. *Cell* 18, 1025-1033.

Pryzwansy KB, Martin LE, Spitznagel JK. (1978) Immunocytochemical localization ofmyeloperoxidase, lactoferrin, lysozyme and neutral proteases in human monocytes and neutrophilic granulocytes*. J. Reticuloendothel. Soc* 24, 295- 310.

Pucadyil, TJ and Chattopadhyay A. (2006) Effect of cholesterol on lateral diffusion of fluorescent lipid probes in native hippocampal membranes. *Chemistry and Physics of Lipids* 143, 11–21.

Putney JW, Broad LM, Braun F-J, Lievremont J-P, Bird GJ. (2001) Mechanisms of capacitative calcium entry. *J Cell Sci* 114, 2223-2229.

Putney JW. (1999) "Kissin' cousins": intimate plasma membrane-ER interactions underlie capacitative calcium entry. *Cell* 99, 5-8.

Putney JW. (2001) Cell biology: Channelling calcium. *Nature* 410, 648-649.

R

Rabinovitch M. (1995) Professional and non-professional phagocytes: an introduction.*Trends Cell Biol* 5, 85-87.

Randriamampita C, Tsein RY. (1993) Emptying of intracellular Ca^{2+} stores releases a novel small messenger that stimulates Ca^{2+} influx. Nature 364(6440), 809-814.

Raucher D. and Sheetz MP. (2000) Cell Spreading and Lamellipodial Extension Rate Is Regulated by Membrane Tension. *J Cell Biol* 148, 127-136

Ravetch JV, Bolland S. (2001) IgG Fc receptors. *Annu Rev Immunol* 19, 275-290.

Ravetch, J.V. and S. Bolland. (2001) "IgG Fc receptors" Annu Rev Immunol.

Rechsteiner M, Rogers SW. (1996) PEST sequences and regulation by proteolysis. *Trends Biochem Sci* 21, 267-271.

Reeves EP, Dekker LV, Forbes LV, Wientjes FB, Grogan A, Pappin DJC Segal AW. (1999) Direct interaction between p47(phox) and protein kinase C: evidence for targeting of protein kinase C by p47(phox) in neutrophils. *Biochem J* 344, 859-866.

Reeves EP, Lu H, Jacobs HL, Messina CGM, Bolsover S, Gabella G, Potma EO, Warley A, Roes J, Segal AW. (2002) Killing activity of neutrophils is mediated through activation of proteases by K^+ flux. *Nature* 416, 291-297.

Reits E, Neefjes J. (2001) From fixed to FRAP: measuring protein mobility and activity in living cells. *Nature Cell Biology* 3, 154-157.

Revathi A , Allen E. (2007) The Forces Behind Cell Movement.*Int. J. Biol. Sci* 3, 303-317.
Reverter D, Strobl S, Fernadez-Catalan C, Sorimachi H, Suzuki K, Bode W. (2001) Structural basis for possible calcium-induced activation mechanisms of calpains. *Biol Chem* 382(5), 753-766.

Rizo J, Sudhof TC. (1998) C2-domains, structure and function of a universal Ca^{2+}-binding domain. *J Biol Chem* 273(26), 15879-15882.

Rizzuto R, Bastianutto C, Brini M, Murgia M, Pozzan T.(1994) Mitochondrial Ca^{2+} homeostasis in intact cells. *J Cell Biol* 126, 1183-1194.

Rizzuto R, Brini M, Murgia M, Pozzan T. (1993) Microdomains with high Ca^{2+} concentration that are sensed by neighbouring mitochondria. Science 262, 744-747.

Rizzuto R, Pinton P, Carrington W, Fay FS, Fogarty KE, Lifshiz LS, Tuft RA, Pozzan T. (1998) Close contacts with the endoplasmic reticulum as determinants of mitochondrial Ca^{2+} responses. *Science* 280, 1763-1766.

Rizzuto R, Simpson AWM, Brini M, Pozzan T.(1992) Rapid changes of mitochondrial Ca^{2+} revealed by specifically targeted recombinant aequorin. *Nature* 358, 325-328.
Robert DP, Misteli T. (2001) Kinetic modelling approaches to in vivo imaging. *Nature Reviews Molecular Cell Biology* 2, 898–907.

Roberts GM, Davies EV, Pettit EJ, Hallett MB. (1997) The timing and magnitude of Ca2+ signaling by CD32 depends on its redistribution on the cell surface. *Exp Cell Res,* 230**,** 303-9.

Rogers S, Wells R, Rechsteiner M. (1986) Amino acid sequences common to rapidly degraded proteins: The PEST hypothesis. *Science* 234, 364-368.

Rohm & Haas (2006) Sodium Deoxycholate*.Pierce Biotechnology* 1-2.

Roos D, Bot A, Schaik M, Boer M, Daha M. (1981) Interaction between human neutrophils and zymosan particles: the role of opsonins and divalent cations. *Journal of Immunology* 126(2), 433-40.

Rosales C, Jones SL, McCourt D, Brown EJ. (1994) Bromophenacyl bromide binding to the actin-bundling protein l-plastin inhibits inositol trisphosphate-independent increase in Ca^{2+} in human neutrophils. Proc Natl Acad Sci USA 91(9), 3534-3538.

Roth, J. (1993) Evaluation of the Influence of Potentia Toxins on Neutrophil Function. *Toxicol Pathol* 21, 141-146.

Rotnes JS, Iversen JG. (1992) Thapsigargin reveals evidence for fMLP-insensitive calcium pools in human leukocytes. *Cell Calcium* 13, 487-500.

Ruban, G.I, Kosmacheva, SM, Goncharova, NV, Van Bockstaele VA, Loiko VA. (2007) Investigation of morphometric parameters for granulocytes and lymphocytes as applied to a solution of direct and inverse light-scattering problems. *J. Biomed. Opt* 12, 044017.

Rutter GA, Theler JM, Murgia M, Wollheim CB, Pozzan T, Rizzuto R. (1993) Stimulated Ca^{2+} influx raises mitochondrial free Ca^{2+} to supramicromolar levels in a pancreatic β-cell line. *J Biol Chem* 268, 22385-22390.

S

Sage SO, Pintado E, Mahaut-Smith MP, Merritt JE. (1990) Rapid kinetics of agonist-evoked changes in cytosolic free Ca^{2+} concentration in fura-2-loaded human neutrophils. *Biochem J* 265, 915-8.

Salmon JE, Browle NL, Edberg JC, Kimberly RP. (1991) Fcγ receptor III induces actin polymerisation in human neutrophils and primes phagocytosis mediated by Fcγ receptor II. *J Immunol* 146, 997-1004.

Sampath R, Gallagher PJ, Pavalko FM. (1998) Cytoskeletal interactions with the leukocyte integrin beta 2 cytoplasmic tail - Activation-dependent regulation of associations with talin and alpha-actinin. *J Biol Chem* 273, 33588-33594.

Sara M. (2010) The bone marrow: a site of neutrophil clearance. *Journal of Leukocyte Biology* 88, 241-251.

Sarah FO andrew LE, Rodger DU, Christopher HA, Adriano RO. (2010) Neutrophil Apoptosis: Relevance to the Innate Immune Response and Inflammatory Disease. *Innate immunity* 2, 216–227.

Savill JS, Wyllie AH, Henson JE, Walport MJ, Henson PM, Haslett C. (1989) Macrophage phagocytosis of aging neutrophils in inflammation. Programmed cell death in the neutrophil leads to its recognition by macrophages. *J Clin Invest* 83, 865-875.

Sawyer DW, Sullivan JA, MandellGL. (1985). Intracellular free calcium localized in neutrophils during phagocytosis. *Science* 230, 663-666.

Sbarra AJ, Karnovsky ML. (1959) The biochemical basis of phagocytosis. I Metabolic changes during the ingestion of particles by polymorphonuclear leukocytes. *J Biol Chem* 234, 1355-1362.

Scannell M, Flanagan MB, deStefani A,Wynne KJ, Cagney G, Godson C, Maderna P. (2007) Annexin-1 and peptide derivatives are released by apoptotic cells and stimulate phagocytosis of apoptotic neutrophils by macrophages. *J Immunol* 178, 4595–4605.

Scharff O, Foder B. (1993) Regulation of cytosolic calcium in blood cells. *Physiol. Rev* 73, 547-582.

Scheel-Toellner D, Wang K, Craddock R, Webb PR, McGettrick HM, Assi LK, Parkes N, Clough LE, Gulbins E, Salmon M, Lord JM. (2004) Reactive oxygen species limit neutrophil lifespan by activating receptor signaling. *Blood* 104, 2557-2564.

Schlaepfer DD, Hunter T. (1998) Integrin signalling and tyrosine phosphorylation: just the FAKs? Trends *Cell Biol* 8, 151-157.

Schmid-Schonbien, G. W., Shih, Y. Y. & Chien, S. (1980) Morphometry of human leukocytes. *Blood* 56**,** 866-75.

Schwab JC, Leong DA, Mandell GL. (1992). A wave of elevated intracellular calcium spreads through human neutrophils during phagocytosis of zymosan. *J Leukocyte Biol* 51, 437-443
Seabold GK, Daunais JB, Rau A, Grant K A, Alvarez VA. (2010). DiOLISTIC labelling of neurons from rodent and non-human primate brain slices. *J. Vis.Exp.* 6, 2081.

Segal AW, Jones OT. (1979) The subcellular distribution and some properties of the cytochrome b component of the microbicidal oxidase system of human neutrophils. *Biochem J* 182(1), 181-188.

Segal AW, Jones OTG. (1978) Novel cytochrome b system in phagocytic vacuoles of human phagocytes. *Nature* 27, 515-518.

Segal AW. (1987) Absence of both cytochrome b-245 subunits from neutrophils in X-linked chronic granulomatous disease. *Nature* 326, 88-91.

Segal AW. (1996) The NADPH oxidase and chronic granulomatous disease. *Molecular Medicine Today* 2, 129-135.

Segal, A.W. (1996) The NADPH oxidase and chronic granulomatous disease.*Mol Med Today*, 2, 129-35.

Segal, A. W. (2005). How neutrophils kill microbes.*Annual Review of Immunology* 23, 197-223.

Selliah N, Brooks WH, Roszman TL. (1996) Proteolytic cleavage of α-actinin by calpain in T-cells stimulated with anti-CD3 monoclonal antibody. *J Immunol* 156, 3215-3221.

Sengeløv H, Nielson MH, Borregaard N. (1992) Separation of human neutrophil plasma membrane from intracellular vesicles containing alkaline phosphatase and NADPH-oxidase activity by free flow electrophoresis. *J Biol Chem* 267, 14912-14917.

Serrander L, Fallman M, Stendahl O. (1996) Activation of phospholipase D is an early event in integrin-mediated signalling leading to phagocytosis in human neutrophils. *Inflammation* 20, 439-450.

Serrander L, Skarman P, Rasmussen B, Witke W, Lew DP, Krause K, Stendahl O, Nüße O. (2000) Selective Inhibition of IgG-Mediated Phagocytosis in Gelsolin-Deficient Murine Neutrophils. *J Immunol* 165, 2451-2457.

Servant G, Weiner OD, Neptune ER, Sedat JW, Bourne HR. (1999) Dynamics of a chemoattractant receptor in living neutrophils during chemotaxis. *Mol Biol Cell* 10(4), 1163-1178.

Shahi M, Haidari F, Rashidi B, Saei A, Mahboob S and Rashidi M. (2011).Comparison of the Effects of Genistein and Daidzein with Dexamethasone and Soy Protein on Rheumatoid Arthritis in Rats. *Bioimpacts* 1(3), 161–170.

Sharma CP, Ezzell RM, Arnaout MA. (1995) Direct interaction of filamin (ABP-280) with the beta 2-integrin subunit CD18. *J Immunol* 154(7), 3461-70.

Shaw SK, Bamba PS, Perkins BN, Luscinskas FW. (2001) Real-time imaging of vascular endothelial-cadherin during leukocyte transmigration across endothelium. *J Immunol* 167**,** 2323-30.

Sherazee N, Alvarez VA. (2013) DiOlistics: delivery of fluorescent dyes into cells. *Methods Mol.Biol* 940, 391–400

Sherwood SW, Kung AL, Roitelman J, Simoni RD, Schimke RT. (1993). In vivo inhibition of cyclin B degradation and induction of cell-cycle arrest in mammalian cells by the neutral cysteine protease inhibitor N-acetylleucylleucylnorleucinal. *Proc Natl Acad Sci* 90, 3353-3357.

Sheterline P, Rickard JE, Boothroyd B, Richards RC. (1986) Phorbol ester induces rapid actin assembly in neutrophil leucocytes independently of changes in $[Ca^{2+}]$i and pHi. *J Muscle Res Cell Motil* 7(5), 405-412.

Sheterline P, Rickard JE, Richards RC. (1984) Fc receptor-directed phagocytic stimuli induce transient actin assembly at an early stage of phagocytosis in neutrophil leukocytes. *Eur J Cell Biol* 34, 80-87.

Sheterline P, Rickard JE. (1989) The cortical actin network of neutrophil leukocytesduring phagocytosis and chemotaxis. In: Hallett MB, ed. The Neutrophil: Cellular Biochemistry and Physiology. CRC Press: Boca Ranton, FL.

Shi, Z and Baumgart (2015) Membrane tension and peripheral protein density mediate membrane shape transitions. *Nature Commun* 6, 5974 .

Shibasaki F, Fukami K, Fukui Y, Takenawa T. (1994) Phosphatidylinositol 3-kinase binds to alpha-actinin through the p85 subunit. *Biochem J* 302, 551-557.

Shiraishi, I. , Takamatsu, T, Minamikawa T, Fujita S. (1992) 3-D observation of actin filaments during cardiac myofibrinogenesis in chick embryo using a confocal laser scanning microscope. *Anat Embryol (Berl)* 185(4):401-408.

Shumway SD, Maki M, Miyamoto S. (1999) The PEST domain of $I_\kappa B\alpha$ is necessary and sufficient for in vitro degradation by μ-calpain. *J Biol Chem* 274(43), 30874-30881.

Simon SI, Burns AR, Taylor AD, Gopalan PK, Lynam EB, Sklar LA, Smith CW. (1995) L-selectin (CD62L) cross-linking signals neutrophil adhesive functions via the Mac-1 (CD11b/CD18) β_2-integrin. *J Immunol* 155(3), 1502-1514.

Sjölin C, Stendahl O, Dahlgren C. (1994) Calcium-induced translocation of annexins to subcellular organelles of human neutrophils. *Biochem J* 300, 325-330.

Smyth JT, Dehaven WI, Jones BF, Mercer JC, Trebak M, Vazquez G, Putney JR. (2006) Emerging perspectives in store-operated Ca2+ entry: roles of Orai, Stim and TRP. *Biochim Biophys Acta* 1763**,** 1147-60.

Southwick FS, Stossel TP. (1983) Contractile proteins in leukocyte function. *Sem Haematol* 20, 305-321.

Spangrude, G. J. (1994). "Biological and clinical aspects of hematopoietic stem cells." Annu Rev Med 45: 93-104.

Springer T A. (1997) Folding of the N-terminal, ligand-binding region of integrin alpha-subunits into a beta-propeller domain. Proc Natl Acad Sci USA 94, 65-72.

Stack JH, Emr SD. (1993) Genetic and biochemical studies of protein sorting to the yeast vacuole. *Curr Opin Cell Biol* 5, 641-646.

Stanley P, Hogg N. (1998) The I domain of integrin LFA-1 interacts with ICAM-1 domian 1 at residue Glu-34 but not GLN-73. *J Biol Chem* 273, 3358-3362.

Stendahl O, Krause K-H, Krischer J, Jerstrom P, Theler J-M, Clark R.A, Carpentier J-L, Lew DP. (1994) Redistribution of intracellular Ca^{2+} stores during phagocytosis in human neutrophils. *Science* 265, 1439-1441.

Stewart MP, Cabanas C, Hogg N. (1996) T cell adhesion to intercellular adhesion molecule-1 (ICAM-1) is controlled by cell spreading and the activation of integrin LFA-1. J *Immunol* 156, 1810-1817.

Stewart MP, McDowall A, Hogg N. (1998) LFA-1-mediated adhesion is regulated by cytoskeletal restraint and by a Ca^{2+}-dependent protease, calpain. *J Cell Biol* 140, 699-707.
Stossel TP. (1989) From signal to pseudopod. J Biol Chem 264(31), 18261-18264.

Strobl S, Fernandez-Catalan C, Braun M, Huber R, Masumoto H, Nakagawa K, Irie A,
Sorimachi H, Bourenkow G, Bartunik H, Suzuki K, Bode W. (2000) The crystal structure of calcium-free human m-calpain suggests an electrostatic switch mechanism for activation by calcium. *Proc Natl Acad Sci USA* 97(2), 588-592.

Sullivan, J.A. (2003) Movie sequence on www.CellsAlive.com.

Suzuki E, Kobayashi H, Kodama Y, Masujima T, Terakawa S. (1997) Video-rate dynamics of exocytototic events associated with phagocytosis in neutrophils. *Cell Motil Cytoskeleton* 38, 215-228.

Suzuki K, Sorimachi H. (1998) A novel aspect of calpain activation. *FEBS Lett* 433(1-2), 1-4.
Swanson JA, Johnson MT, Beningo K, Post P, Mooseker M, Araki N. (1999) A contractile activity that closes phagosomes in macrophages. *J Cell Sci* 122(3), 307-316.

T

Tak T, Tesselaar K, Pillay J, Borghans JA, Koenderman L. (2013) What's your age again? Determination of human neutrophil half-lives revisited. *J Leukoc Biol* 94(4):595-601.
Takano E, Yang M, Maki M, Hatanaka M. (1995) Preference of calcium-dependent interactions between calmodulin-like domains of calpain and calpastatin subdomains. *FEBS Lett*. 362, 93–97.

Terasaki M, Slater NT, Fein A, Schmidek A, Reese TS. (1994) Continuous network of endoplasmic reticulum in cerebellar Purkinje neurons. *Proc.Natl. Acad.Sci.U.S.A* 91, 7510–7514.

Terjung S. (2011) FRAP Tutorial. *EMBL* .[online] available at: www.embl.de/almf. [Accessed on 17 January 2015].

Thelen M, Dewald B, Baggiolini M. (1993). Neutrophil signal transduction and activation of the respiratory burst. *Physiol Rev* 73, 797-822

Theler JM, Lew DP, Jaconi ME, Krause KH, Wollheim CB, Schlegel W. (1995) Intracellular pattern of cytosolic Ca^{2+} changes during adhesion and multiple phagocytosis in human neutrophils. Dynamics of intracellular Ca^{2+} stores. *Blood* 85, 2194-2201.

Theler, J. M., Lew D. P., Jaconi M. E., Krause K. H., Wollheim C. B. and Schlegel W. (1995). Intracellular pattern of cytosolic Ca2+ changes during adhesion and multiple phagocytosis in human neutrophils. Dynamics of intracellular Ca2+ stores. *Blood* 85(8): 2194-201.

Thompson, NL, Axelrod, D. (1980) Reduced lateral mobility of a fluorescent lipid probe in cholesterol depleted erythrocyte membranes. *Biochimica et Biophysica Acta* 597, 155—165.

Thurston G, Jaggi B, Palcic B. (1986) Cell motility measurements with an automated microscope system. *Exp Cell Res* 165, 380-390.

Tian W, Laffafian I, Dewitt S, Hallett MB. (2003) Exclusion of exogenous PIP3 from the membranes of polarising pseudopodia in human neutrophils: its role in stabilising cell polarity. (in press)

Tinel H, Cancela JM, Mogami H, Gerasimenko JV, Gerasimenko OV, Tepikin AV, Petersen OH. (1999) Active mitochondria surrounding the pancreatic acinar granule region prevent spreading of inositol trisphosphate-evoked local cytosolic Ca^{2+} signals. *EMBO J* 18, 4999-5008.

Todd RF III, Petty HR. (1997) Beta2 (CD11b/CD18) integrins can serve as signaling partners for other leukocyte receptors. *J Lab Clin Med* 129, 492-498.
Toker A. (1998) The synthesis and cellular roles of phosphatidylinositol 4,5-bisphosphate. *Curr Opin Cell Biol* 10, 254-261.

Tompa P, Emori Y, Sorimachi H, Suzuki K, Friedrich P. (2001) Domain III of calpain is a Ca^{2+}-regulated phospholipid-binding domain. Biochem *Biophys Res Commun* 280(5), 1333-1339.
Tryggvason K, Koziel H, Kobzik L. (1999) Role of the scavenger receptor MARCO in alveolar macrophage binding of unopsonized environmental particles. *J Exp Med* 189,1497-1506.

Tsujinaka T, Kajiwara Y, Kambayashi J, Sakon M, Higuchi N, Tanaka T, Mori T. (1988) Synthesis of a new cell penetrating calpain inhibitor (calpeptin). Biochem *Biophys Res Commun* 153, 1201-1208.

Tsujita, K, Takenawa T and Itoh T. (2015) Feedback regulation between plasma membrane tension and membrane-bending proteins organizes cell polarity during leading edge formation. *Nature Cell Biology* 17, 749–758.

U-Z

Underhill DM, Ozinsky A. (2002) Phagocytosis of microbes: complexity in action *Annu Rev Immunol* 20, 825-852.

Underhill, D.M. and A. Ozinsky. (2002) "Phagocytosis of microbes: complexity in action" *Annu Rev Immunol*, 20, 825-852.

Ungewickell E, Branton D. (1981) Assembly units of clathrin coats. *Nature* 289, 420-422.

van de Winkel JGJ, Tax WJM, Jacobs CWM, Huizinga TWJ, Willems PHGM. (1990) Cross-linking of both types of IgG Fc receptors, FcγRI and FcγRII, enhances intracellular Ca^{2+} in the monocytic cell line U937. *Scan J Immnol* 31, 315-325.

Van Kooyk Y and Figdor CG. (2000) Avidity regulation of integrins: the driving force in leukocyte adhesion. *Current Opin Cell Biol* 12, 542-547.

Vander AJ, Sherman JH, Luciano DS. (1994) 'Defence mechanisms of the body' in Human Physiology. Ed.6, 699-754. McGraw-Hill, Inc, USA

VanKooyk Y, Weder P, Heije K, Figdor CG. (1994) Extracellular Ca^{2+} modulates leukocyte function-associated antigen-1 cell surface distribution on T lymphocytes and consequently affects cell adhesion. *J Cell Biol* 124, 1061-1070.

Vazquez G, Wedel BJ, Bird GSJ, Joseph SK, Putney JW. (2002) An inositol 1,4,5-trisphosphate receptor-dependent cation entry pathway in DT40 B lymphocytes. *EMBO J* 21(17), 4531-4538.

Vedder NB, Harlan JM. (1988) Increased surface expression of CD11b/CD18 (Mac-1) is not required for stimulated neutrophil adherence to cultured endothelium. *J Clin Invest* 81, 676-682.

Viera OV, Botelho RJ, Rameh L, Brachmann SM, Matsuo T, Davidson HW, Schreiber A, Backer JM, Cantley LC, Grinstein S. (2001) Distinct roles of class I and class III phosphatidylinositol 3-kinase in phagosome formation and maturation. *J Cell Biol* 155(1), 19-25.

Vlahos CJ, Matter WF, Brown RF, Traynor-Kaplan AE, Heywortyh PG, Prossnitz ER, Ye RD, Marder P, Schelm JA, Rothfuss KJ et al. (1995) Investigation of neutrophil signal transduction using a specific inhibitor of phosphatidylinositol 3-kinase. *J Immunol* 154(5), 2413-2422.

Volpe P, Krause KH, Hashimoto KS, Zorzato F, Pozzan T, Meldolesi J, Lew DP. (1988) Calciosome, a cytoplasmic organelle: the inositol 1,4,5 -trisphosphate-sensitive Ca^{2+} store of non-muscle cells? *Proc Natl Acad Sci USA* 85, 1091-1095.

Vossebeld PF, Homburg CH, Schweizer RC, Ibarrola I, Kessler J, Koenderman L, Roos D, Verhoeven AJ. (1997) Tyrosine phosphorylation-dependent activation of phosphatidylinositide 3-kinase occurs upstream of Ca^{2+}-signalling induced by Fcgamma receptor cross-linking in human neutrophils. *Biochem J* 323(1), 87-94.

Wakelin MW, Sanz MJ, Dewar A, Albelda SM, Larkin SW, Boughton-Smith N, Williams TJ, Nourshargh S. (1996) An anti-platelet-endothelial cell adhesion molecule-1 antibody inhibits leukocyte extravasation from mesenteric microvessels in vivo by blocking the passage through the basement membrane. *J Exp Med,* 184**,** 229-39.

Waller A. (1846) Microscopic observation on the perforation of capillaries by the corpuscles of blood and the origin of mucus and pus globules. *London Edingburgh Philos Mag J Sci* 2, 271-280.

Wang C, Hayashi H, Harrison R, Chiu B, Chan JR, Ostergaard HL, Inman RD, Jongstra J, Cybulsky MI, Jongstra-Bilen J. (2002) Modulation of Mac-1 (CD11b/CD18)-mediated adhesion by the leukocyte-specific protein 1 is key to its role in neutrophil polarization and chemotaxis. *J Immunol* 169(1), 415-423.

Wang KK, Nath R, Posner A, Raser KJ, Buroker-Kilgore M, Hajimohammadreza I, Probert A W Jr, Marcoux FW, Ye Q, Takano E, Hatanaka M, Maki M, Caner H, Collins JL, Fergus A, Lee KS, Lunney EA, Hays SJ, Yuen P. (1996) An alpha-mercaptoacrylic acid derivative is a selective nonpeptide cell-permeable calpain inhibitor and is neuroprotective. *Proc Natl Acad Sci USA* 93(13), 6687-6692.

Wang KK, Villalobo A, Roufogalis BD. (1989) Characterization of the fragmented forms of calcineurin produced by calpain I. Biochem J 262, 693-706.

Wang KK, Yuen PW. (1994) Calpain inhibition: an overview of its therapeutic potential. *Trends Pharmacol Sci* 15(11), 412-419.

Wang KK, Yuen PW. (1997) Development and therapeutic potential of calpain inhibitors. *Adv Pharmacol* 37, 117-152.

Weber KS, Klickstein LB, Weber C. (1999) Specific activation of leukocyte beta2 integrins lymphocyte function-associated antigen-1 and Mac-1 by chemokines mediated by distinct pathways via the alpha subunit cytoplasmic domains. *Mol Biol Cell* 10, 861-873.

Weiner OD, Neilsen PO, Prestwick GD, Kirschner MW, Cantley LC, Bourne HR. (2002) A PtdInsP(3)- and Rho GTPase-mediated positive feedback loop regulates neutrophil polarity. *Nat Cell Biol* 4(7), 509-513.

Wendt A, Thompson V, Goll D. (2004) Interaction of calpastatin with calpain: a *review. Biol. Chem*. 385, 465–472.

Westmark CJ, Westmark PR, O'Riordan KJ, Ray BC, Hervey CM, Salamat MS. (2011) ReversaloffragileXpheno types by manipulation of AβPP/Aβ levelsinFmr1KOmice. *PLoSONE* 6:e26549.

Whyte MK, Meagher LC, MacDermot J, Haslett C. (1993) Impairment of function in aging neutrophils is associated with apoptosis. *J Immunol* 150, 5124-34.

Williams AF. (1991) Cellular interactions. Out of equilibrium. *Nature* 352(6335), 473-474.

Williams MA, Solomkin JS. (1999) Integrin-mediated signalling in human neutrophil functioning. *J Leuk Biol* 65, 725-736.

Wilsson A, Lundqvist H, Gustafsson M, Stendahl O. (1996). Killing of phagocytosed Staphylococcus aureus by human neutrophils requires intracellular free calcium. *J Leukocyte Biol* 59, 902-907.

Wintrobe MM. (1967) Clinical Haematology. Lea and Febiger, Philadelphia. Pg226.
Woods A, Couchman JR. (2000) Integrin modulation by lateral association. *J Biol Chem* 275, 24233-242336.

Wymann, MP, Kernan P, Deanleau DA, Baggiolini M. (1989), Respiratory burst oscillations in human neutrophils and their correlation with fluctuations in apparent cell shape. *J Biol Chem* 264, 15829-15834.

Wymann, MP, Kernan P, Vontscharner V, Deanleau DA, Dewald, B, Baggiolini M. (1987) Oscillatory motion in human neutrophils responding to chemotactic stimuli. *Biochem Biophys Res Commun* 147, 361-368.

Yan SR, Berton G. (1998) Antibody-induced engagement of β2 integrins in human neutrophils causes a rapid redistribution of cytoskeletal proteins, Src-family tyrosine kinases and p72syk that precedes de novo actin polymerisation. *J Leuk Biol* 64, 401-408.

Yang HQ, Ma H, Takano E, Hatanaka M, Maki M.(1994) Analysis of calcium-dependent interaction between aminoterminal conserved region of calpastatin functional domain and calmodulin-like domain of mu-calpain large subunit. *J. Biol.Chem*. 269, 18977–18984.

Yin HL, Hartwig JH, Maruyama K, Stossel TP. (1981) Ca^{2+} control of actin filament length. Effects of macrophage gelsolin on actin polymerization. *J Biol Chem* 256(18), 9693-9697.

Yoshifuji, H. et al (2005) Amelioration of experimental arthritis by a calpain-inhibitory compound: regulation of cytokine production by E-64-d in vivo and in vitro. *Int. Immunol* 1, 1327 - 1336.

Zarbock A, Ley K. (2008) Mechanisms and consequences of neutrophil interaction with the endothelium. *Am J Pathol* 172**,** 1-7.

Zicha D, Dunn GA. (1995) An image processing system for cell behaviour studies in subconfluent cultures. *J Microscopy* 179, 11-21.

Zimmerman GA, Prescott SM, McIntyre TM. (1992) Endothelial cell interactions with granulocytes: tethering and signalling molecules. *Immunol Today* 13, 93-100.